Ensuring Technical Product Quality in the Energy Efficient Hot Air Drying of Extruded Fish Feed

Haubjerg, Anders Fjeldbo

Publication date:
2016

Document version
Other version

Citation for pulished version (APA):
Haubjerg, A. F. (2016). Ensuring Technical Product Quality in the Energy Efficient Hot Air Drying of Extruded Fish Feed. Syddansk Universitet. Det Tekniske Fakultet.

Ensuring Technical Product Quality

in the Energy Efficient Hot Air Drying of Extruded Fish Feed

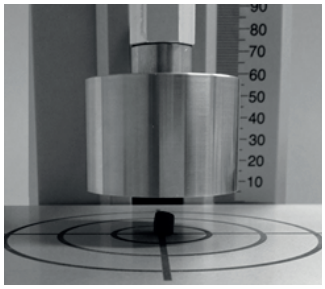

Anders Fjeldbo Haubjerg, M.Sc. Chem. Eng.

Principal supervisor: Associate professor, PhD, Christian T. Veje

Centre for Energy Informatics, Maersk McKinney Moller Institute
Faculty of Engineering, University of Southern Denmark
& Graintec A/S

Doctoral Dissertation (PhD thesis)
Odense, April 15, 2016

SDU

Preface

Feeding the world's ever-growing population whilst safeguarding the planets natural resources for our descendants remains one of the toughest challenges of the human race. Carbon emission must be reduced and climate changes must be slowed down, or even reversed. Political leaders, opinion-formers and environmental associations emphasizes, that the reorganization to a society independent of fossil fuels was actually supposed to be yesterday. In reality though, we are all waiting and wishing that researchers and academia alike soon invent a greener tomorrow. Yet, until the time of bio-sustainable 'super-algae', the established industry will have to look to themselves when faced with increased expense on the consumption of fossil fuels, whilst facing increasing demands in carbon emissions and product quality. This prompts a natural focus on improvement of fossil fuel efficiency to decrease emissions and ensure todays profit, in a business where the accessibility of fossil fuels are natural and vital. The present PhD project was launched aiming to sustain, or even improve product quality, when at the same time trying to increase process energy efficiency.

Over the past few years I have occasionally been asked by friends, families and acquaintances; "what is your PhD project about?" In a casual remark, my wife tell them that it concerns the drying of fish feed. I would observe their witty smiles and their effort to imagine green and red flakes of aquarium fish feed crumble away between their thumbs, to surface on the top of a fish tank filled with guppies and zebrafish. Other times, I elaborate, that the project concern numerical modeling of deep-bed hot air drying processes. Oh yes, and structural mechanics of porous solids. I would then observe their blank eyes and wavering looks, impatiently gesturing that a change of subject is around the corner. Admittedly, many people are not particular passionate about fish feed production – or even drying. With this project, it is my hope that we someday will enjoy to discuss challenges in this world, given the premise that they hold actual relevance, even if they seem unappealing and can be difficult to understand.

This doctoral dissertation concludes the 3-year Industrial PhD project, which was initiated in September 2012. The Industrial PhD project was established in collaboration between Graintec A/S in Vejle, Denmark, and the Centre for Energy Informatics at the University of Southern Denmark. A parental- and a project leave has prolonged the period by 46 weeks, to move termination of the project to April 16, 2016.

Some four years ago, I stumbled upon the advertisement for the Industrial PhD position in the newspaper. My own commitment to this project was immediately awakened, and since that time, it has been an exciting, aggravating, challenging, honorable, tearful and rewarding journey that were never boring! To see it ending, brings pride and relieve that I got this far, and frustration that I did not manage to go further. I am however content to say, that every available inch of me, and the patience of my family, has been put into this project.

I do hope that you will find it interesting.

Acknowledgements

The work presented in this PhD project were carried out at Graintec A/S in Vejle, Denmark, and at the Centre for Energy Informatics at the University of Southern Denmark in Odense. I would like to acknowledge the Danish Agency for Science, Technology and Innovation for making the project possible through financial support (Grant No. 0604–01439). Along the same lines, I would like to express my gratitude towards the management at Graintec A/S for engaging this opportunity; for that, I am grateful and I hope the present project will form basis for a new knowledge platform at Graintec A/S, allowing further maturation of the project, to redeem its full technological and commercial potential.

It has been a privilege for me, as an industrial PhD student, to be able to draw inspiration, guidance and attention from the industry as well as from academia. Dr. Christian T. Veje, my main supervisor at the University of Southern Denmark, is greatly acknowledged for his inspiration, help and encouragement. Without being able to draw on his competences, this project would never have been possible. Benny Simonsen, my company supervisor, have too been a great support, allowing me to use his great knowledge and know-how to establish a technological platform in fish feed production, as well as for keeping me motivated and always willing to elaborate commercial sides to the project. I would also like to thank my co-supervisor at the University, Dr. Bo Nørregaard Jørgensen, for inspiration and motivation, and for visualizing the substance of the project to me, in a wider context. I would like to acknowledge the entire team of supervisors for always being available for honest, inspiring and equal discussions, and for pointing me in the right direction when I needed it the most.

I would like to thank colleagues at Graintec for providing a pleasant working environment and for always being available for discussions; related to the present project as well as related to other, commercial projects. I would also like to thank my former colleague at colleague at Graintec, Sti Løvgreen, for motivating and inspiring me and for sharing his enthusiasm and knowledge. Thank you Lise, for assisting with the graphical layout on front- and back pages.

I would like to thank Aller Aqua A/S in Christiansfeld, Denmark, for letting me use their production and laboratory facilities, for three years! Moreover, thanks to Ole Friis and the staff in the production at Aller Aqua, for being available for inspiring conversations on practical challenges in the industry, particularly within drying.

Wenger Manufacturing Inc. in Sabetha, US, collaborated in the design of a brand new Lab Scale Dryer, manufactured the unit and made it available to use in Denmark. Wenger did this, founded in their genuine interest in the project. Naturally, I feel deeply grateful towards Wenger Manufacturing Inc. for providing an excellent experimental platform and for their engagement in the project; it simply could not have looked the same, without their help. I owe a special thanks to Keith Erdley and Robert Sunderland at Wenger, for inspirational meetings and conversations, and for giving me due feedback on the results obtained.

I would like to take this opportunity to thank my friends; none mentioned none forgotten. Thank you for your support and understanding and for giving me strength to go on. I am looking forward to spending more time with you all.

Finally, I would like to thank my entire family, for keeping me motivated and encouraging me to take this opportunity. I owe my deepest gratitude to my mother and my wife for their invaluable support, not at the least in the final stages of the project. I am truly grateful, and I feel blessed to have a family that have shown unconditional support until the very end.

To my wife, with love. Thank you for enduring and for your never-ending patience.

Abstract

The energy efficiency in the hot air drying of extruded fish feed can often be improved, but some reluctance in the industry exists in this regard, from the risk of compromising the technical quality of the produced feed. The present Doctoral Thesis concern the challenge of improving energy efficiency in the deep-bed hot air drying process, while at the same time conserving the technical quality, and in particular the mechanical durability, of the extruded fish feed pellets. A mathematical model of an industrial deep-bed hot air dryer have been developed and validated experimentally. The numerical model is based on conservation of mass an energy, and is resolved using the finite difference method. The model predicts experimental data at an accuracy, given by coefficients of variation of the root mean square error, at 6 – 13 %. It was found that durable extruded fish feed pellets have viscoelastic character. With this knowledge, influence of the drying parameters on structural properties of the pellets are investigated in the framework of the glass transition theory of viscoelastic biopolymers. It was found that viscoelastic character of extruded fish feed pellets are enhanced, when dried in their rubbery phase. This promotes shrinkage and reduces surface tension. It was found that high temperature, high humidity and high air velocity each improves mechanical durability with significant interacting effects, implying that one high parameter could render high values of the other parameters obsolete. High temperature at the onset of glass transition should however be avoided to avoid increasing hardness and plasticity of the pellets. The developed mathematical model of the drying process allow for prediction and optimization of energy efficiency; additional model output are temporal and spatial pellet moisture and temperature, at any position in the deep bed. Latter details can be used in the final prediction of the mechanical durability. A quality estimate was developed, including, among other spatial pellet parameters from the model, the minimum temperature following evaporative cooling in the drying. The quality estimate was found to be a significant predictor of mechanical durability in the drying process, and was able to account for 44 % of the total variation in mechanical durability in 54 experiments, acknowledging a non-linear relation. The developed model form basis for a multi-objective tool, with the objective to increase energy efficiency, utilizing drying conditions that does not compromise technical quality.

Resumé (danish)

Det er er ofte muligt at øge energieffektiviteten ved varmluftstørring af ekstruderet fiskefoder. Hertil udvises der i industrien oftest tilbageholdenhed, af hensyn til risikoen for at kompromittere foderets tekniske kvalitet. Denne Ph.d. afhandling omhandler den udfordring der ligger i at optimere energieffektiviteten i tørreprocessen, og samtidig bevare den tekniske kvalitet, og i særdeleshed den mekaniske holdbarhed, af de ekstruderede fiskefoderpiller. En matematisk model af tørringen med høj lagtykkelse og ved brug af varm luft er udviklet og valideret eksperimentelt. Den numeriske model er baseret på masse- og energibevarelse og løses ved en central 'finite difference' metode. Modellens nøjagtighed er fundet til at kunne forudsige eksperimentelle tørringer med høj lagtykkelse, med en variationskoefficient for kvadratroden af den gennemsnitlige kvadratafvigelse (CV(RMSE)) på 6-13 %. Det er fundet, at fiskefoder med høj holdbarhed har viskoelastisk karakter. På denne baggrund er tørreparametrenes indflydelse på foderets strukturelle kvalitet og mekaniske holdbarhed undersøgt i regi af glasovergangsteori for viskoelastiske biopolymerer. Det er fundet i projektet, at foderpillernes viskoelastiske karakter øges, når de tørres i en mobil 'gummiagtig' fase. Dette fremmer således også krympning og reducerer trækspændinger på pillens overflade. Det blev i denne kontekst også fundet, at høj temperatur, høj fugtighed og høj lufthastighed hver især øger den mekaniske holdbarhed. Disse interagerer dog således, at én parameter med høj parameter kan gøre effekten af at have høje værdier for de to øvrige parametre overflødig. Ydermere skal høj temperatur ved indtræf af glasovergangen undgås, for at undgå øget hårdhed og plasticitet af pillerne. Den udviklede matematiske model af tørreprocessen muliggør forudsigelse samt optimering af den opnåede energieffektivitet; øvrig output fra modellen er tidslig og rumlig vandindhold og temperatur for en pille placeret et givent sted i tørrelaget. Disse detaljer kan benyttes til en endelig vurdering af foderets mekaniske holdbarhed. Et kvalitetsestimat er udviklet på baggrund af disse detaljer for pillerne. Dette inkluderer bl.a. pillernes minimumtemperatur fra fordampningsafkølingen. Det udviklede kvalitetsestimat blev fundet at være signifikant i kontekst af at forudsige mekanisk holdbarhed af foderet, og var i stand til forklare 44 % af den total varians i mekanisk holdbarhed, målt over 54 tørreforsøg, under antagelse af en ikke-lineær sammenhæng. Den udviklede model danner udgangspunkt for et multiobjektivt optimeringsværktøj der har til formål at øge energieffektiviteten i tørreprocessen, under tørrebetingelser der ikke kompromitterer foderets tekniske kvalitet.

Executive summary

In 2013, 80 million tons of extruded fish feed was produced for finfish, crustaceans and molluscs, worldwide. 7 million tons were produced for marine cage aquaculture, including 3 million tons supplied solely for salmonid species. As much as 7 percent of the produced feed are estimated to be lost to the environment in marine cage aquaculture. A significant part of this loss arises from poor technical quality of the feed, resulting in feed breakage and formation of fines during handling and transport. This imply that for every percent lost to the environment, 70.000 tons of extruded feed was discharged from world marine aquaculture in 2013. For salmonid marine aquaculture alone, each percentage of lost production costs approximately US$ 30 million, using an average feed price at US$ 1.0 / kg. Feed costs in marine cage aquaculture at the same time accounts for more than 50 % of the total production cost. As for costs of feed production, the drying process often account for more than 60 % of the total thermal energy usage. Improvement of energy efficiency in the drying process of extruded fish feed can in many occasions be realized, but often there exist some reluctance in the industry to investigate how changing the drying parameters can improve the energy efficiency, from the risk of compromising the technical quality of the finished product.

This industrial PhD thesis concern the challenge of improving energy efficiency in the drying process of extruded fish feed, while safeguarding, or even improving the technical quality, and in particular the mechanical durability.

Four constituent elements comprise the present thesis;

(i) A mathematical model of the deep-bed hot air drying process have been developed, calibrated and validated experimentally.
(ii) An experimental study have identified those structural properties of extruded fish feed pellet that govern their mechanical durability.
(iii) Drying parameters, and associated mechanisms, directly affecting structural properties and mechanical durability of extruded fish feed have been identified.
(iv) Using details of spatial pellet moisture content and temperature, as output from the developed model, predictions of mechanical durability of extruded fish feed has been correlated to experimental values.

The developed model allows the prediction of spatial moisture content and temperature of the product, during the drying, at any position in the deep bed of a single-zone, single-belt dryer. The model includes process level considerations of applying internal recirculation of drying air, to improve energy efficiency. Optimization of energy efficiency can effectively be realized using a suitable algorithm to minimize the burner load, provided constrains of dryer dimensions, product moisture and capacity, with the drying parameters as free variables. An experimental lab dryer have been designed and manufactured to calibrate and experimentally validate the developed drying model. It was found that the deep-bed model was able to reproduce drying conditions at an accuracy (root mean square error) of 6 – 13 %. Spatial details of moisture and temperature in the pellets are also predicted in the dryer model. These are applied to allow prediction of mechanical durability, as it will appear later in this summary.

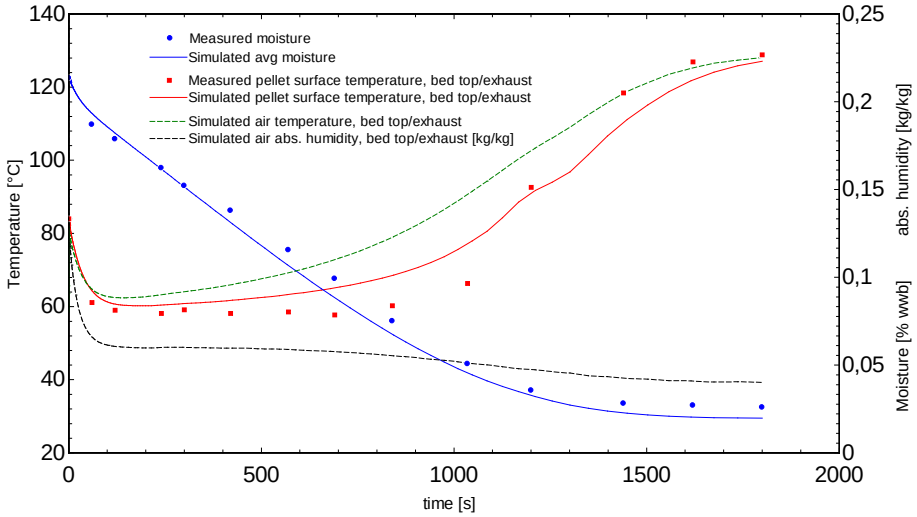

Model reproduction of experimental deep bed drying. Validation parameters are average moisture content and surface temperature of pellets at the top of the drying bed, at the air exhaust side.

By correlating mechanical durability (DORIS) and structural properties, obtained from texture analysis, it has been demonstrated that durable extruded fish feed have viscoelastic character, allowing viscous stress relaxation and an elastic reformation potential, following a deformation. Structural properties of viscoelastic biopolymers can often be characterized using a glass transition theory, implying that they have a soft and viscous, 'rubbery' phase and a distinctively different hard and brittle, 'glassy' phase. It was demonstrated that the observed structural properties of extruded fish feed can be predicted in the proposed framework of glass transition theory, generally stating that a viscoelastic material have a low glass transition temperature at high moisture contents, and vice versa. This implies that water acts as plasticizer, increasing the pellets' viscous character, and that drying in the rubbery phase, at temperatures above the glass transition point, ensures phase mobility and reduces surface tension. At (or immediately before) glass transition onset, drying temperature should generally be lowered to avoid the surface to transcend to its glassy state at a high rate, to avoid build-up of stresses in the pellets. Additionally it is proposed that when glass transition occur at high temperatures, surface non-enzymatic browning reactions are promoted, which in turn decreases the pellets' viscoelastic character, resulting in hard and brittle pellets.

Experimental investigations of mechanical durability and structural properties of extruded fish feed pellets in the drying process have been carried out using the custom-built lab scale hot air dryer. Temperature, humidity and velocity all effect the structural properties and mechanical durability of the feed. It was demonstrated that higher temperature increased the degree of shrinkage, significantly reducing (particularly the radial) diameter. This implies that a high temperature can be applied to dry in the rubbery phase, which in turn will improve the mechanical durability; importantly, the temperature should be reduced prior to the glass transition point, for reasons already mentioned. Increasing humidity generally demonstrated improved mechanical durability and viscoelastic character. This vastly support the glass transition theory, and therefore the same mechanism as stated for the temperature above is proposed; high humidity ensures that pellets will maintain phase mobility (allowing shrinkage), which reduces surface tension while increasing the pellets ultimate tensile strength. A high

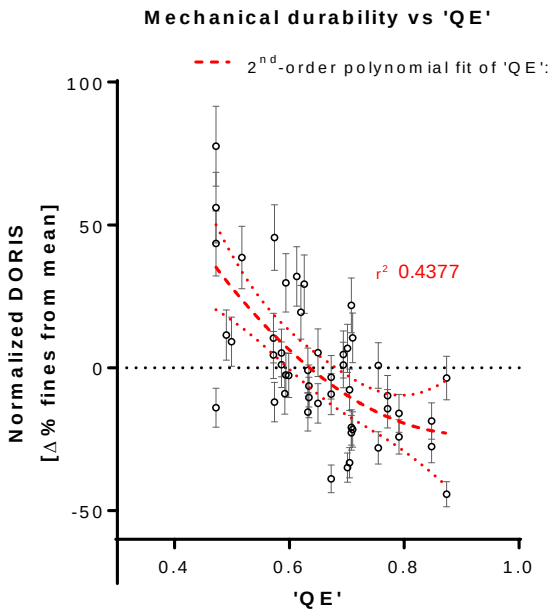

A developed quality estimate, 'QE', can be used to predict mechanical durability (as 'normalized DORIS') in the drying process. 'QE' uses spatial output details for pellets, as obtained from the developed deep-bed drying model

air velocity could additionally be used to hinder early surface glass transition, but more importantly, the air velocity should be kept high to reduce variations through the bed, e.g. avoiding a large temperature drop of the air, which in turn will induce glass transition of pellets at the air exhaust side of the bed. By using the spatial details of pellets' moisture and temperature, as obtained in the drying model, it was demonstrated that a low surface temperature following evaporative cooling significantly reduces the mechanical durability. This is believed to be a direct consequence of achieving an early glass transition in the pellets. A few additional parameters, as obtained from the spatial details of the pellet in the model, were included in a final 'quality estimate' that proved to be a significant effect, for the prediction of mechanical durability. This estimate were able to explain 44 % of the total variation in mechanical durability, across five different experimental design series, totaling 54 different drying conditions.

Following the present PhD thesis, it is proposed that high temperature, high humidity and high air velocity promote viscoelastic character of extruded fish feed pellets, improving their mechanical durability. It should be desirable to constantly be at a position on the glass transition curve, not too far away from the glass transition point, to reduce high product temperatures as well as spatial temperature and moisture gradients at actual onset into the glassy state. In this way, differences in glass transition from surface to center should be minimized.

Glass transition data for extruded fish feed have not been obtained in the present project. These data are obtained, the proposed model will allow for active glass transition temperature control, aiming to improve mechanical durability, by avoiding early glass transition onsets, as well as elevated product temperatures when entering the glassy state. The numerical model developed therefore form basis for a multi-objective optimization tool for the hot air drying of extruded fish feed; objective is to increase energy efficiency whilst utilizing drying conditions that does not compromise technical quality of the fish feed.

Acquiring glass transition data for extruded fish feed have imminent importance to mature application of active glass transition temperature control of the drying process. This should allow the developed model, and the results that demonstrate the mechanism for improving durability in the drying process, to redeem its full industrial potential. Another important task is to expand the developed model to allow computation for multiple drying zones and multiple belts to represent industrial scale hot air dryers for the drying of extruded fish feed.

Nomenclature

Roman

aw	Water activity
A	Area [m²]
Cp	Specific heat capacity [J kg^{-1} K^{-1}]
D	Mass diffusivity [m² s^{-1}]
d	Diameter [m]
E	Evaporation rate [kg s^{-1}]
f	$f(\ldots)$, function of
ΔH_{vap}	Latent heat of evaporation of water [J kg^{-1}]
h	Heat transfer coefficient [W m^{-2} °C^{-1}]
h_m	Mass transfer coefficient [m s^{-1}]
J_m	Mass flux [kg m^{-2} s^{-1}]
J_q	Heat flux [J m^{-2} s^{-1}]
k	Thermal conductivity [W m^{-1} K^{-1}]
K_{eff}	Empirical diffusion type coefficient in Eq. 7 [mol m J^{-1} s^{-1}]
I	Air enthalpy [J kg^{-1}]
L	Length [m]
$\dot{m}$	Feed flowrate [kg s^{-1}]
Mw	Molecular weight [kg mol^{-1}]
M	Air mass flowrate [kg air s^{-1}]
Nu_d	Nusselt's number, $h\,d\,k^{-1}$ [-]
p	Vapor pressure [Pa]
P_l	Capillary pressure [Pa]
Q	Heat load [J s^{-1}]
r	Radius [m]
R	Ideal gas constant [m³ Pa K^{-1}mol^{-1}]
Re_d	Reynold's number, $d\,J_m\,\mu^{-1}$ [-]
S	Source term [-]
S_{iso}	Shrinkage isotropicity [m m^{-1}]
S_B	Shrinkage coefficient [m³ m^{-3}]
t	Time [s]
T	Air temperature [°C]
u	Interstitial velocity [m s^{-1}]
Pr	Prandtl's number, $Cp\,\mu\,k^{-1}$ [-]
v	Superficial bed velocity [m s^{-1}]
V	Volume [m³]
$W_{\%}$	Energy efficiency [%]
$w.b.$	Wet basis
X	Moisture content, wet basis [(kg H_2O)kg^{-1}]
X_d	Moisture content, dry basis [(kg H_2O)(kg dry matter)$^{-1}$]
Y	Air absolute humidity [(kg H_2O)(kg dry air)$^{-1}$]

Greek

ε	Bed porosity [$V_{void}\,V_{tot}^{-1}$] *or* Deformation (structural mechanics) [m]
α	Thermal diffusivity [m² s^{-1}]
ρ	Density [kg m^{-3}]
θ	Pellet temperature [°C]
θ_g	Glass transition temperature [°C]
Δ	Change, difference [-]
∇	Gradient, divergence [-]
ξ	Empirical bed correction factor in Eq. 15
Γ	Permeability [m²]
μ	Dynamic viscosity [kg m^{-1} s^{-1}]
κ	Stiffness of spring (structural mechanics) [N m^{-1}] = [kg s^{-2}]
μ	Viscosity coefficient of dashpot (structural mechanics) [kg s^{-1}]
σ	Stress (structural mechanics) [Pa]
φ	Surface mass flux [kg m^{-2} s^{-1}]
τ	Relaxation time [s]
β	Pellet porosity [$V_{void}\,V_{tot}^{-1}$]
Φ	Chemical potential [J mol^{-1}]

Subscripts

0	Initial
a	Air (incl. humidity)
avg	Average
c	Characteristic
eq	Equilibrium
i	Inlet, node i
j	Node j
k	Node k (air in bed)
Z	Bed depth
l	Liquid [water]
m	Mass
O	Outlet
P	Pellet/particle
q	Energy
r	Radial direction
s	solid
w	Longitudinal direction
∞	Initial conditions

Superscripts

$\overline{j}$	Mean j, average j
$\overline{\overline{j}}$	Normalized j
$*$	Saturated, saturation
$\dot{\sigma}$	Dot notation; $d\sigma\,dt^{-1}$

List of papers and contribution

The following scientific journal papers have been prepared:

Published:

I: A.F. Haubjerg, C.T. Veje, B.N. Jørgensen, B. Simonsen and S. Løvgreen, Structural Properties and Mechanical Durability of Extruded Fish Feed. Journal of Food Process Engineering 12/2015; 38(6):621-631. DOI:10.1111/jfpe.12192

Accepted, with revisions:

II: A.F. Haubjerg, C.T. Veje, B. Simonsen and B.N. Jørgensen, Convective Deep Bed Drying of Extruded Fish Feed: Development of a Mathematical Model. Submitted to Drying Technology, November 2015. Revised edition submitted to Drying Technology, March 2016.

In submission:

III: A.F. Haubjerg, C.T. Veje, B. Simonsen and B.N. Jørgensen, Convective Deep Bed Drying of Extruded Fish Feed: Model calibration, experimental validation and industrial application.

In preparation (not enclosed):

A.F. Haubjerg, C.T. Veje, B. Simonsen and B.N. Jørgensen, Securing mechanical durability by spatial glass transition control in the hot air drying process of extruded feed.

The following peer-reviewed manuscripts have been presented at conferences and symposia:

IV: A.F. Haubjerg, C.T. Veje, B. Simonsen and B.N. Jørgensen, Experimental Investigation Of Physical Properties And Mechanical Durability Of Extruded Fish Feed In The Drying Process, oral presentation at Eurodrying 2015, Budapest, Hungary; October 21st-23rd 2015.

V: A.F. Haubjerg, C.T. Veje, B. Simonsen and B.N. Jørgensen, A Numerical Model Of The Deep-Bed Drying Of Extruded Fish Feed And Its Experimental Validation, oral presentation at Eurodrying 2015, Budapest, Hungary; October 21st-23rd 2015.

VI: A.F. Haubjerg, C.T. Veje, B. Simonsen, S. Løvgreen and B.N. Jørgensen, Mechanical Durability and Relaxation Times of Dried Extruded Fish Feed, poster presentation at 19th International Drying Symposium, Lyon, France; August 24th-27th 2014 *(1st prize award for poster)*.

VII: A.F. Haubjerg, C.T. Veje, B. Simonsen, S. Løvgreen and B.N. Jørgensen, Mathematical Modeling of the Drying of Extruded Fish Feed and its Experimental Demonstration, oral presentation at 19th International Drying Symposium, Lyon, France; August 24th-27th 2014.

VIII: A.F. Haubjerg, C.T. Veje, B. Simonsen, S. Løvgreen and B.N. Jørgensen, Rheological properties as indicator for physico-chemical processes affecting technical quality of extruded fish feed, poster presentation at Eurodrying 2013, Paris, France; October 2nd-4th 2013.

IX: A.F. Haubjerg, C.T. Veje, B. Simonsen, S. Løvgreen and B.N. Jørgensen, Ensuring technical product quality in energy efficient hot air drying of extruded fish feed: Definition of an industrial research project, poster presentation at 18th International Drying Symposium, Xiamen, China; November 11th-15th 2012.

The following publications have been made in various trade journals:

X: A.F. Haubjerg, Testing durability of fish feed pellets – which to use when and why, International Aquafeed Directory & Buyers' Guide, 2015, vol. 18, p. 22-23, Turret Group Ltd, Rickmansworth, Herts, UK, ISSN 1464018x

XI: A.F. Haubjerg, En grønnere opdrætsfisk – om matematik, tørring og fiskefoder (Danish), Aktuel Naturvidenskab 1/2014, p. 34-37.

Papers I to XI outlined in the present section highlight the majority of the work carried over the course of the PhD project. Content from these appear to a wide extent in the present doctoral dissertation. Particularly, content from papers I and IV appear to a wide extent in section 5 and 6. Section 4 have been prepared based on papers II, III, V and VII.

All papers are enclosed as appendices to thesis. These can be found on the CD-ROM on the last page.

Contents

1 Introduction

Aquaculture is the fastest growing animal food producing sector in the world [1]. In the recent five decades, production of fish from aquaculture has evolved intensively, to comprise 42.2 % of all consumed fish for food, totaling a production of 66.6 million tons of finfish, crustaceans and molluscs in 2012. In 2000 – 2012, production more than doubled at an average annual growth rate at 6.2 percent. Hence, aquaculture is one of few food sectors that outpace the worlds growing population, which at present is 3.2 percent[2]. The World Bank foresees that aquaculture production will sustain growth, and predicts a production of 93.6 million tons in 2030 [3]. In 2013 47.1 million tons of finfish was produced from aquaculture, of which 5.8 million tons is from marine cage aquaculture [4]. Latter required around 7 million tons of compound extruded fish feed to be supplied to the marine aquaculture of finfish in 2013 [1]. Of this amount, approximately 3 million tons are produced for Salmonidae (Atlantic salmon, rainbow trout, whitefish, arctic char, grayling and trout) [4].

Industrial compound fish feed for aquaculture of finfish are extruded cylindrical pellets with diameters typically varying from 2 – 12 mm, cf. Figure 1 and Figure 2. They can be characterized as hard and brittle materials that crack and loose mass (as dust, 'fines'), when applied to mechanical stress. Different assessments of the feed waste to the environment comprises sub-optimal feeding practice [5, 6] and inadequate 'technical quality' [7-9]. Technical quality of the feed describes a pellets ability to: (i) endure mechanical stress during transport without losing mass, (ii) have density, geometry and size to ensure intended sinking properties, (iii) be stabile when suspended in water and (iv) have a moisture content to biologically secure product during storage and transport as well as ensure intended oil absorption. Norwegian Institute of Marine Research has suggested that as much as 7 % of the feed could be lost to the environment in the Norwegian (marine) aquaculture, which predominantly comprise salmonid species fed with relatively large feed pellets [10]. These are typically farmed in floating net cages in the deep fjords of Norway, Chile, UK, Canada and the Faroe Islands. Feed is supplied to the fish by pneumatic conveying from feed barges, which often are supplied with feed in bulk, transported at sea [7].

Figure 1: 12 mm extruded fish feed pellets (salmon grower feed)

Figure 2: Interior of an extruded fish feed pellet

Bulk handling and pneumatic transport sets high demands to the technical quality of the feed pellets, to reduce fragmentation and generated fines. It is not known how much of the total feed waste that is caused by issues related to technical quality, and different values appear in literature. Recent literature indicate numbers between 0.3 and 1.2 % feed waste due to breakage in pneumatic feeding systems [11], whereas a decade ago it was suggested that this number is significantly higher at 3 – 5 % [12]. From above, for each percentage of lost production

due to poor quality, 70.000 tons feed was discharged from world marine aquaculture in 2013, as pollution to marine environments. For salmonid marine aquaculture alone, each percentage of lost production costs approximately US$ 30 million, using an average feed price at US$ 1.0 / kg [11]. The physical quality of the pellets is varying with composition and processing conditions [9, 13-15], including also effects directly related to the drying process [5, 16, 17].

In marine aquaculture, feed costs are estimated to account for 50-70 % of the total production cost, depending on geography, farmed specie and the feeding distribution system used [18, 19]. Also, it is evaluated that around 60 % of the total thermal energy consumption in the production of extruded fish feed can conventionally be accounted to the drying process [20]. The energy efficiency in the hot air drying of extruded fish feed can often be improved, but some reluctance in the industry exists in this regard, from the risk of compromising the technical quality of the produced feed [20]. Hence, lack of knowledge and awareness on the drying process in fish feed production could compromise quality of the feed as well as sustain an ineffective fossil fuel efficiency. This yields excessive production costs and environmental emissions. More knowledge is needed about the processing effects that lead to feed degradation during transport, storage and feeding [5]; the present project aim to elucidate how the drying process parameters influence energy efficiency, as well as the achieved technical quality of extruded fish feed pellets.

2 Background

2.1 Aquaculture

Aquaculture is a highly diversified discipline covering all branches of cultivating freshwater, brackish- or saltwater animals or plants. This comprise, among other disciplines, small family-driven ponds in tropical countries, high-tech indoor production facilities in large ponds, solar-powered seaweed-installations or the cultivation of fish in ponds or in cages in lakes, rivers and marine environments [21].

The principle technique in cultivating fish for human consumption can be dated back to as early as 2000 BC. At this time, the common carp (*Cyprinus carpio*) has been reported to be cultivated in lakes, ponds and lagoons in ancient China. The origins of using cages for holding (or transporting live fish) can be traced back to two centuries ago, to native 'boat people' at the banks of the Mekong basin [22, 23].

Modern aquaculture began to evolve around the 1970's in the deep fjords of Norway, with the rise and development of the marine cage aquaculture of finfish; particularly salmon (*Salmo salar*) and rainbow trout (*Oncorhynchus mykiss*) have shown high export value. These have shown relatively easy to reproduce and domesticate at high densities while giving good filet yield and taste. This development has been sustained by an increasing demand for high quality protein and healthy omega-3 fatty acids [22], in a world where 800 million people suffer from chronic malnourishment. By 2050 world population is expected to increase by around 30 % to 9.6 million, and the largest part of the necessary increase in food production is, by far, deemed to arise from aquaculture [2].

The commercial success of farming salmon and rainbow trout in Norway initiated massive marine cage aquacultural production other places around the world, particularly in Chile, China, UK, Japan, Canada, Ireland, Greece and the Faroe Islands, cf. Figure 3. Aside with the commercial success of marine cage aquaculture of particularly salmon, inland aquaculture in developing countries have also seen a massive growth in recent decades [2]. From 1990 to 2012 aquaculture production in Asia has increased at an average annual growth rate of 8.8 %. In 2012, aquaculture production from developing countries (incl. China) accounted for more than 88 % of the world's total aquaculture production. The annual average fish consumption per capita rose from 9.9 kg in the 1960s to 19.2 kg in 2012[2]. Figure 3 visualizes worldwide cage aquaculture production distribution in 2005, including also the ratio between marine and freshwater species.

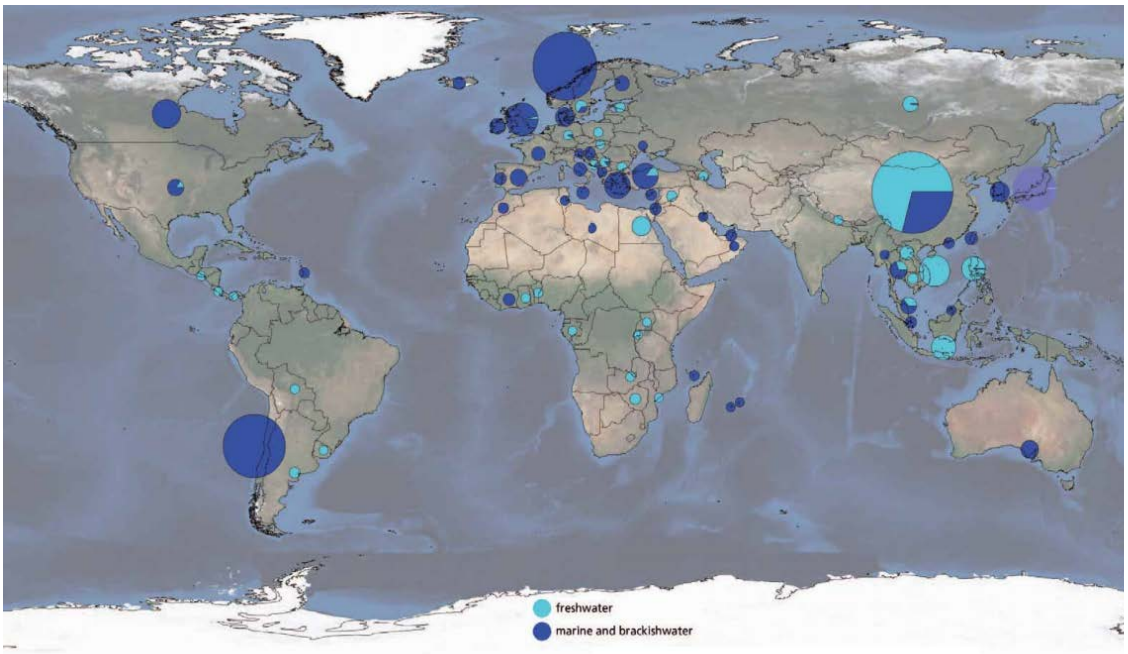

Figure 3: World-wide cage aquaculture production of freshwater and marine (and brackish water) fishes in 2005. The size of the spheres indicate relative production volumes [22].

The development over the past few years, from 2007-2012, have shown persistent growth rates in cultivated marine- and freshwater species, at 4.3 % and 7.0 % respectively. In 2013 freshwater fishes accounted for 86 % of aquaculture production of finfish [4]. Typically, freshwater species are farmed inland in ponds, rivers and lakes, whereas marine species are farmed near coastlines and in the fjords of the sea. Brackish water species could additionally be cultivated either inland or in the seas, obviously depending on the salinity. When distinguishing only between inland and marine aquaculture of finfish, Figure 4 shows how marine and inland finfish aquaculture has evolved since 1950. A segregation between developed and developing countries are included to visualize the massive contribution of inland aquaculture to the total production volumes. Clearly, inland production volumes in developing countries (China, India, Indonesia, Vietnam and Egypt) are massive when compared to marine production in developed as well as developing countries.

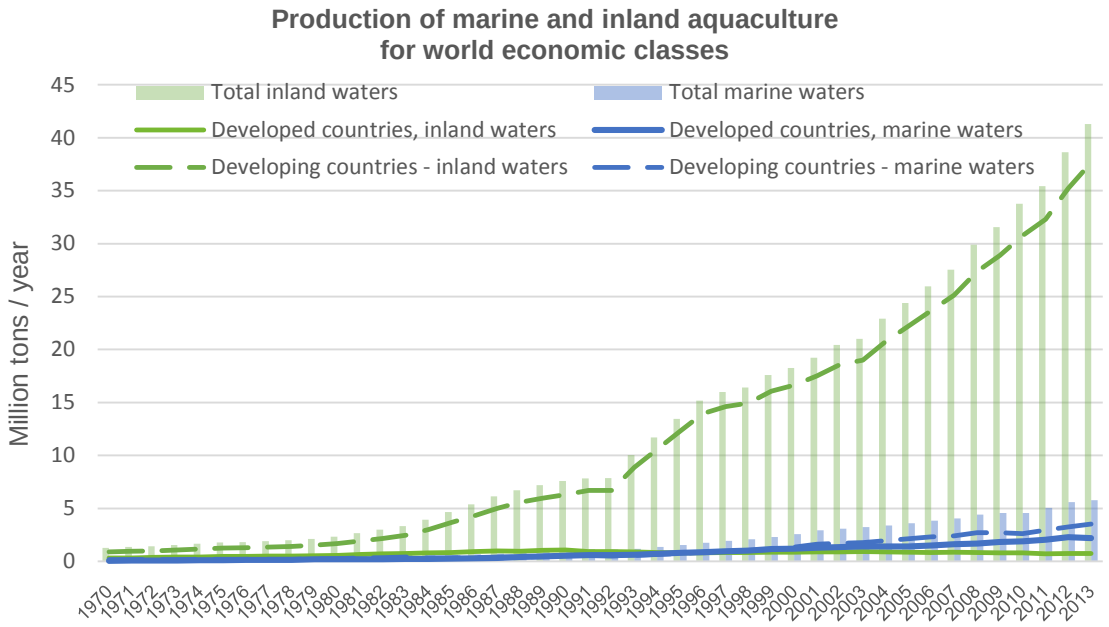

Figure 4: Production data for aquaculture of finfish in marine and inland waters. Inland aquaculture by developing countries constitute an enormous part of the growth in total finfish aquaculture production volumes[4].

The increasing demand for fish has promoted further investments in process intensifications in aquaculture over the last two decades, particular in marine cage aquaculture installations that have proved to have economies of scale [22]. This is additionally motivated by politics in developed countries embracing sustainable and responsible production methodologies. Developments have particularly been on improving cages, disease control, fry hatcheries, feeding techniques and feed distribution and naturally, all aspects in improving feed quality whilst minimizing associated costs [24].

Marine cage aquaculture has over the past years proved to be the most cost-effective production methodology, and is most widespread in developed countries [22], albeit 99.5 % of people employed within aquaculture are located in the least developed or developing countries [21].

Interestingly, production of finfish by marine (and brackish) cage aquaculture was in 2013 only 12 % (5.8 million ton) of the total farmed finfish production (47.1 million ton), but their corresponding value represented 28 % (US$ 26.2 million) of the total value of all farmed finfish (US$ 94.1 million) [2, 4]. This is visualized and elaborated in Figure 5 and Figure 6.

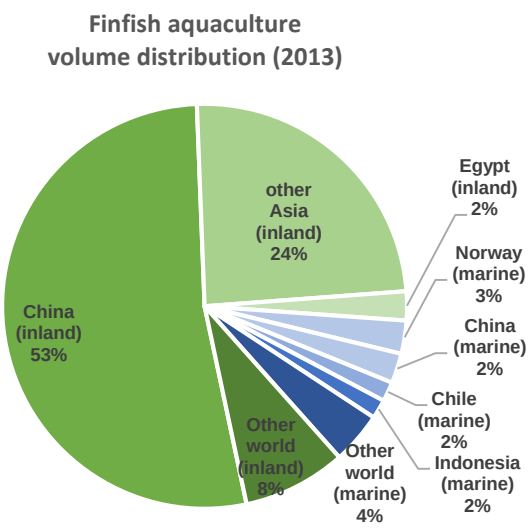

Figure 5: Inland (green) and marine (blue) finfish aquaculture volume distribution for different regions in the world [4].

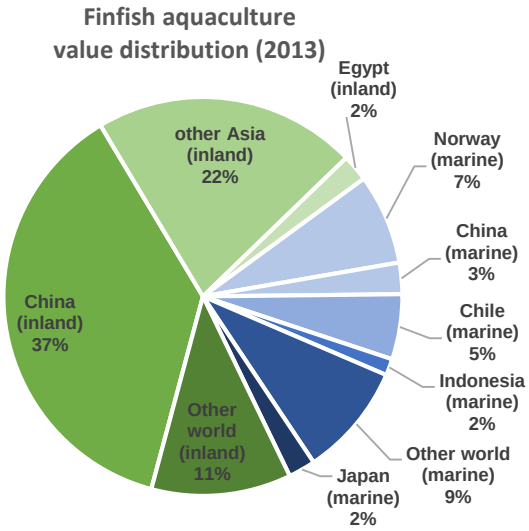

Figure 6: Inland (green) and marine (blue) finfish aquaculture value distribution for different regions in the world [4].

Inland aquaculture of finfish are often carried out in ponds and in penned lakes and lagoons, whilst inland cage aquaculture in large rivers, e.g. the Mekong delta, the Nile, etc. has shown a much higher yields. Certainly, part of the inland finfish aquaculture represented in Figure 4 in the least developed countries are not fed with compound extruded fish feed. It is also difficult to evaluate the actual aquaculture production in these areas. Typically, cages are small (~30 m^3), simple constructions either floating or fixed on poles in the riverbed. If fed with compound extruded feed, manual feeding is carried out using feed supplied in small bags [22]. Modern marine aquaculture is carried out in large cages made of HDPE and steel rims with attached PVC or nylon net cages. Weights are hanging from the nets to keep them open. Cages can be moored or floating and will most often by rectangular or circular and have a steel walkway [22]. The size of each cage in a site will typically range from 90 m – 157 m in diameter [25] with nets as deep as the site allows, typically 20-50 m [24, 25]. Cages typically contain 200,000-400,000 individuals at stocking densities typically varying with specie and local legislation from 10 to 30 kg/m^3 [25]. At a larger Norwegian marine aquaculture site (25 kg/m^3) with 10 cages of 40,000 m^3 each, the daily feed consumption will be 100-400 ton day, at daily feeding rates of 1 – 4 % of net body weight [26].

2.2 Extruded fish feed production

Commercial compound fish feed are particulate cylinders (for fry, granulates) that often range in size from 2-12 mm, cf. Figure 1 and Figure 2 on page 1. The feed are roughly made by grinding, dosing, mixing and cooking raw materials under pressure in an extruder, before drying, coating with oil and cooling. The finished feed are hard and brittle pellets that often have oil encapsulated in its highly porous structure. Larger feed cylinders (> 6 mm) tend to be approximately equilateral while smaller pellets generally have lengths exceeding their diameter.

2.2.1 Raw materials

The composition of main nutrients obviously depend on the cultivated species; the Atlantic salmon for example demand high protein (40-50 %) and lipid contents (30-40 %), whilst carp feed generally can include more carbohydrate. Proteins are generally the most expensive raw materials, followed by oil with carbohydrates being the most inexpensive source of energy in fish diets. In many diets, carbohydrates are not essential but included to reduce costs, and for making use of their binding properties. Other than main nutrient groups, also minerals and vitamins are necessary and specialized additives like pigments and binders could optionally be supplemented [18, 26].

Only a decade ago, sources of protein and lipids were predominantly fishmeal and fish oil. From 2003 to 2013, prices for these have risen almost 3- and 4-fold, respectively. This has induced a transition to include vegetable alternatives into the feed diets; however, the fish still need a certain amount of fish oil and fishmeal to be rich in omega-3 fatty acids. Today, aquaculture uses 75 % of the world's produced fish oil, including 25-33 % in salmon feeds [2]. RAFOA (Research on Alternatives to Fish Oil in Aquaculture) under the fifth framework of the EU targets an inclusion level in salmon feed of 8-12 % fish oil and 12-16 % fishmeal, and targets 0 % of either in carp feeds [18]. Protein sources, other than fishmeal, today includes soybean meal, krill meal, gelatin, maize gluten, wheat gluten, pea meal, field bean meal, sunflower, brewer's yeast and blood- and meat meal. Lipids, other than fish oil, include vegetable oils and tallow and carbohydrate sources are largely comprised from wheat meal and gelatinized starch [18].

2.2.2 Dosing, grinding and mixing

Feed ingredients are unloaded from boat or truck, sifted and stored in raw material silos or tanks. Raw material components are grinded (typically in hammer or roller mills) to reduce particle size for ease of mixing and to promote mechanical durability. Fine grinding of raw materials have also shown to yield good mechanical durability of the feed, as larger particles (> 1 mm) act as fissure points. On the other hand, fine grinding of the raw materials greatly add to costs of production [16, 20].

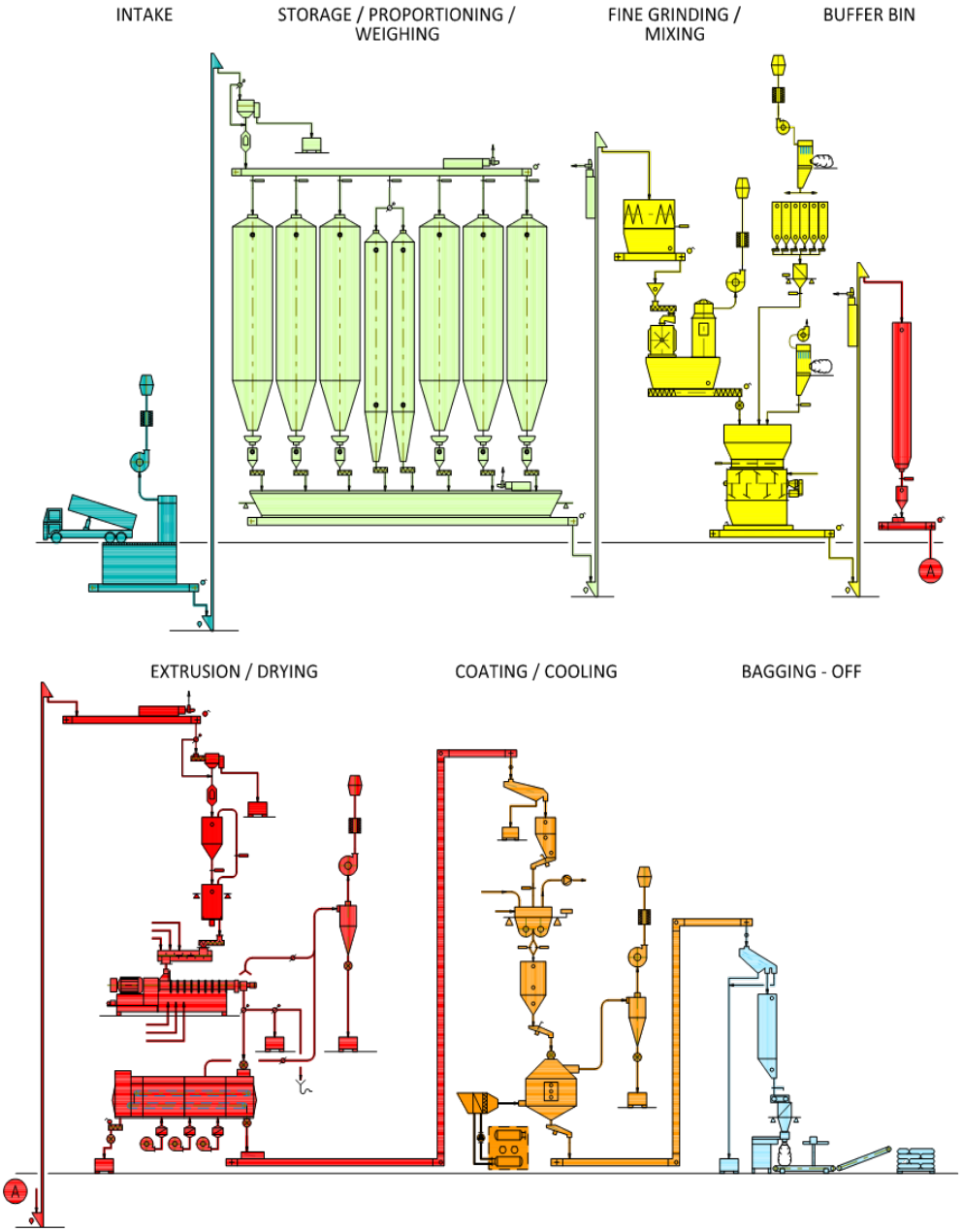

Figure 7: Flow diagram for the production of extruded fish feed (GRAINTEC A/S)

Accurate dosing of each raw material component is important to achieve the desired meal composition. The raw materials are mixed and the complete meal is conveyed to the conditioning process.

2.2.3 Conditioning

In transforming dry meal (~6 % moisture w.b.) into moist feed pellets, the conditioning process is the first step. Steam conditioning increases the temperature and moisture content, and the meal mix is transformed into a hot meal dough (80-95 °C), that is fed to the extruder. Raising the temperature of the feed activates inherent (or added) binders, and promotes gelatinization of starch and denaturation of proteins to increase digestibility by the fish. Last but not the least, the conditioning process helps hygienizing the feed mix. Retention times in the conditioning process range from 20-255 s [16]. Conditioning steam quality (liquid fractions) and pressure are other parameters that are often engineered, to improve durability of the pellets as influenced from the conditioning process, accounting also for the starch and protein contents [27-29].

2.2.4 Extrusion

In the extrusion process, steam and water is added and temperature and pressure is elevated across several sections in the extruder barrel. Other than thermal energy, a single screw, or two 'twin screws', applies mechanical energy onto the feed dough, while transporting the dough through the barrel towards the die plate. The feed dough exists the extruder barrel in holes in the die plate, and a rotating knife transforms the dough into moist feed pellets. When the feed exists the extruder barrel, the sudden pressure decrease causes immediate expansion of moisture in the pellets into steam. Hence, the extrusion process allows a high liquid absorption rate for improvement of starch gelatinization and protein denaturation, while immediately removing much of this moisture as steam, when ejecting the dough from the barrel. In addition, steam evaporated from inside the pellets causes a highly porous interior. This allows control of sinking properties as well as post-extrusion lipid addition, at lowered pressures. Other advantages in the extrusion process includes a thorough sterilization of the feed ingredients as well as the option of producing different geometries and color blends, mostly relevant to other industries, e.g. in pet food [14, 15, 27, 28].

2.2.5 Drying

The pellets ejected from the extruder typically have moisture contents of 22-27 % (w.b.) and saturated steam temperature at atmospheric pressure, 100 °C. The pellet continuously flash off moisture when existing the extruder, while in transport to the drying process. This step is done either on a conveyor belt or pneumatically in an 'airlift'. These processes are quite distinct; the conveyor belt has little airflow over the pellets for relatively long time (10-30 s), and the airlift has a high airflow across the pellet surface, for a duration of only a few seconds. Typically the flash off in either transport process could cause a reduction in moisture of 2-3% and a temperature reduction of 15-30 °C, obviously depending on size of pellets, moisture content out of the extruder and the transport method used. In the drying process, hot air is used to dry the pellets to a moisture content of around 8-10 %, with the obvious aim to avoid biological decomposition. Furthermore, while removing water from the pores cre-

ated in the extrusion process, the porous network in the pellets are made available for subsequent lipid adsorption. Parameters in the drying process include air temperature, humidity and velocity as well as pellet retention time. Combination of these parameters comprise a range of different industrial scale dryers that additionally will define pellet availability and orientation, relative to the airflow. Additionally, industrial scale dryers are typically compartmented into separate drying 'zones', each making use of different drying air parameters and flow patterns, as well as pellet retention times and orientations. The drying process has a high thermal energy consumption, often comprising more than 60 % of net thermal energy, 46 % of the total energy and 29 % of the total energy costs (UK energy prices, December 2015), among all processes in the fish feed production, cf. Figure 8 and Figure 9.

2.2.6 Precooling and vacuum coating

Following the drying, the energy content in the feed is increased by the addition of lipids. Vacuum coating is a highly effective way of doing this, in exploiting the porous interior of the dry feed pellets. An additional precooling step is often necessary to reduce pellet temperature, following the drying process. Sometimes this step is embedded physically into the dryer. The absolute pressure in the vacuum coating process is around 200 mbar, so temperature of the pellets should not be above 60 °C to prevent residual water from boiling. On the other hand, the temperature should not be too low, to avoid increase in viscosity and restriction of lipid flow into the pores. Oil is sprayed through nozzles into the coater. While mixing thoroughly, vacuum is held for a few minutes and released slowly. Other than increasing the energy content, pellet density is also increased. Hence, pellet sinking properties are predominantly governed from the extrusion and vacuum coating processes.

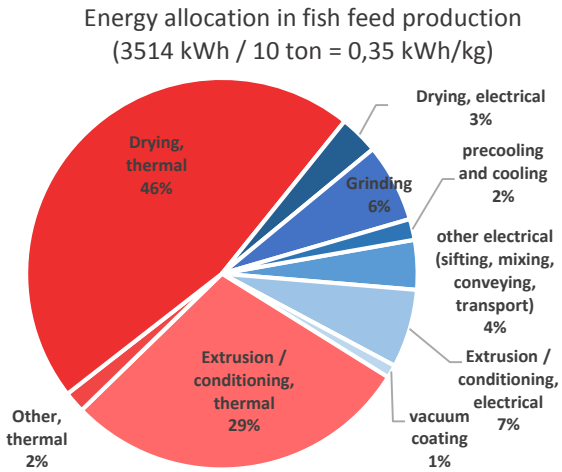

Figure 8: Allocation of energy consumption in the production of extruded fish feed [20].
Red=thermal-, blue=electrical energy contributors.

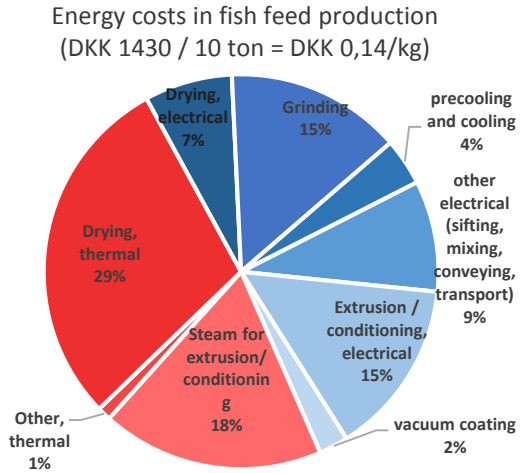

Figure 9: Costs of energy for different processing step in the production of extruded fish feed [20].
Red=thermal-, blue=electrical energy contributors.
Industrial gas / electricity prices: "UK DECC Quarterly Energy Prices", December 2015.

2.2.7 Cooling and storage

After coating the pellets with oil, the pellets must be cooled to avoid condensation issues during storage, and to avoid leak of adsorbed fat. The pellets are often cooled to around 12-15 °C, depending on local storage conditions (humidity and day-nighttime temperature fluctuations). A horizontal belt-cooler or vertical counter-flow cooler are the types of coolers most often used in industry. The pellets are then packed in bags, or stored in silos awaiting bulk loading and transport.

2.2.8 Handling and transport

At larger industrial inland farms, feeding could be carried out by conveying on belt- or vibrating feeders, or the feed could be blown out in the ponds using compressed air, directly from the feed trucks [26]. Marine aquaculture sites are supplied with feed by boat, loaded either in bulk or in big bags. Feed is conveyed to the cages from on-site feed-barges or floating silos in small HDPE tubes, using compressed air or water as transport medium [7]. Automated feeding systems, using underwater feed cameras and bottom waste collectors, in the cages become increasingly standard practice in the biggest marine aquaculture sites [22, 25].

A recurring motif in fish feed production is to direct all raw material ingredients towards ingestion by the fish. While at handling and transport in feed production facilities, feed waste is captured and reintroduced as 'rework' into the raw material ingredient portfolio. For this reason, feed waste is majorly the part of the feed production that is lost and dispersed into aquatic environments, under the influence of post-processing effects. Technical quality of the feed is a common nomenclature used to describe a pellets ability to: [30, 31]

- Endure mechanical stress during handling and transport.
- Have density, geometry and size to ensure intended sinking properties.
- Have a moisture content to biologically secure product during storage and transport
- Be stabile when suspended in water.

Each of above pellets properties contribute to the ratio between net feed intake and produced volume, yet for slightly different reasons. The most obvious property is the ability to endure mechanical stress during handling, without breaking or creating fines. Fines are ultimately scattered on water surfaces, due to surface tension, and are not eaten by the fish. Broken pellet chips sink at unintended velocities (if at all), and are therefore expected to have a lower intake ratio than unbroken pellets. As outlined above, the pellet density will also influence the sinking velocity (and consequently, intake ratio). High oil-uptake pre-requisites light, porous pellets with a fine pore distribution. Narrow pores and low moisture content can be expected to make pellets less prone to post-processing oil-leak, when load is applied onto the pellets, e.g. in big bags or when stores in silos. These effects are expected to arise from increased adsorptive capacity with narrow pores and increased lipophilicity with decreasing (free) moisture content. Hydrophobic effects from the correct amount of oil adsorbed in the pellets will in addition increase water stability, when suspended. As it appears, the stated properties above are to some extent interrelated, explaining the use of a common denominator, 'technical quality'.

3 Research objective

3.1.1 Justification

The challenge of reducing energy consumption in the drying process whilst improving feed quality, to reduce feed waste to the environment, is the key incentive behind the work carried out in the present industrial PhD project. Reducing the energy consumption in the drying process by a 5 percent target value, at an annual production of 80 million tons of extruded feed for finfish, crustaceans and molluscs, 600 GWh savings are estimated worldwide, at 7.5 kWh saved per ton. This is around 70 MW – or the equivalent of erecting ~20 large offshore wind turbines, each year. If only one percent of an annual production of 80 million tons of extruded aquafeed are estimated to be lost to the environment [11] this accounts for an annual lost production of around a US€ 0.5 billion (at an average price of US$ 0.60 / kg). A target reduction of net feed attrition by 20 % will consequently reduce feed wasted as pollution to the aquatic environments by 160.000 tons, at a production value of approximately US$ 100 million.

In context of the industrial side to this PhD project, additional motivation is caused by increased competition arising in the industry as an immediate response to the high growth rate over the recent (and coming) years. This development can be expected to cut away links between fish farmers and equipment suppliers. Indeed, fish farming companies begin to erect feed production facilities and increasingly, equipment suppliers offer engineering services with the supply of their equipment. This trend challenges the available room for Graintec in traditional technology supply, and therefore new technology solutions are needed aiming to improve efficiency, reduce costs as well as improve the green profiles of the company in fish feed production.

3.1.2 Methodology

This project is specifically directed towards extruded fish feed pellets that in a given configuration, based on choice of dryer type, will be subjected to heat transfer and concurrent dehydration. One method for detailed analysis will be mathematical modelling of the governing physical phenomena, i.e. simultaneous heat and mass transfer in a deep layer ('bed') of porous feed pellets. Parallel experimental investigations will be used as a necessary tool, for investigation of feed behavior in the drying process, as well as for model calibration and validation.

As it will appear from the following section 4, drying of porous media is generally well described and several experimental investigations and descriptive models exists on this topic. Approaches for the mathematical modelling are numerous; yet, these normally fall in one of two main groups:

- The microscopic, or particulate, approach addresses temporal and spatial moisture- and temperature distribution in particles with a given geometry.

- The macroscopic approach describes the drying on a 'process level'. This model type predicts temporal and spatial moisture- and temperature distribution in a dried portion of sample (e.g. a bed of feed pellets) and the drying media. As the bed is treated as a homogenous substance, the spatial variation across the bed is of particular interest in this type of model.

The project is divided into four constituent elements, which together comprises the research objective, but their individual resolution each contributes also single-handedly with development potential for the fish feed production industry.

(v) Development, calibration and validation of a mathematical model of the complete drying process (section 4.5 + 4.6)
(vi) Qualitative assessment of feed rheology and feed durability (section 5.3)
(vii) Experimental investigation of drying parameters on final technical quality (section 6.2)
(viii) Model prediction of feed quality measures in the hot air drying process (section 6.3)

3.1.3 Statement of intent

With the purpose of reducing feed waste in aquaculture and energy consumption in the drying process, the present PhD project aims to predict energy consumption as well as structure and technical quality of extruded and dried fish feed pellets, given knowledge of applied drying parameters.

The potential of obtaining a multiphysical description of parameters in the drying process, which governs specific energy consumption and gives rise to formation of structural properties in protein-rich porous extruded fish feed pellets constitutes the research value in this project. The developed model should provide reliable forecasts of the drying process and associated energy consumption, but also of the corresponding 'technical quality', given any input of drying conditions.

4 Energy efficient drying of extruded fish feed

4.1 Drying technologies for extruded fish feed

A 'dryer' may be defined as an apparatus that removes solvent from a solute. The drying apparatus is defined from its i) product handling technique, ii) energy supply, iii) drying media and iv) physical conditions. Combinations of these yield up to 400 different types of dryers [32], although only a fraction of these is practically feasible.

The continuous drying of porous, particulate solids severely limits the product handling techniques. Typically, these are belts, decks and fluidized or agitating beds. The energy supply can be direct or indirect. Direct heating typically involves heating the drying media and heat is transferred to the products by convection. Indirect heat supply comprise radiation and conduction. Conduction dryers employ energy to the solids from contact with tubes, jackets or coils, typically carrying steam. Whilst this process can be more energy efficient, these dryers are more appropriate for slurries, or very wet solids, that will endure mechanical agitation, to avoid heat damage to the product. In addition, commercial available conduction dryers have inferior heat transfer area/dryer volume ratios, when compared to convection dryers, to support large production volumes that ensure economies of scale in the production of extruded fish feed [32, 33].

Drying of animal feed pellets are traditionally carried out using air as the drying medium [27], yet in the early 90's some fish feed producers have experimented with using oil as drying medium [34]. In the latest decade, much attention has been on using superheated steam as the drying medium, due to the associated high energy efficiency [33], but the technology is not yet practically feasible for feed products [35]. This is predominantly due to the need for a viable mechanical vapor re-compression technology, particularly for application in vacuum to protect the product from heat damage. Superheated steam drying is considered an industrial game-changer in many industries, but finds much resistance in the market [36]. Superheated steam drying of extruded animal feed pellets has been carried out in the pet food industry, on a pilot scale [35]. To the knowledge of the author, no full-scale superheated steam dryer for extruded animal feed pellets exists. Superheated steam as drying media, even if promising, prerequisites further industrial maturation that falls outside the scope of the present project; the potential of this technology in the feed production industry is indeed acknowledged. To reflect opportunities in the drying process, immediately available by the industry, only hot air will be considered as drying media in the present project.

The convective hot air drying of extruded fish feed is conventionally carried out in fluidized bed dryers, vertical deck dryers or in horizontal conveyor dryers. Fluidized bed dryers are most often applied for smaller pellets and granules. They are typically compact and have a sanitized design, but often they are not as efficient in energy, without employing external recirculation of drying air that requires immense air volumes to be moved. The remaining two candidates that govern the market in drying of extruded feed pellets, above ~ 3-4 mm pellets in diameter, is the vertical deck dryer, Figure 10, and the horizontal belt dryer, Figure 11.

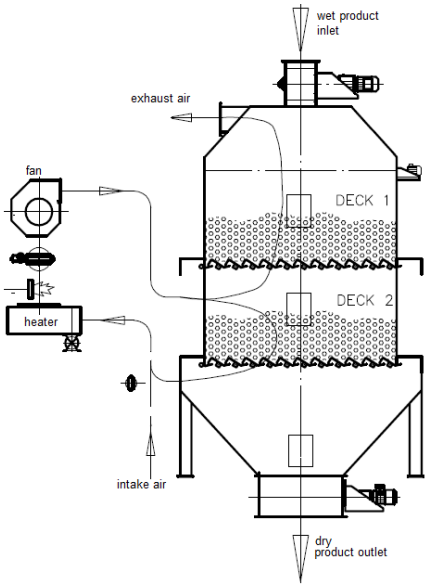

Figure 10: Vertical deck dryer with two decks. Recirculation of drying air is controlled by dampers [37].

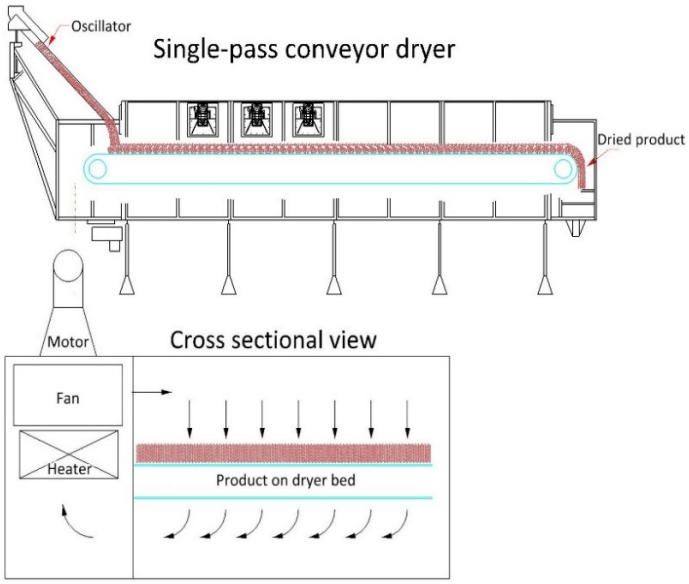

Figure 11: Horizontal conveyor dryer. A side-plenum for internal recirculation of drying air is shown in the cross sectional view [37].

The drying of extruded fish feed in above dryers usually have capacities of 5-15 tons/h. Typically the horizontal dryer have 1-4 belts and the vertical dryer 2-10 decks. Furthermore, the dryers are physically compartmented into several drying zones that have different temperature and/or humidity. Drying air is recirculated internally, inside the dryer cabinet. Retention time, bed depth, airflow, air temperature and air humidity vary across the bed – and in each zone. In addition, the temperature and moisture of the pellets vary across the bed and along the length of a belt (or in the vertical deck dryer, over time). Often, the perpendicular airflow direction is reversed, when moving from one zone to another. Clearly, for the challenge of optimizing energy efficiency in the drying process, a clear trajectory is needed from the chosen set of drying parameters, to the specific energy consumption per kg water evaporated. To achieve this, a mathematical model of the drying process of extruded fish feed is needed. Already in this aspect, an inherently simplifying approach is to develop a model that asses the drying in a single zone, only. Multiple models of a single zone can subsequently be compiled into a complete model of a dryer, with multiple zones and decks or belts. Whilst the two dryer types depicted above have different product transport techniques, retention times and position on the horizontal belt dryer should be easily interchanged. This means that the developed model can be equally well applied for all convective hot air dryers that have perpendicular airflow through a stationary deep bed of extruded fish feed.

4.2 Energy efficiency

The overall energy balance for the dryer is constituted from contributions from feed, air and non-adiabatic losses, cf. Eq. 1.

$$\mathcal{Q}_{\text{dryer, real}} = \mathcal{Q}_{\text{o,feed}} + \mathcal{Q}_{\text{o,air}} + \mathcal{Q}_{\text{loss}} - \mathcal{Q}_{\text{i,feed}} - \mathcal{Q}_{\text{i,air}} \qquad \text{Eq. 1}$$

$\mathcal{Q}_{\text{dryer, real}}$ represents the actual energy input to the dryer. From psychrometrics, the ideal drying process is the isenthalpic and adiabatic saturation of air with water [38]. The air saturates adiabatically with water, and is exhausted from the dryer at a lower temperature and a higher humidity. The differences in heat load of the air are therefore comprised from the increase in humidity of the drying air and a sensible contribution for heating the air. When also accounting for no heat transfer to the product or the surroundings, the ideal energy balance appear from Eq. 2. As it appears, if the air is exhausted at ambient temperature, the net heat load to the dryer becomes the latent heat of evaporating the water, at ambient temperature.

$$\mathcal{Q}_{\text{dryer, ideal}} = \Delta H_{\text{vap}} E \qquad \text{Eq. 2}$$

The energy efficiency, W, can now be defined as the ratio between the ideal and the actual heat load to the dryer, Eq. 3. The choice of reference temperature for the sensible heat load depends on terminology; here, the product inlet temperature is chosen.

$$W_{\%} = \frac{\mathcal{Q}_{\text{dryer, ideal}}}{\mathcal{Q}_{\text{dryer,real}}} = \frac{\Delta H_{\text{vap}}\big|_{\theta_i} E}{\Delta \mathcal{Q}_{\text{feed}} + \mathcal{Q}_{\text{loss}} + \Delta H_{\text{vap}}\big|_{\theta_i} E + \mathcal{Q}_{\text{air,heat}}} \cdot 100\,\% \qquad \text{Eq. 3}$$

It follows from Eq. 3 that energy efficiency are increased from a high evaporation rate, E, whilst using little sensible heating of air, $\mathcal{Q}_{\text{air,heat}}$, and product, $\Delta\mathcal{Q}_{\text{feed}}$, and obviously also minimizing other losses, $\mathcal{Q}_{\text{loss}}$. Obviously, some of these conditions immediately contradicts thermodynamic requisites for the drying to occur. Energy efficiency is often stated as energy required to evaporate 1 kg of water, e.g. 1.0 kWh/kg give an energy efficiency at $W_{\%}$=62.7 % (using $\Delta H_{\text{vap}} = 0.627$ kWh/kg)

A traditional approach to achieve high energy efficiency, is to ensure that the exhaust air have a high absolute humidity, i.e. so that the heated air have been 'utilized well' when exhausted. This a sound approach to achieve a high energy efficiency, but the methodology of how to obtain such conditions in the industry exists mostly as empirical knowhow in the minds of drying engineers and technologists. Often, it prescribes using a high degree of internal air recirculation and a relatively low amount of make-up air. Furthermore, founded in the appearance of characteristic drying curves, a declining temperature gradient is often used, to gain from high temperatures when the surface is wet and protected from heat damage, from evaporative cooling (constant drying rate), and to avoid subsequent heat damage of the product, when the drying is gradually limited by diffusion (falling drying rates). Essentially this has induced the use of multi-zone dryers in the industry. Establishing a model of the hot air deep-bed drying will allow direct optimization of energy efficiency (minimization of $\mathcal{Q}_{\text{dryer}}$), using a number of free drying parameters. As it will follow, the presented model only encompass a single drying zone (and belt), but the model can be expanded to multiple zones, to allow optimization of energy efficiency on industrial scale hot air fish feed dryers.

4.3 State of the art in particulate modeling of convective hot air drying processes

Several authors have made reviews on the classification of drying models [39-41]. Katekawa and Silva [40] have reviewed different strategies adopted for the development of drying models both considering, and more often, neglecting product shrinkage. Their review represents an appropriate starting point in outlining what is often named as a 'conceptual mathematical drying model', which is based on the early pioneer work by Lewis almost 100 years ago [42], and on models presented by Whitaker [43] and Luikov [44] in the 1970's. These rely on conservation balances for moisture and heat in the product, and consists of an unsteady term, a convection term, a diffusion term and a source term.

Katekawa and Silva [40] describe how each term in the balance equations can be altered using assumptions for the phenomenological description of temporal and spatial variations in composition and dimensional changes, e.g. evaporation and shrinkage. General model assumptions fall within:

- Number of components and phases: Binary mixtures (solid material and liquid water only), ternary mixtures (including water vapor) or quaternary mixtures (including air). This assumption relates to the amount of balances needed to solve the problem and if porosity is non-constant, from a non-linear shrinkage behavior.

- Material properties: Homogeneous or heterogeneous material formed from drying. Isotropic or anisotropic transport properties. This assumption will influence the complexity and phenomenological relations used to describe each term, e.g. invoking interface relations in the boundary conditions.

- Phase continuity: Phases can be assumed continuous or dispersed. Assumptions made here will influence the nature of the relations used in the diffusion terms, to describe the driving force for moisture- and energy transfer.

- Dimensionality and geometry: Often used geometries are spheres, cylinders or slabs. The latter two can be solved in two- or three dimensions or in one dimension considering infinite cylinders or slabs. Due to the symmetry of a sphere, they easily solve in three dimensions.

The general case of the conservation equation for moisture comprise a transient term, a convective term, a diffusive term and a source term – it appears below [40]:

$$\rho_s \frac{\partial X_d}{\partial t} + \rho_s \nabla \boldsymbol{v}_s X_d = \nabla \cdot \boldsymbol{J}_m + S_m \qquad \text{Eq. 4}$$

X_d is moisture content on dry matter basis (kg H_2O/kg dry matter), t is time, $\boldsymbol{v}_s$ is a convective velocity component for the solid, ρ_s is the solid density, $\boldsymbol{J}_m$ is the mass flux given by Eq. 5 – Eq. 7 and S_m is the mass source term. The mass source term will in drying processes often relate to the rate of evaporation and will for instance be used for ternary multiphase systems with liquid and vapor balances. Katekawa and Silva stress that the convective term in Eq. 4

should be included, so that shrinkage is included as a non-empirical relation using the actual non-constant solid phase velocity. This must however be measured or calculated from a stress/strain relationship. As opposed to this recommended methodology of including shrinkage, they report that shrinkage is often included as a direct function of water removal by formulating an empirical relationship between water removal and one or more material dimensions. The mass flux can be described using a Fick's law relationship, Eq. 5 (kg m^{-2} s^{-1}). Here D is the diffusion coefficient, which is dependent on product temperature, -moisture content and shrinkage (porosity, β) – and therefore also of position in the pellet [32]. Alternative approaches for dispersed multiphase systems are to apply some form of Darcy's law for the description of moisture flux, as in Eq. 6, or even to use a chemical potential gradient to drive the moisture flux, rather than using moisture content gradients, Eq. 7. Liquid capillary flow, surface diffusion, Knudsen diffusion, Poiseuille flow are some of the other transport mechanisms, aside from liquid and vapor diffusion, that is believed to govern mass transfer in the drying of porous solids [39]. This greatly adds to the complexity of achieving an exact solution. It is therefore common praxis to lump all these effects into an effective diffusion type coefficient, to be used in the selected mass flux expression. In Eq. 6, Γ is the permeability, μ is the viscosity and ∇P_l is a liquid pressure gradient. In Eq. 7 Φ_i is the chemical potential gradient at position i, and K is an effective diffusion type coefficient.

$$\boldsymbol{J}_{\mathrm{m}} = \rho_{\mathrm{s}} D \cdot \nabla X \qquad \text{Eq. 5}$$

$$\boldsymbol{J}_{\mathrm{m}} = \rho_{\mathrm{s}} \frac{\Gamma}{\mu} \cdot \nabla P_{\mathrm{l}} \qquad \text{Eq. 6}$$

$$\boldsymbol{J}_{\mathrm{m}} = \rho_{\mathrm{s}} K \cdot \nabla \Phi_i \qquad \text{Eq. 7}$$

Wang et al. [45] have presented a quaternary modelling approach of fixed-bed drying processes using a combination of Fick's law and Darcy's law for the description of mass transfer from liquid capillary flow, gas flow and vapor diffusion. Here, Darcy's law is used for the description of liquid capillary flow. Yiotis et al. [46] have suggested that this is the main transport mechanism for mass transport in most porous food materials. Obviously, such approaches rely on a vast amount of available data (or assumptions) for product characteristics, e.g. permeability, pore vapor density, capillary pressures, etc.

The general conservation equation for energy during the drying process is [40]:

$$\rho_l \cdot Cp_l \frac{\partial \theta}{\partial t} + \boldsymbol{v_l} \cdot \nabla(\theta \cdot Cp_l \cdot \rho_l) = \nabla \cdot \boldsymbol{J_q} + S_q \qquad \text{Eq. 8}$$

In Eq. 8 Cp_l is the specific heat capacity of water, ρ_l is the density of water, θ is the product temperature, $\boldsymbol{v_l}$ is a convective velocity component and S_q is the energy source term, which often holds the evaporative energy load. The convective heat transport is very often omitted, as this will be much less significant than the conductive heat transfer will. The conductive energy flux, $\boldsymbol{J_q}$, can be described using Fourier's law, Eq. 9, where k is the thermal diffusivity.

$$J_q = k \cdot \nabla \theta \qquad \text{Eq. 9}$$

Boundary conditions at the pellet surface are used to describe mass- and heat transfer to/from the drying media using external transfer coefficients. Hence, different drying models are often distinguished by their approach of evaluating thermal conductivity, moisture diffusivity and external mass and heat transfer coefficients at the boundary level [39, 40].
The coupled systems of partial differential equations are typically solved numerically, especially the cases where shrinkage is taken into account. In this case, it becomes a moving boundary problem, and the finite difference method could be applied by computing the boundary condition at each time step. Other than finite difference methods, finite element and finite volume methods are also used frequently in numerical modelling of drying processes.

Dryer models might also differ in appearance of conservation equations, approach to including shrinkage, temperature and moisture dependence of coefficients as well as a range of other assumptions that lead to inclusion or neglecting terms to describe the concurrent mass- and heat transport. Recent advances on models that describe moisture and heat distribution within a single pellet, both neglecting and including shrinkage, will be reviewed in the following section. Some models have a more industrial approach and treat moisture and heat distribution on process level, e.g. across a drying bed. These models will be subject to a review in section 4.4.

Hussain et al. [47] published in 2003 their work on two-dimensional heat and moisture transfer in cylindrical objects using a finite-difference approach. The intention with their work was to contribute with a solution methodology for the mathematical modelling of cylindrical porous objects subjected to drying and to compare the results experimentally for drying apples and broccoli. In their study, shrinkage was neglected and thermo-physical properties and drying air conditions were assumed constant. Under these assumptions, the model was represented by two-dimensional Fourier and Fick equations for the description of spatial heat and mass transport.

It is generally accepted that the diffusion coefficient possess a dependency on moisture content and on temperature [32]. Rossello et al. have also presented a non-isotropic mass transfer model for the drying of cylindrical green beans. However, isotropicity and spatial independency is often assumed for the diffusion coefficient, lumping all non-isotropic mass transfer effects into a single global transport constant; an 'effective diffusion coefficient [48]. In many occasions authors incorporate variations of the diffusion coefficient with product temperature, by adopting an Arrhenius type dependency [47, 49-56], Eq. 10.

$$D = D_0 \cdot \exp\left(\frac{-E_A}{R\theta}\right) \qquad \text{Eq. 10}$$

The pre-exponential moisture diffusivity, D_0, and the activation energy, E_A, are empirical coefficients characteristic for the moisture diffusivity in the particular feed pellet matrix at temperature, θ. R is the gas constant (8.314 J K^{-1} mol^{-1}). A series of experiments at different air temperatures can be used to find the temperature dependency, plotting ln(D) vs $1/\theta$. - E_A/R and D_0 are found from the slope and intercept, respectively [57]. Hussain et al.[47]

determined pre-exponential moisture diffusivity, D_0, and activation energy, E_A, for carrot slabs and used these in their model validation against drying data from other groups that have investigated drying of broccoli [58] and apples [55], respectively. The model by Hussain et al. mismatches with experimental data in the beginning of the drying period for broccoli, and at the end of the drying period for apples. Some of these deviations is explained from the fact that the temperature dependency on the diffusion is described from an empirical relationship for carrots. The questionable results substantiate the need for product specific moisture diffusivities in modelling the drying of porous moist objects. Only recently, Lambert et al. demonstrated a reverse methodology for identifying moisture diffusivities from deep-bed drying experiments, rather than applying the more typical strategy using thin layer drying experiments [56, 59].

Ljung et al. presented in 2011 [60] their work on convective drying of iron ore pellets. Their drying model only included the warm-up phase and the constant drying rate period. Moisture and temperature distribution are found using expression for diffusivities, i.e. equivalents of Eq. 4 and Eq. 8. The constant-rate drying rate and wet-bulb temperature is assessed thermodynamically by using that at equilibrium all energy transferred to the product is used for evaporation. The moisture flux from this expression is balanced with the moisture flux at the pellet-air interface, described from a mass transfer coefficient and a driving force. Using this approach, the wet-bulb temperature at the surface temperature was found. The methodology applied by Ljung et al. is a sound approach to describing the constant-rate drying period and thermodynamically evaluating the wet-bulb temperature.

4.3.1 Shrinkage

When porous biomaterials are dried, it is often seen that the water removal result in some degree of shrinkage, i.e. reduction of volume over the course of the drying process. The approaches of including this phenomenon into models of the drying process are quite different, as the shrinkage often will be non-linear with the water removal (from the degree of collapse at different moisture contents), and the degree of shrinkage in different materials are differ significantly.

Misra and Young included in 1980 for the first time shrinkage into their drying model of soybeans [53]. They assumed shrinkage in linear proportion with level of dehydration and a completely elastic solid phase. In 1995 Wang and Brennan [54] confirmed Misra and Young's shrinkage hypothesis. They formulated a mathematical model of simultaneous heat and moisture transfer during the drying of potato. They use simple Fick and Fourier descriptions of moisture and heat transport, coupled with conventional flow analogies, for evaluating external heat and mass transfer coefficients. Moisture-solid interactions for the description of moisture transport across the boundary layer are taken into account using sorption isotherms. Sorption isotherms relate moisture content in a product to its water activity. From the name, it appears that a particular sorption isotherm will be relevant for a single temperature, only. Hence, multiple sorption isotherms for a product, at different temperatures, are generally needed. Shrinkage is evaluated to be 5% at the end of the drying, and is assessed linearly

from start to end. A finite difference procedure is used to solve the coupled partial differential equations, PDE's, including and neglecting the 5% shrinkage. It is evident that the model that includes shrinkage has a better match with experimental data, for the drying of potato cubes. Queiroz and Nebra [61] investigated in 2000 the effect of shrinkage on the drying kinetics of bananas under different air conditions. They make use of a simple diffusion model, Eq. 4 + Eq. 5, and only assess mass transport. Their approach to considering shrinkage is empirical, fitting radius and moisture content by linear regression, to a set of correlation coefficients, Eq. 11.

$$\frac{R}{R_0} = a + b \cdot X + c \cdot \left(X_0 - X_{eq} \right) \cdot \left(\frac{X - X_{eq}}{X_0 - X_{eq}} \right) \qquad \text{Eq. 11}$$

In Eq. 11, X_{eq} is the equilibrium moisture content, X_0 is the initial moisture content, R_0 is initial radius and R is actual radius. The authors determined constant mass transfer and diffusion coefficients, fitting the models to the experimental results by minimizing the sum of square error. It was found that a better fit of the experimental data could be obtained when the empirical shrinkage model was included into the model.

Jin et al. [62] presented their model of broccoli drying at the International Drying Symposium in 2012. They utilized a novel approach - the so-called 'free volume theory of diffusion' coupled with the Maxwell-Eucken theory for two-component food systems. Latter describes the effective diffusion as composed from a contribution from the diffusion of water in the continuous- (solid) and dispersed phases (air). The diffusivity of water in the polymer broccoli matrix is found using the free-volume theory, which involves a set of 'free volume parameters' for both liquid and solid constituents. The free volume parameters include, among many other empirical constants, the glass transition temperature and the specific volume. Whereas these parameters obviously can be obtained for pure water, obtaining a set of free-volume parameters for the solid phase obviously constitutes a challenge. Jin et al. use free-volume parameters for sucrose for the solid broccoli matrix.

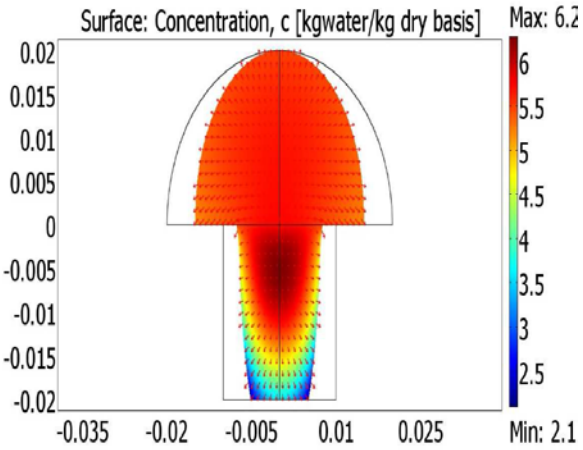

Figure 12: Moisture content and shrinkage of broccoli after 10 hours of drying at 50 °C [62].

A great advantage of this approach is that the effective diffusivity could be described non-empirically as a function of moisture content and temperature. Figure 12 describes spatial moisture distribution within the material after 10 hours of drying at 50 °C, including also the shrinkage. Fundamentally, shrinkage will induce a continuously moving mesh and boundary conditions (for numerical evaluation), which constitutes a major challenge on the introduction of shrinkage into drying models. Jin et al. therefore make use of a commercial PDE solver package, for solving this problem in two dimensions with the effective diffusion coefficient arising from Maxwell-Eucken- and free-volume theories.

The work published by Jin et al. is unique since it does not rely on an empirically based diffusion coefficient, but rather calculates an effective diffusivity from physical relations and an assumed composition of the dried specimen. The effective diffusivity is limiting the drying rate when the diffusion is slower than evaporation from the surface, i.e. for low moisture contents. It is interesting to observe in Figure 12, that after 10 hours of drying, a 'falling-rate phase' has started for the stalk, whereas the diffusivity is still high enough in the porous floret to support a constant rate phase (uniform spatial moisture distribution). Unfortunately, the authors have not benchmarked their results against experiments, which in best case make their suggested model a promising hypothesis. In addition, free volume parameters are needed for the solid matrix that constitutes the drying specimen; at present, such has not been identified for extruded fish feed, and those of sucrose can certainly not be used. Like Queiroz and Nebra [61], Jin et al. assess shrinkage in the radial direction using a linear and purely empirical relation – originally developed by Simal et al. with good results [58], Figure 13.

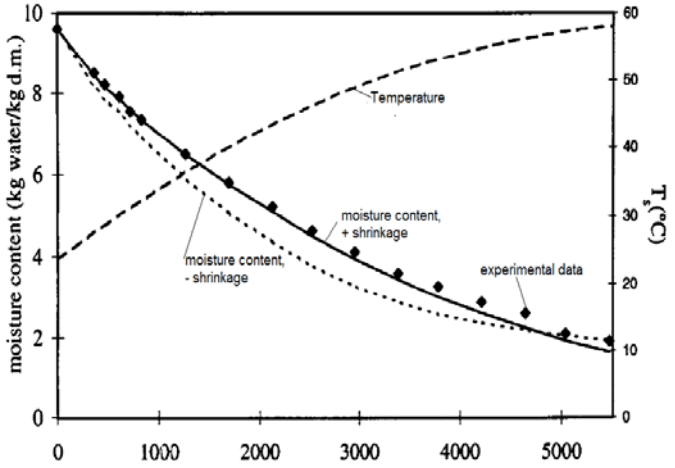

Figure 13: Shrinkage model benchmarked against experimental data for broccoli drying by Simal et al. [58]

Mayor et al. [41] made in 2004 a review on the different approaches to including shrinkage as well as a description of the physical shrinkage mechanism. Generally, the factors that influence shrinkage is, other than the amount of removed water, the mobility of the solid matrix and factors that influence the drying rate. Mayor et al. recommends the fundamental shrinkage model given by Eq. 12, which nevertheless requires information on the evolution of porosity.

$$\frac{V}{V_0} = \frac{1}{(1-\beta)}\left[1 + \frac{\rho_0 (X - X_0)}{\rho_l (1 + X_0)} - \beta_0\right] \qquad \text{Eq. 12}$$

In Eq. 12 V is volume, ρ_l is liquid density and β is porosity. ρ_0 , V_0 and β_0 are initial density, volume and porosity, respectively. Mayor et al. also finds that only 12 of 54 drying models included in their review, included shrinkage on a fundamental type, e.g. by including porosity, constituent concentrations and/or information on initial and equilibrium moisture densities, as in Eq. 12.

Hence, for almost 4 out of 5 drying models presented in literature shrinkage is included as either (non-)linear empirical relations with material- and geometry specific shrinkage coefficients, i.e. the types given by Eq. 11 [48, 52, 58, 61-65], or by invoking an ideal shrinkage hypothesis with volume reductions corresponding to the evaporated water, assuming a completely elastic solid phase [66, 67].

Importantly, both of above approaches include shrinkage based on either assumptions or information that is not readily available. This imply, that when shrinkage is disregarded, it will effectively lump the effect from shrinkage into other coefficients in the drying model, e.g. the diffusion coefficient. It can be argued that neglecting shrinkage can be justified given that the alternative is based on guesses, estimates, or additional fitting parameters.

4.3.2 Analytical approaches

Welty et al. [68] and Rosselló et al. [51] has given the analytical solution for Eq. 4 and Eq. 5 for an infinite slab and an infinite cylinder. Several assumptions must be made on applying

the analytical solution for water transport in two dimensions considering Fick's law as unsteady-state mass balance. Shrinkage and convective mass transfer at the pellet surface is omitted, i.e. the surface of the solid is in equilibrium with the air for the time considered. In addition, the effective diffusivity is constant and found from fitting the analytical solution to experimental data, by minimizing the sum of square error, from regression analysis, as for the numerical approaches.

Sahin et al. [69] describes how the analytical solutions can be applied for multidimensional objects by invoking a geometric shape factor. The shape factor works as a correctional expression, relative to the drying time for an infinite slab. The geometric shape factor for a finite cylinder (a fish feed pellet) is also given. The authors obtain drying times at an accuracy of ± 10% of experimental drying times. For each material and set of experimental data, they must still find geometry specific diffusion- and transfer coefficients, using regression analysis.

4.3.3 Equilibrium and transport data

Very few experimental data exist in the literature on the drying of extruded fish feed. In fact a study made in 2011 by Pacheco et al. [19] is the only one that could be found in literature by the author. They carried out series of thin layer drying experiments with spherical shaped pellets at diameters of 6-8 mm, aiming to model the drying process using semi-empirical expressions. They also determine moisture adsorption isotherms for the extruded fish feed at temperatures from 30 °C – 70 °C. *Ad*sorption isotherms imply that moisture are added (adsorbed) to the product in the measurements. This equilibrium data were obtained by maintaining constant air temperature in a sealed chamber containing saturated salt solutions (to have constant humidity) and initially dry, extruded fish feed pellets. At constant pellet mass, the equilibrium moisture content of the material is achieved for the particular temperature and humidity (~water activity). The kinetic and equilibrium data obtained by Pacheco et al. are visualized in Figure 14 and Figure 15, respectively.

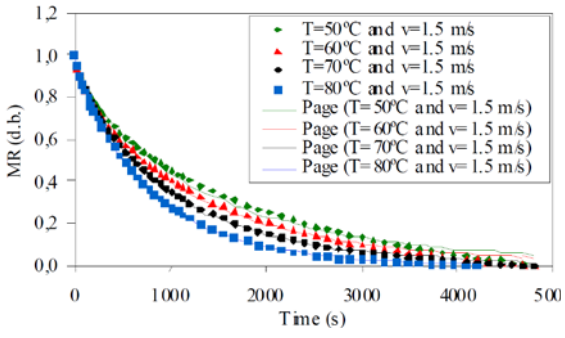

Figure 14: Thin layer dryings of ~7 mm spherical extruded fish feed pellets at temperatures from 50 – 80 °C. The data are fitted to semi empirical expression from Page [32]. Y-axis are normalized dry basis moisture content [kg/kg dry matter] [19].

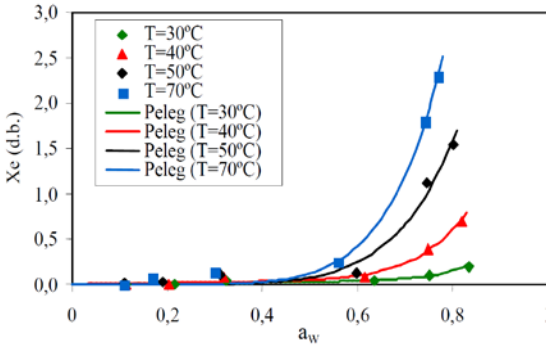

Figure 15: Experimental adsorption isotherms of extruded fish feed at 30 °C – 70 °C. The data are fitted to semi-empirical expressions by Peleg [70]. Y-axis are normalized dry basis moisture content [kg/kg dry matter] [19].

Yu et al.[50] presented in 2008 a gravimetric method for determining moisture diffusion coefficients using an 'automated water sorption instrument'. They made use of an analytical

solution of Fick's second law for one-dimensional moisture diffusion in a thin slab, minimizing the sum of square error against experimental data, to obtain the diffusion coefficient. The temperature dependency of the diffusion coefficient were successfully determined using an Arrhenius type dependency, cf. Eq. 10. The activation energy of the diffusion coefficient could be determined by a plot of ln(D) vs reciprocal product temperature. This illustrates the importance of including the temperature dependency of the diffusion coefficient into the modelling of drying processes.

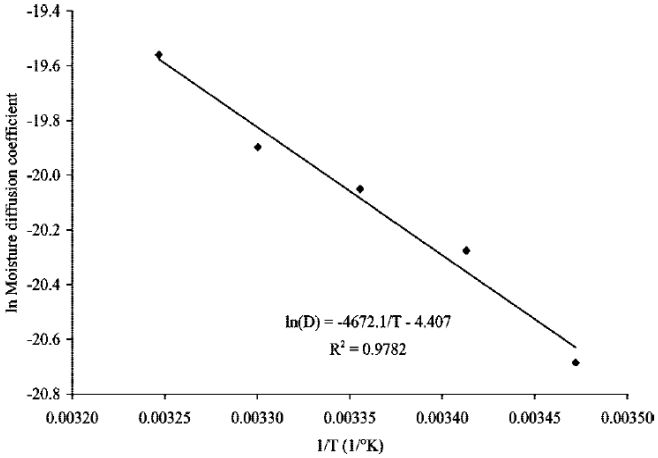

Figure 16: Influence of temperature on moisture diffusion coefficient as measured by Yu et al.[50]

It can be found from Figure 16 that the diffusion coefficient for cornstarch increases by a factor 3 when going from 15 °C to 35 °C. The authors make use of very refined equipment that precisely measures gravimetric changes during the desorption process, whilst controlling relative humidity and temperature very accurately. However, if humidity and temperature can be reasonably controlled, this methodology could easily be transferred onto a larger scale process (e.g. several kg of material). Obviously, this methodology will infer a bulk diffusion coefficient for all of the dryer bed, i.e. 'a porous slab' rather than a coefficient describing the diffusive desorption behavior in a cylindrical pellet. Hence, an application of such method to the drying of extruded fish feed pellets will effectively be a fit of the experimental data, 'lumping' all effects and inaccuracies into the diffusion coefficient parameter. This is not necessarily a bad option for the description of a specific drying process, yet the flexibility towards changing drying and product conditions is obviously compromised. By extending this method by Yu et al. to larger scale processes, it effectively becomes the methodology used in the majority of publications, which have drying models that build on an empirically derived effective diffusive coefficient. Chirife [71] made early work on listing effective moisture diffusivities as well as activation energies for the Arrhenius dependency on temperature, for a range of products with different moisture contents and temperatures.

The source terms in Eq. 4 and Eq. 8 will often be zero, but can be included if radiation-, water spray- or other effects are present in the drying process. The description of external heat and mass transfer at the boundary layer can be described from an external transfer coefficient and a driving force. The driving force arise from pellet-air interface conditions (e.g.

temperature gradient, vapor pressure gradient, etc.), and the transfer coefficients are found empirically or from external flow correlations.

Whitaker et al. have provided a correlation for the heat transfer coefficient for air flowing normal to a single circular cylinder[72], Eq. 13.

$$\mathrm{Nu} = \left(0.4 \cdot \mathrm{Re}^{1/2} + 0.06 \cdot \mathrm{Re}^{2/3}\right) \cdot \mathrm{Pr}^{0.4} \frac{\mu_a}{\mu_0} = \frac{h \cdot L_c}{k_{air}}$$

$$\mathrm{Re} = \frac{\rho_a v_{i,a} L_c}{\mu_a} \qquad \mathrm{Pr} = \frac{c_{p,a} \mu_a}{k_a} \qquad \text{Eq. 13}$$

L_c is the characteristic length, $v_{i,a}$ is the interstitial velocity. ρ_a , k_a, $c_{p,a}$, μ_a and μ_0 are the density, thermal conductivity, specific heat capacity and dynamic viscosity of the air. μ_0 is the dynamic viscosity of the air at the interface condition.

In non-free flow applications it is expected that coefficients obtained, when using the correlation from Whitaker, will over-predict the *average* pellet heat and mass transfer, when using an interstitial windside Nusselt number in the correlation [73]. For instance, Kaya et al. have used CFD to investigate the spatial distribution of heat and mass transfer coefficients in the numerical modelling of drying of cylindrical moist objects [74]. They found that the heat and mass transfer coefficients each vary approximately a factor ten from the front to backside of the moist cylinder, relative to the direction of airflow. Average transfer coefficients are sufficient for many applications; however, for a detailed analysis of uneven solid phase displacement and stress build-up, non-isotropic transfer rates should be important to evaluate. Local external transfer coefficients will vary with geometry, air temperature and air humidity but in particular to air velocity and direction of airflow The heat transfer coefficient for airflow perpendicular to a flat plate can be a factor of more than 50 times larger, relative to parallel airflow over a flat plate. For this reason, average transfer coefficient are more often used [32]. Simal et al. have reported a heat transfer coefficient at 51 W m^{-2} K^{-1} for the monolayer drying of moist 7 mm cylindrical bodies using perpendicular airflow at 2.7 m s^{-1} [58]. Sakai and Hayakawa used 17.4 W m^{-2} K^{-1} in modeling the drying of cylindrical shaped composite food [75] and Lambert et al. used 20 W m^{-2} K^{-1} in their model for deep-bed drying of feed pellets [56]. Mujumdar also give heat transfer coefficients for parallel airflow over a flat plate from Eq. 14 [32].

$$h = 20.4\, G^{0.8} \qquad \text{Eq. 14}$$

As it appears, Eq. 14 correlates very well with obtained coefficients by Simal [58], Sakai and Hayakawa [75] and Lambert [56, 59], indicating that parallel air flow govern the mode of convective heat and mass transfer in the drying of particulate solids.

The external mass transfer coefficient, h_m, can be estimated when knowledge of the external heat transfer coefficient, h, is established or vice versa. This connection arise from the similarities of heat and mass transfer and can be described from the Chilton-Colburn analogy, which is widely used in the modeling of hot air drying processes, e.g. to obtain knowledge of the mass transfer coefficient [56, 60, 73, 76]. The Chilton-Colburn analogy is highly relevant

for single particles in free flow, where heat and mass transfer arises from particle-fluid convection alone. For neighboring pellets, radiation to and from the evaporating surface cannot be neglected [77]. Additionally, external mass transfer is hindered at surfaces not available by flowing air, e.g. at pellet-pellet contact points, stagnant air enclosures, etc. In opposition, heat transfer is supported by conduction and radiation in these points. For these reasons, it is expected that the heat transfer coefficient is significantly larger, relative to the mass transfer coefficient, than what can be expected from the Chilton-Colburn analogy, and an empirical derived correction factor, ξ, is introduced into Eq. 15. Aachenbach have demonstrated that this effect is particular strong for low Reynolds numbers, and found that the effect of heat conduction via points of contact elevated the Nusselt number by 3-5 times at Re<250, relative to the expected value [78]. These observations and challenges is also highlighted by Larachi et al. [79], Adeyanju and Manohar [77] and Sander et al. [80], and should be taken into account when numerically evaluating the effective interrelation between external heat and mass transfer coefficients.

$$\frac{\overline{h}}{\overline{h}_m} = \xi \rho_a Cp_a \mathrm{Le}^{(2/3)} \qquad \text{Eq. 15}$$

Le is the Lewis number and ξ is the correction factor introduced to allow use in non free-flow applications. Hence, for particles in free-flow, this becomes one to give the Chilton-Colburn analogy.

The transfer coefficients can also be estimated empirically, which is useful to assess the applicability of the correlations used, e.g. Eq. 13, or to make use of the obtained transfer coefficients in the model, if the correlations found are not providing a satisfactory reproduction of the drying process. For empirical estimates of transfer coefficients in drying, the heat transfer coefficient is more easily found than the mass transfer coefficient [80]. This seems reasonable as surface temperatures are more easily measured over the course of a drying process than surface moisture content. Also, Barati and Esfahani reported that for drying processes with Biot numbers less than unity, surface and center temperatures are approximately equal [76]. This should indeed be true for small fish feed pellets subjected to convective hot air drying, and a lumped capacitance method can be used to find the heat transfer coefficient, if the surface temperature of the pellets is monitored during the drying. Effectively, this can be done by minimizing sum of square error for the solution for surface temperature in Eq. 8, against the experimental measured surface temperatures [81].

4.4 State of the art in modeling the convective deep-bed drying at process level

Particulate drying models that assess spatial temperature and moisture distribution over time necessitate that the properties of the drying air are well defined and constant with time. In reality, it is difficult to obtain constant drying air conditions all over the solid surface due to pellet-pellet and pellet-wall contact points, as well as wind- and leeside variations. When the solids are positioned in a monolayer (or a 'thin' layer), relative to the direction of airflow, it is common practice to consider the drying air conditions to be constant. Obviously, as monolayers are stacked, air conditions cannot be assumed constant, but changes when passing from one layer to the next.

Some research, particular within grain drying, have been engaged in formulating deep-bed models of the drying process. In these studies, the driving force for heat and mass transfer at the boundary layer will change owing to air conditions changing as it passes the bed of moist solids [82-88]. For deep-bed drying of small particles like grain, it is customary to address the solids drying at particulate level (e.g. 'grain') and include a single thin-layer drying expression as the solid mass conservation balance [89]. Hence, for many deep-bed drying models spatial details for the dried solids at different position in the bed are not addressed [89-96].

Mirzahoseinkashani and Kasiri [97] have provided a model that describes simultaneous energy and mass transfer between the material (grain) and the drying medium (air). This model encompass conservation balances for energy and mass for both material and air, but does not evaluate spatial temperature and moisture gradients in the product. Empirical expressions are used for grain porosity and specific surface area available for the drying air in the bed (bed porosity, ε).

Karim and Hawlader [67] have investigated the drying of tropical fruits in a tunnel dryer. They use a binary type conservation model to assess simultaneous moisture and heat transport in the solid material, and also include an experimental convective velocity component for the solid, i.e. a 'shrinkage velocity', which is considered to be proportional to the amount of water evaporated. They include an 'equipment model' to account for the changing conditions of the drying air, when travelling through the tunnel. This allows including a spatial moisture and temperature gradient through the dryer. Dependency of product moisture and temperature on the position in the tunnel is however not considered, which reduces the coupling between the 'material model' and the 'equipment model'. This is further simplified by applying a driving force expression for evaporation at the product surface, based on moisture contents (rather than by vapor pressure). In addition, bed porosity and thermal properties of air are assumed constant. From the simplifications made, their approach of coupling material and equipment models is useful in engineering applications and a relatively shorter computation time can expected, than if the coupling between air and product is stronger (particularly considering the variation of product conditions with position in the tunnel). Figure 17 shows the air temperature in the tunnel over time, for the drying of banana slabs.

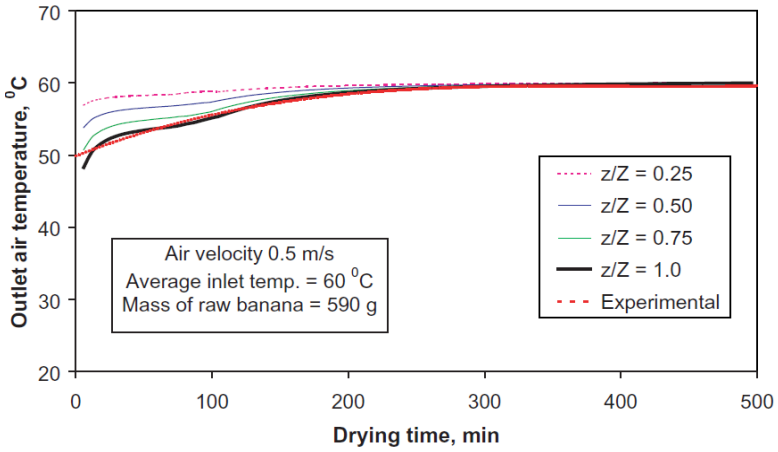

Figure 17: Predicted and experimental air temperatures over time. Z is drier length and z is distance from inlet[67].

Pang and Xu [98] presented a model for the deep-bed drying of woody biomass using a horizontal belt dryer. They assess moisture and temperature variations across the dryer bed as a function of position on the belt (i.e. time) for the air and for the woody biomass, which at particulate level are considered to have uniform temperature- and moisture profile. The direction of the airflow changes when the product has travelled half the distance of the dryer belt. They use mass and energy conservation balances for the drying air, whereas a semi-empirical relation is given for the drying rate, using different expressions for a constant-rate drying phase and two subsequent falling-rate phases.

Wang et al. made in 2012 an experimental study of deep-bed drying of extruded fish feed pellets in fixed beds [99]. They investigated the effect of moisture non-uniformity through the bed, resulting from effects of airflow rate and alternating airflow directions. Not surprisingly, they found that alternating airflow directions improved moisture uniformity through, which effectively is in support of present industrial practice, i.e. that airflow is alternated when the feed moves from one zone to the next.

Stákic and Tsotsas [100] simulated an atypical drying process using ambient air to dry (and cool) hot coal particles. The bed specific surface area is included in the semi-empirical expression for the drying rate, which also comprises a mass transfer coefficient and surface moisture content correlated from sorption isotherms. Shrinkage and variations in bed porosity is disregarded in this model, and as for the other models, spatial variations of temperature and moisture within the particulate coals are not assessed. The fact that the material act as heating source for the drying air makes the appearance and application of the model slightly different, but the approach should be similar to particulate deep-bed hot air drying models. Figure 18 illustrates moisture content whereas Figure 19 shows the temperature evolution for coal and air across the height of the bed, for various drying times.

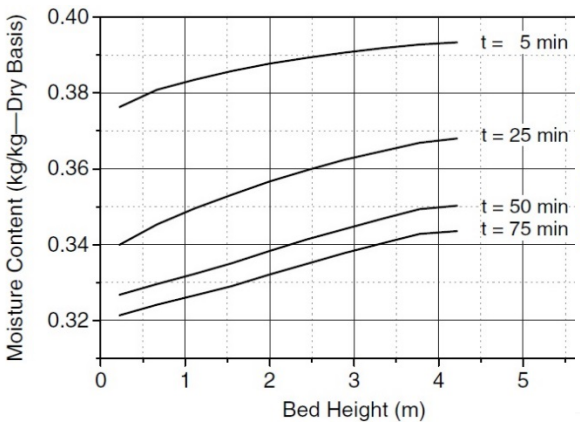

Figure 18: Moisture distribution across a dryer bed for different drying times [100].

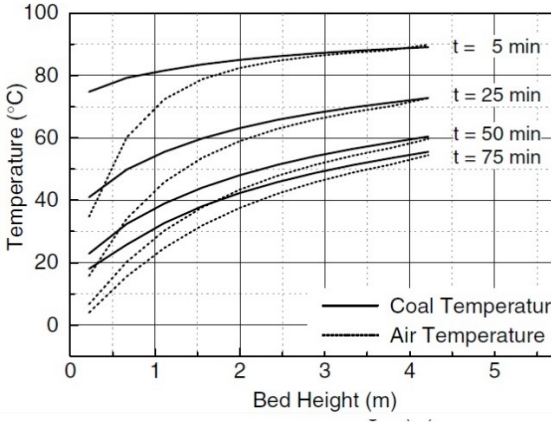

Figure 19: Temperature distribution across a dryer bed for different drying times [100].

Schmalko et al. [91] use a combination of analytical and numerical approaches in their model for the drying of a deep bed of twigs and leaves in a horizontal belt drier. Conservation balances are used for the humidity and temperature of the air as well as for the temperature of the product. The drying rate of the product is however described from an analytical solution to Fick's second law. Again, moisture and temperature gradients in the solids are ignored. Numerically, Schmalko et al. use the finite difference method, dividing the bed into nodes in horizontal (length/time) and vertical (height) directions, cf. Figure 20. Zare and Chen [92], Zare et al. [90] and Naghavi et al. [93] all use a similar approach for the deep-bed drying of paddy and rice, only using empirical thin-layer drying expressions to provide the drying rate.

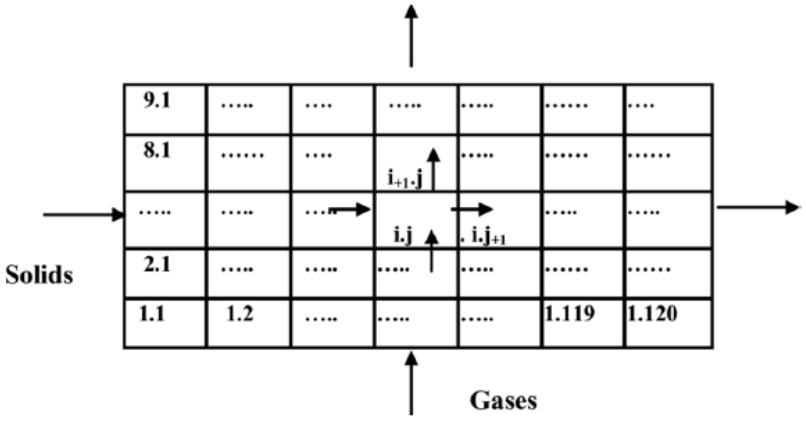

Figure 20: Division of the solid bed in a horizontal conveyor dryer into nodes by Schmalko et al [91].

Over the past few decades, little literature have been published, to the knowledge of the author, on model approaches that account for heat and mass transfer for the drying media when travelling through the bed while also assessing spatial details of temperature and moisture in particulate solids, at any position in the bed. Of course, this is numerically challenging, as introduction of spatial details in the solids induce at the least another dimension (for spherical solids). Furthermore, it is expected that the coupling with the drying air becomes particularly strong if surface heat and mass fluxes holds dependency of temperature and water content at the product surface as well as in adjacent drying air. Nevertheless, García-Perez et al. [101] and Lambert et al. [56] indeed demonstrated deep-bed convective hot air drying

models for grape stalks and animal feed pellets, respectively, which at the same time assesses spatial and temporal details of the drying air, as well as spatial moisture and temperature of the dried solids, across the depth of the dryer bed. García-Perez et al. use 10x9 nodes in their finite difference scheme, for the deep bed and for the product, respectively; time is the independent variable. The product is represented as three infinite cylinders and a sphere (~a grape stalk). The model by García-Perez et al., was programmed in FORTRAN and the resulting 740 non-linear simultaneous ordinary differential equations (ODEs) were solved using the Runge-Kutta algorithm in 0.6 hours on a 1.8 GHz laptop [101].

In the following section, a numerical drying model will be presented for the deep-bed drying of extruded fish feed. The model accounts for changing air conditions as it travels through a bed of moist feed pellets, over time. The temporal description in the drying model falls parallel to the horizontal position in a large-scale conveyor dryer. The presented model shall be able to predict also spatial temperature and moisture evolution over time, for single pellets at any position in the drying bed. While this approach is infrequently encountered in numerical deep-bed drying models, it is additionally taken into account in this model, that part of the drying air is recirculated internally, after passing the dryer bed. This makes the proposed deep-bed drying model new to its kind.

4.5 A numerical model of the deep-bed drying of extruded fish feed

A mathematical model for description of the deep-bed drying of cylindrical extruded fish feed pellets must account for changing air conditions, as it travels through the bed. Time is the independent variable and the temporal coordinate in the drying model falls parallel to the horizontal position in a single-belt conveyor dryer. The model shall be able to predict also spatial temperature and moisture evolution over time, for single pellets at different position in the drying bed. Additionally, it should be included that part of the drying air is recirculated internally, after passing the dryer bed. The modeling problem is illustrated in side- and tail views in Figure 21 and Figure 22, respectively.

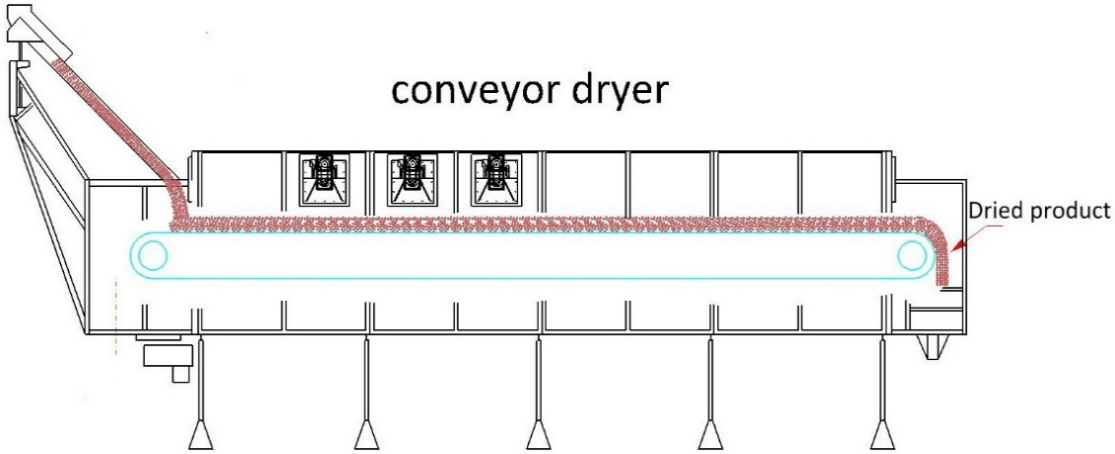

Figure 21: Side view of a single-pass horizontal conveyor dryer. Retention time, dryer size and product flow rate will determine the depth of the product layer, the 'bed depth'.

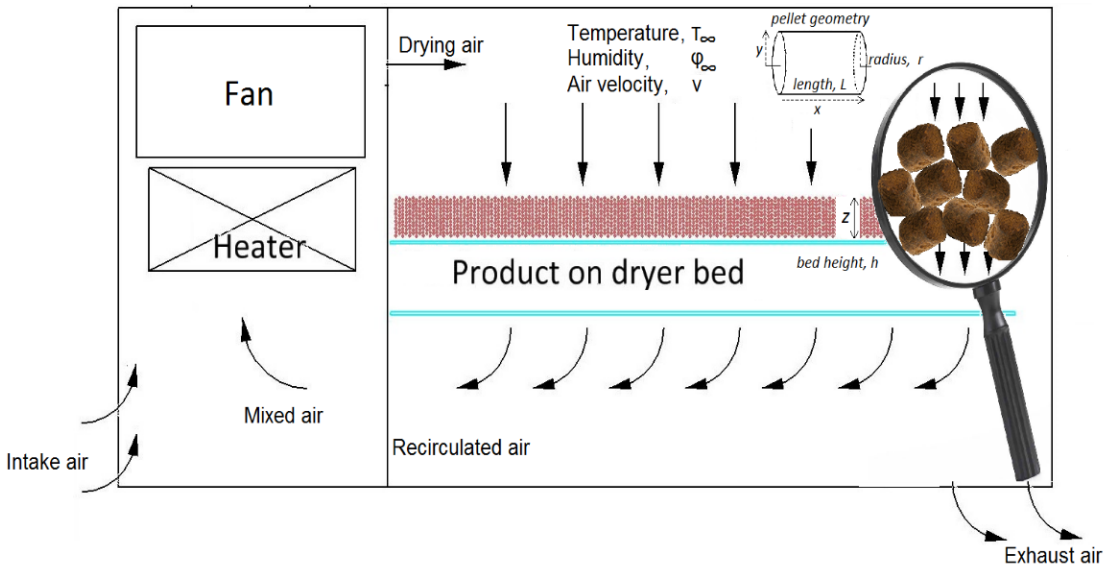

Figure 22: Tail view illustration of a single-pass horizontal conveyor dryer

The model should be comprised from three parts, describing:

- A transient model of heat and mass transfer in a single porous fish feed pellet, considering either cylindrical or assumed spherical geometry. The drying of a single pellet is subjected to constant interfacing air conditions at a given position in the bed (section 4.5.1).
- The changes in air conditions over time, and across the drying bed (section 4.5.2).
- An overall energy/mass balance of the dryer that accounts for the internal recirculation of drying air (section 4.5.3).

The model aim to be efficient in predicting overall energy efficiency for a particular drying process, whilst providing also spatial details of the products in use for the evaluation of technical quality in chapters 5 and 6. The possibility of using the model alongside production, for optimization, require the model to converge significantly faster than the actual retention time of a pellet in the drier (20-40 minutes). In the effort to make application of the model industrially attractive, a resolution time of maximum ~4 minutes is sought. For this, certain simplifying assumptions should certainly be considered. The simplifications considered are identified from that their inclusion otherwise would prerequisite information that is not readily available, using empirical estimates that does not contribute to accuracy – but certainly negatively affect convergence time.

The following simplifying assumptions are considered [93, 101, 102]:

- Pellet shrinkage will be neglected. Therefore, bed shrinkage is also neglected.
- Isotropic diffusion is the transport mechanism for heat and mass transfer in the pellets.
- Pellet-to-pellet conduction and radiation are not included.
- Evaporation and heat transfer occur only at the pellet surface.
- The dryer/bin walls are adiabatic, with negligible heat capacity.
- Airflow is plug-flow and does only have an axial velocity component.
- Vapor diffusion in the air is considered negligible compared to the convective mass transfer.
- As discussed in section 4.1, the model shall represent only a single drying zone, i.e. bed depth and inlet bed temperature, -humidity, -airflow and -airflow direction are constant.

The cylindrical geometry of the feed pellets are an important attribute in accurately describing heat and mass transfer within pellets and on their boundary. For identifying regional moisture and temperature extremes, the asymmetric character of a cylinder certainly holds important details, and ideally, cylindrical geometry should be included in the model. On the other hand, the product dimensionality of the problem could be reduced from 2D to 1D, which will be very significant when identifying the amount of non-linear coupled ODEs, following the discretization. For example, if García-Perez et al. [101] should choose to include (finite) cylindrical geometry in their model, which solved in 0.6 hours, the amount of non-linear simultaneous ODEs can be estimated to increase from 740 to $740^{3/2} \approx 20,000$. For this reason, the desire of including cylindrical geometry seems to be incompatible with a desire to achieve a relatively short resolution time. In the following section 4.5.4, it is desired to provide a

direct comparison of the solutions for the drying of a single cylinder and an equivalent sphere, applying different geometrical similarities (constant volume, -diameter, etc.), to evaluate if spherical geometry is a reasonable assumption and which geometrical similarities to choose. The model presented in the following sections will therefore include details for the resolution using cylindrical coordinates as well as for assuming spherical shaped pellets.

4.5.1 A transient model of heat and mass transfer in a single porous fish feed pellet

A numerical model using constitutive heat and mass transfer equations is adopted to model the drying of a single extruded fish feed pellet in hot air [73]. The model shall be able to predict spatial moisture and temperature evolution in the feed pellet over time, as influenced by surrounding air conditions. Both cylindrical and spherical geometry are considered. The finite difference method is used as the numerical resolution strategy. When simulating the drying of a feed pellet with finite cylindrical geometry, two dimensions must be considered, assuming radial symmetry. Only one dimension is necessary for considering spherical geometry.

The general case of the conservation equations for mass and energy were given by Eq. 4 and Eq. 8, respectively (pages 17-18). The convective velocity component for the solid, v_s, is zero, from neglecting shrinkage, and from the general assumption that diffusion is the primary transport mechanism in extruded feed pellets, which generally have a narrow pore network [103]. Evaporation occur on pellet surface, and this is accounted for in the boundary conditions. Source terms will be zero, as no external effects induce mass and heat transfer on the pellets. Supposedly, if the drying were assisted by e.g. radiation such effects could be included in source terms.

For cylindrical fish feed pellets the mass conservation balance, Eq. 4, is reduced to Eq. 16, considering that internal moisture flux is described from a Fickian relation, Eq. 5. The conservation equation for moisture in spherical feed pellets can be reduced to Eq. 17.

$$\rho_p \frac{\partial X_{r,w}}{\partial t} = \frac{1}{r}\frac{\partial}{\partial r}\left(\rho_p D r \frac{\partial X_{r,w}}{\partial r}\right) + \frac{\partial}{\partial w}\left(\rho_p D \frac{\partial X_{r,w}}{\partial w}\right) \qquad \text{Eq. 16}$$

$$\rho_p \frac{\partial X_r}{\partial t} = \frac{1}{r^2}\frac{\partial}{\partial r}\left(\rho_p D r^2 \frac{\partial X_r}{\partial r}\right) \qquad \text{Eq. 17}$$

In above, ρ_p is pellet density, X is moisture content (wet basis), t is time and r and w denote radial- and longitudinal coordinates, respectively. Moisture diffusivity, D, is assumed to be isotropic with spatial variation described from the temperature. This is normally estimated using an Arrhenius type dependency, cf. Eq. 10.

For cylindrical fish feed pellets the energy conservation balance, Eq. 8, is reduced to Eq. 18 by considering energy flux from Fourier's law, Eq. 9. The conservation equation for energy in spherical feed pellets can be reduced to Eq. 19.

$$\rho_p Cp_p \frac{\partial \theta_{r,w}}{\partial t} = \frac{1}{r}\frac{\partial}{\partial r} kr \frac{\partial \theta_{r,w}}{\partial r} + \frac{\partial}{\partial w} k \frac{\partial \theta_{r,w}}{\partial w} \quad \text{Eq. 18}$$

$$\rho_p Cp_p \frac{\partial \theta_r}{\partial t} = \frac{1}{r^2}\frac{\partial}{\partial r}\left(kr^2 \frac{\partial \theta_r}{\partial r} \right) \quad \text{Eq. 19}$$

In Eq. 18 and Eq. 19, the thermal conductivity, k, is assumed isotropic with a spatial dependency from Fourier's law, Eq. 9. Cp is the heat capacity and θ is the pellet temperature. The solution to Eq. 16 and Eq. 18 will provide temporal and spatial moisture and temperature distribution in a single, cylindrical feed pellet. For spherical geometry, solving Eq. 17 and Eq. 19 will apply.

Spatial boundary conditions, Eq. 20 – Eq. 24, apply for the resolution of the coupled PDEs, Eq. 16 and Eq. 18, at pellet surface and, from symmetry, at pellet center. At the symmetric center of the cylinder, longitudinal, w, and radial, r, distances are defined to be zero, $w = 0$ and $r = 0$. Surfaces of the cylinder therefore appear when the radial distance equals cylinder radius, $r = R$, and when longitudinal distance is half the length of the pellet, $w = L/2$. Boundary conditions are exemplified for cylindrical coordinates here[56, 73]. They appear equivalently for spherical coordinates.

$$\frac{\partial X_{0,w}}{\partial r} = \frac{\partial X_{r,0}}{\partial w} = \frac{\partial \theta_{0,w}}{\partial r} = \frac{\partial \theta_{r,0}}{\partial w} = 0 \quad \text{Eq. 20}$$

$$\frac{\partial X_{\mathrm{R},w}}{\partial r} = \frac{h_m}{D_{\mathrm{R,w}} \cdot \rho_{\mathrm{R,w}}} \cdot \frac{Mw_{H_2O}}{\mathrm{R}} \cdot \left(\frac{\omega_\infty \cdot p^*_{H_2O}\big|_{T_\infty}}{T_\infty} - \frac{aw_{N,j} \cdot p^*_{H_2O}\big|_{\theta_{\mathrm{R},w}}}{\theta_{\mathrm{R},w}} \right) \quad \text{Eq. 21}$$

$$= \frac{\varphi_r}{D_{\mathrm{R,w}} \cdot \rho_{\mathrm{R,w}}}$$

$$\frac{\partial X_{r,\mathrm{L}/2}}{\partial r} = \frac{h_m}{D_{r,\mathrm{L}/2} \cdot \rho_{r,\mathrm{L}/2}} \cdot \frac{Mw_{H_2O}}{\mathrm{R}} \cdot \left(\frac{\omega_\infty \cdot p^*_{H_2O}\big|_{T_\infty}}{T_\infty} - \frac{aw_{r,\mathrm{L}/2} \cdot p^*_{H_2O}\big|_{\theta_{r,\mathrm{L}/2}}}{\theta_{r,\mathrm{L}/2}} \right) \quad \text{Eq. 22}$$

$$= \frac{\varphi_w}{D_{r,\mathrm{L}/2} \cdot \rho_{r,\mathrm{L}/2}}$$

$$k_{\mathrm{R},w} \frac{\partial \theta_{\mathrm{R},w}}{\partial r} = -h\left(\theta_{\mathrm{R},w} - T_\infty \right) + \phi_r \Delta H_{vap;\,\mathrm{R},w} \quad \text{Eq. 23}$$

$$k_{r,\mathrm{L}/2} \frac{\partial \theta_{r,\mathrm{L}/2}}{\partial r} = -h\left(\theta_{r,\mathrm{L}/2} - T_\infty \right) + \phi_w H_{vap;r,\mathrm{L}/2} \quad \text{Eq. 24}$$

T_∞ and ω_∞ are surrounding air temperature and relative humidity, $p^*_{H_2O}$ is the saturated vapor pressure, φ is the surface moisture flux, ΔH_{vap} is the latent heat of evaporation of water, Mw is molecular mass, R is the ideal gas constant and h and h_m are heat and mass transfer coefficients, respectively. The water activity, aw, depends on temperature and moisture content of the product. This is obtained from equilibrium data, or 'sorption isotherms', for the product.

Eq. 23 and Eq. 24 represent the concurrent counterbalancing contributions to product temperature: conductive heating and evaporative cooling. Temporal boundary conditions (*t=0*) for pellet temperature and moisture are known from upstream processing conditions, i.e. outlet conditions from the extruder and a contribution from the transport process to the drier inlet.

A finite difference formulation is used in the numerical resolution of Eq. 16, Eq. 18 and Eq. 20 to Eq. 24. Discretization of the cylindrical feed pellet is shown in Figure 23. The pellets are assumed to possess symmetry around the longitudinal axis, and the pellet can be mirrored at its center point. As mentioned, the drying of a single pellet is modeled using only its half length and half diameter. As it appears from Figure 23, radial nodes, *i*, and longitudinal nodes, *j*, are used to segregate the cylinder into small area elements, and heat and mass balances for each element are written using the central finite difference formulation. The level of discretization is N, so it follows that,

$$\Delta w \Delta r = \frac{L}{2N}\frac{R}{N} \qquad \text{Eq. 25}$$

where Δw and Δr represent node lengths in longitudinal and radial directions.

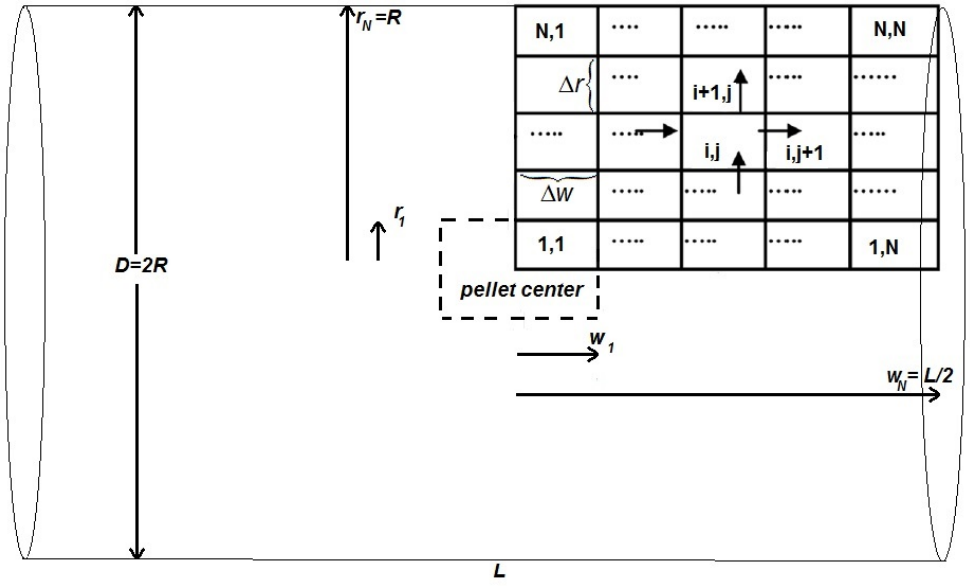

Figure 23: Discretization of cylindrical fish feed pellets

Eq. 26 and Eq. 27 describe the discretization procedure for the drying of a single cylindrical pellet using the central finite difference formulation, for any *i,j* position in the pellet.

$$\frac{\partial X_{i,j}}{\partial t} = \frac{1}{r_{i-½}} \cdot \frac{D_{i+½,j} \cdot r_i \cdot \dfrac{X_{i+1,j} - X_{i,j}}{\Delta r} - r_{i-1} \cdot D_{i-½,j} \cdot \dfrac{X_{i,j} - X_{i-1,j}}{\Delta r}}{\Delta r} + \frac{D_{i,j+½} \cdot \dfrac{X_{i,j+1} - X_{i,j}}{\Delta w} - D_{i,j-½} \cdot \dfrac{X_{i,j} - X_{i,j-1}}{\Delta w}}{\Delta w} \qquad \text{Eq. 26}$$

$$\frac{\partial T_{i,j}}{\partial t} = \frac{1}{Cp_{i,j}\rho_{i,j}r_{i-½}} \frac{k_{i+½,j}\cdot r_i \cdot \frac{T_{i+1,j}-T_{i,j}}{\Delta r} - r_{i-1}\cdot k_{i-½,j}\cdot \frac{T_{i,j}-T_{i-1,j}}{\Delta r}}{\Delta r} + \frac{1}{Cp_{i,j}\rho_{i,j}} \frac{k_{i,j+½}\frac{T_{i,j+1}-T_{i,j}}{\Delta w} - k_{i,j-½}\frac{T_{i,j}-T_{i,j-1}}{\Delta w}}{\Delta w} \quad \text{Eq. 27}$$

Boundary conditions stated in Eq. 20 – Eq. 24 are applied in the expressions for $\partial X_{i,j} / \partial t$ and $\partial \theta_{i,j} / \partial t$ at pellet center and surface coordinates, in Eq. 28 to Eq. 31 [47, 54, 93].

$$\left.\frac{\partial X}{\partial t}\right|_{1,1} = \frac{1}{r_{½}} \cdot \frac{D_{1+½,1}\cdot r_1 \cdot \frac{X_{2,1}-X_{1,1}}{\Delta r} - 0}{\Delta r} + \frac{D_{1,1+½}\cdot \frac{X_{1,2}-X_{1,1}}{\Delta w} - 0}{\Delta w} \quad \text{Eq. 28}$$

$$\left.\frac{\partial T}{\partial t}\right|_{1,1} = \frac{1}{\rho_{1,1}Cp_{1,1}r_{½}} \cdot \frac{r_1 \cdot k_{1+½,1}\frac{T_{2,1}-T_{1,1}}{\Delta r} - 0}{\Delta r} + \frac{1}{\rho_{1,1}Cp_{1,1}} \frac{k_{1,1+½}\frac{T_{1,2}-T_{1,1}}{\Delta w} - 0}{\Delta w} \quad \text{Eq. 29}$$

$$\left.\frac{\partial X}{\partial t}\right|_{N,N} = \frac{1}{r_{N-½}} \cdot \frac{r_N \cdot D_{N,N}\frac{\phi_r}{\rho_{N,N}\cdot D_{N,N}} - r_{N-1}\cdot D_{N-½,N}\cdot \frac{X_{N,N}-X_{N-1,N}}{\Delta r}}{\Delta r} + \frac{D_{N,N}\cdot \frac{\phi_w}{\rho_{N,N}\cdot D_{N,N}} - D_{N,N-½}\frac{X_{N,N}-X_{N,N-1}}{\Delta w}}{\Delta w} \quad \text{Eq. 30}$$

$$\left.\frac{\partial T}{\partial t}\right|_{N,N} = \frac{1}{\rho_{N,N}Cp_{N,N}r_{N-½}} \cdot \frac{r_N \cdot k_{N,N}\frac{-h\cdot\left(T_{N,N}-T_\infty\right)+\phi_r\cdot\Delta H_{vap;N,N}}{k_{N,N}} - r_{N-1}\cdot k_{N-½,N}\frac{T_{N,N}-T_{N-1,N}}{\Delta r}}{\Delta r} + \frac{1}{\rho_{N,N}Cp_{N,N}} \cdot \frac{k_{N,N}\frac{-h\cdot\left(T_{N,N}-T_\infty\right)+\phi_w\cdot\Delta H_{vap;N,N}}{k_{N,N}} - k_{N,N-½}\cdot\frac{T_{N,N}-T_{N,N-1}}{\Delta w}}{\Delta w} \quad \text{Eq. 31}$$

Boundary conditions for moisture and temperature at all remaining positions e.g. $\partial\theta/\partial t\big|_{N,1}$, $\partial\theta/\partial t\big|_{j,N}$, $\partial\theta/\partial t\big|_{i,1}$ etc. are computed from appropriate combination of respective terms within Eq. 28 to Eq. 31.

Discretization of pellets with assumed spherical geometry can be demonstrated using equivalent approach. From symmetry, discretization is for spheres only necessary along the radial coordinate.

At this stage, resolution of the pellet level model necessitate:

- Product/material properties; thermal conductivity, k, heat capacity, Cp, density, ϱ
- Heat and mass transfer coefficients, h and h_m.
- Moisture diffusivity in the pellets.
- Water activity as a function of surface moisture and temperature (sorption isotherms).

4.5.1.1 Material properties

Specific heat capacity and thermal conductivity of solid, dry fish feed is assessed based on the composition of a model food comprised from protein, carbohydrates, fat, fibers and ash. The relative contributions from each constituent to the particular physical property is given by Choi and Okos [104]. Material properties of porous, moist products are then balanced in accordance with volumetric compositions of air (from porosity, β) and actual moisture content, X (wet basis), during the drying process, cf. Eq. 32 and Eq. 33. It is assumed that the feed pellets have a constant porosity and that the dry matter/moisture content ratio does not cause the material properties to change. Of course, this assumption will not be valid for very large moisture contents, where water to a much larger extent can be expected to fill up the pores.

$$k_{feed}(X) = \beta \cdot k_{\text{air}} + (1-\beta)\cdot\left(k_{dry}\left(1-X\right) + k_{\text{H}_2\text{O}}\,X\right) \qquad \text{Eq. 32}$$

$$Cp_{feed}(X) = \beta \cdot Cp_{\text{air}} + (1-\beta)\cdot\left(Cp_{dry}\left(1-X\right) + Cp_{\text{H}_2\text{O}}\,X\right) \qquad \text{Eq. 33}$$

Porosity, $\beta = V_{void} / V_{tot} = 0.509 \pm 0.021$ is given by Draganovic et al. [105], for a commercial salmon grower feed diet, as measured from X-ray microtomography.

The density of the product is evaluated differently, in that a porous, dry feed pellet is used as basis for the dry material. Increasing moisture content will now inevitably elevate the density, from an increase in mass, rather than from changing dry matter/water ratio. Density of dry porous feed pellets are more easily measured than their thermal properties, which additionally improves the applicability for using different feed types. The expression used for pellet density appear from Eq. 34.

$$\rho_{\text{pellet}}(X) = \rho_{\text{dry feed}} + \rho_{\text{dry feed}}\frac{X}{1-X} \qquad \text{Eq. 34}$$

4.5.1.2 Heat and mass transfer coefficients

Heat and mass transfer coefficients can be related from similarities of heat and mass transfer, and can be described from the Chilton-Colburn analogy, Eq. 35 / Eq. 15. An empirical correction factor, c, is included to describe situations where mass transfer is hindered to a greater extent than heat transfer. This effect will arise in non free-flow applications, and at the least at pellet-support contact points as discussed in section 4.3.

$$\frac{h}{h_m} = \xi \rho_a Cp_a \mathrm{Le}^{(2/3)} \qquad \text{Eq. 35}$$

Correlations for cylinders in free-flow (e.g. Whitaker et al., Eq. 13) can be used to find a heat transfer coefficient, and from Eq. 35 a mass transfer coefficient can be obtained. Ideally, one should only integrate over the pellet area that is subjected to free-flow, when solving the non-steady state heat and mass balances. However, in actual applications it is more feasible to have the suitable net transfer coefficients reflect that the transfer area is below the total pellet exchange area, and that the pellet will have a variety of wind- and lee-sides. In reality, the pellet can also be expected to have a contact point with, at the least, its support. This means, that when using the correlation from Whitaker et al., the *average* pellet heat and mass transfer coefficients are easily over-predicted, when using an interstitial windside Nusselt number in the correlation [73].

The drying of a 'single particle' is often simulated using a 'thin layer' drying, yet only a few layers of pellets will have a rigorous contact point network, and will certainly not be a single particle in free flow. Even a ~monolayer of pellets all exposed to the same drying air will have contact to each other, to their support and, some of them, to the walls. This means, that a thin layer drying of a few pellet layers should be applicable for empirically assessing net transfer coefficients, whilst constant air conditions can reasonably be assumed through the thin layer. As surface temperatures are more easily measured over the course of a drying process than surface moisture content, the heat transfer coefficient is more easily found experimentally than the mass transfer coefficient [80]. For drying small particles (Biot number < 1), the lumped capacitance method can be used to find the heat transfer coefficient, if surface temperatures over time is measured [76]. This is effectively done by minimizing the sum of square error for the solution of surface temperature against the experimental measured surface temperatures. By doing so, one would have to exclude the empirical correction factor in Eq. 35, effectively making use of the Chilton-Colburn analogy for evaluating the mass transfer coefficient. However, if at the same time the average moisture content is measured, multi-parameter non-linear regression analysis can be used to find the correction factor in Eq. 35, by minimizing the total sum of square error between model and experimental values of surface temperature and average moisture content.

4.5.1.3 Moisture diffusivity

The moisture diffusion coefficient, *D*, effectively lumps all effects of internal mass transfer within the pellet into a single parameter. For this reason, a moisture diffusion coefficient is very rarely calculated or known a priori, and therefore it needs to be found empirically. This means, that this parameter need to be included as an additional parameter in a multi-parameter non-linear regression analysis. From the nature of diffusion as molecular motion, it could indeed be expected that there is a temperature dependency on several of the effects contributing to the net moisture diffusivity. This temperature dependency is often described from an Arrhenius relationship. Moisture content is reported to have only a minor effect, and the influence from porosity evolution should be more relevant for strongly shrinking products [106]. Eq. 10 / Eq. 36 describe the temperature dependency of the moisture diffusivity, used in present model.

$$D = D_0 \cdot \exp\left(\frac{-E_A}{R\theta}\right) \qquad \text{Eq. 36}$$

The temperature dependency of the moisture diffusivity can be found using a number of thin-layer drying experiments at different drying air temperatures. Graphical analysis of obtained moisture diffusivities, from non-linear regression analysis, and average product temperatures are classically used to identify D_0 and E_A in Eq. 36. As an alternative approach, temperature dependency of the moisture diffusivity could be found simultaneously with the heat and mass transfer coefficients, in a 4-parameter non-linear regression analysis. This approach will obviously be inherently time consuming, possibly requiring days or weeks to find the global minimum of the total sum of square error.

4.5.1.4 Sorption isotherms

Pacheco et al. have recorded four set of sorption isotherms for extruded fish feed at low drying temperatures from 30 °C to 70 °C [19]. At the most, this partially satisfies application in this model, since feed temperature could be much higher temperature than 70 °C. Considering the evaporative cooling effect, the ideal sorption isotherm interval should cover temperatures between 50 and 120 °C.

Sorption isotherms must be recorded for a particular 'reference' feed recipe at air temperatures in all of above interval. Temperature dependency for sorption isotherms in other feed recipes can be generated from a recorded sorption isotherm at a single air temperature, assuming that the temperature dependency recorded for the reference feed recipe can be reused. This means that only a single sorption isotherm at a reference temperature need to be found, for all other feed recipes, by shifting equilibrium moistures up/down, relative to the reference feed recipe at the reference temperature, cf. Eq. 37.

$$X_{\mathrm{Eq}}(aw)\big|_{\theta} = X_{\mathrm{Eq,\ ref.\ feed}}(aw)\big|_{\theta} \cdot \left(1 + \frac{X_{Eq}(aw)\big|_{\theta_{\mathrm{ref}}} - X_{\mathrm{Eq,\ ref.\ feed}}(aw)\big|_{\theta_{\mathrm{ref}}}}{X_{\mathrm{Eq}}(aw)\big|_{\theta_{\mathrm{ref}}}}\right) \qquad \text{Eq. 37}$$

Whilst this is a rough assumption, it allows a large catalogue of equilibrium data to be more easily acquired, when applying the model for different feed recipes.

When the sorption isotherms are recorded, the pellet level model can be computed, using $D = f\left(D_0, E_A\right)$ h and $h_m = f(\xi)$ as free parameters that need to be determined from correlations or empirical optimization algorithms, against experimental data. Flow dependency of the external transfer coefficient should also be included, $\mathrm{Nu}_{D_p} = f\left(\mathrm{Re}_{D_p}\right)$.

4.5.2 A transient model of heat and mass transfer at the air-pellet interface

The air will change conditions as it travels through the deep bed of layered pellets. A numerical model is needed for the description of air temperature, humidity and velocity over time, as influenced by velocity and interfacing feed conditions. The approach here will be constitutive mass and heat transfer equations for the air, which as well are resolved using the finite difference method. To take into account the changing feed interface conditions this model needs to be solved simultaneously with the 'pellet level model' [73].

The transient mass balances for air travelling through an area of the drying bed at a height ∂z of cylindrical and spherical pellets is given by Eq. 38 and Eq. 40, respectively [56, 59, 87, 93].

$$\frac{\partial\left(\rho_{a,k}Y_k\right)}{\partial t}=\frac{\partial\left(u_{a,k}\rho_{a,k}Y_k\right)}{\partial z}+\phi_{\mathrm{R},w,k}\cdot a_r\cdot\left(\frac{1-\varepsilon}{\varepsilon}\right)+\phi_{r,L/2,k}\cdot a_{ax}\cdot\left(\frac{1-\varepsilon}{\varepsilon}\right) \qquad \text{Eq. 38}$$

$$\frac{\partial\left(\rho_{a,k}Y_k\right)}{\partial t}=\frac{\partial\left(u_{a,k}\rho_{a,k}Y_k\right)}{\partial z}+\phi_k\cdot a\cdot\left(\frac{1-\varepsilon}{\varepsilon}\right) \qquad \text{Eq. 39}$$

As it appears, the mass balance is simply made up solely from evaporative and convective contributions. Y is the air absolute humidity, ε is the bed porosity and a is the specific surface area/volume ratio. For cylindrical geometry a_r is the radial area/volume ratio and a_{ax} is the axial area/volume ratio – these should add up to the total area/volume ratio. For cylindrical geometry, the surface position will be relevant for the surface moisture flux, φ, with contributions to the flux from radial, r, and axial, ax, surfaces. The expression for the surface flux at the 'corner' of the cylinder at position k is exemplified in Eq. 40. The surface flux using spherical coordinates is given in Eq. 41. $a\left(1-\varepsilon\right)/\varepsilon$ express the surface area of pellets per volume of air and subscript k denotes air node k. u_a is the interstitial air velocity, given by v_a / ε where v_a is the superficial bed velocity. The total pressure in Eq. 38/Eq. 39 need to be similar to the pressure valid for the recorded sorption isotherms. In practical terms, this means atmospheric pressure.

$$\varphi_{\mathrm{R},L/2,k}=\left.\frac{\partial X}{\partial t}\right|_{\mathrm{R},L/2,k}=h_m\cdot\frac{Mw_{H_2O}}{\mathrm{R}}\cdot\left(\frac{\omega_k\cdot p^*_{H_2O}\big|_{T_k}}{T_k}-\frac{aw_{\mathrm{R},L/2,k}\cdot p^*_{H_2O}\big|_{\theta_{\mathrm{R},L/2,k}}}{\theta_{\mathrm{R},L/2,k}}\right) \qquad \text{Eq. 40}$$

$$\varphi_k=\left.\frac{\partial X}{\partial t}\right|_k=h_m\cdot\frac{Mw_{H_2O}}{\mathrm{R}}\cdot\left(\frac{\omega_k\cdot p^*_{H_2O}\big|_{T_k}}{T_k}-\frac{aw_{\mathrm{R},k}\cdot p^*_{H_2O}\big|_{\theta_{\mathrm{R},k}}}{\theta_{\mathrm{R},k}}\right) \qquad \text{Eq. 41}$$

Evaporation is assumed to take place at the surface at temperature $\theta_{\mathrm{R},k}$. This means that the ratio for sensible heating of air/water will also change, as will the latent heat of evaporation.

In the energy balance for the air, Eq. 42 (cylindrical) and Eq. 43 (spherical), a reference temperature, T_0, with associated latent heat of evaporation, $\Delta H_{\text{vap}}^{0}$, is introduced to account for these changes during the drying process [93].

$$\frac{\partial\left(\rho_a\left(Cp_a+YCp_v\right)T_k\right)}{\partial t}=-\frac{\partial}{\partial z}\left(\rho_a\left(Cp_a+Y_kCp_v\right)T_k\,u_{a,k}\right)$$
$$+a_r\left(\frac{1-\varepsilon}{\varepsilon}\right)\left(\phi_{\mathrm{R},w,k}\left(\begin{array}{l}Cp_v\left(T_k-T^0\right)+\Delta H_{\text{vap,k}}-\\Cp_w\left(\theta_{\mathrm{R},w,k}-T^0\right)-\Delta H_{\text{vap}}^{0}\end{array}\right)+h\left(T-\theta_{\mathrm{R},w,k}\right)\right) \qquad \text{Eq. 42}$$
$$+a_w\left(\frac{1-\varepsilon}{\varepsilon}\right)\left(\phi_{r,\mathrm{L}/2,k}\left(\begin{array}{l}Cp_v\left(T_k-T^0\right)+\Delta H_{\text{vap,k}}-\\Cp_w\left(\theta_{r,\mathrm{L}/2,k}-T^0\right)-\Delta H_{\text{vap}}^{0}\end{array}\right)+h\left(T-\theta_{r,\mathrm{L}/2,k}\right)\right)$$

$$\frac{\partial\left(\rho_a\left(Cp_a+YCp_v\right)T_k\right)}{\partial t}=-\frac{\partial}{\partial z}\left(\rho_a\left(Cp_a+Y_kCp_v\right)T_k\,u_{a,k}\right)$$
$$+a\left(\frac{1-\varepsilon}{\varepsilon}\right)\left(\phi_k\left(\begin{array}{l}Cp_v\left(T_k-T^0\right)+\Delta H_{\text{vap,k}}-\\Cp_w\left(\theta_{\mathrm{R},k}-T^0\right)-\Delta H_{\text{vap}}^{0}\end{array}\right)+h\left(T-\theta_{\mathrm{R},k}\right)\right) \qquad \text{Eq. 43}$$

In Eq. 42 and Eq. 43, physical properties of air and vapor are given by '*a*' and '*v*' subscripts.

Boundary conditions for air heat and mass transfer are absolute humidity, Y_∞, and temperature, T_∞, of the drying air introduced at the top (or bottom, depending on the air flow direction) of the bed, cf. Eq. 44 and Eq. 45. Initial condition for air temperature is approximated by assuming it to equal the initial product temperature, Eq. 46. The initial condition for the humidity of the drying air is approximated given by equating the initial water activity of the product (from the sorption isotherms) with the relative humidity, ω, of the drying air, cf. Eq. 47.

$$Y_0=Y_\infty \qquad \text{Eq. 44}$$

$$T_0=T_\infty \qquad \text{Eq. 45}$$

$$T_{k,t=0}=\theta_{k,t=0} \qquad \text{Eq. 46}$$

$$Y_{k,t=0}=Y\left(T=\theta_{k,t=0},\omega=aw(\theta_{k,t=0},X_{avg,k,t=0}=X_{avg,k,t=0})\right) \qquad \text{Eq. 47}$$

The assumption that latent heat supplied for the evaporation of moisture solely arise from the product surface is likely a rough assumption. Some of the energy should be supplied from the air in immediate vicinity to the 'film' forming at the air-pellet interface. It is considered that the concurrent pellet-air conduction will quickly demonstrate the actual difference in air- and pellet surface temperatures, corresponding to their relative thermal heat conductivities with addition also of a convection term for the air.

4.5.3 A static model of heat and mass transfer in an industrial hot air dryer with internal air recirculation

Many industrial dryers internally recirculate part of the drying air back to the heater, after passage of the drying bed. This recirculation loop needs to be taken into account to obtain the actual drying air conditions before passage of the drying bed. A static 'process level model' will therefore need to be included, to provide the actual drying air conditions, which in turn will alter the product- and air conservation balances. As the introduction of the recirculation loop will use a reiterative approach, the computation time should be expected to increase by the number of iterations necessary until convergence within a given accuracy is achieved [73].

The static process level model alone is useful to benchmark the performance of a particular dryer, with or without use of internal recirculation of drying air. This is useful to identify opportunities for operating the dryer differently, typically aiming to lower the overall energy consumption. The transient pellet and air level models seek to solve the temporal and spatial moisture and temperature evolution of the feed pellets. An obvious characteristic of using the static process level model alone is the fact that drying kinetics is omitted, and temperature and moisture of the feed leaving the dryer are specified.

A number of energy- and mass balances comprise the description of the static process level model. Figure 24 re-illustrate the tail-end view of the dryer, additionally identifying and referencing relevant heat and mass conservation balances, Eq. 48 – Eq. 66. Note that for these equations absolute air humidity, Y, and air enthalpy, I, is chosen as representatives for knowledge of the air conditions. Obviously, for each reference condition in the dryer, any other two parameters in the dryer should suffice, e.g. temperature and relative humidity. The remaining air conditions can be found from psychrometric relations. In the balance equations for water in the air, Eq. 49, Eq. 55, Eq. 59 and Eq. 62, absolute humidity is calculated on a wet basis, rather than dry basis, e.g. $Y_i/(1+Y_i)$.

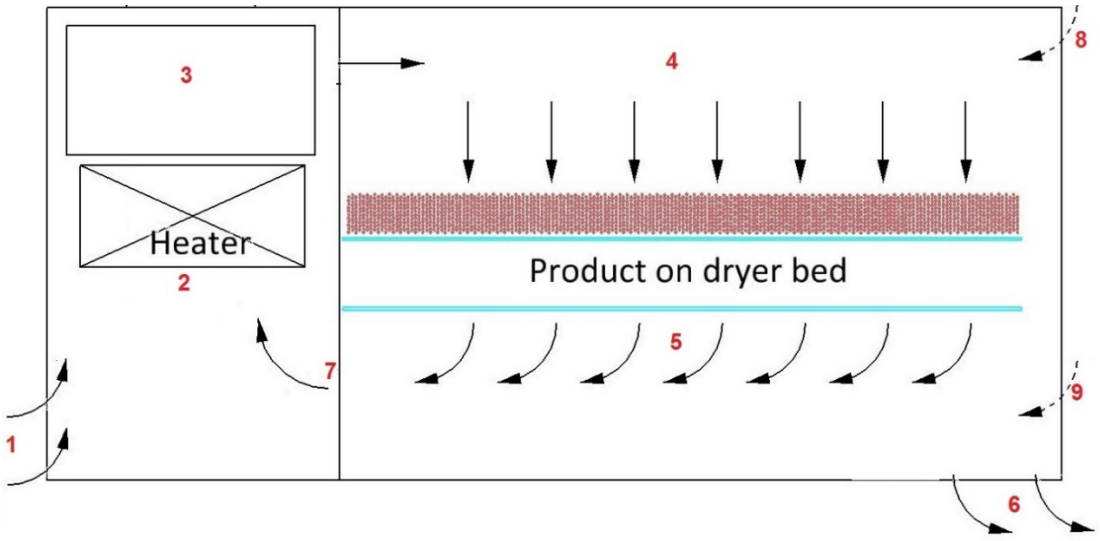

Figure 24: Tail-end view of a conveyor dryer. Designations of air conditions for use with mass- and energy balances are given with red numbers.

Recirculation

Mass: $M_2 = M_1 + M_7$ Eq. 48

Water: $M_2 \frac{Y_2}{1+Y_2} = M_1 \frac{Y_1}{1+Y_1} + M_7 \frac{Y_7}{1+Y_7}$ Eq. 49

Energy: $M_2 I_2 = M_1 I_1 + M_7 I_7$ Eq. 50

Heater

Mass: $M_2 = M_3$ Eq. 51

Water: $Y_2 = Y_3$ Eq. 52

Energy: $Q_{\text{burner}} = M_2 \cdot (I_3 - I_2)$ Eq. 53

False air, pre-bed

Mass: $M_4 = M_3 + M_8$ Eq. 54

Water: $M_4 \frac{Y_4}{1+Y_4} = M_3 \frac{Y_3}{1+Y_3} + M_8 \frac{Y_8}{1+Y_8}$ Eq. 55

Energy: $M_4 I_4 = M_3 I_3 + M_8 I_8$ Eq. 56

Dryer

Mass: $M_4 + \dot{m}_{\text{feed, in}} = M_5 + \dot{m}_{\text{feed, out}}$ Eq. 57

Feed: $\dot{m}_{\text{feed, in}} \cdot (1 - X_{\text{avg,in}}) = \dot{m}_{\text{feed, out}} \cdot (1 - X_{\text{avg,out}})$ Eq. 58

Water: $M_4 \frac{Y_4}{1+Y_4} + X_{\text{feed, in}} m_{\text{feed, in}} = M_5 \frac{Y_5}{1+Y_5} + m_{\text{feed, out}} X_{\text{feed, out}}$ Eq. 59

Energy: $Q_{\text{feed,in}} + M_4 I_4 = Q_{\text{feed,out}} + M_5 I_5 + Q_{\text{loss}}$ Eq. 60

Exhaust

Mass: $M_5 + M_9 = M_6 + M_7$ Eq. 61

Water: $M_5 \frac{Y_5}{1+Y_5} + M_9 \frac{Y_9}{1+Y_9} = M_6 \frac{Y_6}{1+Y_6} + M_7 \frac{Y_7}{1+Y_7}$ Eq. 62

Energy: $M_5 I_5 + M_9 I_9 = M_6 I_6 + M_7 I_7$ Eq. 63

Recirculation

Mass: $M_7 = \gamma M_6$ Eq. 64

Water: $Y_7 = Y_6$ Eq. 65

Energy: $I_7 = I_6$ Eq. 66

The 19 equations from Eq. 48 – Eq. 66 holds 36 variables, which means that 17 variables should be specified to solve the system. Each inlet condition account for three variables (absolute humidity, Y, specific energy content, I and mass flow rate, M). With knowledge of air conditions at positions 1, 8 and 9 in Figure 24, eight variables remain. The feed flowrate, $\dot{m}_{\text{feed, in}}$, feed energy flow (temperature), $\dot{Q}_{\text{feed, in}}$, and initial feed water content, $X_{\text{avg, in}}$, should be known. $\dot{Q}_{\text{loss}}$ is either known or set to zero, from the assumption of adiabatic dryer walls with negligible heat capacity. Temperature set-point of the dryer will specify either I_3 or $\dot{Q}_{\text{burner}}$ and damper position for recirculation, γ, can be specified either directly or by specifying I_6. The remaining two parameters are the temperature ($\dot{Q}_{\text{feed, out}}$) and moisture content of the feed leaving the dryer, $X_{\text{avg, out}}$. By coupling the static process level model to the transient pellet level model the temperature and moisture content of the feed leaving the dryer are evaluated (Eq. 16/Eq. 17 and Eq. 18/Eq. 19 in section 4.5.1 for cylindrical/spherical geometry). This will be applicable for a thin product layer. Introducing the model for heat- and mass transfer at the pellet-air boundary layer (the 'air' level model section 4.5.2), will account for the air changing conditions as it travels through a deep layer.

Exhaust air conditions (humidity and temperature) can be found from the overall mass and energy balances in the static process level model (Eq. 59 and Eq. 60). However, these could equally be found from temporal averages of the solution for Y_Z and T_Z (in Eq. 38/Eq. 39 and Eq. 42/Eq. 43, for cylindrical/spherical coordinates). In practice, it should be easier to use Y_5 from Eq. 59 to find air exhaust humidity. As it appears, the inclusion of the air level model (section 4.5.2) is reasoned from an accurate evaluation of the driving force in each control volume of a deep bed, rather than from a deficiency in the number of degrees of freedom.

Coupling the static process level model, with recirculation of drying air, onto the transient pellet- and air level models should elevate the computation time significantly. This can be expected since each iteration evaluating temperature and humidity of the recirculated drying air involves the full resolution of feed moisture and temperature out of the dryer. In many applications, it will often be sufficient to calculate dryer inlet air conditions (including recirculation) from estimates of moisture and temperature outputs, and then use these values to compute the actual product moisture and temperature outputs, from the transient coupled

pellet- and air level models. One or two iterations should be sufficient for many industrial applications, and in practice, it might often be sufficient to do the calculations using a few manual iterations, using a separate process-level model and a coupled pellet- and air level model.

4.5.4 Influence of feed geometry

In order to reduce computation time, it will be investigated how the drying of cylindrical shaped feed pellets differ from the solution using an assumed spherical geometry. It should also be considered which geometrical similarities for the sphere that will demonstrate the best possible match against the drying of a cylindrical pellet.

Pellet-level solutions are compared below in Figure 25, solving Eq. 16 + Eq. 18 for cylinders and Eq. 17 + Eq. 19 for spheres. Constant air temperature, -velocity and -humidity are used. Boundary conditions are given (in the case of cylinders) by Eq. 20 – Eq. 24, using the discretization procedure exemplified from Eq. 26 - Eq. 31. For the purpose of this comparison values of constant moisture diffusivity, D, and heat transfer coefficient, h, is used from an earlier study; D = 9.9 E-09 $m^2\ s^{-1}$; h=12.5 W $m^{-2}\ °C^{-1}$ [81]. Also, the mass transfer coefficient is obtained from the un-corrected Chilton-Colburn analogy (Eq. 15, $\xi = 1$) Moisture desorption isotherms are implemented using 2D interpolation of data that are presented in section 4.6.2, page 52, using surface moisture and temperature, to find the prevailing surface water activity used in the expressions for the driving force, Eq. 40 – Eq. 41.

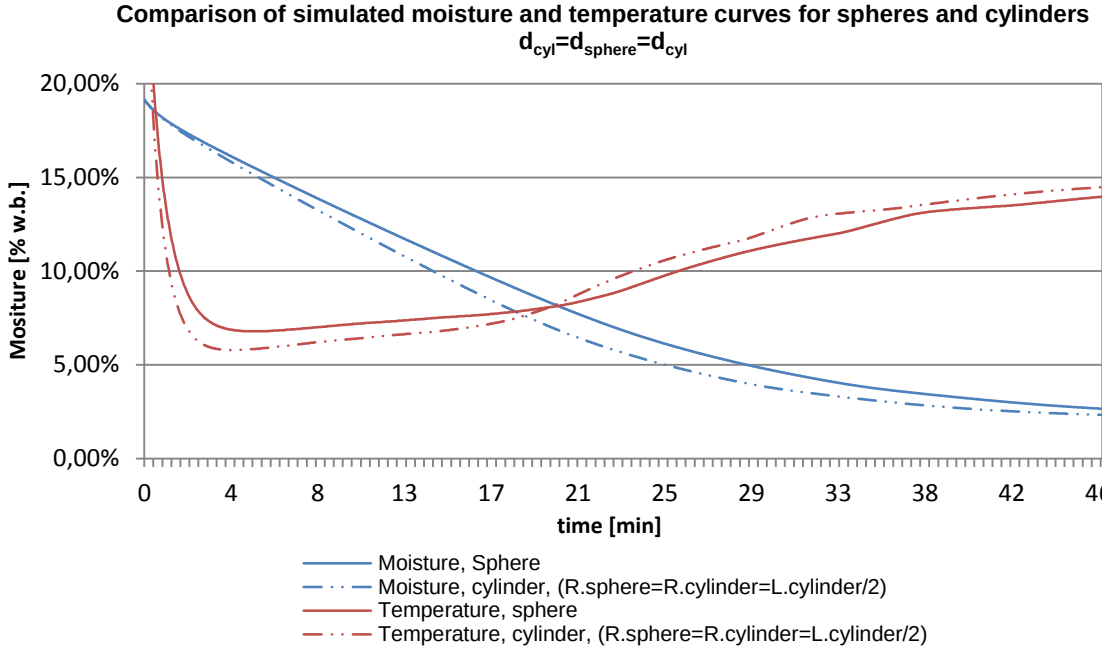

Figure 25: Pellet level solution for a sphere (D=4.5 mm) and an equilateral cylinder (D=4.5 mm; L=4.5 mm) at T=70 °C, 7 g H_2O/kg dry air.

From Figure 25, the equilateral cylinder dries faster than the sphere, particular in the beginning of the drying period, and also cools down and heats up slightly faster than the sphere. This aligns with expectations, that the sphere should be geometrically unmatched in its ability to retain moisture (and temperature). As it appears from Table 1, a sphere and an equilateral

cylinder with similar diameters possess similar surface area/volume ratio, and the volume and net surface area of the sphere is significantly smaller.

SHAPE	SPHERE	FEED CYLINDER	EQUILATERAL CYLINDER
DIAMETER	$2r_s = 2r_c$	$2r_c$	$2r_c$
LENGTH	-	L_c	$L_c = 2r_c$
SURFACE AREA	$A_s = 4\pi r_s^2$	$A_c = 2\pi r_c(L_c + r_c)$	$A_c = 6\pi r_c^2$
VOLUME	$V_s = \frac{4}{3}\pi r_s^3$	$V_c = \pi r_c^2 L_c$	$V_c = 2\pi r_c^3$
AREA/VOLUME, (A/V)	$(A_s / V_s) = \frac{3}{r_s}$	$(A_c / V_c) = \frac{2(r_c + L_c)}{r_c L_c}$	$(A_c / V_c) = \frac{3}{r_c}$

Table 1: Geometrical relations for spheres and different cylinders

In order to improve the match between cylindrical geometry and assumed spherical geometry, it should not be relevant to consider increasing the volume of the sphere (i.e. to assume similar volumes), as the surface area/volume ratio consequently will drop, and the drying rate of such a sphere will decrease. It is expected that the faster drying time of the cylinder over the sphere arise from the cylindrical geometry comprising 'corners' with bidirectional evaporation, which in turn increases local rate of diffusion in these regions. This effect should be lowered if the cylinder is non-equilateral (e.g. longer), which also lowers the surface area/volume to that of an equivalent sphere. Typically, feed cylinders are not equilateral, particular smaller pellets have lengths exceeding their diameter.

To account for the geometrical advantages of a cylinder over a sphere, a geometrical correction factor should be found, in support to the assumption of spherical geometry in the deep-bed drying of cylindrically shaped fish feed pellet. Eq. 67 gives the sphere radius to obtain matching area/volume (A/V) ratio with non-equilateral cylinders, including also the correction factor that accounts for geometrical differences.

$$(A_c / V_c) = (A_s / V_s) \cdot \varsigma_{\text{sphere}} \Leftrightarrow \frac{2(r_c + L_c)}{r_c L_c} = \frac{3}{r_s} \cdot \varsigma_{\text{sphere}} \Leftrightarrow r_s = \frac{3}{2} \frac{r_c \cdot L_c}{r_c + L_c} \cdot \varsigma_{\text{sphere}} \qquad \text{Eq. 67}$$

Figure 26 show that pellet level solutions for a sphere and a non-equilateral cylinder have a good match for similar diameters, *d*, when length of the cylinder is 4/3 times the diameter, $¾ \cdot L_c = d_c = d_s$. This corresponds to a correction factor of $\varsigma_{\text{sphere}} = 0.92$, cf. Eq. 67.

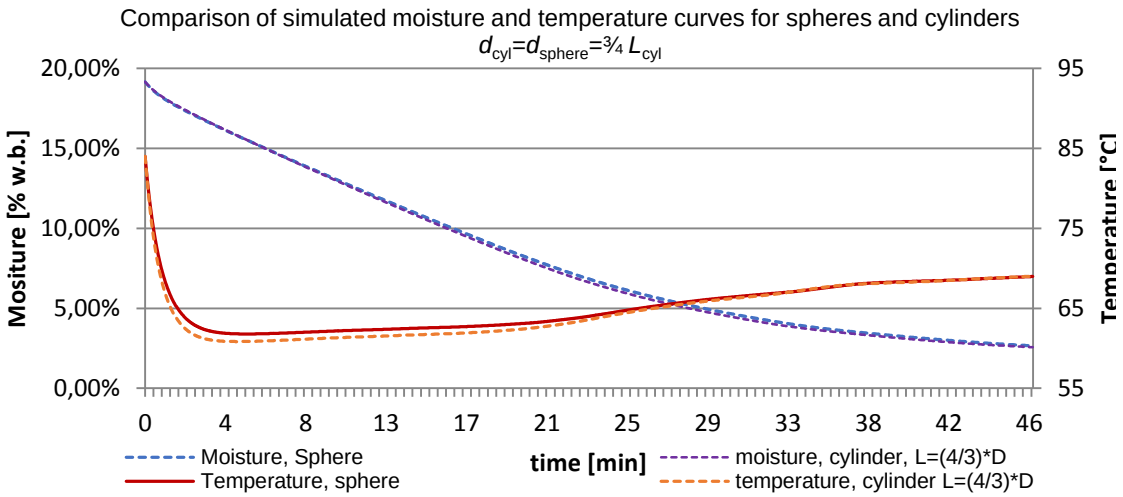

Figure 26: Pellet level solution for a non-equilateral cylinder (d=4.5 mm, L=6mm) and a sphere with diameter corrected to achieve similar area/volume ratio, (Eq. 67, D=4.5 mm). Drying conditions are v_{air}=1 m/s, T=70 °C, Y=7 g H_2O/kg dry air

Figure 27 illustrates spatial distribution of temperature and moisture for the pellet level solution of the drying of an equilateral cylinder (d=12 mm) and a sphere, with diameter corrected using Eq. 67 and $\varsigma_{sphere} = 0.92$, at 100 °C, 7 g H_2O / kg dry air at superficial bed velocity of 1 m/s. As expected, the cylindrical geometry exhibit more extreme local moisture and temperature differences; this is particularly obvious when looking at the solution for the 'corner' of the cylinder, as compared to the surface of the sphere.

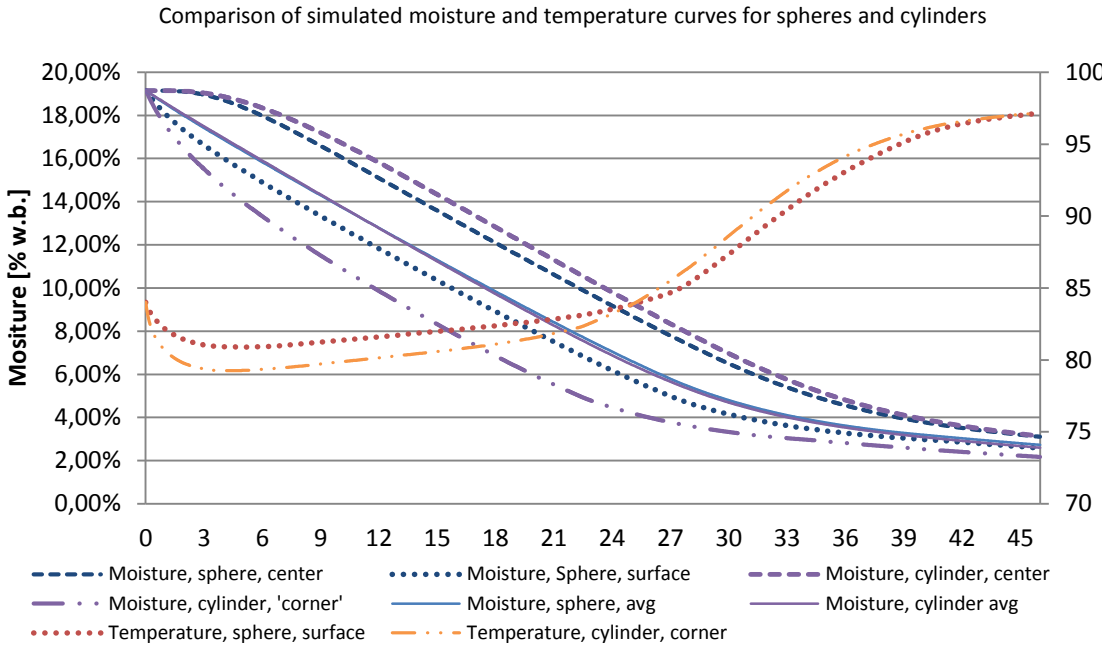

Figure 27: Comparison of pellet level solution for surface/center temperature/moisture for spheres and cylinders. To ease readability, only surface- and corner temperatures of the cylindrical solution are depicted.

4.5.5 Model resolution

To make use of the model presented in section 4.5, transfer coefficients and equilibrium data need to be calibrated toward the used drying conditions. Specifically these are;

- Moisture desorption isotherms for a reference feed, in the temperature range 50 – 100 °C
- Moisture diffusivity, D, and its temperature dependency (D_0 and E_A in Eq. 36, page 40)
- Interrelation of the heat- and mass transfer coefficient (ξ in Eq. 35, page 39)
- The external heat transfer coefficient, and its air flow dependency, $\mathrm{Nu}_{D_p} = f\left(\mathrm{Re}_{D_p}\right)$

The choice of software for implementing the numerical model is Engineering Equation Solver, 'EES'. This tool has the advantage of having built-in thermodynamic properties of moist air and simultaneously compiles and solves up to 12.000 equations with 12.000 variables, which is suitable for the implementation of the finite difference method onto sets of coupled partial differential equations. In addition there exists and option of creating distributable programs of a finished model, with a user-friendly interface [107]. As equations are compiled and solved by EES simultaneously, the outside process level loop posed challenges, when feeding the whole set of model equations to EES simultaneously (i.e. pellet-level, bed-level and process-level). As an alternative approach, the outside process level iteration loop are easily done manually or can simply be implemented by calling separate models after each other, as submodules, until satisfactory convergence. EES is not a particularly good programming software for handling logic commands, and other software packages might be superior to optimize and handle the outside process level iteration procedure, when maturing and developing model equations into a commercial software of a complete industrial scale dryer, with multiple belts and segregated air zones.

4.6 Model calibration and validation

4.6.1 Design of a batch lab-scale dryer

To the knowledge of the author, no laboratory scale dryer has previously been used to simulate the industrial scale deep-bed drying of extruded fish feed; particular when considering measurements of temperature and moisture of the product, as well as temperature and humidity of the drying air. The lab scale hot air dryer was therefore specially designed and manufactured (Wenger Manufacturing Inc., Sabetha, US), with the purpose of calibrating and validating the proposed model, as well as for investigating the influence on drying parameters on the mechanical properties and durability of the pellets [30, 108, 109], which is subject to discussion in section 6. A sketch of the custom-built lab dryer is provided in Figure 28, and from the pictures in Figure 29 and Figure 30. The dryer allows control of air velocity and temperature and has a manual steam injection valve for humidifying the drying air. The dryer comprise a ducting section for conditioning and mixing of the drying air, a removable drying chamber and an exhaust hood. Inlet and outlet air conditions (temperature, humidity) are measured continuously by the built-in SCADA system using Vaisala HMT 330 humidity sensors.

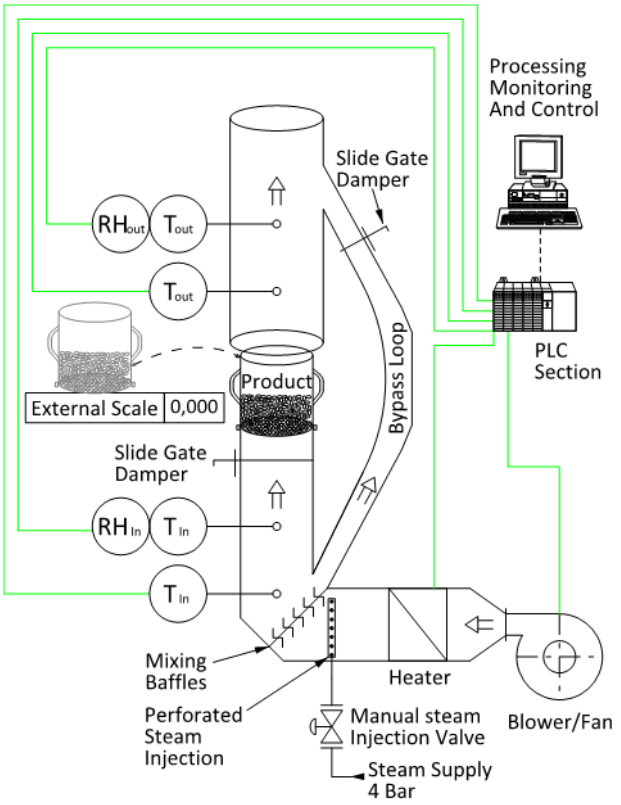

Figure 28: Conceptual layout of custom built hot air dryer for feed pellets.

Exhaust superficial bed air velocity is measured above the drying chamber using an external anemometer. Product moisture is monitored intermittently based on a loss-in-weight principle by weighing the drying chamber at 1-3 min intervals. Data are captured using a PLC and transferred to the built-in SCADA software. Average surface temperatures of topmost pellets are measured using an external IR camera (FLIR E40) during the weighing operations, which generally lasts 4-6 seconds. For safety reasons, air can be routed to an optional bypass loop during weighing operations, when very hot and humid drying air is used. [73, 81, 110].

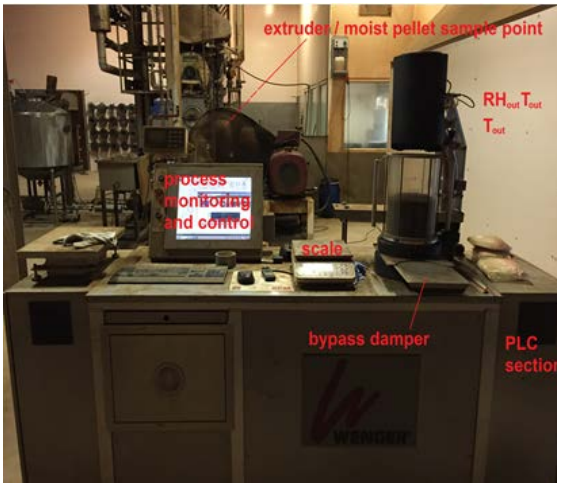

Figure 29: Front side of the custom designed Lab Scale Dryer and vicinity to the extruder, where moist pellets were taken out. External IR camera not shown.

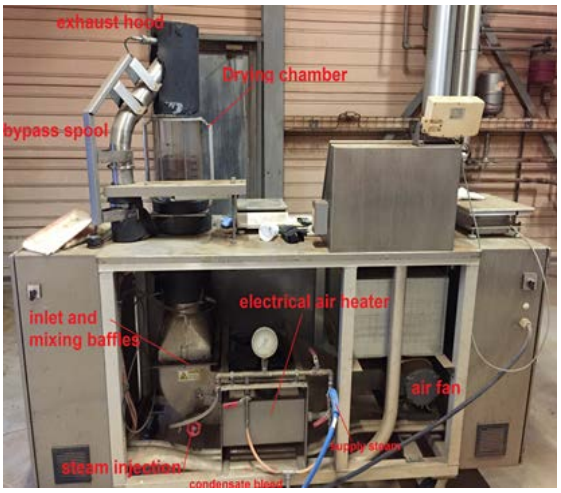

Figure 30: Back side of the Lab Dryer, illustrating the 'air conditioning section'

Extruded fish feed pellets are sampled from the extruder outlet (typically at 22-25 % moisture, w.b., 100 °C), and transferred to the drying chamber. The transfer process is carried out manually and last 20-30 seconds. During this time, the pellet generally cools to 80-85 °C and loses 2-4 % moisture, w.b. At the end of each drying, the end moisture content was found by drying in an oven at 105 °C for 24 hours. This allows the initial moisture content to be back calculated, assuming the total mass loss during the oven drying to be water.

From the prototype nature of the experimental setup and the custom-built laboratory scale batch hot air dryer, a number of challenges were identified. To address the expected accuracy of the system, as well as to aid future design of lab scale hot air dryers, these are discussed below:

- The cylindrical drying chamber need to come off the air conditioning hood when weighing; this induce significant inaccuracies in actual drying time exposed to the drying air. Significant air temperature and humidity fluctuations is also seen in this measurement period, due to the sudden change in backpressure. For this reason, exhaust humidity and air temperature were not found to be as well suited as validation parameters for the model, as the average moisture content and surface temperature of the pellets. Furthermore, the air temperature before the drying chamber was fluctuating ± 2-3 °C, due to the influence of the upset condition on the PID air temperature controller, when removing and repositioning the drying chamber.

- The humidity sensors installed in the dryer (Vaisala HMT 330) has quite high uncertainties when dealing with high temperature and high humidity applications. This effect arise from the specified accuracy for the *relative humidity*, at ±2 %. At 100 °C with 10 % RH, the accuracy in terms of absolute humidity becomes 69 ± 22 g/kg. Even so, this challenge apply equally to humidity measurements in industrial scale hot air dryers.

- The air heater was following the air fan and preceding the steam injection valve. This sequence are properly not ideal in supporting optimal air homogeneity, and the design should easily be improved in future work / version of lab dryers, by moving the fan closer to the drying chamber, to mix the moist, hot air in the fan.

- Manual measurements to find surface temperature of topmost pellets were carried out, using an external IR camera. Surface temperature was found by image analysis, averaging the surface temperatures of the approximate central part of the bed top. The estimated inaccuracy of the manual picture analysis is ± 2 °C and adds to the specified apparatus inaccuracy of ± 2 °C, totaling an approximate accuracy of ± 4 °C for measurements of pellet surface temperatures.

Three different series of thin layer drying experiments were carried out for calibrating the model, determining

- sorption isotherms;
- moisture diffusivity and;
- flow dependency of external transfer coefficients

An additional drying series was carried out to perform a complete validation of the deep-bed drying model. The four series of drying experiments are presented in the following sections, 4.6.2 – 4.6.5.

4.6.2 Sorption isotherms

Extruded fish feed pellets are sampled from the extruder outlet and transferred to the cylindrical drying chamber in the batch dryer, cf. Figure 38, page 59. A thin layer was used to assume constant air temperature. Moisture (equilibrium) is monitored ex situ by removing and weighing the drying chamber. An initial high air humidity was established and at equilibrium, sample weight and inlet air humidity was noted. Humidity was decreased in the drying chamber to establish new equilibrium conditions. Each equilibrium state was achieved when sample weight was constant over time, and thus becomes a single data point in the isotherm. A new equilibrium state was typically achieved after 1-2 hours. After equilibrium was reached at lowest (ambient) air humidity, pellets were sampled for moisture analysis to back-calculate moisture content for all data points. This methodology was repeated for each constant temperature, 'isotherm'. As moisture is removed when creating the isotherm, it is technically a *de*sorption isotherm, as opposed to *ad*sorption isotherms that rely on increasing moisture content. Isotherms recorded by Pacheco et al. are adsorption isotherm. Adsorption and desorption isotherms can differ slightly, so some of the incoherency with Pacheco et al. can be ascribed to the sorption hysteresis phenomenon [111].

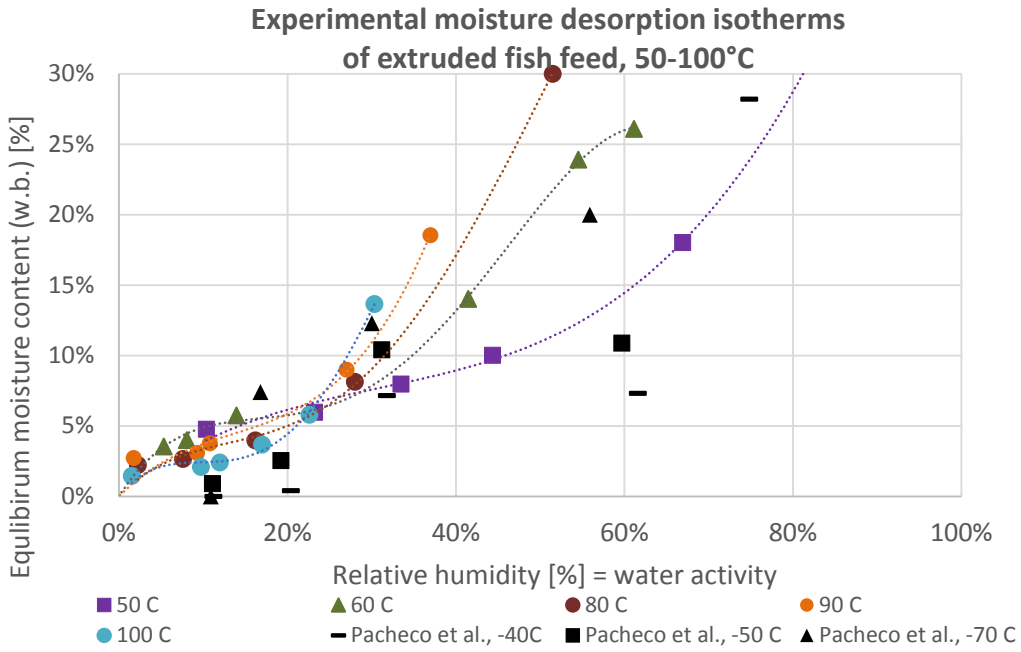

Figure 31: Experimental desorption isotherms as compared to isotherm. Polynomial approximations are to guide the eye. The uncertainties for each measurement point are dominated from the accuracy of relative humidity, i.e. ± 2 % RH, as stated by Vaisala for the sensor HMT 330.

Desorption isotherms recorded at 50 °C to 100 °C, is shown in Figure 31. A comparison is made to adsorption isotherms recorded by Pacheco et al. [19] at slightly lower temperatures (50 – 70 °C). In the region where the influence of temperature on the isotherms is largest (i.e. > 10 % moisture, w.b.), the feed pellets will in the drying tend to have temperatures from 70 – 90 °C, so the illustrated set of five recorded sorption isotherms should cover the range of relevant pellet temperatures. In addition, coherency is generally good as compared with data from Pacheco et al., when considering also the effect of hysteresis, extrusion conditions and recipe. As mentioned, the isotherms recorded by Pacheco et al. were *adsorption* isotherms on fully processed fish feed (coated and cooled); this is believed to cause the larger part of the observed variations to the desorption isotherms recorded in present study. The recorded set of equilibrium data are applied directly into the modeling software, by 2-dimensional interpolation, to find *aw* at a particular surface temperature and moisture content. At this point, the deep-bed model can be run using h, h_m *(or* ξ*)* and D as free parameters, in a non-linear least squares regression analysis, minimizing the total sum of square errors against the experimental recorded moisture contents and temperatures.

4.6.3 Temperature dependency on moisture diffusivity

Thirteen thin layer drying experiments were carried out at different drying temperatures, all other variables held constant. Six thin layer drying experiments were carried out for pellets with a diameter of 6 mm, and seven thin layer drying experiments were carried out for 4.5 mm pellets. Temperatures used was in the range from 60 °C – 130 °C. Figure 32 – Figure 35 illustrate overall moisture content and surface temperature, as recorded for the thin layer drying experiments for 4.5 mm and 6 mm pellets, respectively. Constant air temperatures between 60 and 130 °C was used in the different drying experiments, as annotated.

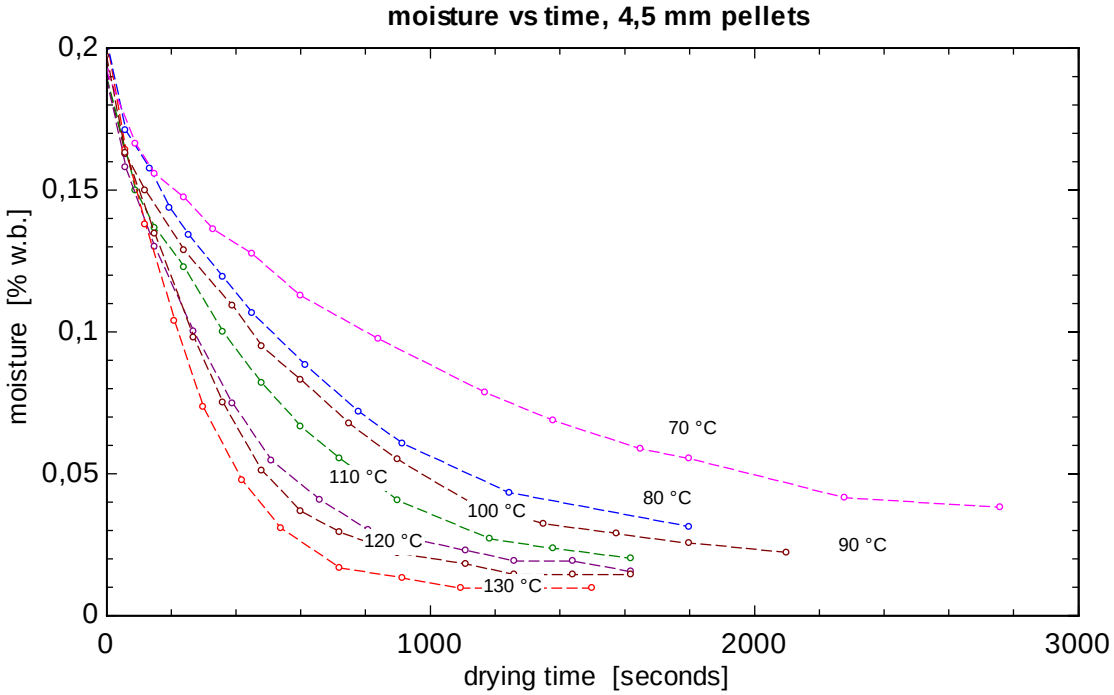

Figure 32: Moisture recordings for thin layer drying experiments of 4.5 mm pellets (dotted lines connects the data points).

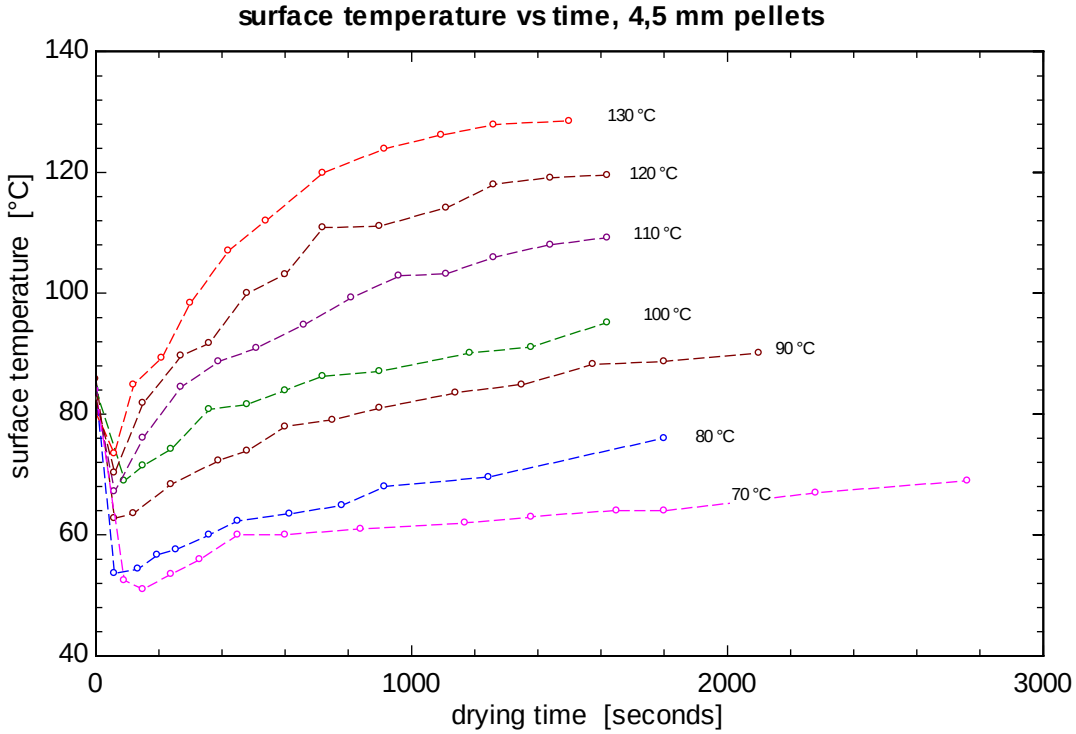

Figure 33: Recordings of surface temperature for thin layer drying experiments of 4.5 mm pellets (dotted lines connects the data points).

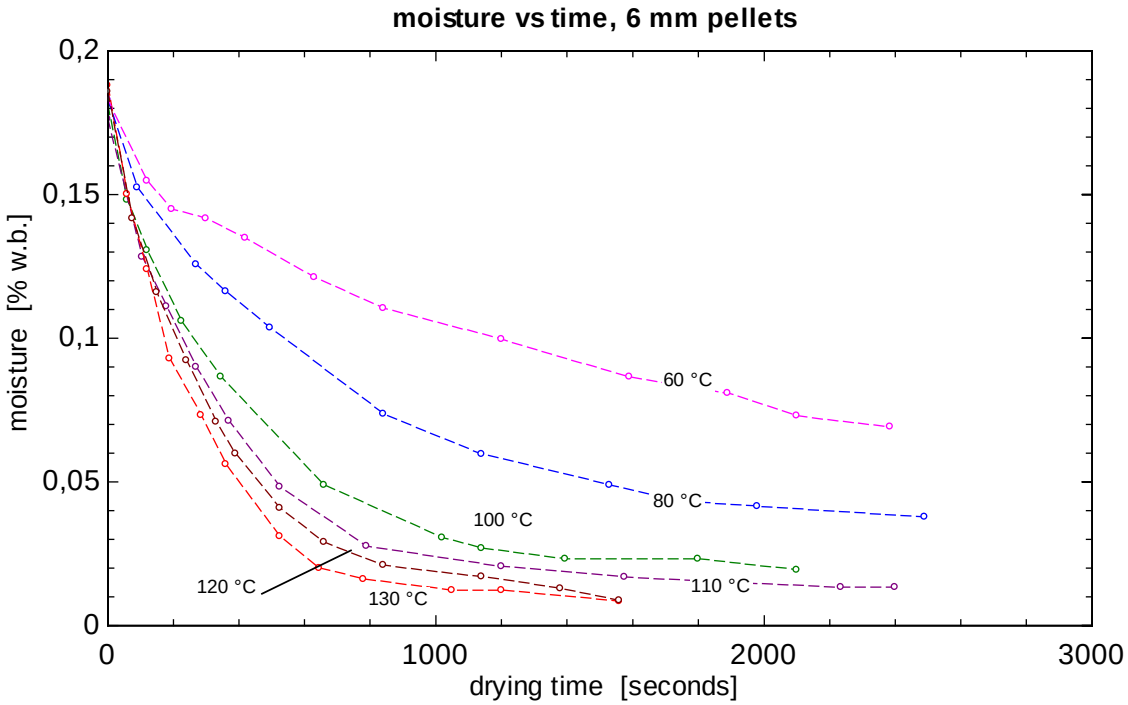

Figure 34: Moisture recordings for thin layer drying experiments of 6 mm pellets (dotted lines connects the data points).

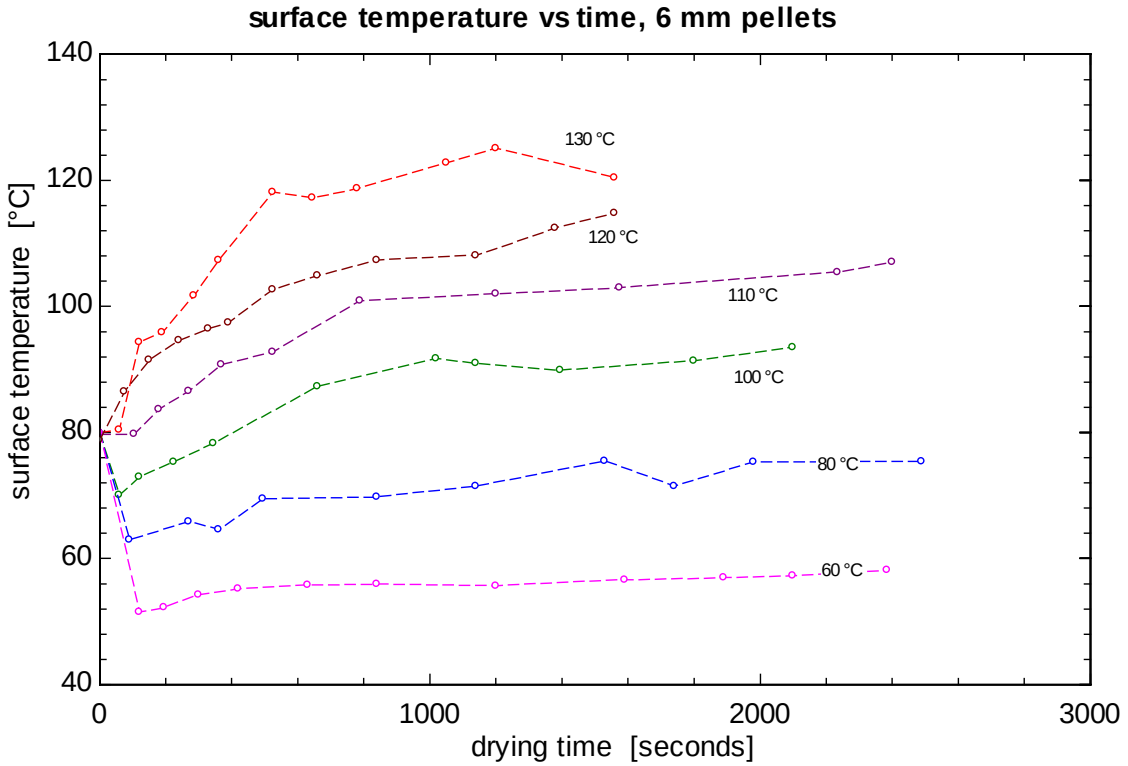

Figure 35: Recordings of surface temperature for thin layer drying experiments of 6 mm pellets (dotted lines connects the data points).

The objective is now initially to find the actual relation between the external mass- and heat transfer coefficient. In doing this, the coefficients are each assumed constant and similar, for

each thin-layer drying at different temperature, but at constant air velocity. An initial multi-parameter non-linear regression analysis was carried out to determine the interrelation of the heat and mass transfer coefficients, through ξ, and the heat transfer coefficient, h, for each of the two pellet sizes. This was done by minimizing the total weighted root mean square error, $WRMS_T$, for the solution of surface temperature and average moisture content, against the experimental data, cf. Eq. 68.

$$\mathrm{WRMS}_T = \sqrt{\sum_{i=1}^{N_{data}} \left(\frac{\hat{X} - X_e}{X_e} \right)_i^2} + \sqrt{\sum_{i=1}^{N_{data}} \left(\frac{\hat{\theta}_R - \theta_{R,e}}{\theta_{R,e}} \right)_i^2} \qquad \text{Eq. 68}$$

N_{data} are the amount of experimental data points, X_e and $\theta_{R,e}$ are experimental data, $\hat{X}$ and $\hat{\theta}_R$ are predicted (simulated) values. The DIRECT algorithm by Jones et al. [112], was used for minimizing the total error. This minimization algorithm is well suited to find a global minimum, even if a range of local minima exists [107].

Table 2 lists average and standard deviations of ξ, h and D from non-linear least square regression analysis for both feed sizes, using all three parameters as free parameters in the multi-parameter regression analysis, minimizing the total sum of square error against the experimental values (Figure 3 and Figure 4).

Table 2: Multi-parameter non-linear regression analysis finding ξ_{bed}.

	4.5 mm	6 mm	Average
ξ (Eq. 35 p. 39)	4.2 ± 1.5	4.0 ± 1.0	**4.1** ± 1.3
h (W m^{-2} K^{-1})	12.2 ± 1.4	22.1 ± 2.9	
D (m^2 s^{-1})	7.9 E^{-10} ± 2.0 E^{-10}	1.1 E^{-9} ± 4.8 E^{-10}	

In table 3, ξ is fixed at the obtained average value from table 2. h and D are free parameters in the subsequent dual-parameter non-linear least squares regression analysis.

Table 3: Multi-parameter non-linear regression analysis finding heat transfer coefficients

	4.5 mm	6 mm	Average
ξ (table 2)	4.1	4.1	**4.1**
h (W m^{-2} K^{-1})	**14.3** ± 2.5	**24.1** ± 2.4	
D (m^2 s^{-1})	7.5 E^{-10} ± 2.1 E^{-10}	1.1 E^{-9} ± 5.4 E^{-10}	

Eventually, this procedure allows a fixed average value for h and ξ to be used when determining the temperature dependency of the moisture diffusivity. This ensures differences between obtained diffusivities in each drying run to be ascribed solely to the difference in air temperature. The differences in the moisture diffusivity is investigated in Figure 36, from a plot of $\ln(D)$ vs $1/\theta$, for each of the two pellet sizes. This allows to determine $-E_A/R$ and $\ln(D_0)$, from respectively the slope and the intercept of the best linear fit line between the points, cf. Eq. 36, p. 40. Note that the average product temperatures, θ, was found in each experiment by (i) integrating measured surface product temperature over time to find the

temporal average and (ii) assuming little difference between average surface temperature and average pellet temperature (lumped capacitances).

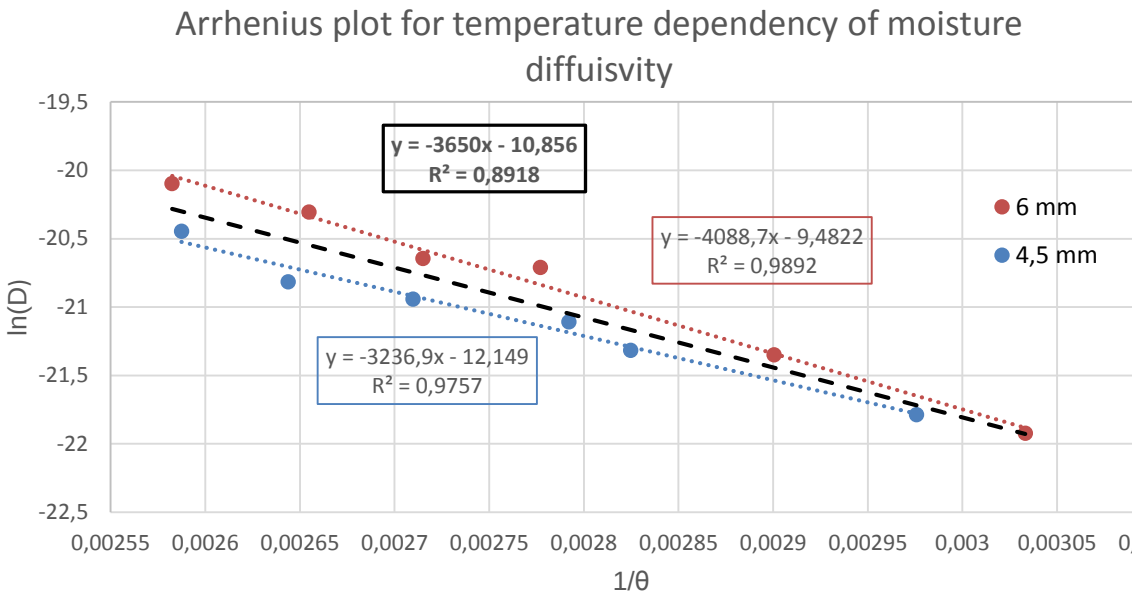

Figure 36: Investigation of the temperature dependency on the moisture diffusivity in an Arrhenius plot. The black dashed line indicate the average between experiments using 6 mm and 4.5 mm pellets.

$$D_0 = \frac{e^{-10.856}}{2} = 1.93 \cdot 10^{-5} \frac{m^2}{s} \qquad \text{Eq. 69}$$

$$E_A = \left(\frac{-3650 \cdot (-8.314)}{2} \right) \frac{J}{mol} = 30.4 \frac{kJ}{mol} \qquad \text{Eq. 70}$$

The above temperature dependency imply that the moisture diffusivity will increase by a factor of 2.3 when increasing the temperature from 15 °C to 35 °C, as compared to a factor 3 obtained as reported for cornstarch, by Yu et al[50].

4.6.4 The heat transfer coefficient and its air flow dependency

Five thin layer drying experiments was carried out at different airflow velocities for 6 mm pellets, all other variables held constant. Superficial bed velocities used were between 0.5 – 1.5 m/s. The heat transfer coefficient is now the single free parameter in the model. The temperature dependency of the moisture diffusivity is defined from Eq. 69 and Eq. 70 and the heat and mass transfer coefficients are interrelated from Eq. (9), using the interrelation of the heat- and mass transfer coefficient, ξ, as found from Table 2.

The overall heat transfer coefficient, h, is found for each of the five thin layer drying experiments at different pellet Reynolds numbers; again, non-linear regression analysis is applied, minimizing the total sum of square error against the experimental values of moisture and surface temperature. The obtained results are shown in Figure 37.

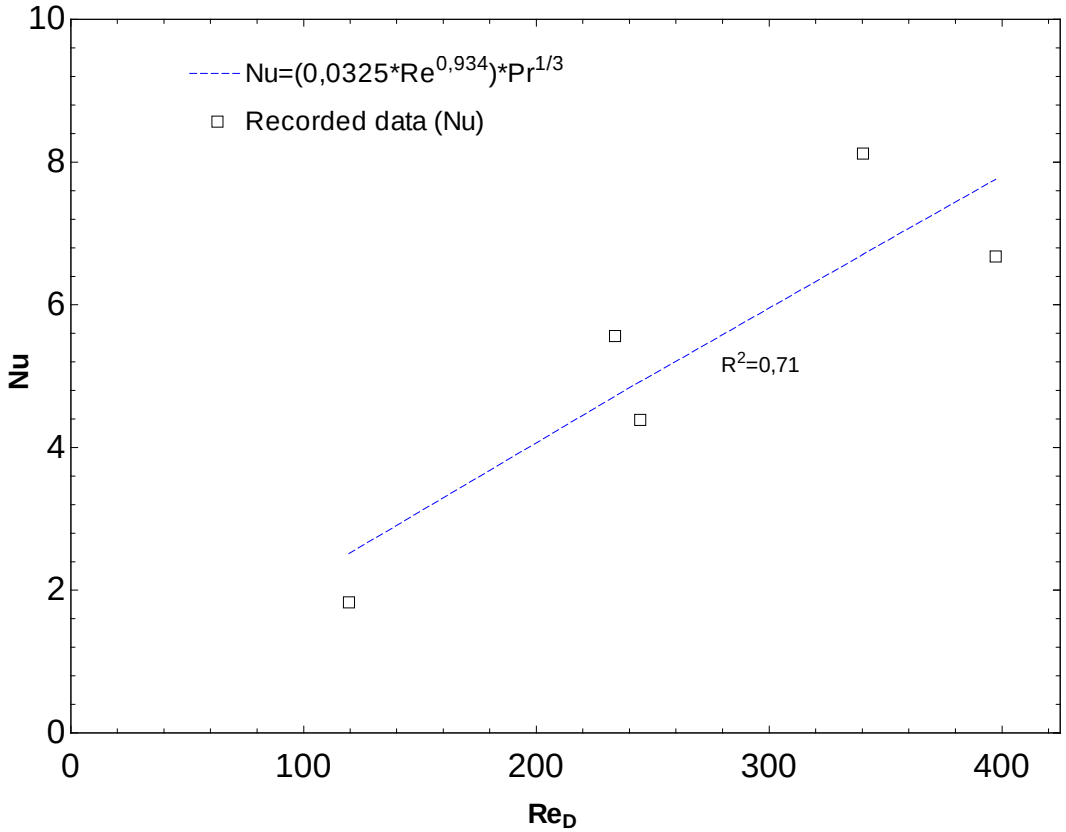

Figure 37: Obtained heat transfer coefficients from non-linear regression analysis for different Reynolds numbers – all other variables are constant.

An empirical external flow correlation by Hilpert [113] is used to fit the data obtained in Figure 37. Exponential and pre-exponential coefficients in the Hilpert correlation are found from regression analysis using the obtained data; the expression appear from Figure 37 and from Eq. 71.

$$\mathrm{Nu}_d = \frac{h \cdot d}{k_a} = 0.0325 \cdot \mathrm{Re}_d^{0.934} \qquad \mathrm{Re}_d = \frac{d \cdot J_m}{\mu_a} = \frac{v_a \cdot \rho_a \cdot d}{\mu_a} \qquad \text{Eq. 71}$$

Pellet diameter, d, is used as basis for Nu and Re calculations, v_a is the superficial bed air velocity and k_a, μ_a and ρ_a are air conductivity, viscosity and density for the drying air, respectively.

4.6.5 Model validation

At this point, model transfer coefficients have been calibrated from thin layer drying experiments; external transfer coefficients, including their interrelation and airflow dependency as well as effective moisture diffusivity and its temperature dependency. The performance of the model can now be evaluated, when stacking thin layers of assumed spherical pellet (with geometrical correction factor) into a deep bed, i.e. allowing the air to change conditions as it travels through the bed. Validation parameters are bed average moisture content, as found gravimetrically, and the surface temperature of the topmost pellets. Exhaust airflow conditions are also validation parameters, yet their accuracy can be expected to be inferior, when compared to the measurements on the product. This is expected due to the intermittent weighing procedure, idle temperature loss in the drying chamber and inaccuracies of the Vaisala sensors for hot, humid air, as discussed in section 4.6.1.

Figure 38: Cylindrical drying chamber on the specially designed lab scale batch dryer with automatic temperature control and manual humidity and air velocity control.

Deep-bed validation is carried out using the same recipe (feed type) as used for determining the sorption isotherms. Six validation experiments are carried out in total, each using different combinations of temperature, feed size, humidity and air velocity. One experiment have three replicates to elucidate the experimental accuracy, and in this experiment, all air exhaust conditions were additionally logged throughout the drying. A picture of the drying chamber containing a deep bed is illustrates in Figure 38.

Figure 39 to Figure 44 illustrate the performance of the deep-bed model using calibrated transfer coefficients from preceding sections. Temperature, humidity and pellet diameter vary in the different drying experiments. One deep-bed drying experiment was carried out on 6 mm pellets using dry air at 120 °C with a high bed velocity (Figure 39) and six deep-bed drying experiments were carried out on 3 mm pellets. One of these drying experiments uses humid air at 90 °C and low bed air velocity (Figure 40), whilst two other experiments utilize hot drying air at 130 °C. Dry air is used in one of these two hot air drying experiments at 130 °C (Figure 41), and humid air at increased bed air velocity is used in the drying illustrated in Figure 42. Essentially this represents an increased internal recirculation of drying air. Figure 43 and Figure 44 visualize the experimental accuracy for pellet and air measurement, respectively, for the deep-bed drying using 130 °C dry air. Three repetitions are used for these drying conditions.

Table 4: Overview of deep-bed drying experiments using different drying conditions, as well as obtained CV(RMSE) values for pellet moisture and pellet surface temperature (at exhaust side).

Figure		**37**	**38**	**39**	**40**	**41**
Pellet size, d	mm	6	3	3	3	3
Humidity, Y	g/kg	8	30	9	40	6
Temperature, T_{air}	°C	120	90	130	130	130
Bed depth, Z	m	0.16	0.16	0.16	0.16	0.15
Superficial bed velocity, v_{air}	m/s	1.3	0.9	0.7	0.9	0.8
CV(RMSE)$_X$	*%*	*9.2*	*7.8*	*9.5*	*7.1*	*12.4*
CV(RMSE)$_{\theta\text{-}surf}$	*%*	*8.9*	*5.9*	*9.8*	*6.5*	*12.7*

An overview of the deep-bed drying experiments is provided in Table 4, with belonging coefficients of variation of the root mean square error, CV(RMSE). This measure is calculated as the ratio of the root mean square error to the mean, cf. Eq. 72 and Eq. 73. CV(RMSE) are calculated for model predictions of pellet average moisture contents, $\hat{X}$, and exhaust-side pellet surface temperatures, $\hat{\theta}_{\text{R},\xi_{\max}}$. Subscript e are experimental values, N_{data} are the amount of data points, and $\overline{X}$ and $\overline{\theta}$ are temporal averages from N_{data} experimental observations.

$$\text{CV(RMSE)}_X = \frac{\text{RMSE}_X}{\overline{X}} = \frac{\sqrt{\dfrac{\sum_{i=1}^{N_{\text{data}}} \left(\hat{X} - X_{\text{e}}\right)_i^2}{N_{\text{data}}}}}{\overline{X}} \qquad \text{Eq. 72}$$

$$\text{CV(RMSE)}_\theta = \frac{\text{RMSE}_\theta}{\overline{\theta}} = \frac{\sqrt{\dfrac{\sum_{i=1}^{N_{\text{data}}} \left(\hat{\theta}_{\text{R}} - \theta_{\text{R,e}}\right)_i^2}{N_{\text{data}}}}}{\overline{\theta}} \qquad \text{Eq. 73}$$

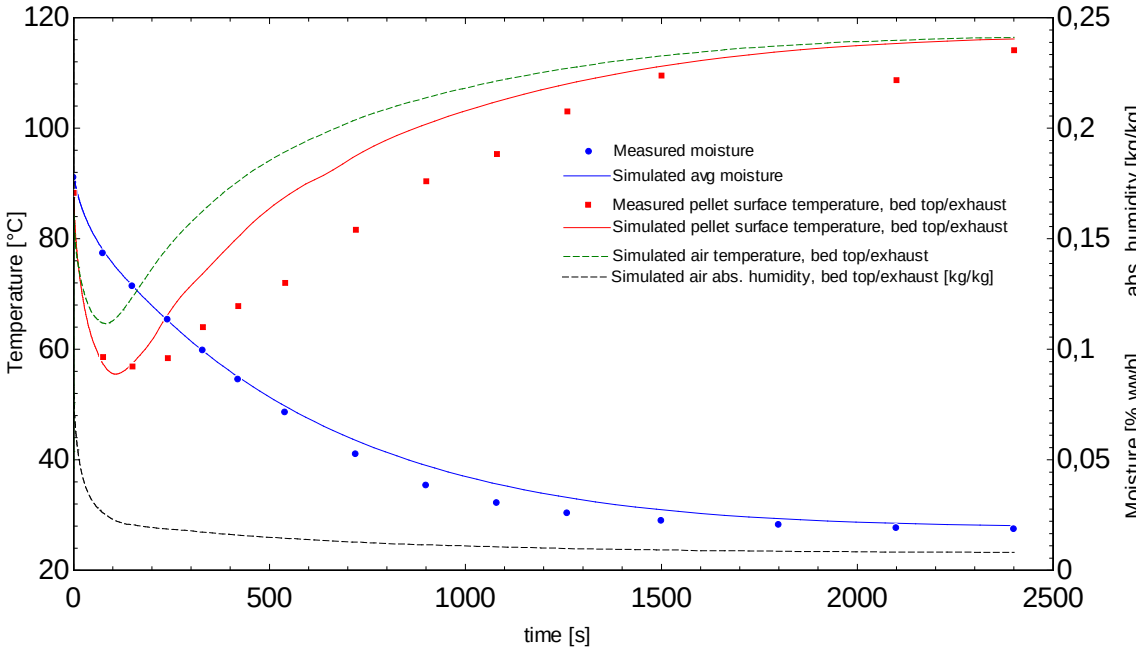

Figure 39: Deep-bed drying of 6 mm extruded fish feed pellets using dry air at 120 °C and 8 g H_2O/ kg dry air. Superficial bed velocity is 1.3 m/s and bed height is 16 cm. Coefficients of variation of the RMSE for pellet moisture, and surface temperature predictions are 9.2 % and 8.9 %, respectively.

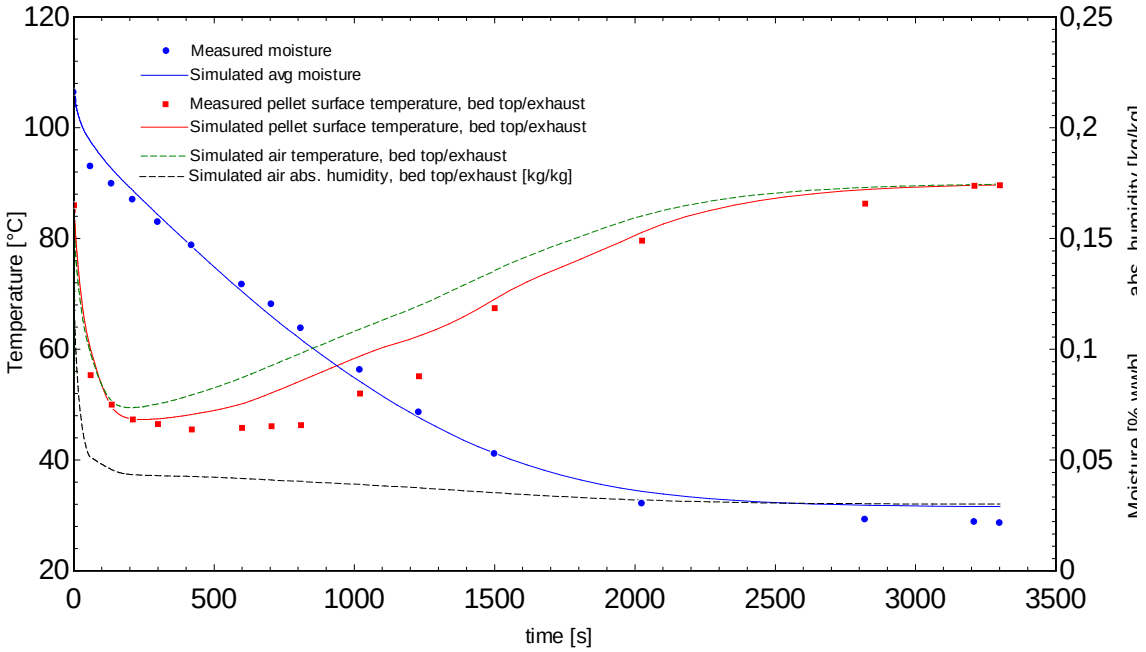

Figure 40: Deep-bed drying of 3 mm extruded fish feed pellets using humid air at 90 °C and 30 g H_2O/ kg dry air. Superficial bed velocity is 0.9 m/s and bed height is 16 cm. Coefficients of variation of the RMSE for pellet moisture and surface temperature predictions are 7.8 % and 5.9 %, respectively.

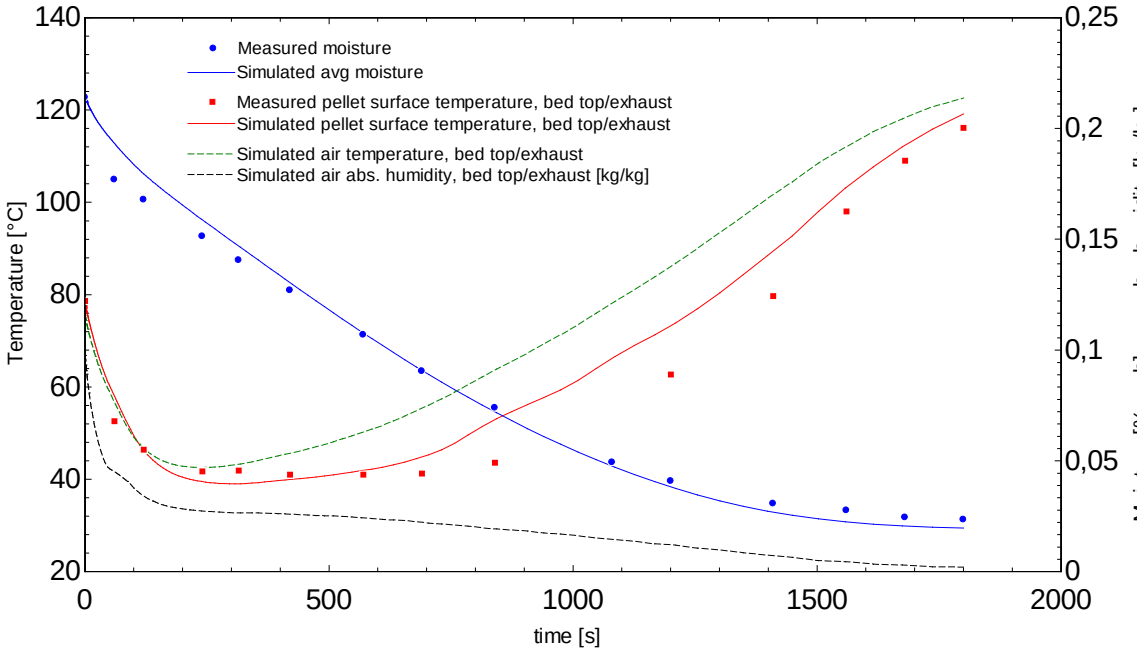

Figure 41: Deep-bed drying of 3 mm extruded fish feed pellets using dry air at 130 °C and 9 g H_2O/ kg dry air. Superficial bed velocity is 0.7 m/s and bed height is 16 cm. Coefficients of variation of the RMSE for pellet moisture and surface temperature predictions are 9.5 % and 9.8 %, respectively.

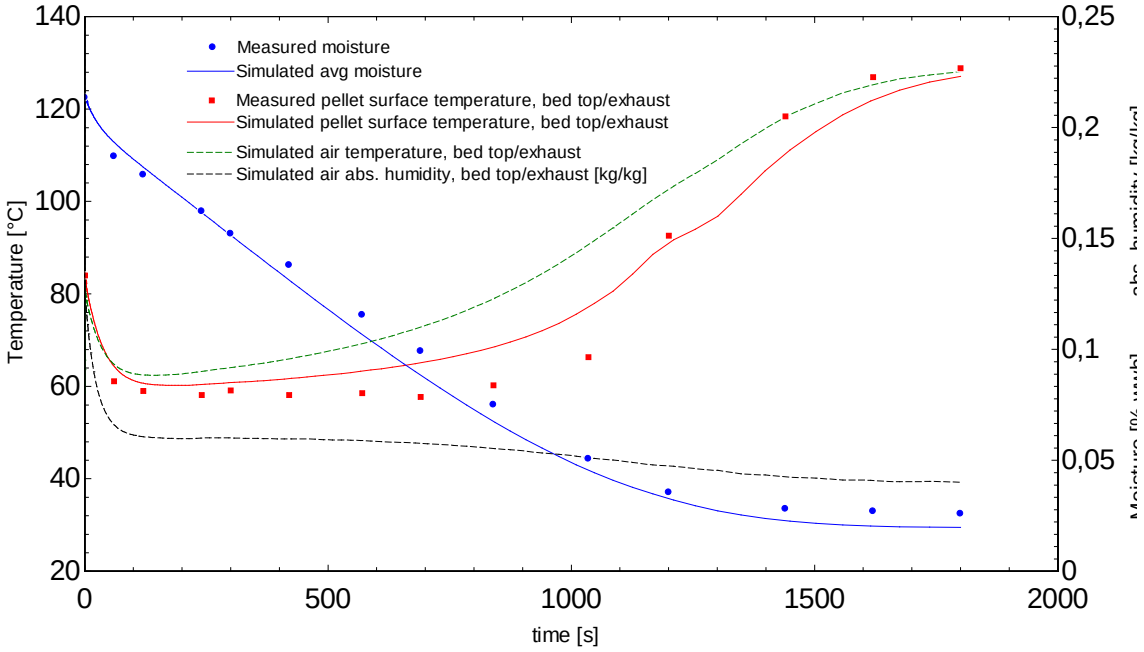

Figure 42: Deep-bed drying of 3 mm extruded fish feed pellets using humid air at 130 °C and 40 g H_2O/ kg dry air. Superficial bed velocity is 0.9 m/s and bed height is 16 cm. Coefficients of variation of the RMSE for pellet moisture and surface temperature predictions are 7.1 % and 6.5 %, respectively.

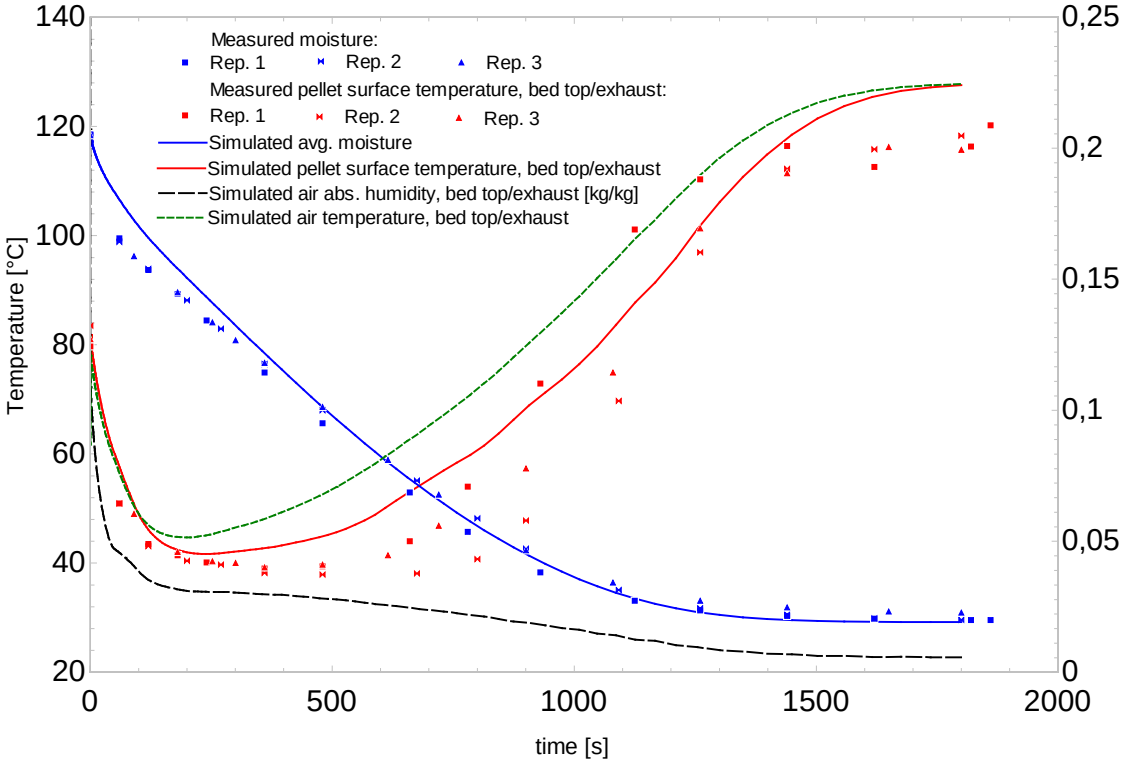

Figure 43: 3 repetitions of the deep-bed drying of 3 mm extruded fish feed pellets using dry air at 130 °C and 6 g H2O/ kg dry air. Superficial bed velocity is 0.8 m/s and bed height is 15 cm. Coefficients of variation of the RMSE for moisture and temperature predictions are 12.4 % and 12.7 %, respectively.

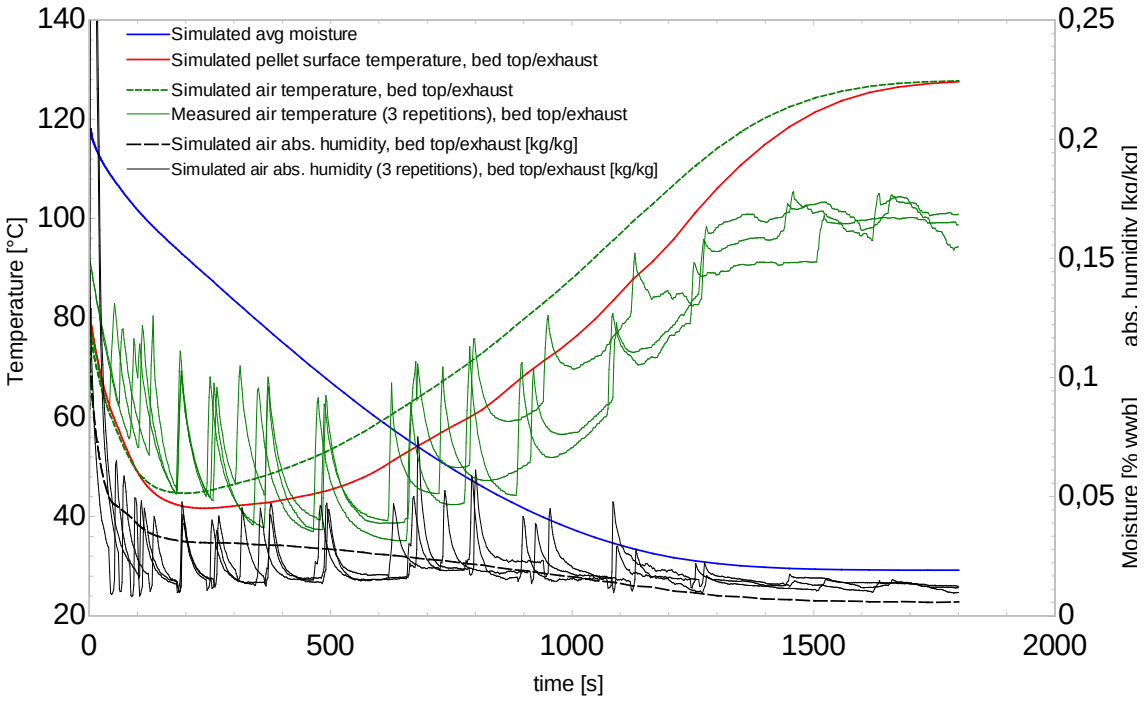

Figure 44: Recorded exhaust air temperature and humidity data for the 3 repetitions of the drying in Figure 13.

The model generally rely on the obtained transfer coefficients from the thin layer drying experiments to lump all effects, so that the deep-bed drying model can be established by 'stacking' thin layers, considering changes in the air state passing each layer. Hence, effects that are stronger in a deep bed than in a thin layer are essentially not assessed. This regards

especially to the increased non-adiabatic behavior of the deep-bed system relative to the drying experiments in a thin-layer. Pellets in a thin layer are largely exposed to the dryer set-point temperature, 'T_∞'. For pellets in a deep bed, there is a proportional contribution of heat loss through the bed wall. This effect is evident in Figure 44, where exhaust air is significantly lower than the adiabatic equilibrium approached by the simulation. This effect should be diminished when applying the model onto large industrial scale dryers, where the bed width/height ratio is significantly larger than in the experimental setup used in this work. It is noted that the exhaust air temperature in Figure 44 does also still not reach the measured pellet temperatures. The exhaust temperature sensor is located in an air pickup hood ~40 cm above the pellets. An additional non-adiabatic cooling (or mixing with ambient air) must exist in this section, as the air immediately exhausted should naturally have temperatures at or above the measured surface pellet temperature. This substantiates that the use of the exhaust air measurements is not as feasible in the validation of the model, as bed average moisture and surface temperature of topmost pellets, at air exhaust. The measured air humidity however correspond relatively well with the simulated values, taking into account the influence on the air humidity measurements of the intermittent moisture and temperature measurements.

The influence on air temperature due to the pressure drop across the deep bed is also not evaluated in the model, and is an additional effect that cannot be lumped into the obtained transfer coefficients obtained from thin-layer drying experiments. This effect should not be expected to be diminished when applying the model in industrial scale.

Sorption isotherms are recorded gravimetrically using the lab dryer, by conditioning air humidity to the desired water activity for each individual isotherm and awaiting equilibrium. As this is a very time-consuming process, the recorded isotherms are from different productions / days, for the different isotherms (albeit obviously using the same recipe and size). Slight variations in extrusion parameters and raw material conditions will be reflected on the accuracy of the isotherms, due to upstream variations in the product. The isotherms govern important drying characteristics, like flash-off and duration of approximately constant rate drying (i.e. if wet-bulb temperature is reached at the surface of the pellets) as well as, obviously, the equilibrium moisture content. From the deep-bed validation experiments in Figure 39 – Figure 43 it is seen that the extent of flash off is not fully reproduced in the model. As this is particularly pronounced for the drying experiments using the smaller 3 mm pellets and dry air, it should be reasoned from the spatial initial conditions of the pellets changing in the transfer period, rather than great inaccuracies from the sorption isotherms. When the experimental drying starts, moisture has in the transfer period (~20-30 seconds), to some extent, already diffused toward the surface creating a high degree of flash off in the bed. The simulation does not include this transfer period; effectively the 'transfer period' is another 'drying zone' at ambient conditions, but at an unknown approximately stagnant air velocity. If the transfer process is pneumatic, (in an 'airlift') with a specified air-pellet interface velocity this could be included in the model. This should be subject to further work

From Figure 39 – Figure 43, it is also seen that the simulation does not fully reproduce the extent of the drying occurring at a constant pellet surface (~wet-bulb) temperature, as seen experimentally. This phenomenon occur when the net heat flux to the pellet is zero, e.g.

when the water activity at the surface of the pellet is unaltered in a region of different surface moisture contents, resulting a 'constant drying rate'. Experimental and model discrepancies should therefore in this regard be partially induced from inaccuracies in the recorded sorption isotherms. Furthermore, local moisture differences (and water activities), relative to the direction of airflow, will additionally increase deviations in the model predictions of surface temperature.

The model fit of the average moisture content is generally good (at $CV(RMSE)_X$ ranging from 7 % - 12 %), albeit slightly different average 'slopes' of the drying curve is witnessed in the experiments. This is naturally caused from several phenomena. The empirical transfer coefficients obtained from non-linear regression analyses in the thin layer drying experiments effectively lumps all phenomena into the empirically obtained moisture diffusivities and external heat- and mass transfer coefficients. Hence, the obtained coefficients will aim to make up for inaccuracies caused by e.g. the extent of flash off or obtained equilibrium moisture. The model assumes spherical geometry of the pellets, with a geometrical correction factor, and does not include shrinkage and moisture dependency on the moisture diffusivity. The effect of these simplifications are also lumped in the transfer coefficients in the non-linear regression analyses. The obtained accuracy on the moisture predictions are comparable to values found in literature; as mentioned earlier Sahin et al. obtained drying times at an accuracy of ± 10% of experimental drying times [69].

From Figure 39 to Figure 43 it can be seen that the model generally predict a more rapid heating of the pellets subsequent to the evaporative cooling. $CV(RMSE)_\theta$ ranges from 6 % - 13 % for predictions on pellet surface temperatures. Where one quantity of this inaccuracy, as mentioned, arise from the sorption isotherms, another quantity certainly arise from measuring the lee-side surface temperature of the topmost pellets, relative to the airflow. This is supported from the effect being stronger for the larger 6 mm pellets, which presumably have more stagnant lee-side conditions, as well as a greater distance (and Biot numbers) to conduct temperature from the wind-side of the pellets.

An untraditional approach in the present work is the introduction of a bed correction factor into the Chilton-Colburn analogy. This modification is based on recommendations and remarks elsewhere [77-80], as explained earlier. The bed correction factor is roughly representing the total pellet surface area relative to the surface exchange area available for convection. Achenbach demonstrated that at low Reynolds numbers the effect of heat conduction via points of contact elevated the Nusselt number by 3-5 times, relative to the expected value. The bed correction factor used in this work is 4.1 and corresponds well with the empirical findings by Achenbach. The effect of heat conduction and radiation on the Nusselt number, relative to the convective contribution, is obviously lowered at increasing Reynolds numbers. This is not included into this model, using the same bed correction factor for all bed air velocities. It is estimated that the Reynolds numbers used in the deep-bed drying of extruded fish feed will be low, relative to the conductive and radiative contributions to the Nusselt number. Therefore, the constant bed correction factor should not be expected to yield large inaccuracies across bed air velocities conventionally encountered at $0.7 \pm 0.3\ m/s$.

Traditionally, the dependency of Reynolds numbers on Nusselt numbers is expanded from circular cylinders in free flow onto packed beds, by optimizing pre-exponential coefficients to match empirical data [72, 114]. In this work an empirical correlation by Hilpert is used to evaluate the interrelation between *particle* Nusselt and Reynolds numbers [113], when embedded in a packed bed. In the model presented in this work, the convective heat transfer to a pellet is found by integrating over the total pellet area, whilst in reality, only the net surface exchange area available for convection comprise the convective heat transfer between the drying air and an individual pellet. This means that the obtained Nusselt number should be lower than the expected pellet-air Nusselt number at the interstitial pellet Reynolds number. Obtained heat transfer coefficients in the model fall within 10-35 W $m^{-2} K^{-1}$ for superficial bed air velocities at 0.4 – 1.3 m/s. It is noted that the exponent coefficient found on Re in the Hilpert type expression, Eq. 71, is nearly one, effectively indicating that the influence of pellet diameter is small. Lambert et al. used a heat transfer coefficient of 20 W $m^{-2} K^{-1}$ in their deep-bed model for the drying of chicken feed pellets, which is certainly comparable to the obtained range of values in the present work [56]. The thin layer drying experiments used for the external flow correlations, Figure 7, is not ideal at R^2=0.71, for the proposed Hilpert type correlation. However, some uncertainty must be expected, as the obtained heat transfer coefficient will encompass residual variations like measurement inaccuracies, variations in depth of the thin layers, air homogeneity at different airflows as well as any changes in parameters upstream the drying process. Furthermore, the number of drying experiments in an experimental series is limited to be using only the feed from a single production run, where no parameters is altered upstream the drying process. In addition, only available time slots in between scheduled (or particularly unscheduled) production halts can be considered.

It is evaluated that the inaccuracies witnessed in the deep-bed validation experiments are generally good, and will not be large enough to be disturbing practical application of the model, to effectively monitor, control and optimize the overall energy efficiency in the continuous drying process. The accuracy might even improve in large-scale dryers that operate closer to adiabatic conditions. When transporting pellets in an airlift at a specified air velocity, initial conditions of the pellets can be simulated using the airlift as a separate 'drying zone'. This should capture the extent of the initial flash off. When transporting the pellets on a belt at unknown, and ~stagnant air conditions, the model will be limited to 'start the drying' at the dryer inlet, and some inaccuracies in the extent of flash off can be expected. In this work, pellet surface temperatures were measured at their lee-side, relative to the airflow. The match between the average surface temperature and the model fit should be, to some extent, improved. Only one feed type was used in this work. When changing feed type, pellet density and nutritional composition can simply be altered in the model input, but the difference in moisture diffusivity remains a challenge. Ideally, carrying out a single thin-layer drying to evaluate the difference in average diffusivity should suffice, retaining the temperature dependency on the moisture diffusivity from this work. It is evaluated that the sorption isotherms can be applied across different feed recipes. In several studies, sorption isotherms are typically applied over a broad range of products [19, 32, 56]. The introduction of different feed types into the model is subject to future work.

4.7 Model output and application

The presented model evaluates temporal temperature and moisture content of air and of feed pellets, across a deep bed. This holds potential in accurately evaluating the energy efficiency of the dryer, as specified in consumed energy per amount of water evaporated, per product produced or at any other reference desired. As the spatial conditions within the feed pellets, at any position in the deep bed are also evaluated, another potential of the model is to evaluate technical quality attributes of the feed, e.g. mechanical durability, nutritional devaluation or structural properties of the extruded feed pellets. As it shall appear from section 6, predictions of spatial temperature- and moisture in the pellets are indeed important parameters in the evaluation of mechanical durability, particular the extent of evaporative cooling. Latter seem to be evaluated well by the model, as the larger portion of the RMSE for the temperature clearly appears when temperature increases after the evaporative cooling. The capabilities of the model to reproduce accurate temperature- and moisture gradients within the pellets are strictly only evaluated, as a function of other validation parameters. Additionally, the actual regional extremes of the cylinder remain hidden, with the assumed spherical geometry. This feature could however easily be reintroduced by evaluating the drying process for a cylinder at certain reference positions in the bed, when knowledge of prevailing airflow conditions are established.

Figure 45 and Figure 46 illustrate some of the output that can derived from the model, simulating the drying of 8 mm pellets for 12 minutes at 15 cm bed depth (e.g. an initial drying zone, a 'zone 1'), using vastly different drying air conditions. Both simulations illustrated use same product and capacity and dries from 21 % to 15 % average moisture, but has different energy efficiencies, as well as spatial temperature and moisture content profiles. This is in sharp contrast to the similar appearance of the average moisture content lines in the two figure / drying conditions. The drying in Figure 45 illustrate the drying using hot and dry air at 140 °C flowing at a low velocity through the bed depicting average temperature and moisture content as well as center- and surface temperatures and moisture contents, for pellets positioned at both air inlet and air outlet positions. This roughly exemplifies a dryer without internal recirculation of drying air, using a low velocity of the air to "maximize the utilization of the drying air through the bed"; a common misperception in the industry [20]. It follows that 1.06 kWh is used to evaporate 1 kg water, i.e. energy efficiency is 60 %, when compared to the latent heat of water at average surface temperature. Temperature of the pellets at the exhaust side of the bed becomes low, due to low air velocity (and obviously, a corresponding low air temperature at the exhaust side). Figure 46 illustrate the same product being dried to the same average moisture content, applying internal recirculation of drying air that increases humidity and velocity. The air temperature is lowered until the same average moisture content is obtained as in Figure 45. It follows that the specific energy efficiency are 0.82 kWh/kg water evaporated, or 77 %. The humidity and air velocity used in Figure 46 imply a ratio of recirculated airflow / exhaust airflow at 6.0.

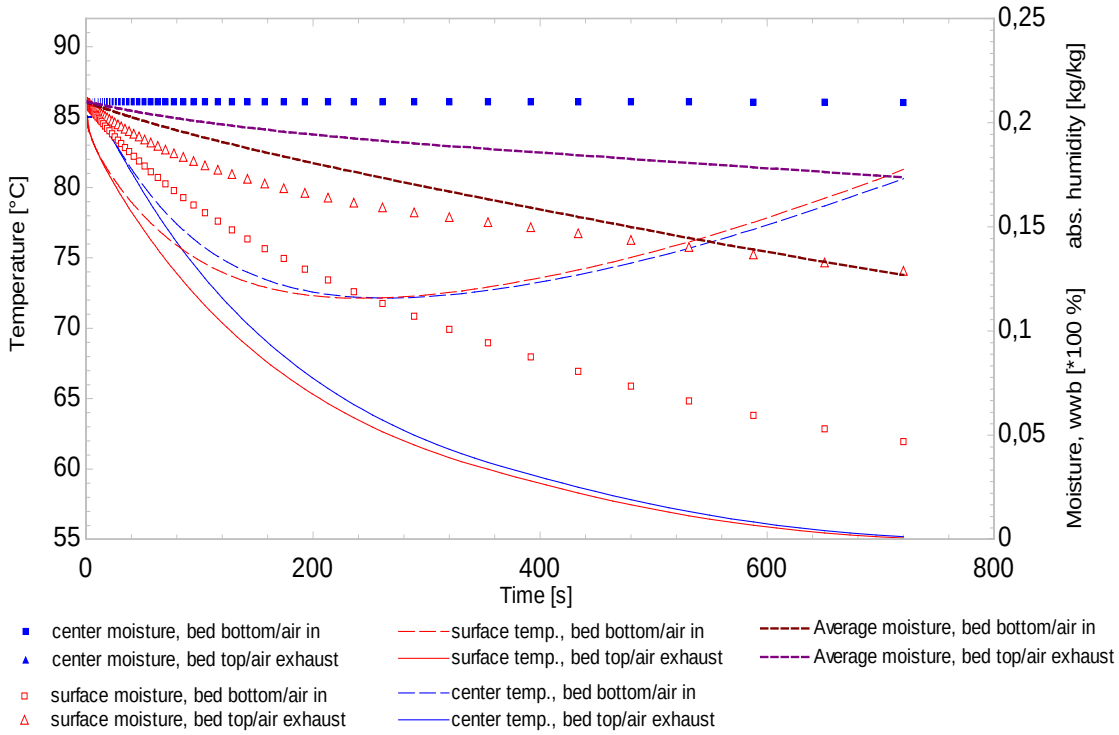

Figure 45: A 'zone 1' drying at low air velocity using hot, dry air. Bed depth=12 cm, v=0,25 m/s, T=140 °C, Y=0,008 kg/kg, d=L=8 mm, X_i=21 % (w.b.), X_o=15 % (w.b.). Energy efficiency is 1.06 kWh/kg or 60 %.

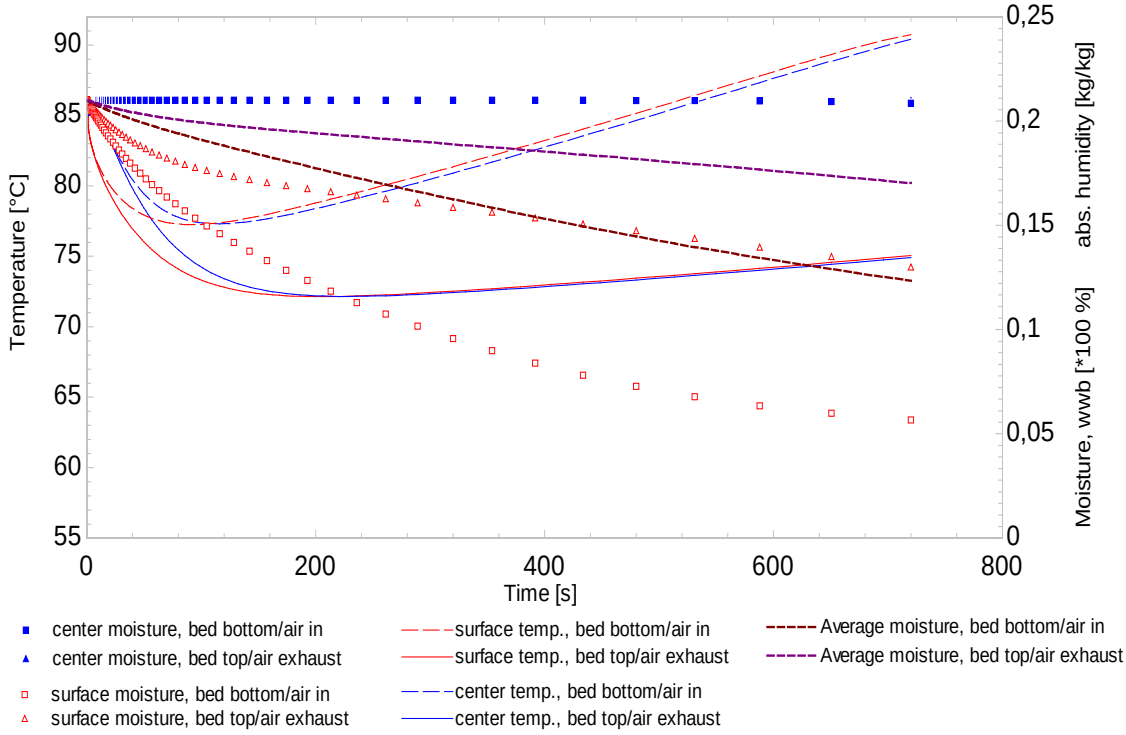

Figure 46: A 'zone 1' drying at high air velocity using humid air. Bed depth=12 cm, v=0,75 m/s, T=107 °C, Y=0,080 kg/kg, d=L=8 mm, X_i=21 % (w.b.), X_o=15 % (w.b.). Energy efficiency is 0.82 kWh/kg or 77 %.

It is interesting to notice that for both drying conditions used, drying does not initiate at the center of the pellets, whereas evaporative cooling of the surface surely imply a lowered temperature – also in the center (which in turn lowers the local moisture diffusivity). The rate of convective heat transfer will determine the extent of cooling of the pellets, at surface as well as in the center. Clearly, a high convective heat transfer rate, from using high air velocities, imply an increase in the obtained minimum temperature. Furthermore, it is found that spatial temperature gradients in the pellets are generally equilibrated earlier, when using humid air at high velocity, compared to using hot air at high temperatures. Despite using 140 °C dry air at low-velocity, no pellet temperature above 85 °C is found anywhere in the bed, in this stage / 'drying zone 1'.

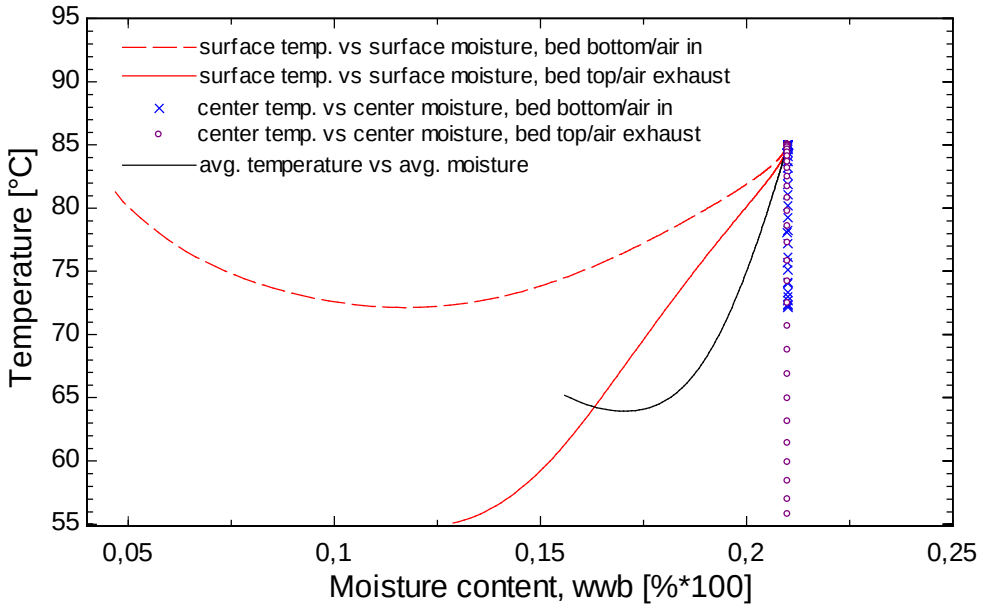

Figure 47: Local temperature versus local moisture content for the drying in Figure 45 using dry, hot air at low velocity

Figure 47 and Figure 48 visualizes spatial details of the product dried in Figure 45 and Figure 46, respectively, by plotting temperature as a function of moisture content, throughout the drying. The plot includes global bed averages, but also local extremes (surface and center) for pellets in bottom (air inlet) and top (air exhaust) of the bed. Clearly, the local details in the pellets deviate significantly from the average values. Again, by comparing Figure 47 and Figure 48 it is clearly seen that the high convective heat transfer rate (high velocity), strongly counteracts the effect from evaporative cooling, effectively increasing the minimum temperature obtained by the pellets, during the drying. This effect can also be retrieved from Figure 49 that visualizes energy distributions for the two different dryings. Here, the lowering of the pellet temperatures actually contributes energy to the overall drying process; yet, the energy efficiency is inferior when compared to the drying using humid air at high velocity, i.e. applying internal recirculation of drying air.

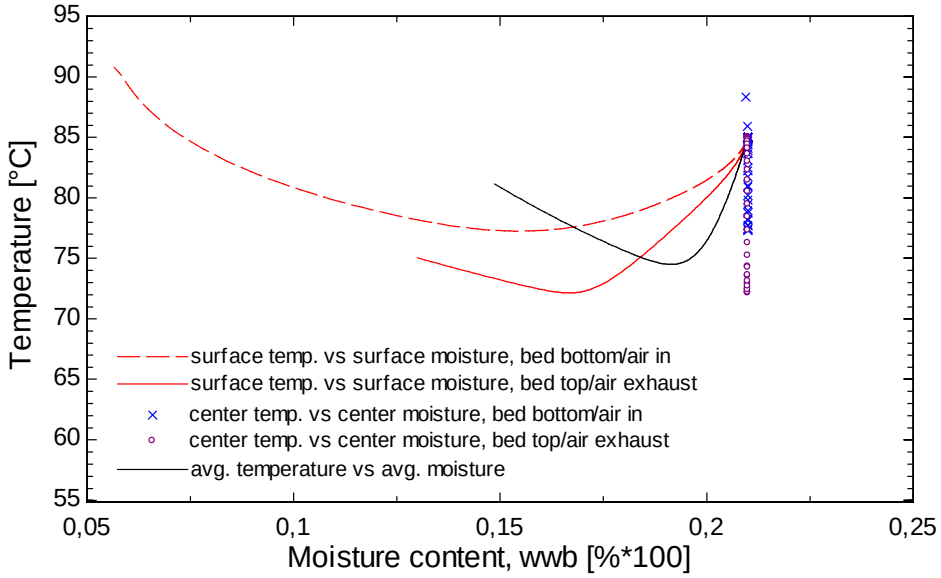

Figure 48: Local moisture content versus local temperature for the drying in Figure 46 using humid air at high velocity

When using dry, hot air at low velocities the energy efficiency is significantly lowered from a large amount of energy allocated to heating the air, despite some energy is obtained from the pellets and their residual water content. This is illustrated in the right hand side bar plot in Figure 49.

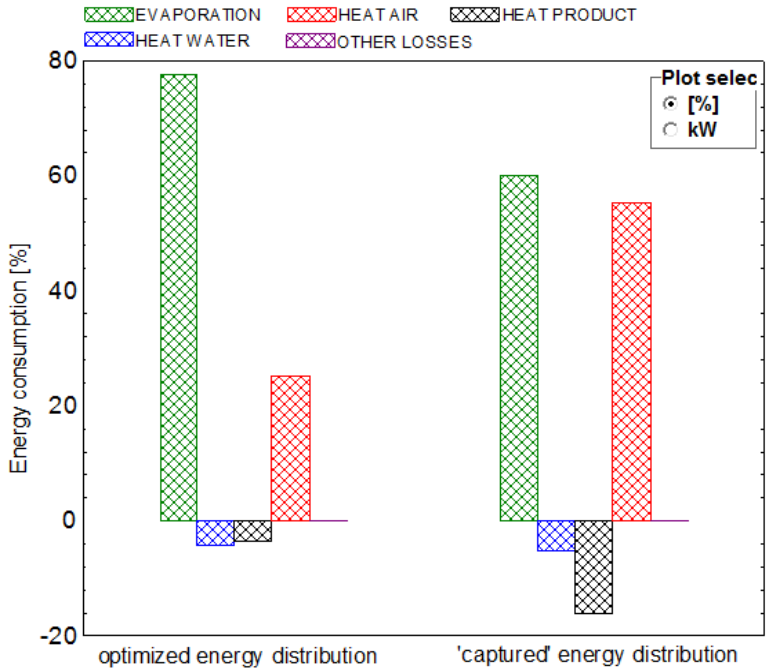

Figure 49: Energy distribution for the two different 'zone 1' deep-bed dryings in Figure 45 (right) and Figure 46 (left). The energy consumption (in percent) that is used to evaporate the water

At present stage, the deep-bed drying model does not encompass electrical power estimates for exhaust and recirculation fans, motors, gears, drives, dampers, etc. For example, in the two different approaches outlined above, for the 'zone 1 deep-bed drying', an increased electrical fan power required for providing internal recirculation of the air should be significant. With reference to the discussion in the background section, comparing thermal and electrical

power consumption in fish feed production (Figure 8, page 10), this aspect is at present stage disregarded in the model. If characteristic fan curves are provided for the recirculation/exhaust fans, it should however be relatively simple to estimate additional fan power required to provide air recirculation inside the dryer cabinet. Disregarding this aspect (at current stage of the model) is additionally motivated by that inherently different airflow and fan setups are used at different production sites, and often exhaust fans are not equipped with VFDs to realize electrical power savings, e.g. at reduced airflows.

The model encompass a single temperature zone at a fixed bed depth. By sequencing multiple models, reusing model output as new initial conditions will allow the model to reproduce large-scale industrial dryers with multiple belts and temperature zones with changing airflow directions. Sequencing multiple models into a commercial software tool for the complete simulation of commercial dryers with multiple heat zones and multiple stages should be subject to future work. The programming package should handle logic commands well, to be useful for handling the multi-stage nature of the complete dryer, as well as the outside process level loops to allow for either internal zone-wise, or external overall recirculation of drying air.

The resolution time for the deep-bed model for pellets with assumed spherical geometry is currently 187 – 218 seconds, using 10 nodes in the product radius and 10 nodes in the bed height, when computed on a 64 bit windows laptop with an Intel Icore i5 CPU at 2.6 GHz with 4 GB RAM installed. The range arises from that the computation time can be reduced, when initial value estimates are improved. The stated times corresponds to the resolution of a single 'process level' iteration loop, finding pellet moisture content and temperatures, at a given bed inlet air conditions. Three process level iterations will bring the total computation time to 9-11 minutes. This time exceed the targeted 4-minute threshold, however it is significantly shorter than the resolution time of an equivalent model by García-Perez et al. [101], at 36 minutes, using similar discretization, however at 70 % of the stated computer power. It is evaluated that severe improvement of computer power could reduce the resolution time, to a level closer to the 4-minute threshold. When combining process- and bed level models, the performance of the model could additionally be improved by specifying an allowed amount of process level iterations, when recirculating the drying air. This procedure should be subject to further work. This becomes particular relevant when multiple model segments are combined into a commercial type dryer software, to simulate the deep-bed hot air drying process of extruded fish feed in industrial scale dryers with multiple belts and drying zones.

The model includes process level considerations of applying internal recirculation of drying air, to improve energy efficiency. Optimization of energy efficiency can effectively be realized using a minimization algorithm of the burner load, provided constrains of dryer dimensions, product moisture and capacity and allowing one or more drying parameters to be free variables in the optimization. The presented model serves as a platform to provide this opportunity; actual optimizations have not been carried out in the present project.

5 Technical quality of extruded fish feed

5.1 Physical transformations in the drying process

Spatial and temporal description of product temperature and moisture content, as well as temperature and humidity of drying air, gives a complete description of drying efficiency, drying time and dryer capacity. Hence, impacts from drying conditions, configuration or even design specifications of the dryer can be analyzed. This do however not contribute to an understanding of physical or chemical transformations to the product, as a response to the exposed set of drying conditions. In the mathematical model of the drying process, shrinkage has been disregarded, and its effect was effectively lumped into transfer and surface exchange coefficients, from regression analyses. It should however be of imminent importance to address the influence of shrinkage when evaluating product transformations in the light of evaluating product quality aspects, during the drying process. This section review current knowledge on physical properties of food and biomaterials, during hot air drying, with particular focus on the most important phenomena that should govern product transformations, crack evolution and failure.

Important physical properties of dehydrated biomaterials are porosity, pore connectivity, surface exchange area, tortuosity, isotropicity, glass transition temperatures, and density. Ideally these hygrophysical properties should influence technical quality indicators like rehydration capacity, wettability, mechanical properties and durability [115].

Dissa et al. [116] and Schmalko et al. [117] use a very simple approach of monitoring product density, shrinkage (isotropicity) and porosity in the drying of cylindrical spirulina samples. Shrinkage and density are found by continuous measurements of mass and product dimensions. Porosity, shrinkage and shrinkage isotropicity are found from relations given by Eq. 74, where S_B is shrinkage coefficient, S_{iso} is shrinkage isotropicity, β is porosity, t is time, V is volume, V_0 is initial volume, ρ is density, ρ_0 is density of the solid material and d and L are diameter and length of the cylindrical product [116].

$$S_B = \left(1 - \frac{V(t)}{V_0}\right) \qquad S_{iso} = \frac{\frac{d_0 - d(t)}{d_0}}{\frac{L_0 - L(t)}{L_0}} \qquad \beta(t) = 1 - \frac{\rho(t)}{\rho_0} \qquad \text{Eq. 74}$$

May and Perré [118] and Dissa et al. [116] related the drying rate against actual and initial surface exchange area. They found that the transition from constant-rate to falling-rate drying could only be verified if the drying rate is related to the actual surface exchange area. Hence, critical moisture content of the product could be determined with good accuracy using this approach. Interestingly, they showed that porosity evolution for the majority of biomaterials is occurring primarily at low moisture contents. This also means that shrinkage largely can be expected to occur in the constant-rate phase with high product moisture contents. This was generally confirmed in that shrinkage was highly anisotropic and nonlinear, particularly for large diameter samples. May and Perré [118] found that radial shrinkage is

predominant for carrot and apple samples, longitudinal shrinkage is predominant for potato samples, whereas shrinkage occur isotropic for avocado. Dissa et al.[116] also found longitudinal shrinkage predominant in the drying of spirulina samples. Hence, it is difficult to deduce any pattern on shrinkage isotropicity in the drying of cylindrical samples.

In the drying of rice, it has been suggested that failure and crack formation occur from moisture content gradients within a single grain, causing tensile and compressive stresses. Solid materials will generally be more prone to failure, following tensile rather than compressive stresses [115]. During the drying process, the surface will naturally dry at a faster rate than the kernel, causing tensile stresses at the surface. For this reason, fissures could start to emerge at the surface during the drying process, if the stress exceed the material strength [119, 120]. At the end of the drying process, there will be a moisture migration from the moister kernel to the dryer surface. If the kernel shrinks in this process, compressive stress in the kernel will direct further tensile stress towards the outer layers of the material [121]. For a solid phase that allow complete stress communication, stress gradients within the material should be leveled out from the water migration and from solid phase mobility (shrinkage). Obviously, as moist biopolymers are dehydrated, they will per definition loose phase mobility, from loss of water that act as plasticizer in biopolymers [122].

According to Slade and Levine, the glass transition theory of biopolymers [123] imply that a change in state of the material – from rubbery to glassy – can occur during processing or storage. The transition will occur at the glass transition temperature, θ_g, which is as strong function of the plasticizer (water) content that imparts local mobility of adjacent large polymer chains. Generally, θ_g will increase with decreasing plasticizer content. This imply that during the drying process, an initial rubbery biopolymer could be turned glassy by removal of water or by decrease in temperature. The phase change will imply significant changes in viscoelastic properties of the material. Particularly, viscosity of the material could rise by a factor of 10^5 Pa s [115]. This implies that shrinkage will only occur in the rubbery phase at temperatures above the glass transition temperature at the prevailing moisture content. Due to spatial moisture and temperature gradients arising within the material during drying, the onset of glass transition through the material will also have a spatial gradient. This applies equally to downstream processing steps, if glass transition occur at temperatures below those achieved in the drying – yet gradients might be less significant. Non-uniform shrinkage followed by a gradual loss of phase mobility complicates the prediction of surface tension and failure of the dried material. From above considerations, it should follow that stresses in materials, during drying, can be minimized by:

- Using drying temperatures well *below* the glass transition temperature, essentially drying in the glassy state [115].
- Using low drying rates (e.g. high humidity) at temperatures well *above* the glass transition temperature to allow phase mobility and shrinkage during dehydration. At surface glass transition onset, the drying rate should be lowered by also lowering the temperature [120].

The two approaches mentioned above are obviously quite different. Already in 1971, Ban investigated the use of high temperature drying of moist rice (18 – 24 % w.b.). They found

that drying at 130 °C to a moisture content at 13.5 % and subsequently lowering the air temperature, produced the least amount of fissures. Crossen and Siebenmorgen [124, 125] further demonstrated that the level of fissuring in rice can be significantly reduced by including tempering periods to equilibrate spatial gradients in moisture content, while strictly remaining in the rubbery phase. They emphasize that tempering phases applied in the drying should be relatively long. If tempering phases are (too) short and intermittent, glass transition could be initiated in the center of the material, which is believed to cause high level of crack formation [120]. Siebenmorgen have determined glass transition temperatures of two different rice varieties using dynamic mechanical analysis, DMA. These appear from Figure 50. The points indicate an observed transition to the glassy state. Below the line formed from connecting the points (the glass transition temperature curve), the rice will be glassy, and above the line, the rice will be 'rubbery'. As it appears from the inaccuracy of the measurements, there should be a significant transition phase around the proposed glass transition temperature curve. Red and blue dashed lines have been added by the author of the present thesis, to roughly illustrate the two approaches mentioned above. When drying in the glassy state (freeze-drying being the radical example) the porosity of the product will be high, as no (or little) shrinkage will occur. Oppositely, when drying in the rubbery phase, a high degree of shrinkage should be expected, and the porosity of the dry product will be significantly lower. Demands to the product characteristics should therefore also be included when evaluating the two distinct strategies. A high porosity should allow for large quantities of post-processing adsorbates (e.g. lipids) to be added to the product, but the break strength of the product could be expected to be lower than a denser product, dried in the rubbery phase.

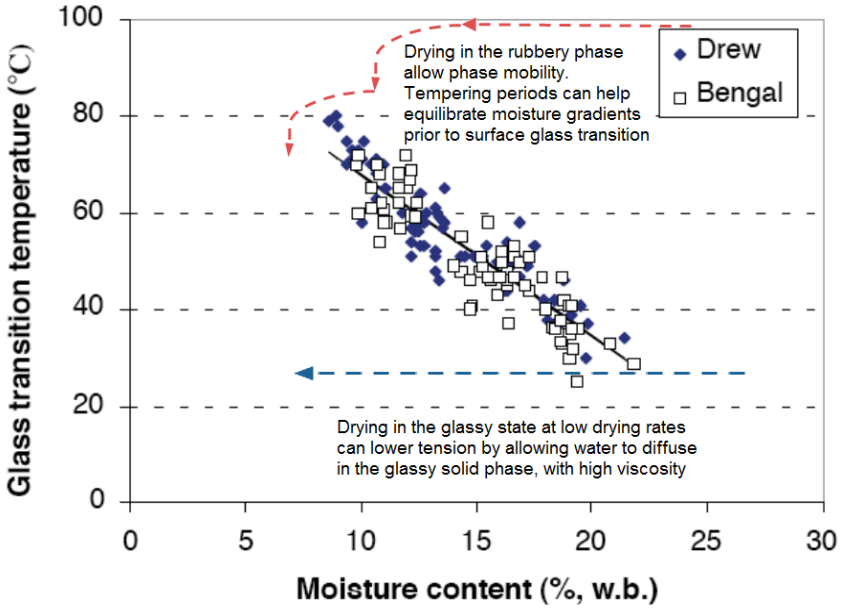

Figure 50: Example of experimentally obtained glass transition temperatures for two different varieties of rice kernels ('Drew', 'Bengal') at different moisture content[126]. The inserted red and blue lines represent two distinct approaches to minimize fissures, i.e. drying in the rubbery or in the glassy state. Adapted from Prakash [120].

Boudhrioua et al. [127] have investigated changes in the texture of bananas during drying as a response to ripeness and drying time. They used a texture analyzer to correlate hardness of

bananas and drying time. They found that radical change in textural properties of bananas occurred at a certain drying time; the bananas lost their deformability and became fragile and brittle. They confirmed by DMA that this is related to elevation of the glass transition temperature following the loss of plasticizer (moisture). When the glass transition temperature rises above the storage temperature, the bananas remained brittle and 'glassy'. Hence, in the drying process it should be important to possess knowledge on the entrance of the product into the glassy state, in order to optimize drying conditions for the altered structural and physical properties. When the surface has entered its glassy state, but the center part is still mobile and rubbery, enforcing a high drying rate will increase compressive and tensile stresses in the product, increasing the risk for material failure [120]. Hence, it follows that in ideality the material should spatially enter the glassy state at the same time. This is supported from that smaller materials will have fewer material cracks and fissures during the drying, in proportion with their characteristic length and time-scale of internal diffusion [115].

Achanta and Okos [115] describe in their review on predicting quality of dehydrated food, that the transition into the glassy state in drying processes is also largely responsible to the formation of 'crust' on the dry product surface. This is due to that the dryer surface will pass into the glassy state before the center of a product, which will greatly reduce moisture diffusivity and therefore decrease shrinkage. Crust formation (or "case-hardening") will therefore turn a homogenous material into a composite material consisting of a dry, dense crust and a more moist and porous center. They describe that crust formation will generally take place, when high drying rates were used to transcend through the glassy state, whilst a thicker and less dense crust can be expected if drying (or product) conditions is used to prolong the period in the rubbery phase, and transcend to the glassy state at lower drying rates. They repeat that biomaterials will shrink until they pass into the glassy state. Beyond this point evaporated water are replaced by air and the product will become more porous. At this point, drying can also be expected to increase tension in the material, due to mass transfer in the immobile glassy solid phase.

Katekawa and Silva investigated in 2009 [128, 129] how the glass transition phenomenon influences shrinking kinetics in their case study on the drying rate of banana. Their objective was to demonstrate that shrinkage stops when glass transition occurs at the pellet surface. They compared product sorption isotherms and correlations for glass transition temperatures to find the surface glass transition temperature at a given set of drying conditions (temperature and relative humidity), using product desorption isotherms to find equilibrium moisture content at the surface, given specific drying conditions. From Figure 51 it can be found that the surface glass transition point occur at 20 °C and 0.11 g/g moisture, when drying at 30 °C and 40 % relative humidity – and therefore the transition does not occur during the drying. Likewise, it can be found that the relative humidity of the drying air should be at least ~14 % at this temperature to ensure a glass transition temperature of 30 °C, which should just allow the sample to remain in the rubbery state throughout the drying, promoting phase mobility and shrinkage to reduce surface tension. Conversely, the drying temperature would have to be ~46 °C to ensure drying to proceed in the rubbery phase, if dry air is used.

This approach can therefore be used to find a target air humidity and/or target drying temperature, to remain in the rubbery phase, or to engineer a particular desired onset of glass transition given a targeted product moisture content.

Figure 52 shows the drying of banana samples using dry air at 30 °C. Here it is demonstrated that at the point where the temperature of the product falls below the glass transition temperature, shrinkage is indeed hindered as the surface has passed into the glassy state, and there will subsequently be a risk to form a dense crust at high drying rates (i.e. to cause 'case-hardening'). Obviously, 30 °C is a low temperature in many hot air drying processes. Fruits are often dried at these low temperatures to preserve nutritional value, and as in above study, to avoid gelatinization of the banana starch. Gárcia et al.[130] have investigated glass transitions temperatures for whey protein/cassava starch systems. For such systems glass transition temperatures exceed 80 °C at a moisture contents around 10 % and approach 120 °C at 5 % moisture content. This interval is more than likely to interfere with the temperatures conventionally used in the hot air drying of extruded fish feed pellets.

Despite the seemingly coherence between shrinkage, glass transition temperatures, onset of the falling-rate phase and critical moisture contents no clear connection has been made between these phenomena and product characteristics. Critical moisture content is used to describe when the drying flux drops, whereas the transition into the glassy state will just be one

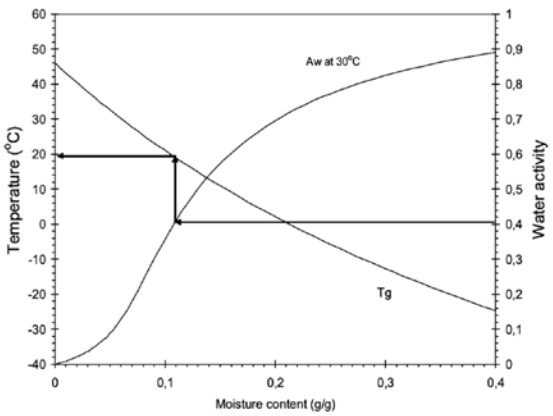

Figure 51: Sorption isotherm and glass transition temperature vs moisture content for drying at 30°C and 40 %RH [128].

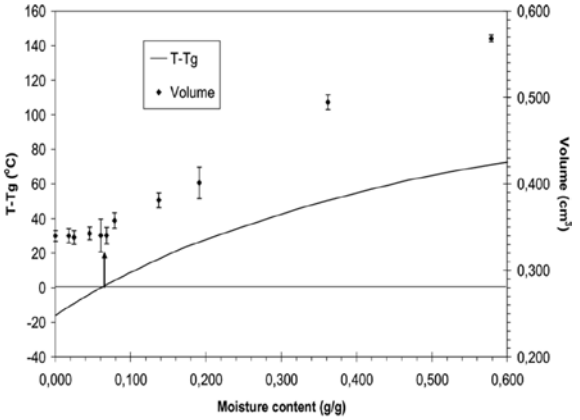

Figure 52: Shrinkage of banana stops (constant volume), once the glass transition temperature reaches the drying temperature at the relative humidity (here 0 %RH) [128].

phenomenon (among several) that contributes to this effect. Hence, it is not evident if one governs the other or if they act independently.

Kowalski [131] presented in 2010 a thorough study on the mechanical aspects of drying cylindrical capillary-porous materials with special emphasis on drying-induced stresses, which create deformation and crack propagation in the product. The author aims to describe these matters using mathematical modelling, and in particular by monitoring the 'acoustic emission' of the product. Acoustic emission is the analysis of acoustic waves released due to rapid release of elastic energy accompanied with deformations, glass transitions, crack formation etc. This has the advantage that drying rate can be increased in periods of little acoustic emission and vice versa. A conventional ternary conservation model is used with a Darcian

approach to describe the moisture transport and Fouriers law for the energy transfer into the material. Momentum conservation equations and a conventional relation that describe stress and strain evolution in an elastic material are used to address radial, longitudinal, circumferential and shear stresses as well as displacements in the product. The results from the mathematical modelling of stress evolutions are compared to the results obtained in the acoustic emission analysis. Interestingly, it was shown that the acoustic emission signal strength and the computed evolution of circumferential stress at the cylinder surface corresponded surprisingly well. This is illustrated in Figure 53 and Figure 54.

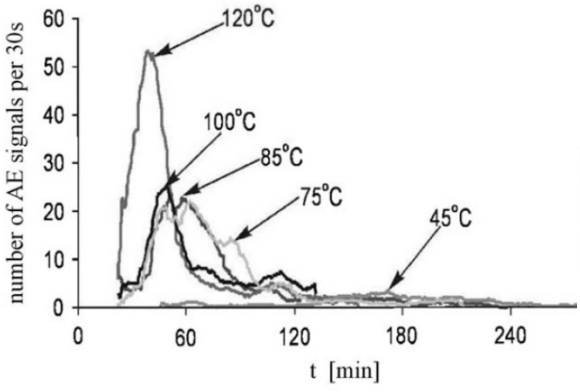

Figure 53: Acoustic emission measured in a cylindrical capillary-porous material as a function of time [131].

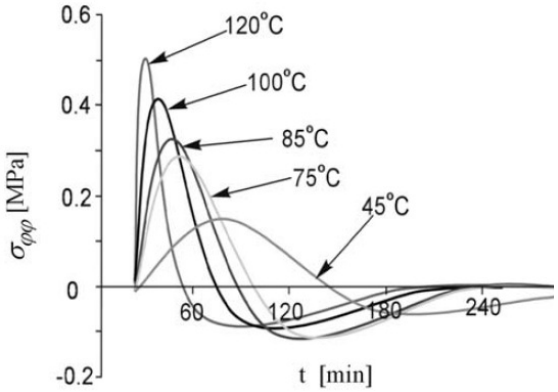

Figure 54: Circumferential stress, $\sigma_{\varphi\varphi}$, at the surface of a cylindrical capillary-porous material computed by a mechanistic model as a function of time [131].

The authors use an energetic strength hypothesis to predict failure and crack propagation in elastic materials. This means, that if the overall stress level experienced by the material supersedes the admissible stress of the material, fracture will occur. This supports that crack propagation occur when surface tension exceeds the pellet's tensile strength. They found that when drying an elastic material, a high drying rate (~temperature) will cause the largest stress levels. However, the drying of an elastic material, will largely describe the drying in the glassy, immobile state of a biopolymer, i.e. per definition no viscous force relaxation is allowed (as in the rubbery phase). Therefore, the studies by Kowalski et al. actually supports the hypothesis, that applying high drying rates after passage into the glassy state will increase stress and tension in the material, from reduced phase mobility, i.e. 'shrinkage' [65, 131]. In a later study, Kowalski and Rybicki have indicated that the stress build-up, during the drying of viscoelastic materials are significantly less than for the drying of elastic materials [132]. This suggests that certain structural properties should give less stress build-up during the drying, and therefore have superior mechanical durability. This provide motivation for investigating those structural properties of extruded fish feed pellets that could demonstrate good mechanical durability.

5.2 Characterizing technical product quality of extruded fish feed

The quantity of raw material ingredients that are lost and dispersed to the aquatic environment, rather than directed towards ingestion by the fish, are caused by lack of technical quality. It is reiterated that technical quality of extruded fish feed is a nomenclature encompassing several characteristics that describes a pellets ability to: [30, 31, 133]

- Endure mechanical stress during transport, handling and feeding without losing mass.
- Have density, geometry and size to ensure intended sinking properties.
- Have a moisture content to biologically secure product during storage and transport, and ensure intended oil adsorption.
- Be stabile when suspended in water.

Density, dimensions and water stability are important pellet characteristics for the final 'technical quality'. Density and dimensions depend however largely on the extrusion and oil coating parameters, when considering a constant moisture content out of the dryer. Also, it has been reported that the water stability is not influenced from the drying process [5]. The feed loss from post-processing attrition accounts for a large part of the total feed loss, and it is acknowledged that here exists an inherent dependency on the drying process [16, 17]. This attrition following mechanical stresses can generally be separated into contributions from abrasion-, collision- and compression type forces. Quality assessment of attrition generally seek to mimic the extent of one or more of the effects that a pellet is exposed to in its post-processing lifetime [9, 16, 31].

Thomas and van der Poel [27, 134, 135] have reviewed methods for assessing post-processing attrition of pelleted animal feed, and give a general recommendation to distinguish methods that address either 'hardness' and 'durability', separately. This is reasoned from that their results will not necessarily provide the same conclusion towards the physical state of a product – i.e. this will depend on the actual application and criteria for the product in question. Furthermore, in each of these categories several subgroups exist.

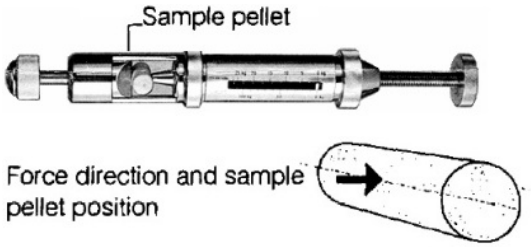

Figure 55: The Kahl pellet hardness tester apply static force, and the break force can be read [134]

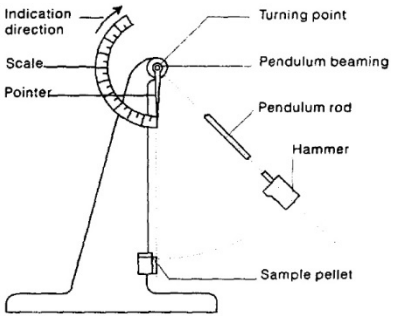

Figure 56: The pendulum pellet hardness test device apply dynamic force [134].

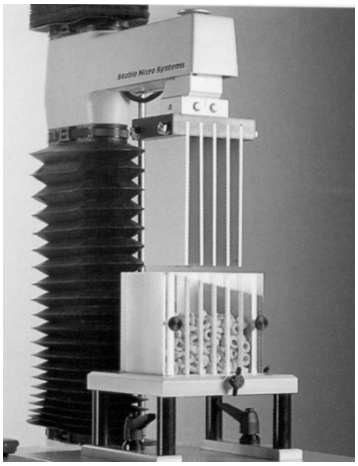

Figure 57: A Kramer shear cell attached onto a texture analyzer (picture: Stable Micro Systems Ltd)

Pellet hardness can be quantified as the force necessary to crush the pellet, and is conventionally carried out using a 'Kahl test device' (Amandus Kahl GmbH) or a texture analyzer [9, 31]. This has importance for enduring loads in silos and big bags, without leaking adsorbed fat. The durability effectively quantifies the amount of fines created (e.g. < 2.5 mm) when the pellets are exposed to a certain amount and type of mechanical stress. The tests is more often carried out in post-production, but can also be done in situ, particular for larger production runs. For testing hardness, static or dynamic force can be applied; the most distinct apparatuses here are the 'Kahlen' and the 'pendulum' pellet hardness test devices, Figure 55 and Figure 56. These devices share that the mode of operation is for a single pellet and that the force is applied at a single fixed point causing axial or radial tension only (depending on pellet position). Hansen and Storebakken [136] applied in 2007 a 'texture analyzer' for investigating hardness of individual extruded fish feed pellets. Texture analyzers can be equipped with a number of different probes and test rigs, including also the Kramer shear cell, which allows testing of multiple pellets simultaneously. Here, force is applied at variable positions, causing both axial and radial tension, cf. Figure 57.

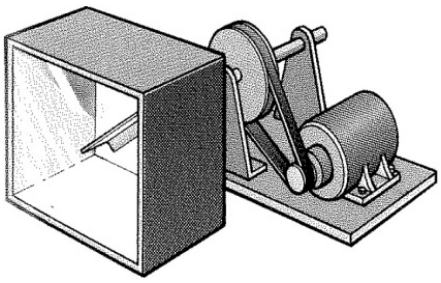

Figure 58: Pfost tumbling box device for measurement of pellet durability. Typical settings: 10 minutes at 50 rpm [134, 137].

Figure 59: DORIS tester for measuring durability against mechanical handling. 'Single-pass' system [9].

Figure 60: The Holmen pellet durability tester. Pellets are transported pneumatically around in a closed circuit (http://www.tekpro.com/nhp200.html).

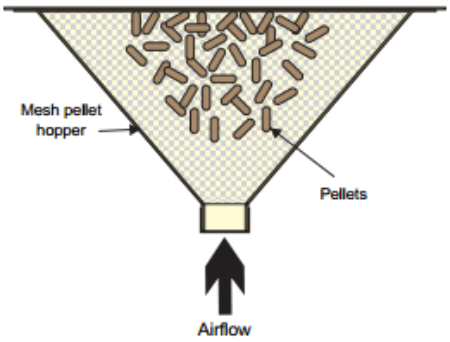

Figure 61: In the Holmen tester, generated fines can be taken out continuously from the installed mesh pellet hopper (2.5 mm).

Durability tests / simulators are particularly common in the fish feed production industry. Some research groups have even built large sections of bulk transportation systems, trying to reproduce the actual stress that the finished product will experience [22]. ASAE Standard S269.4 [27] for testing durability of feed pellets is based on the Pfost 'tumbling box' method, cf. Figure 58. This is strictly the only standardized method for testing durability of feed pellets, yet very few fish feed producers are using this. Sørensen et al. [15] have indicated, when investigating the effect of nutritional and extrusion parameters, on the physical quality of extruded fish feed, that the Pfost tumbling box could not be shown to unveil the same variation in durability pattern as the Holmen durability tester. The DORIS tester (Akvasmart, Bryne, Norway), Figure 59, and the Holmen pellet durability tester (Borregaard Lignotech, Rothschild, USA), Figure 60 + Figure 61, are the two candidates for testing durability of fish feed that are being used in industry [7, 8, 20]. They both aim to replicate part of the post-processing attrition that feed pellets are being subjected to in their lifetime. The DORIS tester uses a rotating paddle that accelerates pellets into a wall. Ultimately, the pellets are collected in a sample collector bin. The DORIS tester will primarily measure the fragmentation of pellets arising from pellet-wall collisions, and is less specific towards abrasion. The Holmen tester has a higher specificity towards mechanical abrasion of edges and corners of a feed pellet for pellet-pellet interactions, but quantifies less of the potential fragmentation

induced from collisions, which are relevant in pneumatic transport and bulk handling. The DORIS tester showed good correlation against durability obtained in a feeding facility, when originally developed [138]. Other research groups have indicated that the DORIS tester seems to correlate well with actual durability obtained from feeding trials, when sampled from some regions in a big bag (i.e. middle section), but not in others [9].

The Holmen tester has sometimes been criticized for measuring too high pellet durability indexes (meaning very durable pellets), owing to its predominant abrasion-type attrition, which for some feed transport modes (i.e. pneumatic transport, bulk handling, silo loading, etc.) will represent the smaller part of the combined attrition [9, 31]. Conversely, when the DORIS tester sometimes get critique to mismatch with customer-experienced durability, it is very likely that the governing attrition in the transport and handling is owing to abrasion; e.g. bagged feed.

Pellet durability has a dependency on storage conditions and – time. Cooler temperatures generally invoke stronger binding interactions from an increased viscosity of the feed matrix, whilst storage time (> 1 month) has been reported to negatively influence attrition owing to abrasion, i.e. durability as measured in the Holmen test [139]. This sometimes makes feed complaints difficult to handle, as feed aboard an open deck containership could easily be exposed to high temperatures and long transport times.

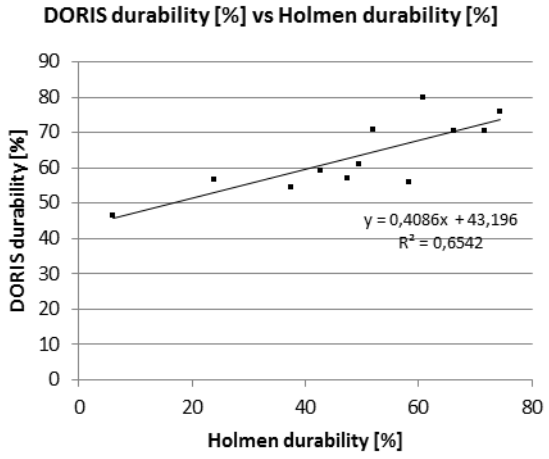

Figure 62: Correlation between durability measurements, when quantified using DORIS and Holmen test apparatuses. Data is from [14].

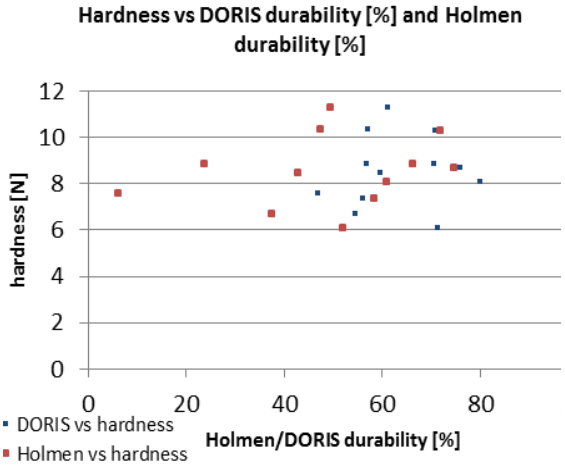

Figure 63: Connection between hardness value (using a texture analyzer) and durability. Data taken from [14].

Feed with admitted claims will often be subjected to a DORIS test and the hardness of the pellets will often be measured afterwards, in trying to identify connections and explanations. This is very often done using the Kahl tester [31]. Presently, there is not a good agreement whether the fragmentation of the pellets into smaller particles and fines, are connected with the hardness of the pellets. A few studies have indicated some coherency between hardness and durability [9, 134], whilst other studies have indicated that the correlation between hardness and pellet abrasion/durability is weak [5, 140, 141]. Sørensen found in another study in 2011 [14] that the correlation of durability, when measured between DORIS and Holmen tests were reasonably good. This correlation is remade in Figure 62. Results obtained using

the DORIS tester were found to be better in identifying main effects (starch source and extruder screw speed) as governing for durability, rather than the interacting effects. It is therefore pointed out that the DORIS tester is the more appropriate durability tester for coated high energy extruded fish feed pellets [14, 133]. Using the results obtained by Sørensen in 2011 [14] it appears from Figure 63 that there is no transferability on hardness values obtained using the texture analyzer and the measure for durability, using either Holmen or DORIS durability testers.

In 2011 Aas et al. [9] investigated pellet degradation of extruded fish feed pellets, with different physical qualities, in a pneumatic feeding system. They made use of a large-scale pneumatic feeding system with a 20 kW rotary blower connected to an air cooler and a rotary feeder/doser, connected to the feed pipe. This had 12 90° bends and a total length of 400 m. They correlated the results obtained in the large-scale pneumatic feeding system from three different 12 mm pellets to hardness and DORIS- and Holmen durability. Latter performed slightly better in re-finding the results obtained in the large-scale pneumatic feeding system; yet it is concluded that no good correlation can be made.

The governing attrition type for large (heavy) pellets can be expected to be collision-type forces, from their relatively high impact momentum. Conversely, very small and light pellets are expected to be more vulnerable towards abrasion than collision, from their high specific surface area and low impact momentum. Intrinsic binding forces increase with starch content [18, 26], so protein rich pellets can be expected to yield higher attrition than starch rich pellets – this effect should however appear for both abrasion and collision type forces. Above considerations imply, that post-processing effects on large protein-rich pellets are represented well by the DORIS test, particularly when handling feed in bulk. Consequently, the DORIS test should find particular relevance in feed production for salmon and rainbow trout, in their grow-out phase [31], and was selected as the method of quantifying mechanical durability of extruded fish feed, in the present study. A principle illustration of the DORIS test apparatus is provided in Figure 64.

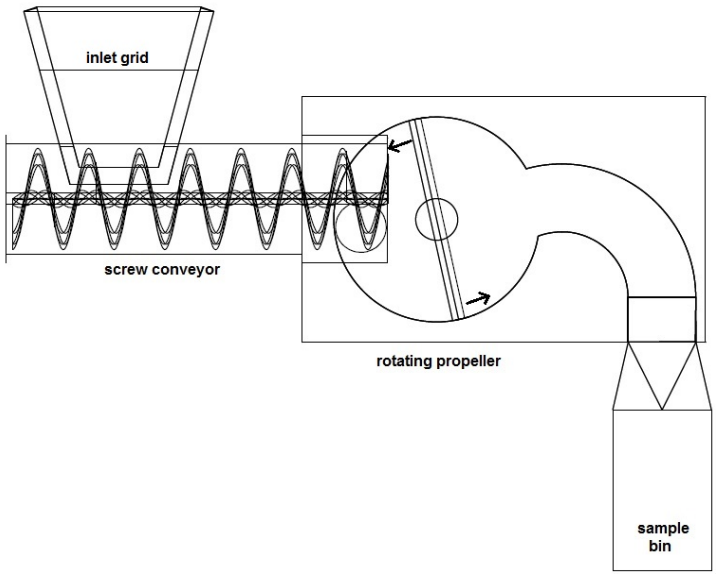

Figure 64: A sketch of the DORIS tester, DORIS tester comprising an inlet grid, a screw conveyor, a rotating fan and a sample collector bin

5.2.1 Application of texture analysis on extruded feed pellets

Hardness has in the fish feed industry conventionally been measured using the Kahl tester [134]. In recent years, this method has largely been replaced with the use of a texture analyzer [14, 136]. Sørensen et al. [133] points out that whilst hardness is often measured with texture analyzers, there is a lack of standardization using this method, as the force needed to crush the pellet obviously should vary significantly with the orientation of the applied force, as well as with the type of probe applied. Not too many thoughts are found in literature on the actual reason behind including 'hardness' as a relevant parameter, in the assessment of technical quality of extruded fish feed. The pellet should be 'hard enough' to endure loadings in a silo, yet a pellet should not be *too* hard, due to the risk of feed indigestion. While texture analyzers have entered laboratories in the fish feed industry, particular as a new tool to measure pellet hardness, little effort has been made in exploring other mechanical properties that a texture analyzer will quantify. Fundamentally, measuring hardness will only have relevance, if that particular mechanical property is of importance in describing the total attrition a pellet will undergo in its post-processing lifetime. From Figure 63 this seem not to be the case, but if other mechanical properties can be found to be descriptive for the mechanical durability, it will be of immediate importance in trying to unravel the effect of drying parameters on the feed durability. A few examples on the application of texture analyzers in other industries are provided in the following.

Texture analyzers were introduced by Bourne in 1978, and is conventionally used apparatus in the food and pharmaceutical industries to assess quality attributes and mechanical properties of many different products. Texture analyzers measures displacement vs. applied force, which elucidates rheological details of a product. Interpretation of the measured force-displacement curve can be used for quantifying a range of different textural properties of a

product [142]. The apparatus is used intensively in the pharmaceutical industry for assessment of hardness and shear strength [143], in the food industry for quantifying rheological and sensory attributes of particular fruits [144, 145] and for assessing structural behavior using Stress Relaxation Tests (SRT) [146-148]. Stress relaxation tests measure a products ability to relax the force applied to it, over long time. Completely elastic materials will show no force relaxation.

Watano et al. [143] introduced the use of the texture analyzer in the pharmaceutical industry for testing hardness of pharmaceutical extruded pellets in 2001, using a knife and a cylinder probe to measure 'shear strength' and pellet hardness, respectively, as a response to different grinding degrees used in the extrusion. Lewicki and Jakubczyk [144] have used texture analyzers to evaluate mechanical properties of apples subjected to convective hot air drying. Multiple samples were subjected to 20 % compression and corresponding stress was recorded, revealing that samples dried at 50-70 °C showed similar hardness and modulus, whereas samples dried at 80 °C exhibited a higher modulus. The authors also recorded stress relaxation (for 180 *s*), to find that samples dried at 80 °C could percentagewise relax most of the stress applied when holding 20 % compression. Mani et al. [145] further expanded on the stress relaxation test using a texture analyzer in their analysis of mechanical properties of biomass pellets from compacted grasses. The stress relaxation curves were normalized and mathematically transformed into a straight line. By this transformation the authors derive an asymptotic modulus, which is "an empirical index for the ability of the compressed material to sustain unrelaxed stresses" [145].

Chong et al. [149] presented their work on mechanical and rheological properties of dehydrated fruits at the 18th International Drying Symposium in 2012 in Xiamen, China. They conducted compression tests using two compression cycles, at slow compression speed to a low level of compression, without breaking the product. This procedure, 'texture profile analysis', TPA, is designed to reflect the behavior of a product while masticating and is often used to quantify quality attributes like chewiness and ripeness of fruits or crispiness of food products, as an alternative to using sensory panels. Modulus and hardness can be directly attained from TPA, but also a range of rheological type attributes can be quantified, like cohesiveness, springiness, fracturability, ductility and resilience. The obtained attributes from TPA are specific to the test parameters used in the analyses. To overcome this dependency, food and pharmaceutical industries, as well as producers of texture analyzers, have tried to standardize test parameters used in TPA analyses of various products in order to avoid the use of test-specific material properties [150-152]. Unfortunately, at the time of writing, no standardized test method could be found. This means that for each application, test parameters should be optimized to maximize the response of a particular test.

TPA and SRT tests will be useful in investigating if a suitable mechanical behavior is characteristic for durable fish feed pellets. If such a connection can be found, this will be important to increase the detail level of analyzing feed durability (if multiple mechanical properties and rheological attributes are of significance towards the obtained mechanical durability). Additionally, this connection could help identify those physical and chemical processes in the drying process, that govern the obtained durability of extruded fish feed pellets.

5.3 Structural properties and mechanical durability of extruded fish feed

An important aspect in the task of relating the influence of drying parameters to the final technical quality of extruded fish feed, is the actual feasibility of measuring improvements in the technical quality, and in particular to ascribe such to the responsible drying parameter. Ideally, a more detailed analysis of the technical quality could reveal footprints, from some of the governing chemical and physical processes in the drying that influence the technical quality in a specific way.

In trying to relate mechanical durability of extruded fish feed to certain structural properties – and to the drying process – the following hypotheses apply:

- The overall mechanical behavior of extruded fish feed pellet can be described using a simple structural mechanics model.
- Mechanical behavior of the pellets gives structural properties that can be quantified using a texture analyzer. Certain structural properties will govern the mechanical durability.
- A specific mechanical behavior of extruded fish feed pellets can be promoted by optimizing parameters in the drying process.

5.3.1 Structural mechanics of extruded fish feed

From classical mechanics it is presumed that mechanical behavior of extruded fish feed can be described from elastic, viscous and possibly also plastic components.

Maxwell materials possess both elastic and viscous properties. In classical mechanics a Maxwell material is modeled as a spring and a dashpot in series [30, 140, 153, 154]. The standard Maxwell model behavior describes the dynamic relation between stress, σ, and deformation, ε, as:

$$\dot{\sigma} = \kappa\dot{\varepsilon} - \frac{\kappa}{\mu}\sigma \qquad \left(\frac{\kappa}{\mu}\right)^{-1} = \tau \qquad \text{Eq. 75}$$

Eq. 75 is written in dot notation, so that $\sigma = \sigma(t)$ and $\dot{\sigma} = d\sigma / dt$; κ is the stiffness of the spring and μ is the viscosity coefficient for the dashpot. There is a time dependency on the viscous component. If a sudden stress is imposed, the resulting deformation will be composed from a rapid elastic deformation and a time-dependent viscous, irreversible deformation. At constant deformation, stress will decay exponentially by the relaxation time, τ.

Kelvin-Voigt materials possess both elastic and viscous behavior [154]. In classical mechanics, a Kelvin-Voigt material is comprised by a spring and a dashpot in parallel. Stress, σ, and deformation, ε, are described from:

$$\sigma = \kappa\varepsilon + \mu\dot{\varepsilon} \qquad \text{Eq. 76}$$

Kelvin-Voigt materials exhibit completely reversible deformations, which exponentially decays towards the deformation for a purely elastic material. On release of stress, the material will exponentially decay towards its reference state.

Maxwell and Kelvin-Voigt materials comprise some important characteristics in the description of mechanical behavior of biomaterials, but also have significant downsides when it comes to predicting the structural behavior of extruded feed. Maxwell materials successfully describe irreversible deformations through viscous stress relaxation; however, deformation is a linear function of time. Kelvin-Voigt materials do not encompass stress relaxation or irreversible deformations. However, for a constant stress, the deformation will inevitably reach some finite value, which obviously is an important characteristic of a solid material.

The 'standard linear solid model' is represented in classical mechanics as a spring and a Maxwell arm arranged in parallel. This allows stress relaxation at constant deformation, and a non-linear time-deformation relation for a constant stress. This type of model could be further expanded to the 'Generalized Maxwell model',

Figure 65, which has several Maxwell elements arranged in parallel. This represents molecular constituents of varying length, each contributing to the relaxation of the material. Shorter molecular segments will relax faster than longer [153-155]. The Generalized Maxwell model with *j* Maxwell arms have dynamics governed by Eq. 77:

$$\dot{\varepsilon} = \frac{\dot{\sigma} + \sigma\sum_j \tau_j - \varepsilon\kappa_{eq}\sum_j \tau_j}{\kappa_{eq} + \sum_j \kappa_j} \qquad \text{Eq. 77}$$

In Eq. 77, subscripts *eq* is the equilibrium modulus of the material and *j* denote the j^{th} Maxwell arm.

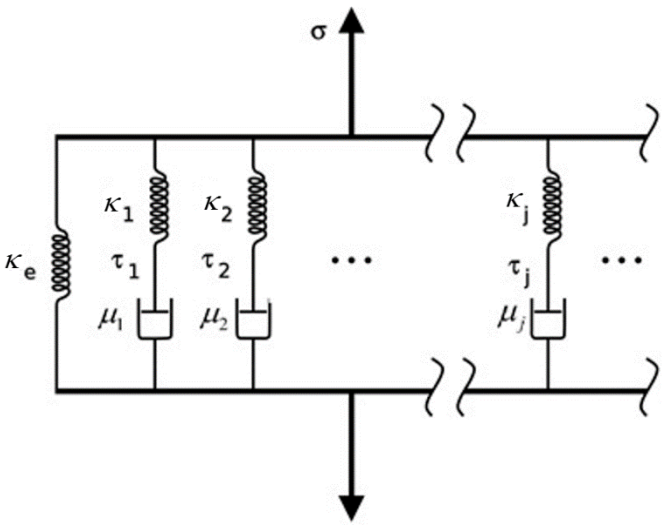

Figure 65: The 'Generalized Maxwell model' for viscoelastic materials [153].

Whereas the Generalized Maxwell model will be very suitable for modelling the behavior of linear viscoelastic materials, it will not account for plastic deformations.

The viscoplastic standard linear model has a parallel slider-dashpot system in series with the standard linear solid model, which will include this effect, cf.

Figure 66 [156, 157]. For this model, there will be a yield stress, F_P, above which a dashpot will contribute with an irreversible deformation [158].

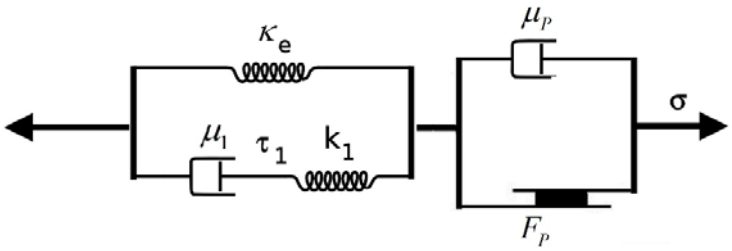

Figure 66: A 'standard linear viscoplastic model' for viscoelastic materials exhibiting plastic deformation at yield stress, F_P. Adapted from Tschoegl [153] and Irgens [157].

5.3.2 Experimental correlation of mechanical durability and structural properties

The mechanical durability has been assessed using the DORIS apparatus and structural properties of the feed is obtained from TPA and SRT analyses, using a texture analyzer [30, 108, 140].

To elucidate the connection between mechanical durability and structural properties, the correlations are made using a range of different types of fish feed. Experimental series was made for extruded fish feed pellets of similar size. Nine different types of 6 mm pellets and six different types of 8 mm pellets, each from two different feed producers, were used for the experiments. Feed types were sturgeon, freshwater trout, rainbow trout, turbot and salmon feeds – all products had been fully processed and were commercially available, yet some had been stored for a few months longer than other had. The feed was kept airtight by double bagging and stored at 17-20 °C between the two sets of experiments. Generally, maximum 24 hours passed from the durability test to the textural analyses for the individual feed types [30]. The texture analyzer (Perten TVT 300-XPH) was equipped with a 100 kg load cell and a 50 mm cylindrical probe, cf. Figure 67. The structural attributes are computed automatically by the Perten TVT texture analyzer software, based on the obtained SRT and TPA force-displacement graphs. For each feed type, measurements were carried out on 24 pellets, using 12 repetitions for each orientation of the pellet, 'vertical' and 'horizontal'.

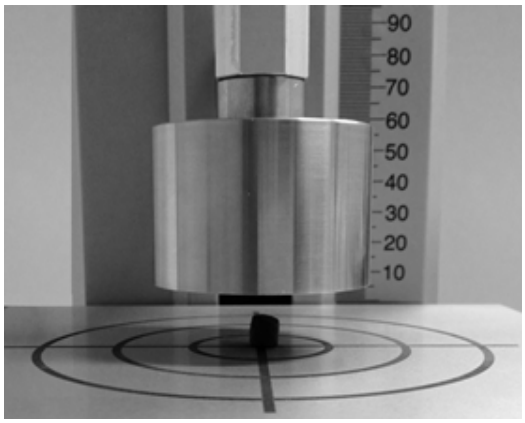

Figure 67: Texture analyzer equipped with a cylindrical probe (ruler in background in mm)

The physical meaning and graphical interpretation of each structural attribute is described below [151]:

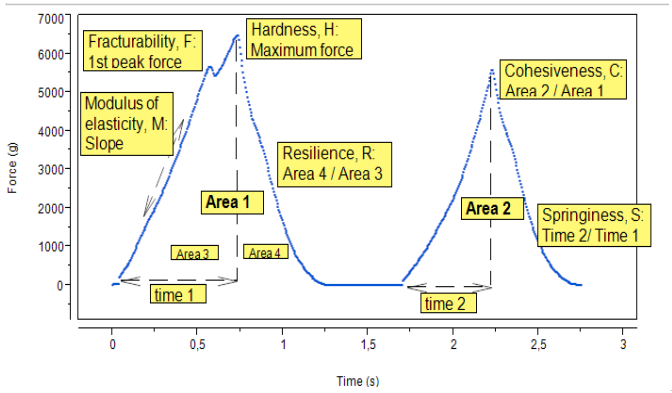

Figure 68: Graph from texture profile analysis, TPA, with designations and calculations of structural attributes.

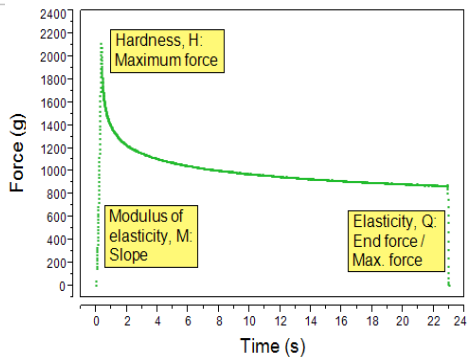

Figure 69: Graph from stress relaxation test, SRT, with designations and calculations of structural attributes.

From TPA, Figure 68:

Hardness: Maximum force recorded. Typically occurs at the point of ultimate compression.

Cohesiveness: Ratio between areas of second and first force-deformation curve. Cohesiveness can be interpreted as the materials' ability to withstand a second deformation, in a specified 'waiting time' after the initial deformation. If deformations are completely reversible, cohesiveness attains a value of 1.

Springiness: Ratio between times for reaching maximum deformation for second and first cycles. Springiness is a measure of how well the pellet physically springs back after a deformation.

Resilience: Ratio of areas under the first force-deformation curve while withdrawing from and while compressing the pellet, respectively. This is a measure of pellet's instant elastic properties, fighting to regain its original position.

Modulus: Can be interpreted as the stiffness of the material, and fall roughly parallel to the hardness, at constant deformation speed (in absence of fracturability). As this falls parallel to hardness, this property is omitted in the screening of effects.

Fracturability: A property that will identify the first crack in the pellet, on deformation. This property does not always appear, and is omitted in the screening of effects.

From SRT, Figure 69

Elasticity: Measured as the ratio between force after a holding time and initial force at ultimate compression. A completely elastic material will retain the initial force exerted onto the load cell whilst most biomaterials are expected to exhibit some plastic and/or viscoelastic stress relaxation, and therefore have 'elasticity' less than unity.

For additional experimental details, reference is made to research in this area by Haubjerg et al. [30, 108, 158].

Structural attributes obtained from TPA and SRT were subjected to a screening test to identify those that statistically could be shown to explain most of the variation in mechanical durability. This was done by fitting a linear regression model in the statistical software package SAS JMP 10, using the parameters as variables for predicting mechanical durability. The significance of each parameter in the model was assessed from normal probability plots shown in Figure 70 and Figure 71. The vertical coordinate in this plot represents the normalized value of the parameter estimate (mechanical durability), and the horizontal coordinate represents its normal quantile. Hence, effects that are of little importance are interpreted as noise, and should follow a normal distribution. These can be found on a line with the standard deviation as the slope. Conversely, important effects toward the model estimate are identified as those lying away from this line.

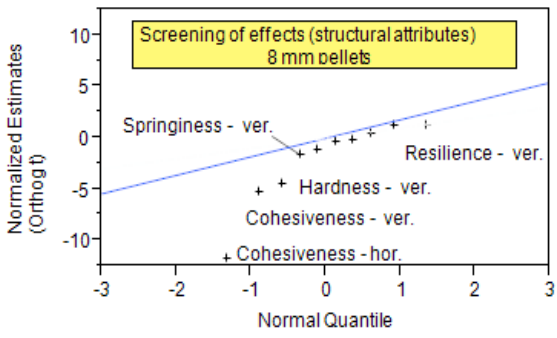

Figure 70: Screening of main effects (structural attributes) for experiments with 8 mm pellets.

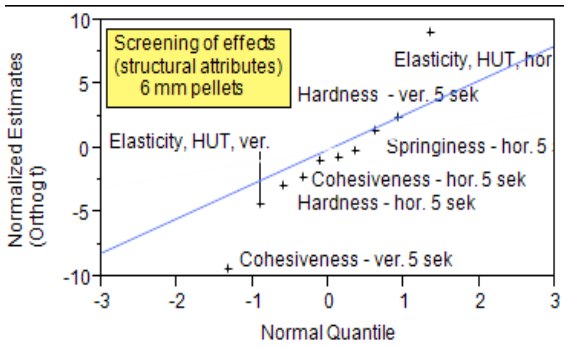

Figure 71: Screening of main effects (structural attributes) for experiments with 6 mm pellets.

It is found that particularly 'cohesiveness' and 'elasticity' explain most of the variation in mechanical durability. Figure 72 and Figure 73 show the dependence of cohesiveness on the mechanical durability as measured by the DORIS test. The figures show that higher cohesiveness will result in better mechanical durability (lower fines content). A linear relationship is assumed for these regression analyses. It appears from the coefficients of determination that cohesiveness alone can explain 43-50 % of the overall variation in mechanical durability, depending on pellet size and orientation of the deformation.

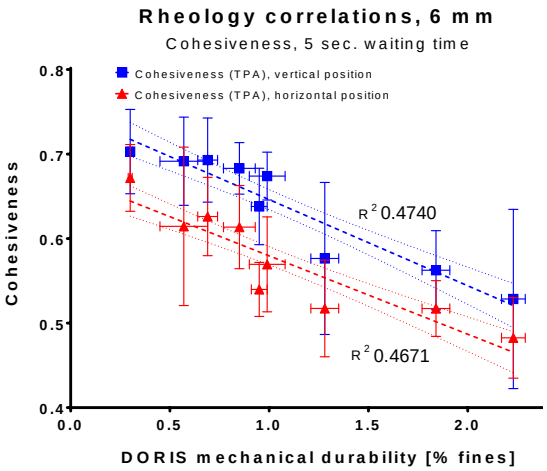

Figure 72: Cohesiveness vs. durability, 6 mm pellets

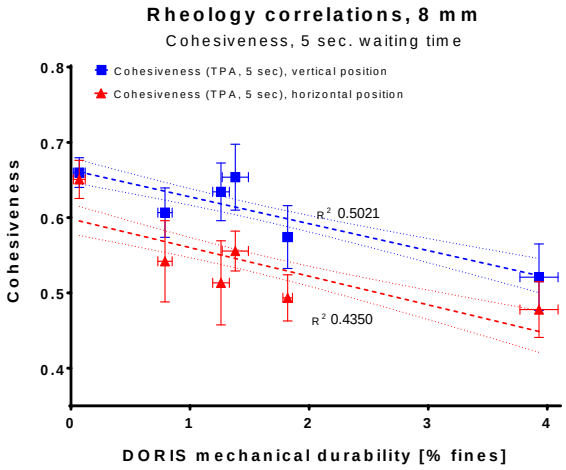

Figure 73: Cohesiveness vs. durability, 8 mm pellets

The elasticity found from SRT also has significance towards determining mechanical durability. This describes the materials' ability to exhibit viscous force relaxation. Figure 74 and Figure 75 indicates that low elasticity will give high mechanical durability, for deformations applied perpendicular to the radial coordinate ('horizontal position'). From Figure 70 and Figure 71 it is found that 'hardness' explain little of the variation in mechanical durability, and only for stress applied in the vertical direction. For the remainder of the measured structural attributes it was not statistically evident that these could describe any of the variation in mechanical durability.

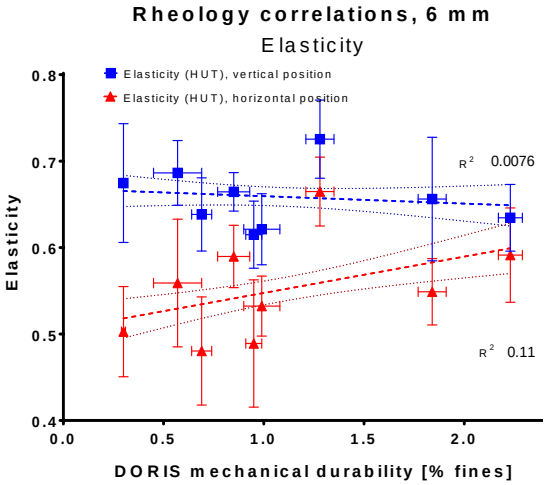

Figure 74: Elasticity vs. durability, 6 mm pellets

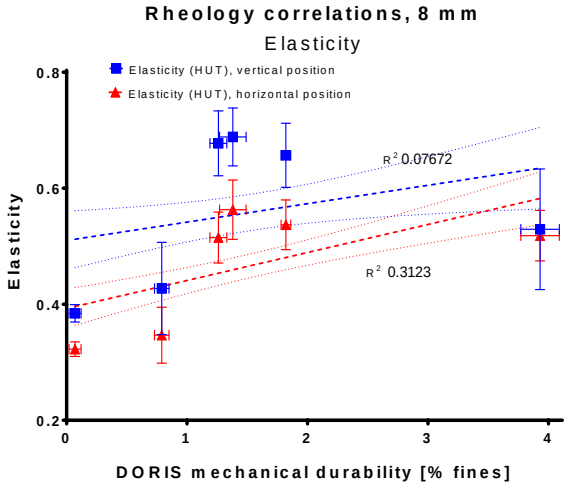

Figure 75: Elasticity vs. durability, 8 mm pellets

From Figure 74 and Figure 75 it appears that that a pellet will have a high durability if the product is able to exhibit viscous stress relaxation, when stress is applied horizontally, i.e. perpendicular to the direction of extrusion (and therefore expectedly to the orientation of the pores) [30]. Importantly, by coupling this observation with the notion following the TPA experiments, that higher cohesiveness increases the mechanical durability (Figure 72 and Figure 73), the structural behavior should be viscoelastic rather than viscous or plastic, i.e. the pellet should be able to return to its original state after a deformation, in order to promote mechanical durability.

The Generalized Maxwell model,

Figure 65, and the 'standard linear viscoplastic model',

Figure 66, each have five model parameters. These parameters can be estimated by minimizing the sum of square error of a model reproduction of a SRT plot against an experimentally obtained SRT plot for an extruded fish feed pellet. Figure 76 illustrates that the SRT model reproduction get very close to the experimentally recorded SRT, which obviously is not so surprising, with five free fitting parameters. The values of the parameters obtained from the regression analysis, for each of the two material models might however be of interest. These appear from Table 5:

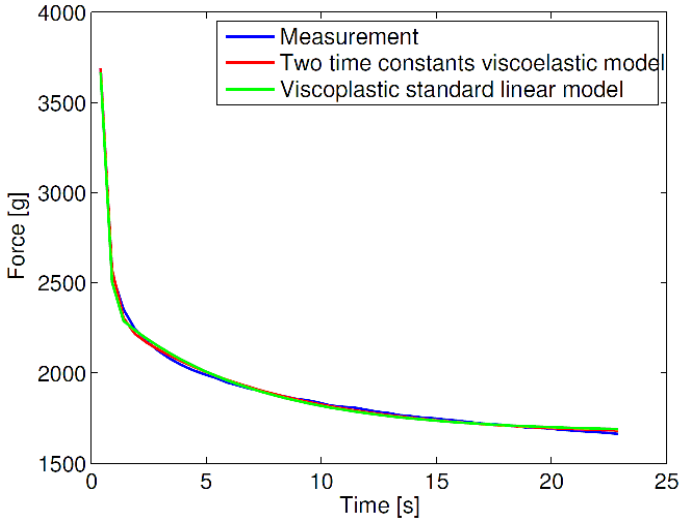

Figure 76: Generalized Maxwell model with 2 time constants and viscoplastic standard linear model fitted against a recorded SRT (load cell error is ± 17 g [151])

Table 5: Obtained parameters from regression analysis of model reproduction of SRT plot against an experimental plot

Parameter	Generalized Maxwell model, Figure 65	Standard linear viscoplastic model, Figure 66
k_e	33100 N/m	56800 N/m
k_1	94400 N/m	26600 N/m
k_2 / F_P	14500 N/m	2270 N/m²
τ_1	0.32 s	5.94 s
τ_2 / μ_P	6.90 s	25100 N·s/m

In the TPA tests, the waiting time in between the two consecutive compressions were 5 seconds. From the regression analysis of the SRT plot, using the two proposed mechanical models, the identified relaxation times were 6.9 and 5.9 seconds, cf. Table 5). This means, that in the TPA tests, certain components within the pellet have not had time to relax to their finite state, at onset of the second compression. If a longer waiting time is used in the TPA experiments, the strength of the correlations between mechanical durability and structural properties could therefore be improved, from the stronger response obtained for the

cohesiveness. This will benefit future analysis and verify the mechanical behavior of durable extruded fish feed pellets.

TPA tests were repeated using 15 seconds waiting time between the two cycles (8 mm pellets only), rather than 5 seconds. The choice of 15 seconds was made to get significantly beyond the characteristic relaxation times identified in Table 5 above. The obtained correlations of cohesiveness with 15 second waiting time against mechanical durability are shown on Figure 77 and Figure 78, for horizontal and vertical orientations, respectively. For comparison, the regression line obtained for the TPA test using 5 seconds waiting time (Figure 73) is also shown (black dotted line).

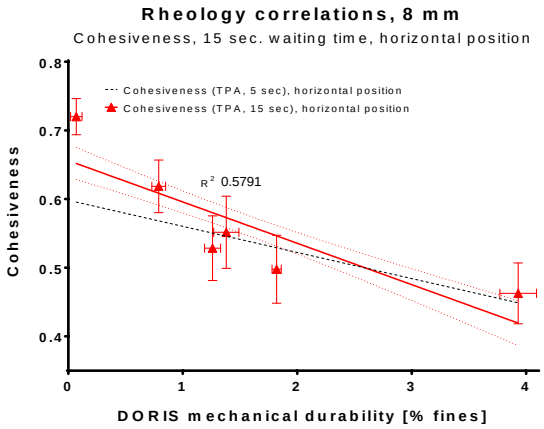

Figure 77: Cohesiveness vs. mechanical durability, 8 mm pellets, 15 sec. waiting time, horizontal position. Error line for regression is shown with red dotted line

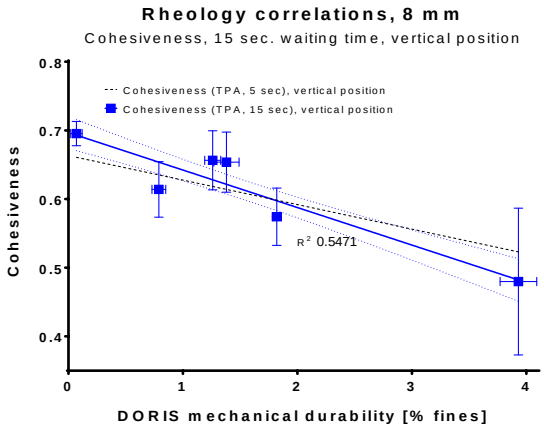

Figure 78: Cohesiveness vs. mechanical durability, 8 mm pellets, 15 sec. waiting time, vertical position. Error line for regression is shown with blue dotted line

From Figure 77 and Figure 78 there is a clear tendency that the durability-cohesiveness correlations were improved by increasing the waiting time to 15 seconds. This is explained from allowing viscoelastic components in the pellets to relax in between the two cycles in TPA. Cohesiveness less than unity are now largely ascribed to plastic, irreversible deformations. Less durable pellets will not gain much cohesiveness by increasing the waiting time.

In summary, from stress relaxation tests, durable pellets should have a low elasticity, meaning that they should be able to exhibit viscous (or plastic) stress relaxation. From texture profile analyses, it is additionally found that a durable pellet should possess a high cohesiveness, i.e. be able to return to its original state following a compression. This is particularly pronounced when sufficient time is allowed for relaxation, in between consecutive compressions. When these pieces of information are coupled, this support a general proposition that a durable extruded fish feed pellet will exhibit viscous stress relaxation and an elastic reformation potential, i.e. viscoelastic behavior.

In the following section 6, it will be investigated whether a viscoelastic mechanical behavior of extruded fish feed pellets can be promoted, by optimization of parameters in the drying process.

6 The influence of hot air drying on the technical quality of extruded fish feed

It is assessed that attrition during handling, storage and transport forms one of the greater challenges, related to technical quality, among commercial fish feed producers, and it is by far the most difficult technical quality parameter to predict and control [20]. This includes breakage of the solid pellet during handling and transport, as well as oil leaks arising from compressive stresses, which will generally occur during storage. Whilst latter issue is strongly related to the coating and cooling of the pellet (and likely to the grinding, conditioning and extrusion processes), the mechanical durability ('breakage') is under strong influence from the drying process, as described in section 5. Other aspects related to the 'technical quality of the feed pellets include sinking properties, water stability, lipid sorption capacity and uniformity – in a single pellet, in the bed and over an entire production run. The importance of each of these technical quality measures, in connection to the drying process, are evaluated below.

Sinking properties of the pellets, as influenced in the drying process, arise directly from their density. Pellets obviously loose mass in the drying process, predominantly due to evaporation of water, but due to shrinkage the net pellet density will not change much [20, 37]. Moisture removal in the drying process are primarily carried out to secure the feed biologically. Thus, the drying process is not very effective for density control and optimization. This is more effectively done in the extrusion and in the coating process, where the degree of expansion and level of oil coating strongly influence the density.

Water stability of feed pellets can be defined as feed loss directly related to the suspension in water. Fines that stick to the surface of the pellets should be included in the evaluation of a pellets durability, by thorough sifting, while in industry some of these fines will inevitably be lost following suspension in water. The influence on water stability in the drying process will be limited, as the most significant influential factors should relate to hydrophobicity and available surface contact area. These are feed recipe, pore width and uniformity (extrusion and grinding) and lipids added in the coating process. The cooling process should also have significant influence, to prevent leakage of lipids that per definition increase hydrophobic character of the pellets.

Lipid adsorption capacity is linked to the porosity, pore connectivity / tortuosity and to the condition of the pellet surface, e.g. if a surface crust has been formed during the drying. Porosity of the pellet is strongly influenced by the expansion in the extrusion process. Tortuosity and pore connectivity are believed to be large influence from upstream conditioning and grinding processes [20]. Lipid sorption capacity in the drying process are essentially influenced from the degree of shrinkage, which occur from drying in the rubbery phase. If the degree of shrinkage in the drying process is known a priori (i.e. from glass transition onset [128]), this could easily be counterbalanced by expansion control in the extrusion process. A certain combination of drying parameters leading to an early surface glass transition onset followed by a drying period using hot air could lead to surface crust formation, cf. section 5 and [115], lowering available surface exchange area for lipid adsorption.

The drying process directly influences moisture and temperature uniformity within individual pellets, as well as between pellets across the depth of a dryer bed. Implementing a liable dryer control strategy could additionally minimize fluctuations in moisture content over a production run, e.g. from changes in inlet moisture content. Moisture gradients in a single pellet could influence (mechanical and durability related aspects set aside) lipid adsorption uniformity, leading to subsequent oil leak from a mostly oil wet surface, when water eventually equilibrates from the center to the surface. Optimization of particularly the moisture uniformity in the bed and over the course of a production run are directly related to the biological stability of the finished product. There should be a limit to how much moisture the product can equilibrate between pellets during storage; typically ± 0.5 % (w.b.) are targeted [20]. A highly dispersed moisture content between individual pellets will likewise influence the coating process, leading to very high oil uptake in some pellets, with associated risk of oil leak, whilst other remain below specifications in oil content. Moisture uniformity through the bed becomes particularly important since reduced deviation in moisture content allow moving the target moisture content closer to a boundary value induced from biology / delivery terms. Essentially, this could render it possible to retain more moisture in the finished product, while using less energy in the dryer. Moisture and temperature uniformity of an individual pellet and between pellets across the depth of the bed, are directly output parameters of the model of the deep-bed drying process, presented in section 4.

From above discussion of technical quality parameters, mechanical durability as influenced from the hot air drying process will be subject to discussion and experimental investigation, in the following sections 6.1 and 6.2, respectively. Section 6.3 takes on the challenge on how to predict mechanical durability of extruded fish feed in the hot air drying process, using a 'glass transition temperature control' methodology.

6.1 Causal relations between the drying process and mechanical durability

Establishing a liable causality between drying parameters and achieved mechanical durability has been an important prerequisite to the discussion of optimizing the mechanical durability (e.g. DORIS) of extruded fish feed, in the drying process. Below, the causal relations chart, Figure 79, intend to help establish a necessary overview on which properties and connections are well known, but more importantly, which that are not. Obviously, not all parameters will influence proposed processes and properties, but some combinations should definitely be highly descriptive towards the viscoelastic properties, which increases the mechanical durability.

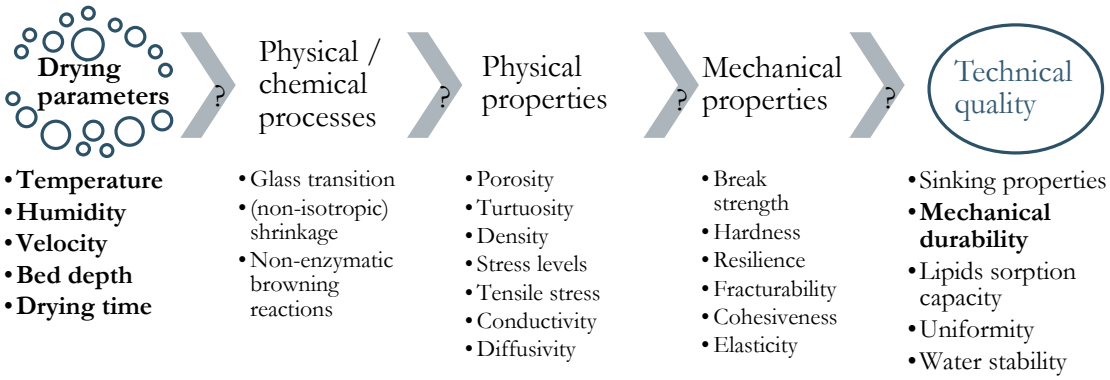

Figure 79: Causal relation chart proposed at an initial stage of the Industrial PhD project. This relates drying parameters to different plausible mechanisms and some descriptive physical and mechanical properties for the obtained 'technical quality'

A general assumption follows from investigations of mechanical durability in the previous section 5, that the onset of glass transition in the drying process influences the extent of stresses built up in the pellet, and consequently its viscoelastic character. The pellet would be more prone to plastic deformation when the glass transition occur (from surface to center) at an early stage in the drying process. This is a generally admitted mechanism for a vast number of amorphous foods and biomaterials [30, 159]. Glass transition will often, but not necessarily, initiate on the dryer pellet surface. Founded in the glass transition theory of biopolymers [123], stresses built up in the pellets should be influenced from:

- Onset of glass transition in the drying process
- Spatial differences in onset of glass transition in the drying process
- Moisture (plasticizer) removed
- Non-enzymatic browning reactions of reducing surface carbohydrates

Above considerations imply that local air temperature, air humidity and air velocity, as well as feed diameter/geometry and final moisture content, should influence the obtained viscoelastic character. Oehme et al. have indeed found that mechanical durability was increasing with moisture content of extruded fish feed pellets. Hence, this should be directly induced from the glass transition theory of biopolymers; decreasing plasticizer content will impart mobility of adjacent biopolymers, reducing the pellets' stress relaxation potential, lowering

their viscoelastic character and therefore also their mechanical durability. Whilst this mechanism is straightforwardly acknowledged, stresses arising from spatial moisture (and temperature) differences will be much less obvious, and necessitate model predictions. This is also highlighted by Katekawa et al. [129], stating that model predictions of average temperature and moisture content are ineffective in evaluating onset of glass transition, in the drying of particulate materials. It follows that this should be particularly important for larger products, which is additionally highlighted by Achanta et al. [115]. Note that non-enzymatic browning reactions (caramelization and Maillard reactions) of reducing surface carbohydrates (dextrin equivalents) could influence the viscoelastic character, by forming a crust that rapidly increases hardness and plasticity of the pellets. This should be particularly relevant at elevated surface temperatures.

6.2 Experimental investigation of physical properties and mechanical durability in the drying process

More than 140 different drying experiments of extruded fish feed pellets have been completed in the present PhD project, to assess the impact from different drying parameters on their mechanical durability and structural properties. 30-40 of the drying experiments were preliminary in their type and analysis, specifically targeted to develop methods and streamline experimental work involved, throughout an experimental design. A recurring issue was the need for strictly constant production conditions out of the extruder, throughout an experimental design series. Furthermore, the size of the produced pellets should be above 5 mm. This is reasoned since larger pellets generally have greater issues with technical quality (from spatial differences, cf. section 5), provide better response in the DORIS test (from impact momentum) and will allow effective subsequent assessment of structural properties in a texture analyzer. Around 40 experiments formed a large experimental design, but unfortunately failed 'as a whole', due to upset production conditions upstream the dryer. These could however be lumped into two smaller groups of experiments, i.e. before and after the upset condition, respectively. 62 experiments were successfully carried out as part of completing 6 different experimental designs, comprising 4 factors as 'drying conditions'. These are air temperature, air velocity, air humidity and final moisture content. Latter is strictly not a 'drying condition' but serve as a factor in two experimental designs, to evaluate if effects from the other factors apply equally, for different extent of drying, i.e. an assessment of the transferability of conclusions across different drying zones in industrial scale dryers.

6.2.1 Experimental method

The custom designed lab dryer (cf. section 4.6.1 and Figure 28 – Figure 30 (pages 50-51) for details and illustrations) was used to provide different drying conditions to the pellets. Generally, a bed height of 3-4 cm were aimed throughout all experiments, to pursue constant drying conditions for all pellets in the layer, yet have sufficient material to conduct replicate analyses. This roughly corresponded to 250 – 350 g of moist pellets. Moisture content during the drying was checked by weighing the cylindrical drying chamber at appropriate times (as infrequent as possible; average 4-5 moisture checks in total). The drying proceeded until the desired moisture content had been obtained. At this point, all pellets were sampled in a plastic bag, sealed and stored at 5 °C. This is to equally distribute moisture in between pellets as well as equilibrate spatial temperature and moisture gradients within pellets. For all experiments, the dried pellets were subjected to testing of mechanical durability. Pellets dried in experiments forming three of the larger experimental designs were additionally subjected to structural analysis in a texture analyzer.

The pellets' mechanical durability are assessed using the DORIS pellet durability tester, cf. Figure 59, page 80 + Figure 64, page 83. All samples were taken out 30 minutes prior to the analyses, and had generally been stored 5-7 days. It was aimed to use around 110 g of pellets to conduct the DORIS test; in post analysis, this turned out to be 112 ± 7 *g*. All material were transferred to sifting analysis on 2.36 mm screen (mesh 8), and sifting was done for 5 minutes

at medium intensity in the laboratory scale vibrating sifter. Fines/fractures are quantified, which effectively becomes the test result. For each experiment, it was tested that the masses added up, before/after sifting, on each side of the screen. From six replicates of the DORIS test, using the same material, it was confirmed that the amount of pellets used in the analyses had negligible impact on the test results (in a 70 – 130 g range). Here the standard deviation of the DORIS test was additionally found to be 7.9 % (e.g. for 2 % result, std. deviation is 0.079 · 2 %). Generally, the desire of conducting the drying experiments in a thin layer, to ensure validity of the intended airflow properties, was directly contradicting the desire of using replicate estimates of mechanical durability in the DORIS test. Replicate estimates were therefore generally preferred to be carried out for the entire drying experiment, restricted by duration and continuity of production. Eleven replicate drying experiments of 8 mm salmon feed pellets were carried out consecutively, to find a standard deviation of 11.9 % for the whole experiment, including determination of the DORIS mechanical durability. The standard deviation of the DORIS durability estimates (7.9 %) are used on all measurements, when conducting statistical analyses. Pellets that were subjected to structural analysis were analyzed using the texture analyzer, within 48 hours of storage at 5 °C, *after* conducting the DORIS test.

For details on the structural analyses experiments, reference is made to section 5.3.2. Pellets were subjected to texture profile analysis, TPA, and stress relaxation tests, SRT, in horizontal and vertical directions. 16 pellets were used in each of the analyses, i.e. 64 pellets from each sample were used for texture analyses, in total. Other than cohesiveness (from TPA, 15 seconds waiting time) and elasticity (from SRT, 22 seconds deformation time), pellet dimensions (diameter / length) and hardness were assessed by the texture analyzer, at the same time. All measurements, except the dimensions, were specific towards the testing parameters (e.g. extent of compression).

6.2.2 Design of experiments

A preliminary requisite for carrying out experimental investigation of the drying parameters' influence on mechanical durability on pellets immediately out of the dryer, was that no interaction effects was encountered when quality is assessed following downstream processing operations, i.e. the coating and cooling processes. This means, that the conclusions derived on the influence of different drying parameters should be similar when measuring durability for the same feed type following the dryer, coater and cooler, respectively. Effectively, this can be investigated by measuring the mechanical durability for different pellets of similar dimensions, following the drying, coating and cooling processes. The results from this initial experiment appear in Figure 80.

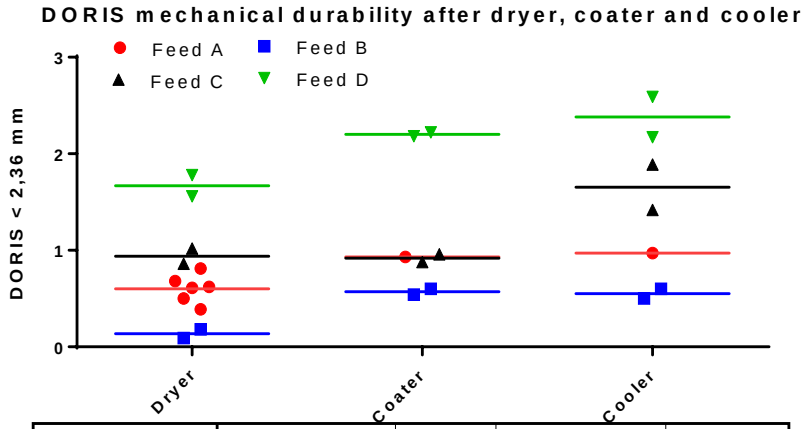

Two-way ANOVA	Ordinary			
Alpha	0.05			
Source of Variation	% of total variation	P value	P value summary	Significant?
Interaction	3.361	0.0633	ns	No
Processing	10.15	< 0.0001	****	Yes
Feed type	74.07	< 0.0001	****	Yes

Figure 80: The influence on drying, coating and cooling processes on mechanical durability, for different feeds.

From investigating Figure 80, it is found that the response on mechanical durability following the coating and cooling processes is similar, across feed types (and associated drying and extrusion parameters). It is therefore deduced that measurements following the lab scale dryer can be extended to make conclusions for the finished product. This can also be deduced from the interaction effect in the two-way ANOVA analysis comprising only ~3 % of the total variation, however with a relatively low associated p-value of 0.06.

Three smaller designs (I-A, I-B and II) were carried out to make rough estimates on the effect of drying air parameters, temperature, humidity and velocity. Two larger designs were subsequently carried out to increase the level of detail, to include also 'end moisture content' as a factor and finally to elaborate the analysis of the drying parameters by investigating structural properties using textural analyses (TPA and SRT). One large design originally included two levels of air velocity, humidity and end moisture content and three levels of temperature (i.e. a 3x2x2x2 full factorial design). Unfortunately, upset conditions at the extruder (shutdown and subsequent slight change in raw materials) did not allow completion of this design as intended. The experiments in this larger design were fortunately sequenced to consider such a situation to arise, and the larger design could subsequently be separated into two 3x2x2 full factorial designs, at low (IV-A) and high (IV-B) air velocities, respectively.

For all designs, the choice of feed type and size was merely based on production scheme and availability. For the designs that includes analyses of structural properties, it was desired to use large pellets, preferably also of the same type.

Table 6: Overview of experimental designs to evaluate the influence of drying parameters on mechanical durability and structural properties. Drying parameters are air temperature, *T*, air humidity, *Y*, air velocity, *v*, and product end moisture content, X_0.

Full factorial design ID	*Type / levels*	*Factors*	*Feed*	*Mechanical durability, section 6.2.3:*	*Structural properties (TPA and SRT), section 6.2.4:*
I-A	2 x 2	T x Y	Sea bass, 6 mm	Figure 81	N/A
I-B	2 x 2	*T* x *Y*	Rainbow trout, 5 mm	Figure 82	
II	1 x 3	*T* x *v*	Cod, 8 mm	Figure 83	
III	4 x 2	*T* x *v*	Sea trout, 8 mm	Figure 84	Figure 87 – Figure 89
IV-A (low *v*)	3 x 2 x 2	*T* x *Y* x X_0		Figure 85	Figure 91+Figure 92
IV-B (high *v*)	3 x 2 x 2	*T* x *Y* x X_0		Figure 86	Figure 90+Figure 93

6.2.3 Results, mechanical durability

Design I-A and I-B investigated the effect of air temperature and air humidity on the DORIS mechanical durability.

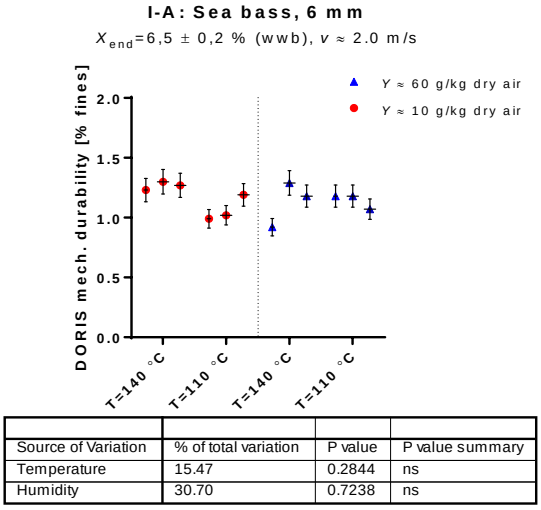

Source of Variation	% of total variation	P value	P value summary
Temperature	15.47	0.2844	ns
Humidity	30.70	0.7238	ns

Figure 81: Full factorial design with two temperature and humidity levels, using a high air velocity.

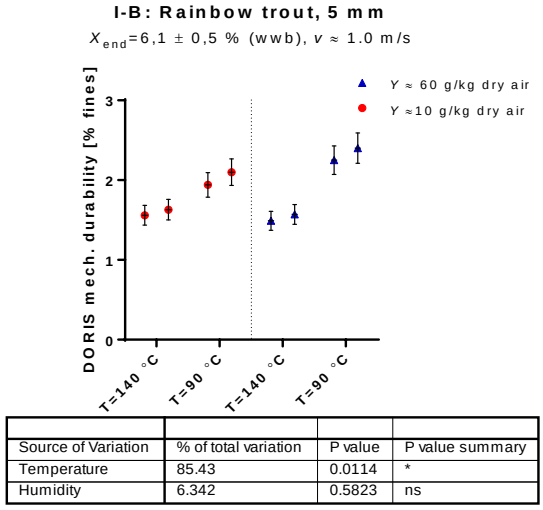

Source of Variation	% of total variation	P value	P value summary
Temperature	85.43	0.0114	*
Humidity	6.342	0.5823	ns

Figure 82: Full factorial design with 90 °C and 140 °C temperature levels and 10- and 60 g/kg dry air humidity levels.

I-A was carried out at a high air velocity and 110 °C and 140 °C. Neither humidity nor temperature were found to be a significant source of variation. Furthermore, all obtained DORIS mechanical durability values were low (global mean of 1.2 ± 0.1 % fines). The choice of using a high air velocity rose from a desire of obtaining uniform air conditions in the bed. Obviously, this comes at the expense of high external transfer coefficients, which influences spatial temperature and moisture profiles in the pellets. A broader range of temperature levels were chosen in I-B, aiming to reiterate if humidity and temperature could not be found to be influencing the mechanical durability. The air velocity was also reduced in trying to allow a stronger effect of temperature in the drying experiments. The experiments in I-B did show

increase in mechanical durability at increasing temperatures (p=0.011), in support of the glass transition theory of biopolymers, cf. section 5. No effect was found from humidity in neither I-A nor I-B.

I-B highlights that there is a significant effect from air temperature, but the difference between I-A and I-B further indicate that there could also be a significant effect from air velocity. This is investigated in experimental design II, which include air velocity as the only factor at three different levels, using three repetitions. Figure 83 illustrate the effect of air velocity quantifying DORIS mechanical durability as 'fines' (> 2.36 mm), but also as larger fractures/'cracks' (< 4 mm). By investigating Figure 83, the effect of velocity seem to be have some importance towards mechanical durability, albeit the statistical material cannot support a p-value below 0.05, which is the significance level (α) normally considered significant and used by many statistical software packages, including the one used in the present thesis (GrahPad Prism 6.0, GraphPad Software Inc., USA). The obtained p-value of 0.074 is low, and indicate that there is a good likelihood that the air velocity has importance toward the mechanical durability (i.e. there should be a ~7 % risk falsely stating that air velocity will be of importance towards the durability).

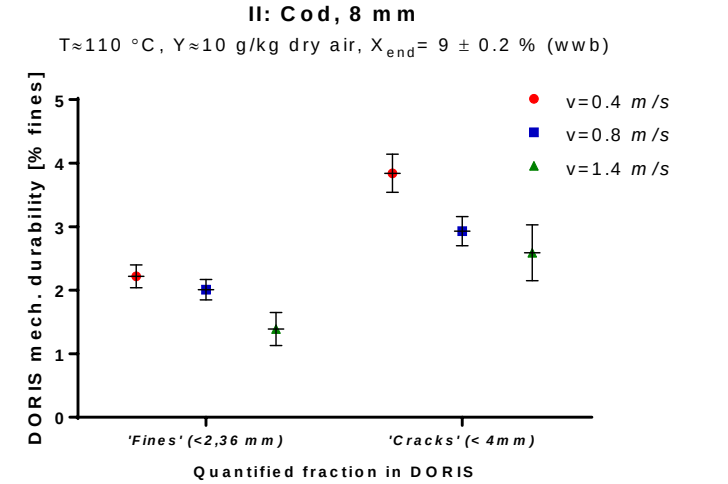

Source of Variation	% of total variation	P value	P value summary
Interaction	3.146	0.5867	ns
Quantified fraction in DORIS	59.09	0.0087	**
Velocity	27.47	0.0744	ns

Figure 83: Full factorial design with three air velocity levels using ambient air humidity (10 g/kg dry air) at 110 °C. Two different size fractions were quantified in the DORIS durability test, to increase the response between the different air velocities.

Experimental design III further investigates the impact of velocity and of temperature, cf. Figure 84. Four levels of temperature and two levels of air velocity is used in the design, using large 8 mm pellets for sea trout. A 2-way ANOVA here found that the air velocity does not have much influence on the durability, but the temperature is likely to have importance across the two air velocities (p=0.10). Linear regression analysis on each data set using constant air velocity gave significantly non-zero slopes for the influence of temperature on DORIS mechanical durability (p≈0.02). This linear fit was able to describe 70 % of the total variation (R^2≈0.7). At low air temperatures, the obtained durability using the two different

air velocities are different; however, there are insufficient data available to conclude if this is a significant difference. If so, this falls parallel to the observations made on the differences between the output of the analyses of I-A and I-B (Figure 81 and Figure 82), specifically, that below a certain temperature the influence of air velocity become increasingly important and, vice versa, below a certain air velocity, the influence of air temperature become increasingly important. This mechanism is in line with the glass transition theory for biopolymers proposing to maintain a rubbery solid phase as long as possible in the drying, to reduce stresses building up in the pellets. Particular in the evaporative cooling (especially of the surface in an early stage of the drying), there should be a relevant risk for the surface to transcend through the glass transition curve, making the crust immobile and 'glassy', cf. discussions in section 5.1.

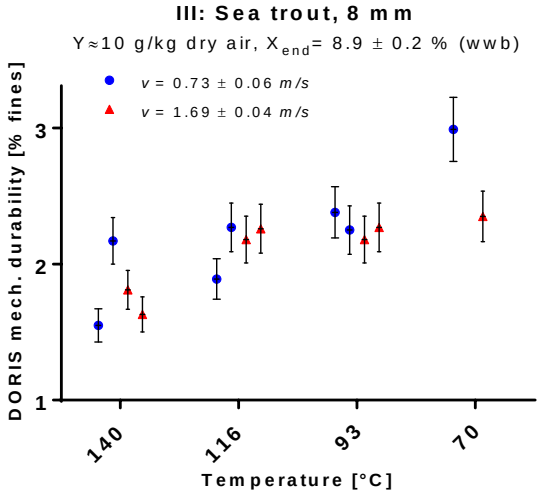

2-way ANOVA; temperature and velocity

Source of Variation	% of total variation	P value
Temperature	73.17	0.1000
Velocity	2.885	0.4278

Effect of temperature (linear regression) for different velocity

Goodness of fit

	v=0.73 m/s	*v*=1.69 m/s
R square	0.6865	0.7205

Is slope significantly non-zero?

	v=0.73 m/s	*v*=1.69 m/s
P value	0.0213	0.0157
Deviation from zero?	Significant	Significant

Figure 84: Full factorial design with four air temperature levels, two air velocity levels. Ambient air humidity is used (10 g/kg dry air) and the drying proceed to end moisture contents of ~9 % (w.b.). Two replicates are used, except at 70 °C due to very long drying times and production scheme limitations.

Significant influence on durability from temperature (p=0.03) and humidity (p=0.04) was found from a 2-way ANOVA on the data obtained from experimental design IV-A. However, this connection could only be confirmed when drying to end moisture contents of 8.6 ± 0.4 % (w.b.). When the drying proceed to end moisture content 6.2 ± 0.4 % (w.b.), the influence on durability of these parameters cannot be found to be particularly strong in a 2-way ANOVA analysis, cf. Figure 85. Using more simple t-tests (or by visual interpretation of the data), it can be found that high air humidity significantly improves durability, for the two lower drying temperatures (p=0.02, analysis not shown). It can also be found that for dry air, high temperature improves durability (p=0.002, analysis not shown).

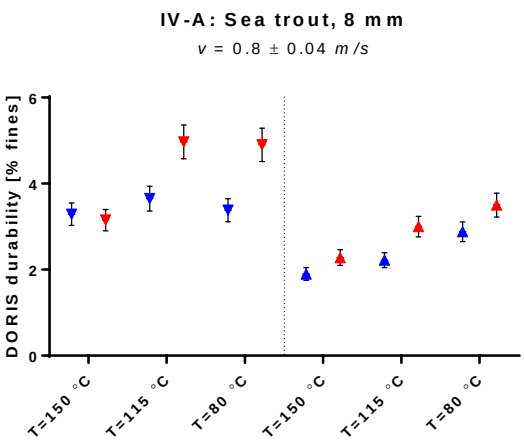

▲ Y ≈ 10 g/kg dry air; X_{end} = 8.6 ± 0.5 % (wwb)
▲ Y ≈ 60 g/kg dry air; X_{end} = 8.6 ± 0.4 % (wwb)
▼ Y ≈ 10 g/kg dry air; X_{end} = 6.4 ± 0.5 % (wwb)
▼ Y ≈ 60 g/kg dry air; X_{end} = 6.0 ± 0.2 % (wwb)

2-way ANOVA, X_{end} = 8.6 ± 0.4 % (wwb)

Source of Variation	% of total variation	P value	P value summary
Temperature	68.05	0.0324	*
Humidity	29.67	0.0363	*

2-way ANOVA, X_{end} = 6.2 ± 0.4 % (wwb)

Source of Variation	% of total variation	P value	P value summary
Temperature	40.32	0.3738	ns
Humidity	35.61	0.2275	ns

Figure 85: Full factorial design with three air temperature levels, two air humidity levels and two 'final moisture content' levels, X_{end}. A 'low' air velocity of 0.8 ± 0.04 m/s is used, originally comprising another level as part of a larger design, merged with IV-B, Figure 86. The two (un-replicated) designs are separated in the analysis due to production halts.

Similar trends can be found in the parallel design IV-B, cf. Figure 86 using a higher air velocity. Here, 2-way ANOVA including all levels and effects cannot statistically validate the significance of temperature and humidity on the mechanical durability. Particularly, for the experiments where the pellets are dried to the higher moisture content (9.2 ± 0.1 % w.b. in IV-B), the influence of temperature and humidity on the durability cannot be re-found in IV-B where a higher air velocity is used. This is explained from an interaction effect between air velocity and air temperature on mechanical durability, as was also seen when comparing experimental designs I-A (Figure 81) and I-B (Figure 82). From the glass transition theory for biopolymers, a high air velocity will render the influence of temperature and humidity insignificant, if the high air velocity will ensure that the rubbery state product, particular in early stages of the drying with evaporative cooling, has significant distance from the glass transition region. This should effectively allow temperature or humidity of the drying air to be lowered, without moving into a glassy state. Yet, the effect of lowered air temperature / humidity should be realized when the drying proceed for a longer time in the glassy state, i.e. the cumulated stresses should become larger. This effect is sought explained from Figure 86: When drying to higher moisture contents, no effects appear; when drying to lower moisture contents, similar patterns as found from previous designs appear – low humidity and low temperatures will yield inferior durability. It is proposed that this effect arises from differences in glass transition onset (i.e. at different average moisture contents), additionally influenced by moisture content gradients providing differences in glass transition onset though the pellet. Founded in this glass transition theory, the ideal drying should promote a spatially uniform glass transition, at a late stage in the drying process. Internal resistance towards heat and mass transfer should naturally render such a scenario impossible, and starting to pile layers in deep beds additionally complicates this, as air properties change through the layer. Yet, aforementioned targets should allow for a global optimization of technical quality of extruded fish feed pellets in the deep-bed drying process.

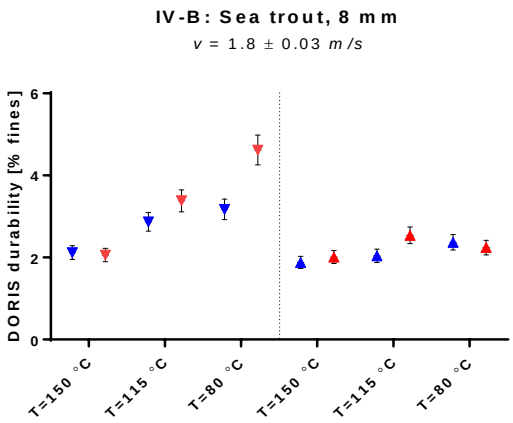

▲ Y ≈ 10 g/kg dry air; X_{end} = 9.2 ± 0.1 % (wwb)
▲ Y ≈ 60 g/kg dry air; X_{end} = 9.1 ± 0.1 % (wwb)
▼ Y ≈ 10 g/kg dry air; X_{end} = 6.2 ± 0.2 % (wwb)
▼ Y ≈ 60 g/kg dry air; X_{end} = 6.1 ± 0.2 % (wwb)

2-way ANOVA, X_{end} = 9.2 ± 0.1 % (wwb)

Source of Variation	% of total variation	P value	P value summary
Temperature	53.90	0.3766	ns
Humidity	13.54	0.4581	ns

2-way ANOVA, X_{end} = 6.1 ± 0.2 % (wwb)

Source of Variation	% of total variation	P value	P value summary
Temperature	73.50	0.1505	ns
Humidity	13.48	0.2869	ns

Figure 86: Full factorial design with three air temperature levels, two air humidity levels and two 'final moisture content' levels, X_{end}. A 'high' air velocity of 1.8 ± 0.03 m/s is used, originally comprising another level as part of a larger design, merged with IV-A, Figure 85. The two (un-replicated) designs are separated in the analysis due to production halts.

6.2.4 Results, structural properties

With reference to Figure 79, taking only the single step from drying parameters to structural properties could reveal details in support and maturation of proposed mechanism for increasing the viscoelastic character and mechanical durability of an extruded fish feed pellet, founded in the glass transition theory of biopolymers.

Pellets dried in designs III, IV-A and IV-B were subjected to structural analysis using a texture analyzer. Parameters assessed were cohesiveness (TPA) and hardness (SRT / TPA) for both vertical and horizontal pellet orientations and elasticity (SRT) for horizontally oriented pellets only, cf. section 5.3.2. The texture analyzer automatically records dimensions of the tested objects, so length and diameter for all pellets were also recorded, which allows to compare shrinkage (isotropicity) between pellets dried using different conditions. This sum up to seven structural property outputs for the three different experimental designs, yielding 21 graphical output opportunities of structural properties for the different experimental designs, each comprising different drying conditions. Seven figures, Figure 87 to Figure 93, are included here, to illustrate significant effects that emerge details on the influence on the individual drying parameters, e.g. to help understand some of the interaction effects mentioned in previous section. Statistical analysis for significant effects and conclusions for remaining data that are not illustrated in figures are listed in Table 7. Additionally, some of the structural properties relate directly to other aspects of technical quality, e.g. shrinkage should relate directly to sinking velocity, through density, as well as to the final lipids sorption capacity.

Figure 87 illustrate geometrical changes in the drying process in experimental design III (temperature and air velocity). It is found that radial shrinkage have significant dependency of temperature as well as on air velocity, with little or no interaction effects. It is proposed that this connection is directly related to the glass transition theory of biopolymers, i.e. a rubbery and mobile phase allow shrinkage. From this hypothesis, it should also follow that increased humidity will promote shrinkage; Table 7 highlights that humidity has been identified as a significant effect in experiments IV-A and IV-B, however for drying to the lower end moisture content only.

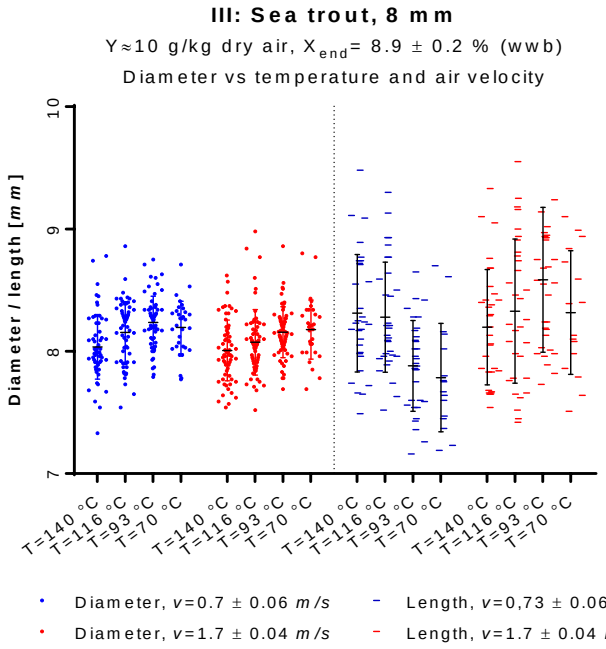

2-way ANOVA; temperature and velocity, diameter

Source of Variation	% of total variation	P value
Interaction	0.3021	0.6894
Temperature	7.999	< 0.0001
Velocity	0.9685	0.0305

2-way ANOVA; temperature and velocity, length

Source of Variation	% of total variation	P value
Interaction	10.30	< 0.0001
Temperature	2.183	0.1281
Velocity	6.756	< 0.0001

Figure 87: Full factorial design III (ref. Figure 84) illustrating the shrinkage in radial and longitudinal directions as influenced from air temperature and air velocity.

The radial shrinkage in particular seem to be governing overall shrinkage in the drying process. The length has much higher variation than the diameter likely due to small variations in production capacity out of the extruder (die speed). This will directly influence the pellet lengths, at constant speed of the rotating knife. The lengths seem to be roughly constant for different temperatures, yet is proposed that the velocity and its interaction effect is significant effects. By investigating the data it can be found that the at the low air velocity, the two lower drying temperatures (93 and 70 °C) actually gave significantly lower lengths than for the other combinations of drying parameters in the design. It is suggested that this could be reasoned from that longitudinal shrinkage occurs when surface tension start to build up upon early entrance into the glassy state. While this should reduce the amount of stresses building up during drying in the glassy state, it will cause non-isotropic stress differences, which could be expected to lead to reduced durability or breakage. This hypothesis adds to the glass transitions hypothesis of biopolymers, and can assist in outlining mechanisms in the drying process that lead to reduced durability.

Figure 88 illustrates the registered peak hardness at the initial compression cycle in the TPA tests. The compression in this method was 6 %. High temperature clearly gives harder pellets ($p=0.005$). At vertical orientation, it could additionally be found that high velocity gave harder pellets. It is proposed that the hardness is strongly related to the degree of shrinkage; pellets with stronger binding forces, from a denser molecular network should be expected to demonstrate higher modulus / 'hardness'. This should also explain how the air velocity does not influence hardness in horizontal directions; from Figure 87 it appears that the degree of radial shrinkage is not *much* different in between high and low air velocities, when comparing the different temperatures (albeit a p-value of 0.03 is found for the influence of air velocity on radial shrinkage).

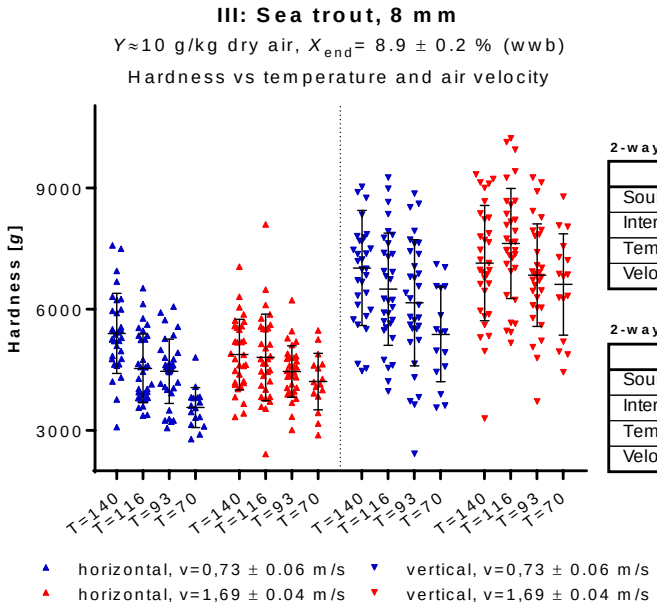

2-way ANOVA; horizontal orientation

Source of Variation	% of total variation	P value
Interaction	4.466	0.0070
Temperature	18.02	< 0.0001
Velocity	0.2347	0.4195

2-way ANOVA; vertical orientation

Source of Variation	% of total variation	P value
Interaction	2.164	0.1401
Temperature	7.250	0.0005
Velocity	6.606	< 0.0001

Figure 88: Full factorial design III (ref. Figure 84) illustrating hardness (at 6 % compression) for vertical and horizontal compression, as influenced from air temperature and air velocity.

Figure 89 demonstrates the influence of air temperature and velocity on cohesiveness, as measured from the TPA test. To support the proposed glass transition theory to control durability, it should follow that the viscoelastic character of the pellet should increase with increasing humidity, temperature and velocity. Experimental design III indeed demonstrate that this is the case for the two latter parameters, with the effect being however only cohesiveness measured in the horizontal direction gave strong significance.

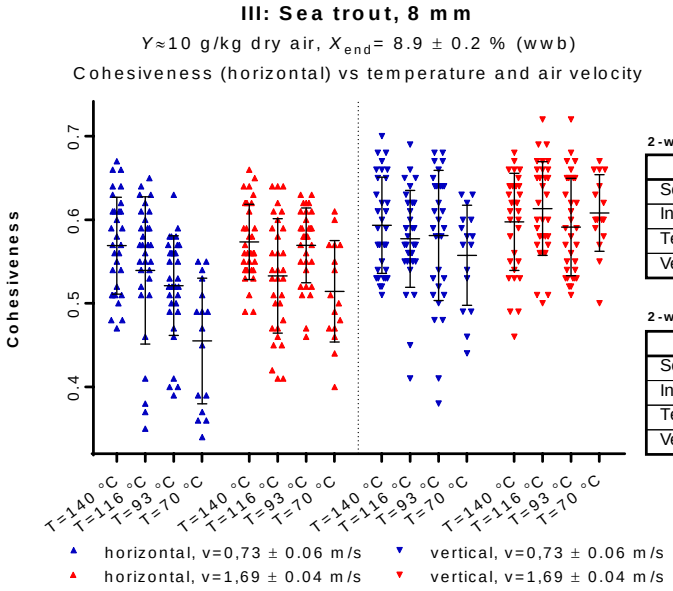

2-way ANOVA; horizontal orientation

Source of Variation	% of total variation	P value
Interaction	3.665	0.0203
Temperature	14.87	< 0.0001
Velocity	3.243	0.0032

2-way ANOVA; vertical orientation

Source of Variation	% of total variation	P value
Interaction	2.059	0.1962
Temperature	0.7232	0.6464
Velocity	3.892	0.0031

Figure 89: Full factorial design III (ref. Figure 84) illustrating cohesiveness as measured from TPA, for vertical and horizontal orientations, as influenced from air temperature and air velocity, v [m/s].

The influence of humidity on cohesiveness (horizontal) is investigated in experimental design IV-B, cf. Figure 90. Here humidity is also identified as an important parameter, however only evident when drying to low moisture contents. Comparing the impact of humidity between

the two 80 °C and 6 % end moisture dryings, it becomes increasingly clear that increased humidity will also increase the viscoelastic character of feed pellets (from increase in cohesiveness), *if* the other drying conditions, at any time during the drying, infer temperature and moisture profiles in the pellet close to the glass transition region. For example, a high air velocity is used in IV-B. This is likely the reason why no effect from temperature nor humidity could be identified when drying to the higher moisture content of 9 %, i.e. the glass transition region have probably not been fully reached, for neither combinations of drying conditions.

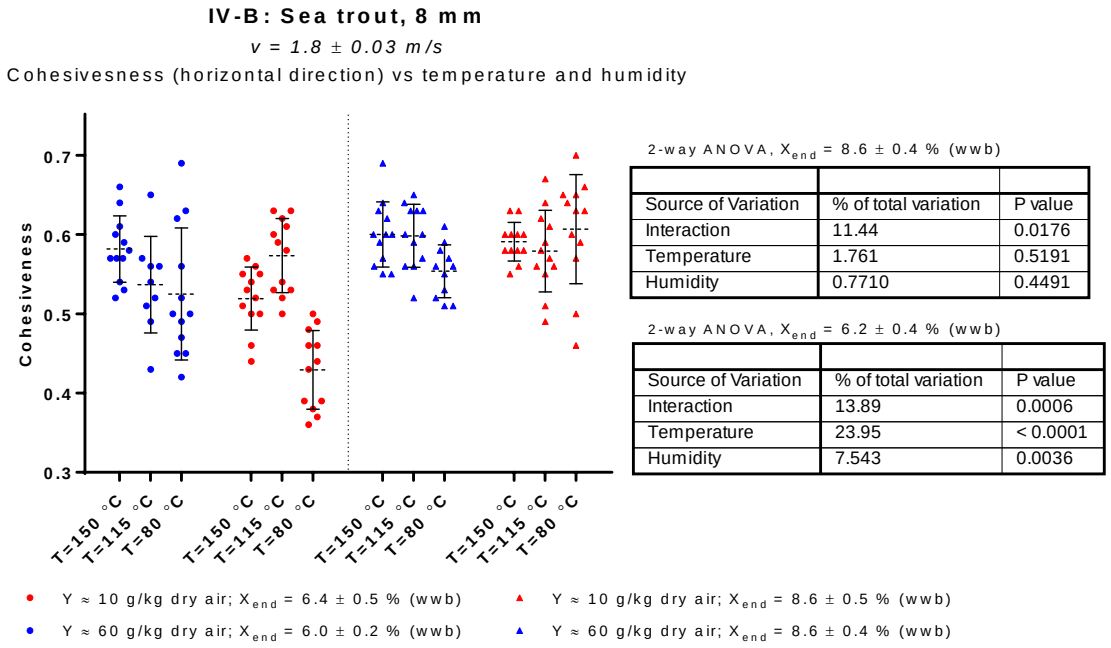

Figure 90: Full factorial design IV-B (ref. Figure 86) illustrating cohesiveness (horizontal direction only) as measured from TPA, for two different end moisture contents; ~6 % and ~9 % (w.b.).

Figure 91 demonstrates the influence of temperature and humidity on elasticity, as measured from the SRT test. Elasticity is another important measure for the viscoelastic character (viscous stress relaxation). In previous studies it was found that this parameter only have significant importance when oriented horizontally in the test, so elasticity was only recorded for pellets in horizontal direction in experimental designs III, IV-A and IV-B. A low value of 'elasticity' allow viscous stress relaxation and therefore increase the viscoelastic character of the pellets. This should essentially increase the durability [30]. One of the most apparent notions in Figure 91 is that pellets with ~9 % water have significantly lower values of elasticity ($p<0.001$, analysis not shown) than the drier pellets at ~6 % water (w.b.). This is not surprising, as moisture should act as plasticizer in the pellets and therefore support their viscous stress deformation potential. Another important notion in Figure 91 is the differences in elasticity for 150 °C air, when drying to ~ 6% moisture (w.b.). The elasticity of the pellets are very significantly increased (i.e. lowering their viscous stress relaxation potential) when using dry air at the high temperature. This is likely reasoned from that, surface glass transition will occur at a very high temperature (and drying rate), resulting in a crisp crust, lowering viscous (and increasing plastic) properties of the pellets – in other words, the pellets

might be "baked" at these conditions. This phenomenon is sometimes called 'case hardening', and it is an important counterbalancing effect to include in the discussion of overall optimization of technical quality. From previous discussions in section 6.2.3 it appears that a high temperature should support a good technical quality. Structural analysis in the present section now demonstrate that this should not always be the case. To overcome the issue of losing viscous stress relaxation potential by having rapid glass transitions at very high temperatures (and drying rates), high humidity can be used, as seen in Figure 91. This could be reasoned from lowering the drying rate by decreasing the driving force for external mass transfer, decreasing spatial moisture gradients. The pellets with these high elasticity values could not be subjected to TPA analysis, as they were simply too hard and brittle, and would too often crack on deformation. Also, their hardness were significantly higher (39 %, p=0.02, analysis not shown, cf. Table 7) than when using high humidity at the same temperature. It is important to note that, in this case, the pellets dried to ~6 % moisture (w.b.) at 150 °C using dry air did not result in lower durability, when compared to having a higher humidity. Of course, it is not optimal to produce fish feed that resembles small 'stones', even if their mechanical durability in the DORIS test seem good. Very hard pellets are known to lower feed conversion rates in the fish, which essentially brings up another issue related to technical quality [20]. Test results in the DORIS should only be comparable when pellets share approximately the same mechanical behavior, highlighting the importance of the present chapter, investigating the effect of the drying parameters on the desired structural attributes rather than solely looking to the testing of mechanical durability.

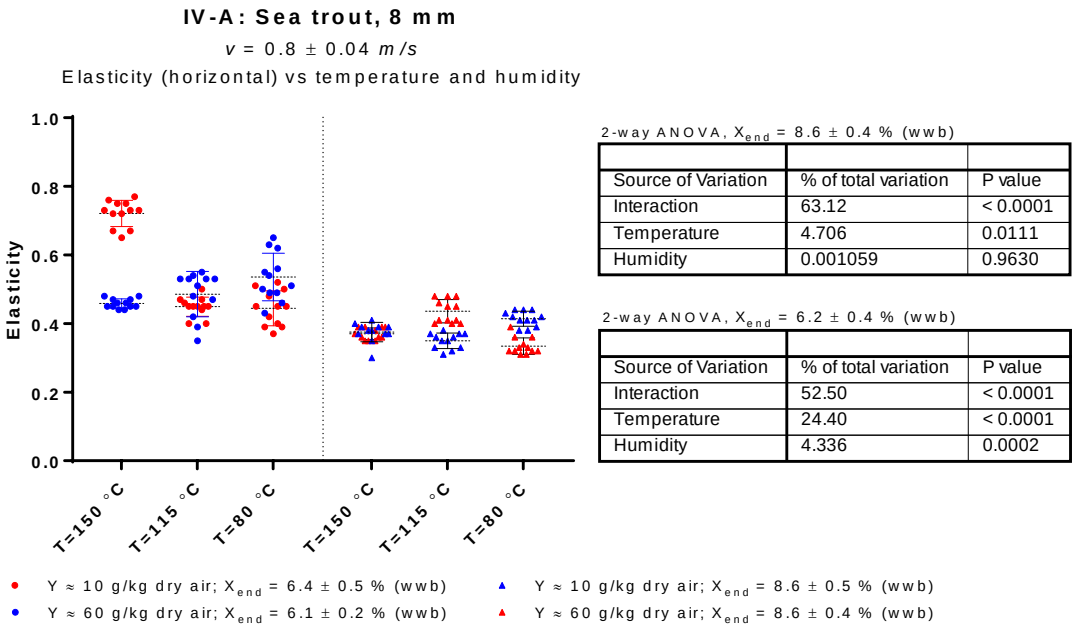

2-way ANOVA, X_{end} = 8.6 ± 0.4 % (wwb)

Source of Variation	% of total variation	P value
Interaction	63.12	< 0.0001
Temperature	4.706	0.0111
Humidity	0.001059	0.9630

2-way ANOVA, X_{end} = 6.2 ± 0.4 % (wwb)

Source of Variation	% of total variation	P value
Interaction	52.50	< 0.0001
Temperature	24.40	< 0.0001
Humidity	4.336	0.0002

Figure 91: Full factorial design IV-A (ref. Figure 85) illustrating elasticity (horizontal direction only) as measured from SRT, for two different end moisture contents; ~6 % and ~9 % (w.b.).

Investigation of the influence of a pellets viscoelastic properties on the obtained mechanical durability is shown in Figure 92 and Figure 93 for experimental designs IV-A (low velocity) and IV-B (high velocity), respectively. The aforementioned drying conditions (using dry and hot air) that led to a susceptible high elasticity are easily identified as an extreme outlier in

this correlation. Generally, high cohesiveness confirm to improve the mechanical durability for both air velocities, whilst the elasticity did not correlate well with durability, for high air velocities (Figure 93, IV-B). It is believed that this difference in the significance of elasticity arise from the strong interaction effects with air velocity, i.e. the high air velocity in IV-B caused only a few combinations of the other drying parameters used in the design to demonstrate significant differences in structural properties and mechanical durability. For example, in IV-B, when drying to the higher moisture content at ~ 9 %, all combinations of temperature and humidity resulted in ~ constant durability, cf. Figure 86.

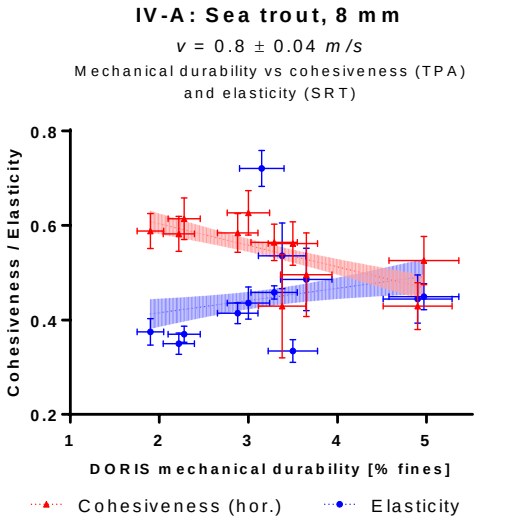

Is slope significantly non-zero?

	Cohesiveness, hor.	Elasticity
P value	< 0.0001	0.0075
Deviation from zero?	Significant	Significant

Figure 92: Experimental design IV-A illustrating coherency between mechanical durability and viscoelastic properties: elasticity (SRT, horizontal direction) and cohesiveness (TPA, horizontal direction).

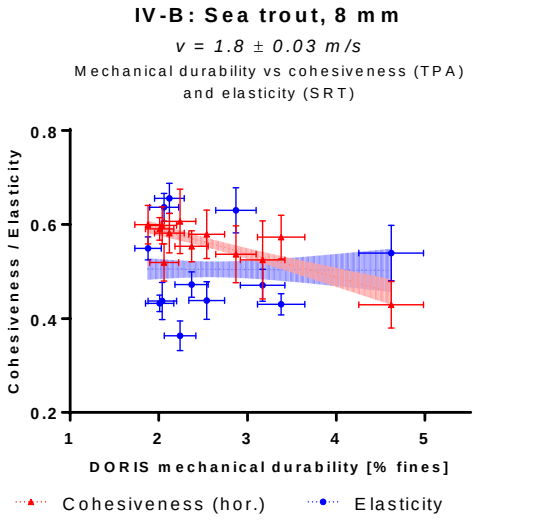

Is slope significantly non-zero?

	Cohesiveness, hor.	Elasticity
P value	< 0.0001	0.9215
Deviation from zero?	Significant	Not Significant

Figure 93: Experimental design IV-B illustrating coherency between mechanical durability and viscoelastic properties: elasticity (SRT, horizontal direction) and cohesiveness (TPA, horizontal direction).

The following Table 7 summarizes all significant effects from the different drying parameters (temperature, humidity, velocity), on structural properties and mechanical durability, as identified in the present and previous sections, respectively. Directions of the effects are intentionally not included, due to the high influence of interaction effects. These interaction effects are believed largely to relate to the vicinity of the glass transition region, caused by combination of other drying parameters than the main effect being tested. For example, in Figure 90 and Figure 91, dissimilar patterns are seen depending on the moisture content that is being dried to, and in Figure 85 and Figure 86 it is seen that the effect of temperature is reduced at high humidity levels. Other interaction effects can be caused from different mechanisms of the parameter. For example, humidity can allow phase mobility and shrinkage at low temperatures, increasing the hardness. At high temperatures, high humidity can help to reduce degree of crust formation, reducing the hardness. In the following section 6.3.1, the influence of each drying parameter will be outlined, including the influence from interacting effects, based on results presented in previous and present sections.

Table 7: Summary of the statistical significance of the drying parameters' influence on structural properties and mechanical durability with their respective p-values to reject the stated H_0-hypothesis.

Effect	H_0-hypothesis Effect does *not* significantly influence:	Applicable at constant parameters		ANOVA P-value	Ref. Fig. – Exp. design ID
		Y / v	X_{end}		
Temperature, T	Mechanical durability (DORIS)	Y=10 g/kg	9 %	*0.10*	III – Figure 84
		v = 0.8 m/s	9 %	0.032	IV-A – Figure 85
		v = 1.8 m/s	6 %	*0.15*	IV-B – Figure 90
	Cohesiveness, vertical	v = 1.8 m/s	9 %	0.005	IV-B – Figure 90
		v = 0.8 m/s		0.009	IV-A – N/A
		Y=10 g/kg		0.003	III – N/A
	Cohesiveness, horizontal	v = 0.8 m/s	9 %	0.022	IV-A – N/A
		v = 0.8 m/s, (excl. 150 °C)	6 %	<0.001	
		v = 1.8 m/s			IV-B – Figure 90
		Y=10 g/kg	9 %		III – N/A
	Shrinkage (radial)	Y=10 g/kg	9 %	0.031	III - Figure 87
		v = 1.8 m/s		0.047	IV-B – N/A
		v = 0.8 m/s		<0.001	IV-A – N/A
	Shrinkage (longitudinal)	Y=10 g/kg	9 %	<0.001	III - Figure 87
		v = 1.8 m/s	6 %		IV-B – N/A
			9 %	0.005	
	Elasticity, horizontal	Y=10 g/kg	9 %	<0.001	III – N/A
		v = 0.8 m/s	6 %	<0.001	IV-A – Figure 91
			9 %	0.002	
		v = 1.8 m/s	6 %	<0.001	IV-B – N/A
			9 %		
	Hardness, horizontal	v = 1.8 m/s	6 %	<0.001	IV-B – N/A
			9 %		
		v = 0.8 m/s	6 %	0.003	IV-A – N/A
	Hardness, vertical	Y=10 g/kg	9 %	<0.001	III - Figure 88
			9 %	<0.001	
Air velocity, v	Mechanical durability (DORIS)	Y=10 g/kg	9 %	*0.43*	III - Figure 84
	Cohesiveness, vertical	Y=10 g/kg	9 %	0.003	III – N/A
	Cohesiveness, horizontal			0.003	III - Figure 89
	Shrinkage (radial)			0.031	III - Figure 87
	Shrinkage (longitudinal)				
	Elasticity, horizontal			<0.001	III – N/A
	Hardness, vertical				III - Figure 88
Humidity, Y	Mechanical durability (DORIS)	v = 0.8 m/s	9 %	0.036	IV-A – Figure 85
			6 %	*0.23*	
		v = 1.8 m/s	6 %	*0.29*	IV-B – Figure 86
	Cohesiveness, vertical	v = 1.8 m/s	6 %	0.105	IV-B – Figure 90
	Cohesiveness, horizontal		9 %	0.004	
		v = 0.8 m/s	6 %	0.117	IV-A – N/A
	Shrinkage (radial)	v = 0.8 m/s	6 %	<0.001	IV-A – N/A
		v = 1.8 m/s	9 %		IV-B – N/A
	Shrinkage (longitudinal)	v = 1.8 m/s	6 %	<0.001	IV-B – N/A
		v = 0.8 m/s		0.058	IV-A – N/A
	Elasticity, horizontal	v = 0.8 m/s	6 %	<0.001	IV-A / Figure 91
		v = 1.8 m/s	6 %		IV-B – N/A
			9 %		IV-B – N/A
	Hardness, horizontal	v = 0.8 m/s	9 %	0.002	IV-A – N/A
		v = 1.8 m/s	9 %	<0.001	IV-B – N/A
			6 %		
	Hardness, vertical	v = 0.8 m/s	9 %	0.01	IV-A – N/A
		v = 1.8 m/s	9 %	<0.001	IV-B – N/A

6.3 Prediction of technical quality parameters in the convective hot air drying process

Previous sections, and Haubjerg et al. [30], demonstrated that viscoelastic mechanical properties promote mechanical durability of an extruded fish feed pellet, allowing viscous stress relaxation and apt reversible deformations, with a characteristic relaxation time of ca. 7 seconds. Based on the glass transition theory of biopolymers presented in section 5.1, and observations in previous section 6.2 on mechanical durability and structural properties for different drying conditions, the following physicochemical processes (Figure 79, page 95) are proposed to govern the viscoelastic character of a mechanically durable feed pellet.

- Water act as plasticizer, increasing the pellets' viscous character.
- Drying in the rubbery phase ensures phase mobility and reduces surface tension.
- Non-enzymatic browning reactions of reducing surface carbohydrates (dextrin equivalents) at elevated temperature can form a crust that rapidly increases hardness and plasticity of pellets.

Note that for the latter of above processes, it was not found that this process lowered the durability, but rather the viscoelastic properties of the feed pellet was dramatically decreased; apparently hard, plastic pellets too show high durability (as do stones), whilst their functional behavior in downstream processing (coating) as well as their digestibility will be doubtful.

The present section aim to combine knowledge obtained on the structural behavior of durable feed pellets and model predictions of spatial moisture and temperature evolution in the drying. Above physicochemical phenomena will be considered, with special emphasis on the glass transition theory. The reactions above are interpreted in section 6.3.1, trying to draw up the causality between different drying parameters and obtained mechanical durability. In section 6.3.2, it will be pursued to predict the mechanical durability using model predictions of spatial moisture and temperature gradients in the pellets, over the course of the drying process. This phase will make use of *all* drying experiments carried out in the experimental phase related to assessment of structural properties and mechanical durability, i.e. experimental designs I-A, I-B, II, III, IV-A and IV-B.

6.3.1 Proposed causalities between drying parameters and achieved technical quality

As it follows from Table 7 and previous discussions, definitive directions of the influence on structure and durability of individual drying parameters are difficult to predict, due to non-linear weighting of the parameters, as well as significant influence of interacting effects. From the glass transition theory, this should arise due to the strong discontinuous behavior emerging, as the product gradually enters its glassy state. A detailed discussion will follow on the influence on structural properties and durability for each drying parameter; temperature, humidity and velocity, including likely interaction effects and non-linear behavior connected to an expected phase transition to a glassy state.

Temperature

Section 6.2 generally visualizes, that higher drying temperatures improve the mechanical durability (Figure 82 + Figure 84 – Figure 86). The fundamental mechanism for this result is proposed to be that when drying occur predominantly in the rubbery phase, the pellet maintains for a long time its phase mobility, which is believed to reduce stress gradients in the pellets. It was demonstrated that higher temperature increased the degree of shrinkage, significantly reducing the radial diameter (Figure 87). The increased shrinkage also gave a harder pellet (Figure 88), presumably from increased bond strength between adjacent large biopolymer molecules. Additionally this could expect to increase the tensile strength of the feed pellet, which makes the effect of allowing phase mobility two-fold; surface tension is lowered whilst at the same time increasing the ultimate tensile strength for crack formation. It was also found that a higher temperature generally enforce pellets' viscoelastic character by increasing their elastic reformation potential ('cohesiveness', Figure 89+Figure 90). The contribution to the pellets' increasing viscoelastic character (and durability) with temperature did not arise from an increase in their viscous stress relaxation potential ('elasticity', Figure 91). Importantly, when drying to a low moisture content, high temperature negatively influenced the pellets viscoelastic character by increasing plasticity and hardness of the pellets. This is proposed to arise following non-enzymatic browning reactions on the surface in the glassy state. As it appears from Figure 91, elevated humidity might help protect the pellets against this phenomenon. It follows that high temperature in the drying ensures phase mobility to reduce surface tension, but once transition to the glassy state occur, it will be important to lower the air temperature to avoid formation of a dense crust that reduces desirable viscoelastic character of the feed pellets.

From a modeling perspective, temperature increases the driving force for heat transfer in a linear behavior, $\propto T$, while the mass transfer, causing initial evaporative cooling of the pellets, are increased in a non-linear behavior. This follows from the influence of temperature through the associated decrease in partial vapor pressure in the surrounding air, $\propto p_{\mathrm{H_2O,air}}$. This should cause the extent of evaporative cooling to rise with elevated temperature, reducing the risk of transitioning into the glassy state owing to evaporative cooling.

Humidity

Increasing humidity could generally demonstrate improved mechanical durability, cf. Figure 85 – Figure 86. This vastly support the glass transition theory, and therefore the same mechanism as stated for the temperature above is proposed; high humidity ensures that pellets will maintain phase mobility (allows shrinkage), which reduces surface tension while increasing the pellets ultimate tensile strength. This mechanism is supported from that increasing humidity reduces the rate of mass transfer (from reducing the driving force), while maintaining a ~ constant heat transfer rate (assuming constant external transfer coefficients, albeit state of the air changes). This can be realized from that humid air has a higher wet bulb temperature than its dry counterpart has. Hence, if a low temperature is used in the drying, and the pellet will enter the glass transition following the evaporative cooling, increased humidity should overcome this issue, decreasing the extent of evaporative cooling. This is witnessed in Figure 86, experimental design IV-B for 80 °C (6.2 % end moisture). From Figure

90 it follows that increased humidity at this temperature indeed elevated the pellets viscoelastic character, particular the pellets' elastic reformation potential ('cohesiveness'). On the other hand, if the temperature is already high enough to overcome early glass transition, increased humidity will alter the pellets structural character and durability to a much less extent (see 115 °C and 150 °C drying experiments to ~6 % moisture in Figure 86). As mentioned, increased humidity might additionally reduce the risk of surface browning reactions, causing a hard crust on the pellets, greatly decreasing the pellets' viscoelastic character (and possibly ruining their value in downstream processing and digestibility altogether). It follows that humidity generally influences structural properties, as well as mechanical durability, positively. In industrial application, the relative humidity of air exhausted from the drying bed will be significantly higher than for the inlet air. Hence, there is a risk of causing condensation in the drying bed, if excessive inlet air humidity is being used.

Velocity

The impact from air velocity should be two-fold, as there will be a direct consequence on the drying behavior of an individual pellet following the external airflow. Additionally, and possibly significantly more important, the air velocity through the bed greatly influences temperature and humidity gradients for the air travelling through the bed. From Figure 84 it followed that the effect of air velocity on a 'pellet-level', did not significantly affect mechanical durability. Nevertheless, it was found that for the drying experiments at a low temperature (70 °C), an increased airflow showed increase in the obtained durability (only one repetition for each experiment was made here, due to production scheme limitations). This is additionally supported by comparing obtained durability values in IV-A, Figure 85, and IV-B, Figure 86, (as originally intended). While not statistically evident, it appears that increasing external airflow can increase a pellets durability. This would be in line with the proposed glass transition theory and pellet level model predictions; increasing external transfer coefficients will cause rate of heat *and* mass transfer to be elevated. This means that the pellet will achieve its state of terminal evaporative cooling earlier, i.e. at a higher moisture content. As the glass transition temperature at the higher moisture content will be lower, elevated air velocity should indeed reduce the risk of achieving an early transition into the glassy, immobile phase. As for the humidity, if the temperature and humidity applied in the drying gives evaporative cooling at a far distance from the glass transition point, the effect of increased air velocity should be low. This could explain how air velocity could not be found to be of significant influence in the analysis of variances, cf. Figure 84. It follows from Figure 89 that velocity indeed has a significant importance towards pellets' elastic reformation potential (cohesiveness); particular it is observed that a high velocity at low temperatures increases the pellets cohesiveness and therefore their viscoelastic character, improving their durability.

From above it is proposed that high temperature, high humidity and high air velocity promote viscoelastic character of extruded fish feed pellets, improving their mechanical durability. It should be desirable for the pellets constantly to be at a 'position' not too far away from the glass transition curve, to reduce spatial temperature and moisture gradients at actual onset into the glassy state. In this way, differences in glass transition from surface to center should be minimized. Theoretically, it will be viable if glass transition occur instantly throughout the pellet. At entrance into the glassy state, the temperature should be reduced to avoid non-

enzymatic surface browning reactions, causing crust formation and a reduced viscoelastic character. Maintaining a high humidity could help reduce this phenomenon. Air velocity should be kept high at all times, to reduce variability through the bed. High levels of humidity and air velocity additionally promotes energy efficiency of the drying process, resembling a high degree of internal air recirculation.

6.3.2 Glass transition temperature control in the hot air drying of extruded fish feed

To justify the impact of glass transition onset on mechanical durability, Figure 94 highlights normalized values for the DORIS mechanical durability vs model predictions of minimum surface temperatures across all drying experiments carried out in the different experimental designs, concerning investigation of structural properties and mechanical durability. Values for the DORIS mechanical durability within different experimental series are normalized to allow comparison across feed types, size, etc. Hence, within each series the obtained mechanical durability is compared to the mean value obtained in the particular series. This highlight drying experiments that increase the amount of fines in the DORIS test, compared to the average value of the particular series. Vice versa, drying experiments with conditions yielding superior quality give fine contents below average, i.e. negative 'Δ% fines' values in Figure 94.

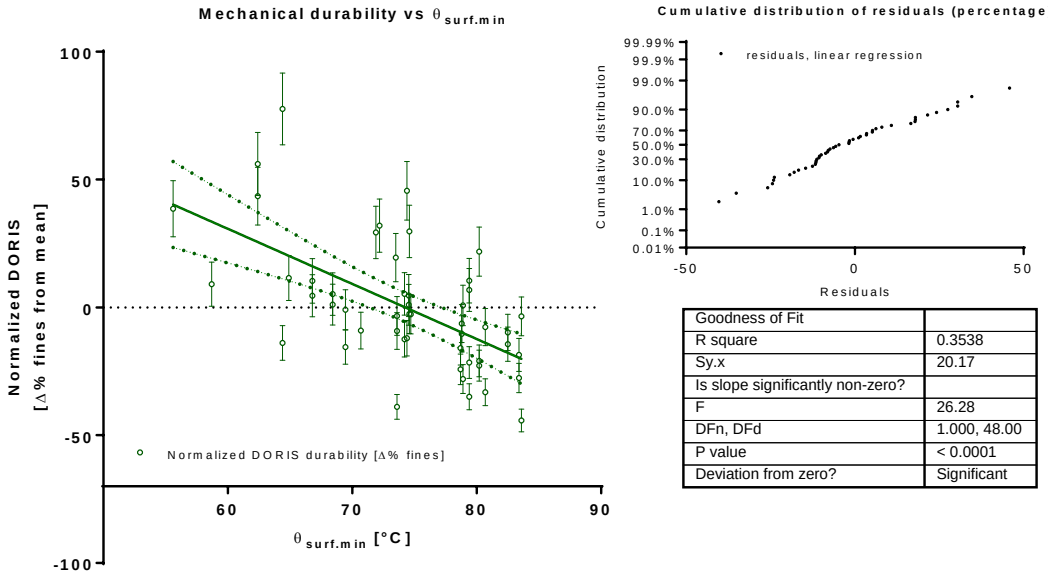

Goodness of Fit	
R square	0.3538
Sy.x	20.17
Is slope significantly non-zero?	
F	26.28
DFn, DFd	1.000, 48.00
P value	< 0.0001
Deviation from zero?	Significant

Figure 94: Normalized measures of obtained mechanical durability in the DORIS test compared to simulated minimum surface temperature in all experiments carried out. Negative values of 'Δ% fines' indicate an improvement in the mechanical durability as compared to the average.

The linear correlation in Figure 94 demonstrate high variance of the data, with a R^2-value of 0.35., i.e. the minimum surface temperature observed, as single main effect, is able to explain 35 % of the total variance. Whilst this value is low, there is a definite trend that higher minimum surface temperatures improve the mechanical durability ($p<0.0001$). The cumulative distribution of the residuals is also plotted to highlight their normal distribution. It should

be stressed that the linear correlation is chosen to demonstrate the significance of minimum surface temperature, rather than to demonstrate an actual linear tendency. Actually, a linear relationship should strictly not be expected due to the expected non-linear behavior of the glass phase transition, i.e. transcending into the glassy region at an early stage in the drying – or not. Whilst it can be concluded that there is a definite tendency that minimum surface temperature impacts durability, the variance of the estimate will be correspondingly high following the low R^2-value. This is illustrated from the 95 % confidence intervals included around the regression line in Figure 94.

Other than the minimum surface temperature, it follows from the glass transition theory that the surface moisture content at the minimum surface temperature should be high, to reduce the risk of transcending into the glassy state following evaporative cooling. As already mentioned it should additionally be theoretically viable to achieve a spatial uniform glass transition onset from the surface to the center. A numerical representation of this ability can be interpreted as a low spatial moisture content gradient at the minimum surface temperature.

As the minimum surface temperature, the aforementioned two parameters can be predicted by the pellet level model. It follows that below model predictions should be important for explaining and predicting the mechanical durability:

- minimum surface temperature, $\theta_{surf.min}$;
- spatial moisture content gradient at minimum surface temperature, $\nabla X\big|_{\theta_{surf.min}}$
- surface moisture content at minimum surface temperature, $X_{surf}\big|_{\theta_{surf.min}}$

Above model parameters are normalized against the mean value of the parameter obtained for each experimental design series. This allows combinations of model predictions trying to identify an optimal quality estimate. Such estimate could possibly improve the correlation (reducing unexplained variance, increasing R^2) against mechanical durability further than using solely θ_{min}, as in Figure 94. The following quality estimate, 'QE' were considered:

$$QE = \frac{\overline{\overline{\theta_{surf.min}}} + a \cdot \overline{\overline{X_{surf}\big|_{\theta_{surf.min}}}}}{\left(1 + \frac{1}{b \cdot \overline{\overline{\nabla X\big|_{\theta_{surf.min}}}}}\right)^{b \cdot \overline{\overline{\nabla X\big|_{\theta_{surf.min}}}}}} \qquad \text{Eq. 78}$$

The double overbars denotes normalization within and experimental design. The function applied in the denominator (with spatial moisture gradient) approaches unity for small spatial moisture content gradients (and e for large values). This is applied to avoid rapidly increasing quality estimates when spatial moisture gradients approaches zero.

Table 8: comparison of linear and 2nd order polynomial regression analyses for different indicative quality estimates

Regression type	$\theta_{surf.min}$	$\overline{\overline{\theta_{surf.min}}}$	'QE'
Linear	$R^2 = 0.35$	0.39	R^2=0.42; $a = 0.4$, $b = \infty$
2nd order polynomial	$R^2 = 0.36$	0.39	R^2=0.44; $a = 0.8$, $b = 25$

Table 8 demonstrates that normalization of the minimum obtained surface temperatures in the model results, to the respective mean value in the experimental series, $\overline{\overline{\theta_{\min}}}$, improves the correlation against mechanical durability. Additionally, by invoking the effect from normalized estimates of the spatial moisture gradient at $\theta_{\text{surf.min}}$, $\overline{\overline{\nabla X|_{\theta_{\text{surf.min}}}}}$, and surface moisture content at $\theta_{\text{surf.min}}$, $\overline{\overline{X_{\text{surf}}|_{\theta_{\text{surf.min}}}}}$, the explanation of the total variance is increased slightly more. As it appear the spatial moisture gradient only describes very little of the total variance ($b = \infty$), and only if a non-linear regression is used, ($b = 25$, cf. Table 8). It can be argued if there is sufficient reasoning for choosing 2nd order polynomial regression rather than using a simpler linear fit, discarding also the influence of spatial moisture gradients, to gain only 2 % additional description of the total variance. As described, it is expected that the influence on the parameters should be non-linear; for this reason, the non-linear description of mechanical durability using 'QE' are included in

Figure 96. Both Figure 95 and Figure 96 should however be equally right in justifying, that the glass transition theory can be used to explain and optimize mechanical durability.

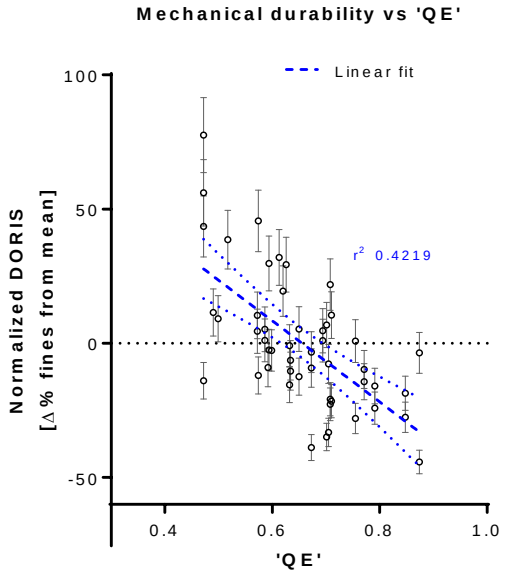

Figure 95: Linear regression of mechanical durability vs 'QE'. Parameters are listed in Table 8.

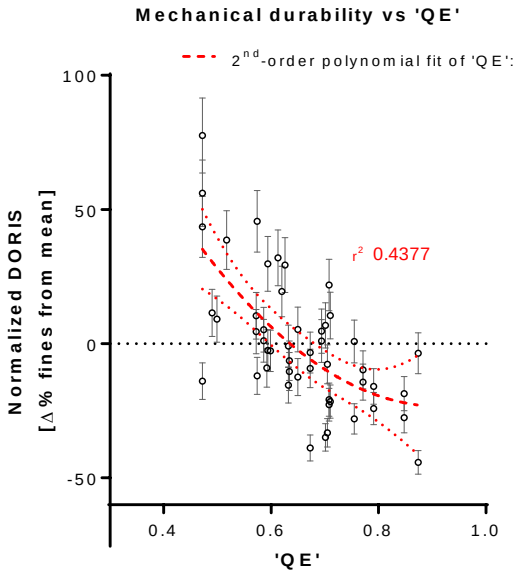

Figure 96: Non-linear regression of mechanical durability vs 'QE'. Parameters are listed in Table 8.

In summary, prerequisites to make use of the glass transitions hypothesis to actively optimize mechanical durability of extruded fish feed in the deep-bed hot air drying process are:

- Complete model of the deep-bed drying of extruded fish feed, including pellet level details of spatial temperature and moisture content (section 4.5).
- Knowledge of moisture diffusivity of the particular feed (or actual drying time and end moisture content, to find diffusivity by equaling modeled and actual drying times).
- Glass transition data for extruded fish feed pellets.

It follows that an inherently important aspect in active optimization of mechanical durability, is the lack of glass transition data for extruded fish feed pellets. Optimization becomes further complicated by optimizing all pellets across the bed depth, while at the same time trying to minimize the specific energy consumption per evaporated amount of water.

The figures below illustrate the impact of increasing velocity (Figure 98), humidity (Figure 99) and temperature (Figure 100) as compared to some reference drying conditions, given by Figure 97. Increasing the different drying conditions give very different impacts on the spatial moisture and temperature curves as compared to a hypothesized glass transition curve. It is interesting to notice that an increase in velocity reduces the drying time by 66 % (increases capacity), but does not stop the pellet surface (and center) to transcend to glassy state in the evaporative cooling – pellet spatial profiles of Figure 97 and Figure 98 are quite comparable.

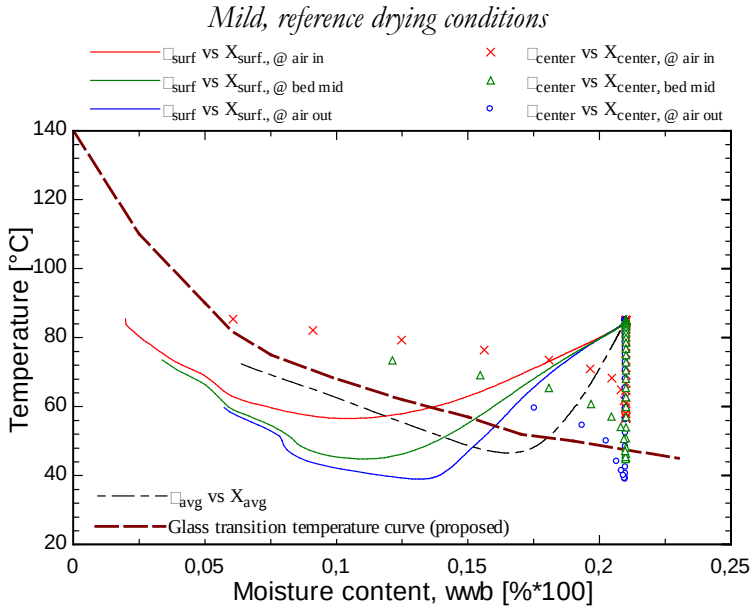

Figure 97: Spatial moisture and temperature profile compared to a proposed glass transition temperature curve for the deep-bed drying of 25 cm 8 mm pellets at 0.7 m/s, 110 °C and 60 g H_2O/kg dry air. Drying time to 6 % average moisture (w.b.) is 107 min.

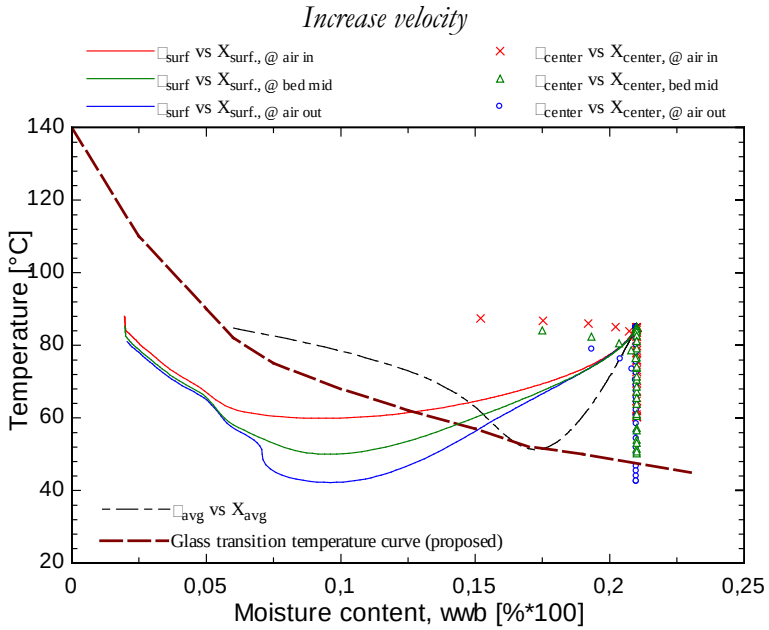

Figure 98: Spatial moisture and temperature profile compared to a proposed glass transition temperature curve for the deep-bed drying of 25 cm 8 mm pellets at 1.5 m/s, 90 °C and 8 g H_2O/kg dry air. Drying time to 6 % average moisture (w.b.) is 36.5 min.

The same pattern is seen when increasing only the temperature, Figure 100, however some delay in the spatial onset of glass transition for pellets closest to the air inlet can be found, whilst the drying time is only improved by 35 % from increasing the temperature set-point by 40 °C. Increasing humidity, Figure 99, significantly alters the spatial profiles of the pellets, and pellets should now remain in their rubbery state, as evaporative cooling becomes very low. Unfortunately, these drying conditions increases drying time to well more than 4 hours.

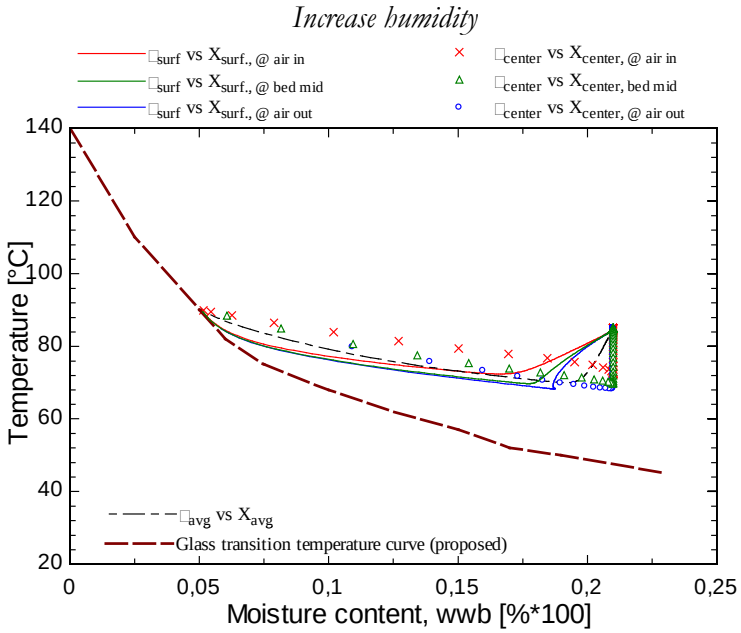

Figure 99: Spatial moisture and temperature profile compared to a proposed glass transition temperature curve for the deep-bed drying of 25 cm 8 mm pellets at 0.25 m/s, 90 °C and 80 g H_2O/kg dry air. Drying time to 6 % average moisture (w.b.) is >240 min.

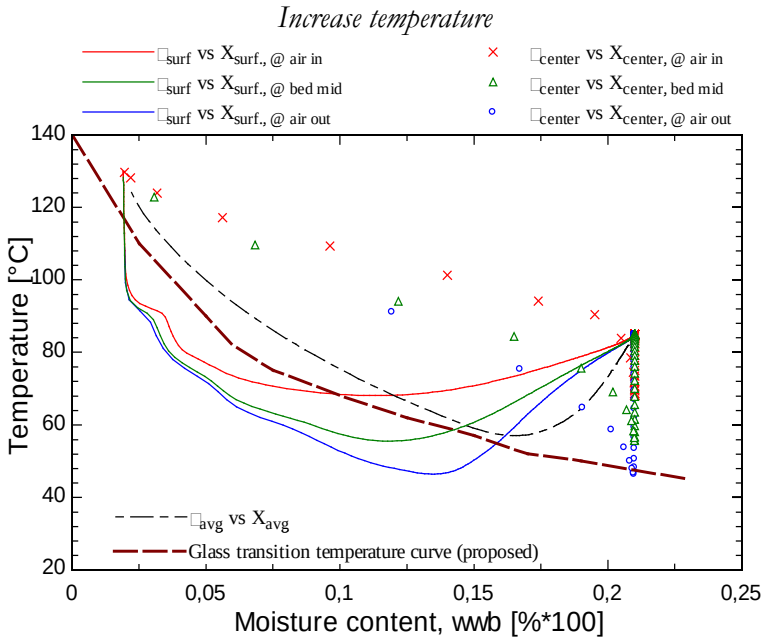

Figure 100: Spatial moisture and temperature profile compared to a proposed glass transition temperature curve for the deep-bed drying of 25 cm 8 mm pellets at 0.25 m/s, 130 °C and 8 g H2O/kg dry air. Drying time to 6 % average moisture (w.b.) is 70 min.

As it appears, optimal drying conditions cannot be achieved by elevating only a single drying parameter, as different drying parameters affect quality, capacity and efficiency differently. Figure 101 and Figure 102 demonstrate two different approaches of avoiding phase transition to the glassy state, following evaporative cooling. In Figure 101, high temperature, velocity and humidity is used, achieving a drying time of only 21 minutes, and the transition into the glassy state occur at 100 °C, rapidly increasing to 120 °C.

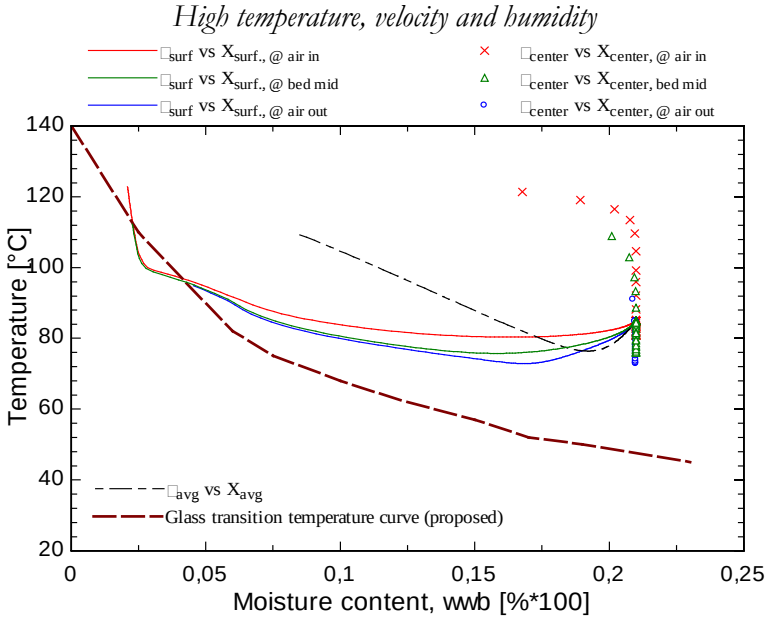

Figure 101: Spatial moisture and temperature profile compared to a proposed glass transition temperature curve. Deep-bed drying of 25 cm 8 mm pellets at 1.5 m/s, 130 °C and 80 g H_2O/kg dry air. Drying time to 6 % average moisture (w.b.) is 21 min.

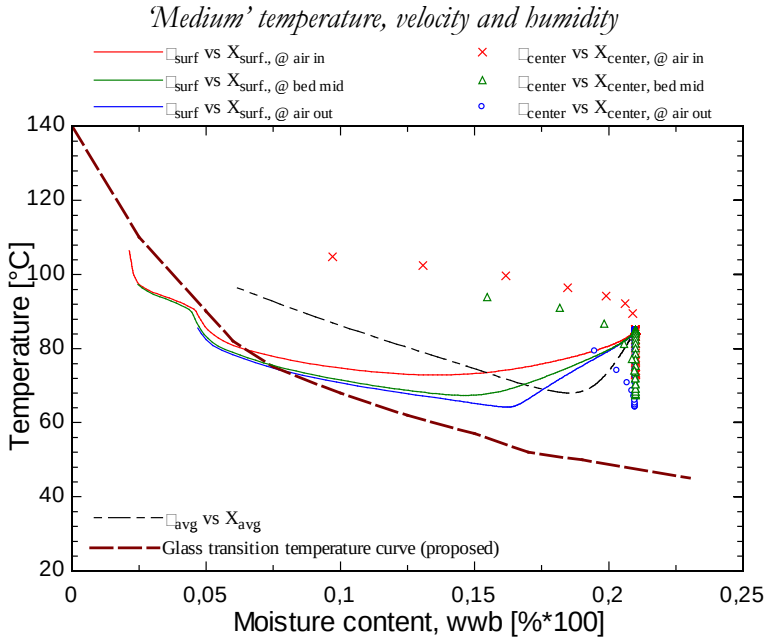

Figure 102: Spatial moisture and temperature profile compared to a proposed glass transition temperature curve. Deep-bed drying of 25 cm 8 mm pellets at 0.7 m/s, 110 °C and 60 g H_2O/kg dry air. Drying time to 6 % average moisture (w.b.) is 46 min.

Figure 102 demonstrate an approach using 'medium' temperature, velocity and humidity to achieve transition into the glassy state at 80 °C. Effective glass transition control, when suitable glass transition data for extruded fish feed pellets are acquired, should consider reducing air temperature (i.e. in a new drying zone) at the onset of glass transition.

In summary, without a priori knowledge of glass transition data of extruded fish feed, durability can be optimized from keeping temperature, humidity and velocity in the first part of the dryer high, as this should reduce the risk for the pellets to transcend into their glassy state. This at the same time reduces drying time and elevates capacity. Using low bed depths in initial stages of the dryer further minimizes this risk. Whilst this approach is already assessed as good drying practice in (some parts of) the industry, little focus is paid to the transfer of pellets into the dryer, as the risk of early glass transition exists already in this pre-drying stage, or at the least preconditions for avoiding early glass transition within the dryer are worsened. When knowledge of glass transition is obtained, it will allow active glass transition temperature control to be applied as a multi-objective optimization tool, minimizing specific energy consumption whilst improving the mechanical durability by avoiding early glass transition onset and elevated temperatures in the glassy state. Such optimization could be constrained by a capacity demand and/or, for existing production lines, by dryer dimensions.

7 Conclusions

A multiphysical description of the drying parameters that govern energy efficiency and improves the structural properties that lead to superior technical quality of extruded fish feed have been carried out in this PhD project. From reviewing literature in related fields and from experimental work carried out in the present project, conclusions are outlined:

An experimentally validated model of the deep-bed hot air drying of extruded fish feed is presented to predict and allow optimization of energy efficiency. Spatial moisture and temperature profiles, over time, for individual pellets in the deep bed are additional model output, which can be used to predict mechanical durability.

The numerical model comprise conservation balances for moisture and temperature in the pellets and in the drying air, and utilize the finite difference method as the resolution strategy. The model is combined with a process level model to allow internal recirculation of the drying air. A custom designed lab scale hot air dryer is used to calibrate and validate the model performance. The model comprise empirically recorded desorption isotherms. Thin-layer drying experiments are carried out to evaluate the temperature dependency of moisture diffusivity and the flow dependency of external heat and mass transfer coefficients. The model is validated using a range of deep-bed drying experiments at different drying conditions. The model reproduces the experimental recorded data well, with a coefficient of variation of the root mean square error, RMSE, at 6 % – 13 % for product moisture and surface temperature. The most significant part of the RMSE can be accounted to initial moisture flash off, and to heating of the pellets, following evaporative cooling. Respectively, this is explained from that, no transfer period is included in the model, and that temperatures are measured on pellet lee-sides. The extent of the evaporative cooling is generally predicted well by the model.

The model holds directly potential in benchmarking and monitoring energy efficiency of drying processes, as well as for investigating opportunities for reducing energy consumption. The model additionally calculates spatial moisture and temperature profile for each individual pellet in the drying bed. This is valuable input in the effort to promote those mechanical properties of extruded fish feed pellets that are known to improve mechanical durability.

Durable feed pellets are viscoelastic, demonstrating viscous stress relaxation and reversible deformation.

From correlations, using a commercial tester for mechanical durability (DORIS) and a texture analyzer, it have been demonstrated that durable extruded fish feed pellet have predominantly viscoelastic mechanical properties. This allow the pellets to show viscous force relaxation during a deformation, yet returning to their original position when force is released. This was additionally supported by proper choice of measurement parameters in texture analysis. Particularly, the response between mechanical durability and viscoelasticity was improved, when allowing complete relaxation for at least 7 seconds following a deformation. The identified structural properties that promote mechanical durability, reducing build-up of stresses in the pellets are supported in literature [132].

Viscoelastic character of extruded fish feed pellets can be described using a glass transition theory. Drying in the rubbery phase enhance viscoelastic character and improves durability. Early transition to the glassy state decrease durability, from a lowered viscoelastic character.

The viscoelastic character and mechanical durability of a single extruded fish feed pellet depend on prevailing air conditions in the dryer. The influence of each of the drying parameters can be ascribed to their impact, following a glass transition theory. This implies that water acts as plasticizer, increasing the pellets' viscous character, and that drying in the rubbery phase ensures phase mobility and reduces surface tension. Additionally it is proposed that surface non-enzymatic browning reactions decrease viscoelastic character of the pellets, when glass transition occur at high temperatures. These conditions did however not reduce mechanical durability, apparently reasoned from distinctively altered structural properties, increasing pellet hardness and plasticity.

It has been found experimentally, that low surface temperatures, following evaporative cooling, significantly reduces the mechanical durability. This is a direct consequence of early glass transition in the drying. It follows that mechanical durability of extruded fish feed can be improved by keeping a high temperature, humidity and velocity in the first section of the dryer. Transition to the glassy state should however occur at a low drying rate, to account for sudden reduction of surface diffusivity and -mobility. This could additionally reduce the potential for non-enzymatic browning reactions on the surface to occur.

Mechanical durability of extruded fish feed in the drying process can be promoted by 'glass transition temperature control' utilizing spatial profiles of the pellets obtained from the drying model.

To predict and optimize mechanical durability by ensuring phase mobility in the drying, spatial predictions from the developed model are included as effects in a 'quality estimate', to:

- Increase minimum surface temperature;
- Increase surface moisture content at the minimum surface temperature; and
- Decrease spatial moisture gradient at the minimum surface temperature.

Acknowledging a non-linear behavior, the quality estimate was able to account for 44 % of the total variation in mechanical durability averaged over 54 different drying experiments, using a 2^{nd} order polynomial fit.

When glass transition data is obtained for extruded fish feed pellets, the proposed model will allow active glass transition temperature control aiming to improve mechanical durability, by avoiding early glass transition onsets, at any point through the bed, as well as avoiding elevated product temperatures when entering the glassy state.

The numerical model developed ultimately form basis for a multi-objective optimization tool for the hot air drying of extruded fish feed; objective is to increase energy efficiency whilst utilizing drying conditions that does not compromise technical quality of the fish feed.

8 Outlook

In the present research project, a tool for modeling the deep-bed drying process of extruded fish feed have been developed, to account for specific energy consumption and to predict spatial details of the pellets in the bed, during the drying process. This falls parallel to a number of interesting findings on the connection between structural properties, mechanical durability and on spatial moisture and temperature evolution in the drying process. Hence, the PhD project terminates at the threshold of a real viable industrial application potential, which motivates further maturation.

Acquiring glass transition data for extruded fish feed have imminent importance to mature application of active glass transition temperature control of the drying process. This should allow the developed model, using the results demonstrating the mechanism for improving durability in the drying process, to redeem its full industrial potential

An important task is to expand the developed model to account for multiple drying zones and multiple belts, with changing air conditions, bed depths and possibly a randomized re-orientation of the pellets when falling from one belt to another. A large part of this work becomes adding the presented model onto itself, until the desired number of drying zones and belt have been reached, each time using product output conditions as new input conditions. Whilst this task should not be particular complex, it will increase industrial application.

As it has been found in the present project, the minimum temperature obtained following evaporative cooling directly influences mechanical durability. This should induce a natural focus in future work on the transfer of the pellets to the dryer. This process is important, as evaporative cooling will obviously start when pellet start to flash off moisture when transported either mechanically, on a conveyor belt, or pneumatically, in an 'airlift'. In some occasions, product quality might already have been compromised before even entering the dryer. This should also induce a discussion to re-think the principles of industrial scale fish feed (and pet food) drying; possibly invoking another drying media in the pellet transport process, e.g. superheated steam

The transfer period from the extruder to the dryer should be added to the model, i.e. as a 'zone 0'. The presented model have limitations in accurately predicting the transfer process, as it will be valid for pellets stacked in a deep bed and subjected to forced convection air flow. Pellets conveyed pneumatically in airlifts are in free flow, and pellet transported on belts have ~stagnant airflow conditions. More work is needed to mature and validate the inclusion of the transfer period to the dryer into the model.

Active multi-objective glass transition temperature control could be realized as an online software for active dryer control, or as an offline tool to evaluate opportunities to improve energy efficiency, whilst safeguarding or possibly improving technical quality. Practically, the multi-objective control could be realized by minimizing the burner load, constrained by dryer dimensions, target moisture and capacity, whilst maximizing the 'quality estimate' for all pellets across the bed. Latter should essentially avoid that (many) pellets transcends through

their glass transition point, until at a desired moisture content. At some average glass transition onset', air temperature can actively be reduced to avoid creating pellets with crisp, hard surfaces.

A practical implication of maturing a multi-objective dryer control software is to investigate the temporal and regional variance of moisture and structural uniformity of pellets produced in a commercial scale extruder, as this will directly influence application of any feed-forward dryer control logic implemented. Along the same lines, it should be investigated if the accuracy of humidity measurements in drying can be improved to provide accurate inlet conditions to the dryer model and for accurately stating the obtained energy efficiency.

Finally, the introduction of a wide variety of feed types and recipes into the model is subject to future work. Possibly this could be established in the framework of allowing customers in fish feed production to make use of the dryer model when providing details of their production run, drying parameters, etc. Minimization of the offset between modeled average moisture content and actual obtained average moisture content for a specific product should largely be ascribed to differences in pellet moisture diffusivities.

Bases on a few experiments in the present project, it has been proposed that longitudinal shrinkage will occur to a certain extent, following entrance into the glassy state. Whilst this reduces the net amount of stresses building up during drying in the glassy state, non-isotropic stress differences are increased. This could in turn be expected to lead to reduced durability or breakage. This hypothesis adds to the glass transitions hypothesis of biopolymers, but more work is needed to find if the mechanism is valid and if it can assist in the prediction of mechanical durability in the deep-bed hot air drying of extruded fish feed.

9 References

1 Ytrestrøyl, T.; Aas, T.S.; Åsgård, T. Resource utilisation of Norwegian salmon farming in 2012 and 2013. 2014, Nofima.

2 FAO The state of World Fisheries and Aquaculture - opportunities and challenges. 2014, Food and Agriculture Organization of the United Nations: Rome.

3 The World Bank FISH TO 2030, Prospects for Fisheries and Aquaculture. 2013.

4 FishstatJ - FAO Glabl Fishery and Aquacultural Statistics Global Aquacultural production (1950 - 2013), Fisheries and Agricultural Organization. 2013.

5 Oehme, M. Feed Utilization can be improved by optimizing physical pellet quality and feeding equipment in salmonid farming in Department of Animal and Aquacultural Sciences. 2013, Norwegian University of Life Sciences: Ås.

6 Oehme, M. et al. Feed pellet distribution in a sea cage using pneumatic feeding system with rotor spreader. Aquacultural Engineering 2012, 51, 44-52.

7 Aarseth, K.A. et al. Reliable pneumatic conveying of fish feed. Aquacultural Engineering 2006, 35 (1), 14-25.

8 Aarseth, K.A. Attrition of feed pellets during pneumatic conveying: The influence of velocity and bend radius. Biosystems Engineering 2004, 89 (2), 197-213.

9 Aas, T.S. et al. Analysis of pellet degradation of extruded high energy fish feeds with different physical qualities in a pneumatic feeding system. Aquacultural Engineering 2011, 44 (1), 25-34.

10 Gjøsæter, J. et al. Effekter av spillfôr på marine organismer in Kyst og Havbruk. 2008, Havforskningsintituttet. 52-55.

11 Samuelsen, T.A. Fishmeal physicochemical properties - Impact on the fish feed extrusion process, phase transitions and physical pellet quality. 2015, University of Bergen.

12 Brooks, K.M.; Mahnken, C.V.W. Interactions of Atlantic salmon in the Pacific northwest environment: II. Organic wastes. Fisheries Research 2003, 62 (3), 255-293.

13 Aas, T.S. et al. Nutritional responses in rainbow trout (Oncorhynchus mykiss) fed diets with different physical qualities at stable or variable environmental conditions. Aquaculture Nutrition 2011, 17 (6), 657-670.

14 Sorensen, M. et al. Pea and wheat starch possess different processing characteristics and affect physical quality and viscosity of extruded feed for Atlantic salmon. Aquaculture Nutrition 2011, 17 (2), 326-336.

15 Sorensen, M. et al. Starch source, screw configuration and injection of steam into the barrel affect the physical quality of extruded fish feed. Aquaculture Research 2010, 41 (3), 419-432.

16 Kaliyan, N.; Morey, R.V. Factors affecting strength and durability of densified biomass products. Biomass & Bioenergy 2009, 33 (3), 337-359.

17 Behnke, K.C.; Kpp; Kpp Feed manufacturing technology: Current issues and challenges; Advances in Equine Nutrition. 115-127 1998

18 Rana, K.J.; Hasan, M.R. Impact of rising feed ingredient prices on aquafeeds and aquaculture production. 2009, Food and Agriculture Organization of the United Nations: Rome.

19 Pacheco, A.C.W. et al. Modeling of drying and adsorption isotherms of the fish feed. Brazilian Archives of Biology and Technology 2011, 54, 577-588.

20 Graintec A/S *Unpublished obersvations:* Numerous energy surveys for customers in pet food and fish feed production, from 1990-2016.

21 Boto, I.; Phillips, S.; D'Andrea, M. Fish-farming: the new driver of the blue economy. 2013, Centre Technique de Coopération Agricole et Rurale: Brussels, Belgium.

22 Halwart, M.; Soto, D.; Arthur, J.R. Cage aquaculture. Regional reviews and global reviews in Fisheries Technical Paper No. 505. 2007, FAO: Rome. 205.

23 FAO History of Aquaculture. 1988, Food and Agricultural Organization of the United Nations: Manila, Philippines

24 Grøttum, J.A.; Beveridge, M. a review of cage culture: northern europe in In M. Halwart, D. Soto and J.R. Arthur (eds). Cage aquaculture – Regional reviews and global overview. 2007, FAO: Rome. pp. 126-154.

25 Oppedal, F.; Dempster, T.; Stien, L.H. Environmental drivers of Atlantic salmon behaviour in sea-cages: A review. Aquaculture 2011, 311 (1-4), 1-18.

26 Craig, S.; Helfrich, L.A. Understanding Fish Nutrition, Feeds, and Feeding in Virginia Cooperative Extension. 2009, Virginia State University.

27 Thomas, M.; van Zuilichem, D.J.; van der Poel, A.F.B. Physical quality of pelleted animal feed. 2. contribution of processes and its conditions. Animal Feed Science and Technology 1997, 64 (2–4), 173-192.

28 Denstadli, V. et al. Enzyme pretreatment of fibrous ingredients for carnivorous fish: Effects on nutrient utilisation and technical feed quality in rainbow trout (Oncurhynchus mykiss). Aquaculture 2011, 319 (3–4), 391-397.

29 Payne, J.D. Improving quality of pellet feeds. Milling Feed and Fertiliser 1978, 161 (5).

30 Haubjerg, A.F. et al. Structural properties and mechanical durability of extruded fish feed. Journal of Food Process Engineering 2015, 38 (6), 621-631.

31 Haubjerg, A.F. Testing durability of fish feed pellets – which to use when and why in International Aquafeed Directory & Buyers' Guide. 2015, Turret Group Ltd: Rickmansworth, Herts, UK. 22-23.

32 Mujumdar, A.S. Handbook of Industrial Drying; 3 ed. CRC Press, Taylor & Francis Group: New York, 2007

33 Mujumdar, A.S. R&D Needs, Challenges and Opportunities for Innovation in Drying Technology, S.V. Jangam and B.N. Thorat. 2010.

34 Holgersen, K. Manager, Aquafeed Technology, Graintec A/S. 2016: personal communication.

35 Schmidt, S. personal communication, Disruptive Dry Process &Technology Leader at MARS. 2014.

36 Mujumdar, A.S.; Devahastin, S. Superheated Steam Drying - An Emerging Technology. 2008: National University of Singapore.

37 Haubjerg, A.F. et al. Ensuring technical product quality in energy efficient hot air drying of extruded fish feed: Definition of an industrial research project in International Drying Symosium. 2012: Xiamen, China.

38 Moyers, C.G.; Baldwin, G.W. Perry's Chemical Engineers' Handbook in Section 12, Pshycrometry, Evaporative Cooling and Solids Drying. 1999, McGraw-Hill Companies Inc.

39 Waananen, K.M.; Litchfield, J.B.; Okos, M.R. Classification of drying models for porous solids. Drying Technology 1993, 11 (1), 1-40.

40 Katekawa, M.E.; Silva, M.A. A review of drying models including shrinkage effects. Drying Technology 2006, 24 (1), 5-20.

41 Mayor, L.; Sereno, A.M. Modelling shrinkage during convective drying of food materials: a review. Journal of Food Engineering 2004, 61 (3), 373-386.

42 Lewis, W.K. The rate of drying of solid materials. Journal of Industrial and Engineering Chemistry 1921, 13, 427-432.

43 Whitaker, S. Simultaneous Heat, Mass, and Momentum Transfer in Porous Media: A Theory of Drying, in Advances in Heat Transfer; P.H. James and F.I. Thomas, Editors Elsevier, 1977; 119-203

44 Luikov, A.V. Systems of differential equations of heat and mass-transfer in capillary-porous bodies (review). International Journal of Heat and Mass Transfer 1975, 18 (1), 1-14.

45 Wang, W.; Ma, H.X.; Chen, G.H. A Model for Drying of Porous Materials: From Generality to Specific Applications. Drying Technology 2011, 29 (13), 1542-1555.

46 Yiotis, A.G. et al. Pore-network modeling of isothermal drying in porous media. Transport in Porous Media 2005, 58 (1-2), 63-86.

47 Hussain, M.M.; Dincer, I. Two-dimensional heat and moisture transfer analysis of a cylindrical moist object subjected to drying: A finite-difference approach. International Journal of Heat and Mass Transfer 2003, 46 (21), 4033-4039.

48 Viollaz, P.E.; Rovedo, C.O. A drying model for three-dimensional shrinking bodies. Journal of Food Engineering 2002, 52 (2), 149-153.

49 Roberts, J.S.; Tong, C.H. Drying kinetics of hygroscopic porous materials under isothermal conditions and the use of a first-order reaction kinetic model for predicting drying. International Journal of Food Properties 2003, 6 (3), 355-367.

50 Yu, X. et al. Determination of the Bulk Moisture Diffusion Coefficient for Corn Starch Using an Automated Water Sorption Instrument. Journal of Agricultural and Food Chemistry 2007, 56 (1), 50-58.

51 Rossello, C. et al. Nonisotropic mass transfer model for green bean drying. Journal of Agricultural and Food Chemistry 1997, 45 (2), 337-342.

52 Rovedo, C.O.; Suarez, C.; Viollaz, P.E. Drying of foods: Evaluation of a drying model. Journal of Food Engineering 1995, 26 (1), 1-12.

53 Misra, R.N.; Young, J.H. Numerical solution of simultaneous moisture diffusion and shrinkage during soybean drying. Transactions of the American Society of Agricultural Engineers 1980, 23 (5), 1277-1282.

54 Wang, N.; Brennan, J.G. A mathematical model of simultaneous heat and moisture transfer during drying of potato. Journal of Food Engineering 1995, 24 (1), 47-60.

55 Feng, H.; Tang, J.; Dixon-Warren, S.J. Determination of moisture diffusivity of red delicious apple tissues by thermogravimetric analysis. Drying Technology 2000, 18 (6), 1183-1199.

56 Lambert, C.; Romdhana, H.; Courtois, F. Reverse Methodology to Identify Moisture Diffusivity During Air-Drying of Foodstuffs. Drying Technology 2015, 33 (9), 1076-1085.

57 Haubjerg, A.F. et al. A numerical model of the deep-bed drying of extruded fish feed and its experimental validation. In Proceedings of 5th European Drying Conference (EuroDrying'2015), Budapest, Hungary, 2015

58 Simal, S. et al. Drying of shrinking cylinder-shaped bodies. Journal of Food Engineering 1998, 37 (4), 423-435.

59 Lambert, C.; Romdhana, H.; Courtois, F. Reversing classical modeling methodology for hot air drying of foodstuffs. In Proceedings of 4th European Drying Conference (EuroDrying'2013), Paris, France, 2013;8

60 Ljung, A.L.; Lundstrom, T.S.; Tano, K. Simulation of convective drying of a cylindrical iron ore pellet. International Journal of Numerical Methods for Heat & Fluid Flow 2011, 21 (6-7), 703-716.

61 Queiroz, M.R.; Nebra, S.A. Theoretical and experimental analysis of the drying kinetics of bananas. Journal of Food Engineering 2001, 47 (2), 127-132.

62 Jin, X.; Sman, R.G.M.v.d.; Boxtel, A.J.B.v. Evaluation of the free volume theory to predict moisture transport and quality changes during broccoli drying. In

Proceedings of 17th International Drying Symposium Magdeburg, Germany, 3-6 October, 2010

63 de Lima, A.G.B.; Queiroz, M.R.; Nebra, S.A. Simultaneous moisture transport and shrinkage during drying of solids with ellipsoidal configuration. Chemical Engineering Journal 2002, 86 (1–2), 85-93.

64 Hadrich, B.; Kechaou, N. Mathematical modeling and simulation of shrunk cylindrical material's drying kinetics-Approximation and application to banana. Food and Bioproducts Processing 2009, 87 (C2), 96-101.

65 Kowalski, S.J.; Mierzwa, D. Numerical Analysis of Drying Kinetics of Shrinkable Products Like Fruits and Vegetables. In Proceedings of 18th International Drying Symposium, Xiamen, China, 11-15 November, 2012

66 Caceres, G.; Bruneau, D.; Jomaa, W. Two-phase shrinking porous media drying: A modeling approach including liquid pressure gradients effects. Drying Technology 2007, 25 (12), 1927-1934.

67 Karim, M.A.; Hawlader, M.N.A. Mathematical modelling and experimental investigation of tropical fruits drying. International Journal of Heat and Mass Transfer 2005, 48 (23–24), 4914-4925.

68 Welty, J.R.; Wicks, C.E.; Wilson, R.E. Fundamentals of Momentum. Limusa: Mexico, 1993

69 Sahin, A.Z. et al. Determination of drying times for regular multi-dimensional objects. International Journal of Heat and Mass Transfer 2002, 45 (8), 1757-1766.

70 Peleg, M. Assessment of a semi-empirical four parameter general model for sigmoid moisture sorption isotherms. Journal of Food Process Engineering 1993, 16 (1), 21-37.

71 Chirife, J. Fundamentals of the drying mechanism during air dehydration of foods; Advances in Drying, ed. A.S. Mujumdar. 1983

72 Whitaker, S. Forced convection heat-transfer correlations for flow in pipes, past flat plates, single cylinders, single spheres, and for flow in packed-beds and tube bundles. Aiche Journal 1972, 18 (2).

73 Haubjerg, A.F. et al. Convective Deep Bed Drying of Extruded Fish Feed: Development of a Mathematical Model. Drying Technology 2015 (submitted november 2015).

74 Kaya, A.; Aydin, O.; Dincer, I. Numerical modeling of forced-convection drying of cylindrical moist objects. Numerical Heat Transfer Part a-Applications 2007, 51 (9), 843-854.

75 Sakai, N.; Hayakawa, K.-I. Two Dimensional Simultaneous Heat and Moisture Transfer in Composite Food. Journal of Food Science 1992, 57 (2), 475-480.

76 Barati, E.; Esfahani, J.A. Mathematical modeling of convective drying: Lumped temperature and spatially distributed moisture in slab. Energy 2011, 36 (4), 2294-2301.

77 Adeyanyu, A.A.; Manohar, K. Theoretical and Experimental Investigation of Heat Transfer in Packed Beds. Research Journal of Applied Sciences 2009, 4 (5), 166-177.

78 Achenbach, E. Heat and flow characteristics of packed beds. Experimental Thermal and Fluid Science 1995, 10 (1), 17-27.

79 Larachi, F. et al. Nu/Sh Correlation for Particle-Liquid Heat and Mass Transfer Coefficients in Trickle Beds Based on Péclet Similarity. Chemical Engineering Research and Design 2003, 81 (6), 689-694.

80 Sander, A.; Kardum, J.P.; Skansi, D. Transport Properties in Drying of Solids. Chemical & Biochemical Engineering 2001, 15 (3), 131-137.

81 Haubjerg, A.F. et al. Mathematical modeling of the drying of extruded fish feed and its experimental demonstration. In Proceedings of 19th International Drying Symposium, Lyon, France, 2014

82 Cenkowski, S.; Jayas, D.S.; Pabis, S. Deep-bed grain drying - a review of particular theories. Drying Technology 1993, 11 (7), 1553-1581.

83 Sun, D.W.; Woods, J.L. Simulation of the heat and moisture transfer process during drying in deep grain beds. Drying Technology 1997, 15 (10), 2479-2508.

84 Sitompul, J.P.; Istadi; Widiasa, I.N. Modeling and simulation of deep-bed grain dryers. Drying Technology 2001, 19 (2), 269-280.

85 Istadi, I.; Sitompul, J.P. A comprehensive mathematical and numerical modeling of deep-bed grain drying. Drying Technology 2002, 20 (6), 1123-1142.

86 Srivastava, V.K.; John, J. Deep bed grain drying modeling. Energy Conversion and Management 2002, 43 (13), 1689-1708.

87 Sitompul, J.P.; Istadi; Sumardiono, S. Modelling and simulation of momentum, heat, and mass transfer in a deep-bed grain dryer. Drying Technology 2003, 21 (2), 217-229.

88 Aregba, A.W.; Nadeau, J.P. Comparison of two non-equilibrium models for static grain deep-bed drying by numerical simulations. Journal of Food Engineering 2007, 78 (4), 1174-1187.

89 Hemis, M. et al. Simulation of Coupled Heat and Mass Transfer in Granular Porous Media: Application to the Drying of Wheat. Drying Technology 2011, 29 (11), 1267-1272.

90 Zare, D. et al. Computer simulation of rough rice drying in a batch dryer. Energy Conversion and Management 2006, 47 (18-19), 3241-3254.

91 Schmalko, M.E.; Peralta, J.M.; Alzamora, S.M. Modeling the drying of a deep bed of Ilex paraguariensis in an industrial belt conveyor dryer. Drying Technology 2007, 25 (12), 1967-1975.

92 Zare, D.; Chen, G.N. Evaluation of a simulation model in predicting the drying parameters for deep-bed paddy drying. Computers and Electronics in Agriculture 2009, 68 (1), 78-87.

93 Naghavi, Z.; Moheb, A.; Ziaei-rad, S. Numerical simulation of rough rice drying in a deep-bed dryer using non-equilibrium model. Energy Conversion and Management 2010, 51 (2), 258-264.

94 Ljung, A.-L. et al. Discrete and Continuous Modeling of Heat and Mass Transport in Drying of a Bed of Iron Ore Pellets. Drying Technology 2012, 30 (7), 760-773.

95 Koop, L. et al. A Dynamic Two-Dimensional Model for Deep-Bed Drying of Mate Leaves (Ilex paraguariensis) in a Single-Pass/Single-Zone Conveyor-Belt Dryer. Drying Technology 2015, 33 (2), 185-193.

96 Zare, D.; Jayas, D.S.; Singh, C.B. Generalized Dimensionless Model for Deep Bed Drying of Paddy. Drying Technology 2012, 30 (1), 44-51.

97 Mirzahoseinkashani, E.; Kasiri, N. Mathematical Modeling of a Cross Flow Conveyor Belt Dryer. Scientia Iranica 2008, 15 (4), 494-501.

98 Pang, S.; Xu, Q. Drying of Woody Biomass for Bioenergy Using Packed Moving Bed Dryer: Mathematical Modeling and Optimization. Drying Technology 2010, 28 (5), 702-709.

99 Wang, Z.H. et al. Drying Kinetics of Extruded Pellets in Fixed Beds. Drying Technology 2012, 30 (16), 1881-1889.

100 Stakic, M.; Tsotsas, E. Modeling and numerical analysis of an atypical convective coal drying process. Drying Technology 2004, 22 (10), 2351-2373.

101 Garcia-Perez, J.V. et al. Simulation of grape stalk deep-bed drying. Journal of Food Engineering 2009, 90 (2), 308-314.

102 Ruiz-Lopez, II et al. Mathematical modeling and simulation of batch drying of foods in fixed beds with airflow reversal. Journal of Food Engineering 2008, 89 (3), 310-318.

103 Draganovic, V. et al. Assessment of the effects of fish meal, wheat gluten, soy protein concentrate and feed moisture on extruder system parameters and the technical quality of fish feed. Animal Feed Science and Technology 2011, 165 (3–4), 238-250.

104 Choi, Y.; Okos, M.R. Effects of Temperature and Composition on the Thermal Properties of Foods. Food Engineering and Process Applications 1986, 1: Transport phenomena, 93-101.

105 Draganovic, V. et al. Wheat gluten in extruded fish feed: effects on morphology and on physical and functional properties. Aquaculture Nutrition 2013, 19 (6), 845-859.

106 Lambert, C. et al. Toward a generic approach to build up air drying models. Drying Technology 2016, 34 (3), 346-359.

107 Klein, S.; Nellis, G. Mastering EES, F-Chart Software. 2015: Madison, WI, USA.

108 Haubjerg, A.F. et al. Prediction of mechanical durability of dried, extruded fish feed using structural mechanics models and experimental justification of relaxation times. In Proceedings of 19th International Drying Symposium, Lyon, France, 2014

109 Haubjerg, A.F. et al. Experimental investigation of physical properties and mechanical durability of extruded fish feed in the drying process. In Proceedings of 5th European Drying Conference (EuroDrying'2015), Budapest, Hungary, 2015

110 Haubjerg, A.F. et al. Convective deep bed drying of extruded fish feed: model calibration and experimental validation. 2016: Submitted to Drying Technology, february 2016.

111 Salin, J.G. Inclusion of the sorption hysteresis phenomenon in future drying models. Some basic considerations. Maderas-Ciencia Y Tecnologia 2011, 13 (2), 173-182.

112 Jones, D.R.; Perttunen, C.D.; Stuckman, B.E. Lipschitzian optimization without the lipschitz constant. Journal of Optimization Theory and Applications 1993, 79 (1), 157-181.

113 Incropera, F.P. et al. Fundamentals of Heat and Mass Transfer; 6th ed. John Wiley and Sons, Inc.: NJ, USA, 2007

114 Wakao, N.; Kaguei, S.; Funazkri, T. Effect of fluid dispersion coefficients on particle-to-fluid heat-transfer coefficients in packed-beds - correlation of Nusselt numbers. Chemical Engineering Science 1979, 34 (3), 325-336.

115 Achanta, S.; Okos, M.R. Predicting the Quality of Dehydrated Foods and Biopolymers — Research Needs and Opportunities. Drying Technology 1996, 14 (6), 1329-1368.

116 Dissa, A.O. et al. Shrinkage, porosity and density behaviour during convective drying of spirulina. Journal of Food Engineering 2010, 97 (3), 410-418.

117 Schmalko, M.E.; Alzamora, S.M. Modelling the drying of a twig of "yerba mate" considering as a composite material Part I: shrinkage, apparent density and equilibrium moisture content. Journal of Food Engineering 2005, 66 (4), 455-461.

118 May, B.K.; Perré, P. The importance of considering exchange surface area reduction to exhibit a constant drying flux period in foodstuffs. Journal of Food Engineering 2002, 54 (4), 271-282.

119 Kunze, O.R.; Calderwood, D.L. Chapter 8: Physical and mechanical properties of rice, in Rice: Chemistry and Technology; E.T. Champagne, Editor American Association of Cereal Chemists: St. Paul, Minn., 2004; 191-221

120 Prakash, B. Mathematical Modeling of Moisture Movement within a Rice Kernel during Convective and Infrared Drying in University of California Davis. 2011.

121 Kunze, O.R. Fissuring of the rice grain after heated air drying. Trans. ASAE 1979, 22 (5), 1197-1201, 1207.

122 Aklonis, J.J. Introduction to Polymer Viscoelasticity, ed. Wiley. New York, 1983

123 Slade, L.; Levine, H. A food polymer science approach to structure-property relationships in aqueous food systems - nonequilibrium behavior of carbohydrate-water systems; Water Relationships in Foods: Advances in the 1980s and Trends for the 1990s, ed. H. Levine and L. Slade. 29-101 1991

124 Cnossen, A.G.; Siebenmorgen, T.J. The glass transition temperature concept in rice drying and tempering. Trans. ASAE 2000, 25 (4), 1037-1040.

125 Cnossen, A.G. et al. An application of glass transition temperature to explain rice kernel fissure occurrence during the drying process. Drying Technology 2001, 19 (8), 1661-1682.

126 Siebenmorgen, T.J.; Yang, W.; Sun, Z. Glass transition temperature of rice kernels determined by dynamic mechanical thermal analysis. Transactions of the Asae 2004, 47 (3), 835-839.

127 Boudhrioua, N. et al. Influence of ripeness and air temperature on changes in banana texture during drying. Journal of Food Engineering 2002, 55 (2), 115-121.

128 Katekawa, M.E.; Silva, M.A. Drying rates in shrinking medium: Case study of banana. Brazilian Journal of Chemical Engineering 2007, 24 (4), 561-569.

129 Katekawa, M.E.; Silva, M.A. On the influence of glass transition on shrinkage in convective drying of fruits: A case study of banana drying. Drying Technology 2007, 25 (10), 1659-1666.

130 García, L. et al. Glass transition temperatures of cassava starch–whey protein concentrate systems at low and intermediate water content. Carbohydrate Polymers 2012, 87 (2), 1375-1382.

131 Kowalski, S.J. Control of mechanical processes in drying. Theory and experiment. Chemical Engineering Science 2010, 65 (2), 890-899.

132 Kowalski, S.J.; Rybicki, A. The vapour-liquid interface and stresses in dried bodies. Transport in Porous Media 2007, 66 (1-2), 43-58.

133 Sorensen, M. A review of the effects of ingredient composition and processing conditions on the physical qualities of extruded high-energy fish feed as measured by prevailing methods. Aquaculture Nutrition 2012, 18 (3), 233-248.

134 Thomas, M.; van der Poel, A.F.B. Physical quality of pelleted animal feed .1. Criteria for pellet quality. Animal Feed Science and Technology 1996, 61 (1-4), 89-112.

135 Thomas, M.; van Vliet, T.; van der Poel, A.F.B. Physical quality of pelleted animal feed 3. Contribution of feedstuff components. Animal Feed Science and Technology 1998, 70 (1–2), 59-78.

136 Hansen, J.O.; Storebakken, T. Effects of dietary cellulose level on pellet quality and nutrient digestibilities in rainbow trout (Oncorhynchus mykiss). Aquaculture 2007, 272 (1-4), 458-465.

137 ASAE Standards S269.4 Cubes, pellets, and crumbles – definitions and methods for determining density, durability and moisture content. 1991, ASAE: St. Joseph, Mich.

138 Askeland, T.; Fjellanger, K.; Flem, N. Historien om DORIS - bedre kontroll med fôrets fysiske kvalitet. 2002; Available from: http://www.skretting.com/internet/SkrettingNorway/webInternet.nsf/wprId/343E7B319AD65597C125740C004095F0!OpenDocument.

139 Zimonja, O. et al. Effects of fibre content in pelleted wheat and oat diets on technical pellet quality and nutritional value for broiler chickens. Canadian Journal of Animal Science 2008, 88 (4), 613-622.

140 Haubjerg, A.F. et al. Rheological properties as indicator for physico-chemical processes affecting technical quality of extruded fish feed. In Proceedings of 4th European Drying Conference (EuroDrying'2013), Paris, France, 2013

141 Kersten, J.; Rohde, H.R.; Nef, E. Principles of Mixed Feed Production, AgriMedia. 2005: Bergen/Dumme.

142 Bourne, M.C. Texture Profile Analysis. Food Technology 1978, 32 (7), 62-66.

143 Watano, S.; Shimoda, E.; Osako, Y. Measurement of physical strength of pharmaceutical extruded pellets. Chemical & Pharmaceutical Bulletin 2002, 50 (1), 26-30.

144 Lewicki, P.P.; Jakubczyk, E. Effect of hot air temperature on mechanical properties of dried apples. Journal of Food Engineering 2004, 64 (3), 307-314.

145 Mani, S.; Tabil, L.G.; Sokhansanj, S. Effects of compressive force, particle size and moisture content on mechanical properties of biomass pellets from grasses. Biomass and Bioenergy 2006, 30 (7), 648-654.

146 Bhattacharya, S.; Narasimha, H.V.; Bhattacharya, S. Rheology of corn dough with gum arabic: Stress relaxation and two-cycle compression testing and their relationship with sensory attributes. Journal of Food Engineering 2006, 74 (1), 89-95.

147 Singh, H. et al. The analysis of stress relaxation data of some viscoelastic foods using a texture analyzer*. Journal of Texture Studies 2006, 37 (4), 383-392.

148 Limanond, B.; Castell-Perez, M.E.; Moreira, R.G. Modeling the kinetics of corn tortilla staling using stress relaxation data. Journal of Food Engineering 2002, 53 (3), 237-247.

149 Chong, C.H.; Figiel, A.; Law, C.L. Mechanical and Rheology Properties of Dehydrated Fruits. In Proceedings of 18th International Drying Symposium, Xiamen, China, 11-15 November, 2012

150 Rosenthal, A.J. Texture Profile Analysis - How important are the parameters? Journal of Texture Studies 2010, 41 (5), 672-684.

151 Perten Instruments Texvol TVT-300XP/XPH Operation Manual, EXX01 v3.42. 2013.

152 Schubring, R. Investigation of factors influencing the instrumental texture profile analysis (TPA) of fishery products. 1. Influence of compression. Deutsche Lebensmittel-Rundschau 1999, 95 (9), 373-386.

153 Tschoegl, N. Representation of Linear Viscoelastic Behavior by Mathematical Models, in The Phenomenological Theory of Linear Viscoelastic Behavior; N. Tschoegl, Editor Springer-Verlag: Berlin Heidelberg, 1989; 314-364

154 Christensen, R.M. Theory of Viscoelasticity. Dover Publications, Inc.: 31 East 2nd Street, Mineola, N.Y. 11501, 2003

155 Tschoegl, N.W. Time Dependence in Material Properties: An Overview. Mechanics of Time-Dependent Materials 1997, 1 (1), 3-31.

156 Nguyen, Q.S. Stability and Nonlinear Solid Mechanics. John Wiley and Sons Ltd.: United Kingdom, 2000

157 Irgens, F. Continuum Mechanics. Springer: 2008

158 Haubjerg, A. et al. Texture profile analysis of extruded fish feed. European Study Group for Industry 2013, 94 (Graintec A/S).

159 Bonazzi, C.; Dumoulin, E. Quality Changes in Food Materials as Influenced by Drying Processes, in Modern Drying Technology, Volume 3; E. Tsotsas and A.S. Mujumdar, Editors Wiley-VCH Verlag & Co. KGaA: Weinheim, Germany, 2011; 1-20

Appendices / CD-ROM

Appendices to this PhD thesis are

- List of tables, page A-2
- List of figures, page A-3
- Digital versions of all papers and contributions made during the PhD project, as outlined in page X. A CD-ROM is found physically on the last page of this thesis, page A-10.

List of tables

List of figures

Digital version of all papers and contributions

If the CD-ROM does not read, or if you do not have a CD-ROM drive installed, please do not hesitate to write me an email at afh@graintec.com or haubjerg@mmmi.sdu.dk.

In any case, I shall be happy to send you the papers as a compressed file, by email.

ISBN 9788793192904

Correspondence should be directed to the author:
Anders Fjeldbo Haubjerg
Phone: + 45 2124 9767
Email: haubjerg@mmmi.sdu.dk, afh@graintec.com

If necessary, correspondence can alternatively be directed to supervisors:

Principal supervisor:
Christian T. Veje, University of Southern Denmark, veje@mmmi.sdu.dk

Supervisor:
Bo N. Jørgensen, University of Southern Denmark, bnj@mmmi.sdu.dk

Company supervisor:
Benny Simonsen, bs@graintec.com GRAINTEC

The Doctoral Dissertation are printed in:

- 10 copies using thermal tape binding (format A4)
- 10 copies using perfect binding, resembling a paperback book (format 170 x 240 mm)

Haubjerg, Anders F. 2016. Ensuring Technical Product Quality in the Energy Efficient Hot Air drying of Extruded Fish Feed. University of Southern Denmark, Philosophiae Doctor Thesis, 2016:4; ISBN-13/EAN 978-87-93192-90-4

Printed by: Print & Sign, University of Southern Denmark

ISBN-13/EAN: 978-87-93192-90-4

Ensuring Technical Product Quality in the Energy Efficient Hot Air drying of Extruded Fish Feed • Anders Fjeldbo Haubjerg